HYDROTHERMAL-BIOLOGICAL COUPLING OF LAKE EUTROPHICATION MODELS

BY
MING-PIN WANG
and
DONALD R.F. HARLEMAN

RALPH M. PARSONS LABORATORY
AQUATIC SCIENCE AND ENVIRONMENTAL ENGINEERING

Report Number 270

Prepared under the support of the
National Science Foundation
Water Resources and Environmental Engineering Program

APRIL 1982

MIT

DEPARTMENT
OF
CIVIL
ENGINEERING

SCHOOL OF ENGINEERING
MASSACHUSETTS INSTITUTE OF TECHNOLOGY
Cambridge, Massachusetts 02139

R82-16

HYDROTHERMAL-BIOLOGICAL COUPLING OF LAKE EUTROPHICATION MODELS

by

Ming-pin Wang

and

Donald R. F. Harleman

RALPH M. PARSONS LABORATORY

AQUATIC SCIENCE AND ENVIRONMENTAL ENGINEERING

Report Number 270

Prepared under the support of the

National Science Foundation

Water Resources and Environmental Engineering Program

APRIL 1982

ABSTRACT

A deterministic model capable of simulating lake response to changes in hydrologic conditions or nutrient input has been developed. This model may provide a convenient means of evaluating management strategies and identifying weak points in our current knowledge. The emphasis of this model development is to minimize the number of calibrated parameters. A summary of the state-of-the-art of hydrothermal modeling in a phosphorus limited condition is presented in this work. It is demonstrated that a mixed layer hydrothermal model, which calculates the daily vertical temperature profile and thickness of the upper fully mixed layer based on the meteorological and hydrological information, is capable of simulating the transport and diffusive process in a stratified lake with a minimum number of calibrated parameters. Since our ability to mathematically represent complex aquatic biological processes is less well developed than our corresponding ability in the geophysical area, field data plays an important role in defining the final biological model structure. Phytoplankton modeling of L227 is used as a case study to illustrate the methodology for arriving at a biological model whose complexity is consistent with the available data. A procedure is indicated for extracting biological rate constants from primary productivity measurement. The extent to which the linked hydrothermal-biological model simulates the phytoplankton dynamics of the following summer is discussed. Finally, the importance of capturing the short term dynamics of the fully mixed layer in the modeling of phytoplankton variation is illustrated by simulation runs. The simulation runs compare phytoplankton predictions of three lake phytoplankton models with different specifications of the daily fully mixed layer dpeths. Both a surface nutrient input case and an intermediate depth nutrient input case are considered.

ACKNOWLEDGMENTS

Support for this study was provided by the National Science Foundation under Grant No. CEE-7906125 administered by Dr. Arthur A. Ezra, Program Director for Water Resources and Environmental Engineering. The lake data used for the testing and verification of the mathematical models were generously provided by Dr. David W. Schindler, Freshwater Institute, Winnipeg. Mrs. Therese Best, Dr. Schindler's former assistant, was most helpful in locating specific data. Many other scientists at the ELA camp of the Freshwater Institute kindly gave their time. Dr. David Lean of the National Water Research Institute, Burlington, provided valuable insights on the phosphorus cycle.

Professors Sallie W. Chisholm, Francois M.M. Morel, Keith D. Stolzenbach, David H. Marks and Dr. E. Eric Adams and Dr. Peter Shanahan of the Ralph M. Parsons Laboratory supplied valuable advice and suggestions during the course of this research and in reviewing drafts of this report. Dr. Dieter Imboden of the Institute of Aquatic Sciences, ETH, Zurich made many helpful suggestions during a two-month visit to the laboratory.

The report was skillfully typed by Elizabeth Quivey with assistance from Margaret Underdown, Carole Solomon, Laureen Young, Liza Drake and Barbara Adams. All computations were carried out at the MIT Information Processing Center.

TABLE OF CONTENTS

Chapter 1

INTRODUCTION

1.1 Background

Lake eutrophication, which causes deterioration of the water quality, has been recognized as a major environmental problem in the past decade. The National Eutrophication Survey conducted by the EPA from 1971 to 1977 indicated that 68% of 800 lakes surveyed were unmistakably eutrophic and of these, 48% were hypereutrophic.

The term "eutrophic", meaning well nourished, was introduced to limnology by Einar Naumann (1919) to classify lake water types. At the time this classification was introduced, Naumann's criteria (1927) for nutrient content were either uncertain or wildly unrealistic and were based on quite inadequate analysis (Hutchinson, 1969). The practical criterion was that when eutrophic water filled a lake, the phytoplankton rendered the water turbid or colored for much of the year. Therefore, the term "eutrophication" refers to the addition of plant nutrient into the water body and more importantly, the adverse effect subsequently induced on the water body.

The preservation of lake water quality has both ecological and economic importances. Floating water plants and debris clog sand filters and cause taste and odor problems for drinking water supply. Moreover, some phytoplankton are toxic to animals and humans. Excessive phytoplankton growth and coloring of the lake water can certainly impair the recreational use of the lake. Fish of higher commercial values generally desire high water quality so that the eutrophication may cause a change of

fish species. Fish kills have been observed after temporary oxygen depletion and H_2S production in the hypolimnion of stratified lakes.

Sedimentation of organic matter is one natural cause of the disappearance of a lake. Therefore, eutrophication, which increases the production of organic material, may accelerate the ultimate disappearance of the lake. This whole sequence of undesirable effects of eutrophication has its origin in the excessive phytoplankton growth. The nutrient itself is of no great environmental harm but its induced effect, which is this excessive phytoplankton growth, is. The emphasis of eutrophication studies, therefore, has been on the phytoplankton dynamics.

In temperature lakes, which will be the focus of this study, phosphorus has often been considered the nutrient present in shortest supply so that an increase in phosphorus supply results in an increase in phytoplankton population. The lake receives its phosphorus through both external sources, which include both point and non-point sources, and internal sources. The distribution of these phosphorus in the lake and their subsequent use for phytoplankton growth are governed by many hydrothermal and biochemical processes.

Several legal or technological control strategies may be used singly or jointly to curtail or reverse the eutrophication process. For example, the reduction of nutrient suppy may be achieved through treatment plant removal of phosphorus, a change in land practices and lake sediment dredging; reduction of the phytoplankton concentration may be achieved by destratification through mechanical mixing. Any of the control schemes is costly and the recovery of the lake may not be instantaneous; therefore, an astute management decision relies on the ability to predict the

effectiveness of each control scheme. However, the intricate interaction between physical and biochemical processes involved in the lake eutrophication process make it difficult to predict lake ecosystem response by mere data inspection. A mathematical model incorporating the important relevant processes provides a convenient method for evaluating these management strategies. The EPA (1971) has strongly endorsed the utilization of this predictive mathematical procedure. However, model use is not limited to prediction. Since the model integrates current knowledge on the biology and hydrodynamics of the eutrophication process, it can also serve as a diagnostic tool in elucidating the effect of specific factors upon lake water quality. The conjunctive use of the model and a field sampling program may greatly assist in our understanding of the eutrophication process.

1.2 Objectives

The modeling of lake eutrophication needs a comprehensive knowledge of both hydrothermal and biological processes. Unfortunately, due to the diverse nature of the eutrophication problems, the existing eutrophication models often show unbalanced treatment of the two processes. Each process has been stressed by one model or another as the most important process in the lake eutrophication. However, the knowledge of the two processes complement each other and each cannot substitute for the other; an unjustified simplification of one area cannot be compensated by an extensive coverage of the other. On the other hand, an all-inclusive model, such as the WRE model developed by Chen and Orlob (1972), introduces a huge number of calibrated parameters. This not only easily generates errors with users

who do not carefully examine the crucial assumptions but also renders no information on crucial processes. Since the construction of the WRE model in 1972, the continuing concern over the lake eutrophication problem has attracted many hydrodynamic engineers and biologists investigating related problems. This interest has improved our ability to model hydrothermal processes and our understanding of the phosphorus cycle. These improvements are valuable in the development of an eutrophication model that would simulate the growth of phytoplankton in the phosphorus-limited environment of a horizontally-stratified, small- to medium-sized lake, which is the scope of this study. The first objective of this study is to develop a lake eutrophication model that is consistent with the data and the nature of the eutrophication process with the minimal number of calibrated parameters. This may be done by incorporating model formulations which capture the underlying mechanisms or whose validity and parameter values can be measured by conventional methods of measurement.

The time scales in the hydrothermal and biological components of the eutrophication model should be compatible. Since the phytoplankton growth rate is in the order of days and the duration of the phytoplankton bloom is in the order of weeks, the hydrothermal variability of a similar time scale should be identified and properly modeled. While all hydrothermal models recognize the separation of the upper fully mixed layer (FML) from the lower quiescent layer of a stratified lake, the movement of the FML has been traditionally described as a slowly varying process. Since the formation of the FML is a result of the delicate balance between the heating/cooling and the wind mixing process, an examination of the time scale of these forcing terms suggests a likely movement of the FML in the order of

days or a week. The second objective of this thesis is to test this hypothesis by using the MIT wind mixing model for the simulation of the FML and to investigate the importance of capturing this FML variability in modeling phytoplankton dynamics.

The constructed model will be applied to lake 227 (L227) of the Experimental Lake Area (ELA) for model calibration and verification. L227 has been artificially enriched with weekly additions of H_3PO_4 and $NaNO_3$ since 1969 and, like all other lakes in the ELA site, L227 has the following advantages: (1) it is free from other uncontrolled man-made pollution; (2) it is stratified and therefore, allows consideration of hydrothermal characteristics; and (3) it lies in a basin sealed by bedrock so that groundwater influence can be neglected. Data obtained from L227 allows various hypotheses to be tested under controlled conditions in a natural aquatic environment.

In general, the major difficulty encountered in model calibration and verification is the estimation of nutrient input. Since L227 was virtually undisturbed before the fertilization experiment and the use of ELA is restricted to experiment only, it is guaranteed that the nutrient experiment can be conducted without the interference of uncontrollable effects. This considerably simplifies the problem of estimating nutrient inputs. The comparison of lake water quality data from different years will then provide an excellent opportunity to test the relative variability of the biological processes rate constants.

Chapter 2

HYDROTHERMAL MODELS

2.1 Introduction

According to Hutchinson (1975), the first scientific exploration of lake stratification was that of De Saussure's (1779) who demonstrated the prevalence of low temperatures at the bottom of Swiss lakes. Subsequently in 1812-1814, Jardine measured the first series of vertical temperature profiles of Scottish lakes. However, Jardine's work was not published until much later by Buchan (1871). Therefore, the first publication demonstrating lake thermal stratification was that of De la Beche (1819) who studied the lakes of the Alps.

The form of the temperature profile during the stratification period is very characteristic. Figure 2.1 is a typical summer temperature profile of a moderately deep lake in a temperate climate. The temperature profile can be divided into three distinctive regions (Birge, 1910):

(1) The epilimnion, the stratum in which the temperature is nearly uniform;

(2) The thermocline, the stratum of rapid cooling whose limits are somewhat arbitrarily fixed as those regions in which the decrease of temperature equals or exceeds 1°C/m;

(3) The hypolimnion, the region below the thermocline and extending to the bottom of the lake. In this region, the temperature falls slowly with the depth and soon approaches a constant value.

The density of the lake water is predominantly governed by its temperature. In the presence of a positive buoyancy, the non-trivial

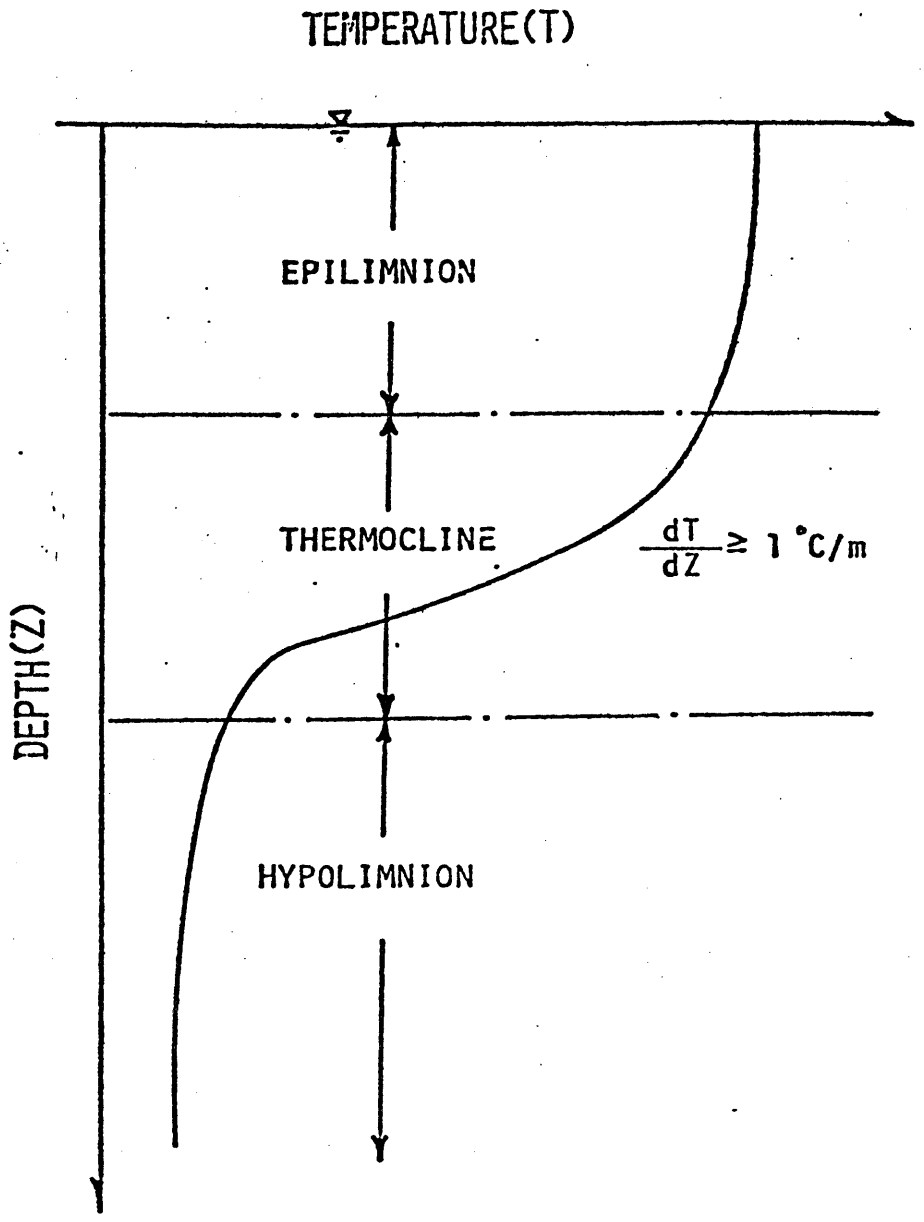

Figure 2.1: Typical Temperature Distribution in a Thermally Stratified Lake and the Definition of Thermocline as Given by Birch (1910)

gravitational body force tends to inhibit vertical motion. When the stratification is strong, this force will dominate over other prevailing forces and the fluid will avoid vertical motions and will mostly flow horizontally (Fischer, Imberger et al., 1978). It appears that more than 70% of the overall vertical temperature difference occurs in the thermocline region. Thus the thermocline leads to a convective decoupling of the epilimnion and hypolimnion.

It is a prerequisite for any water quality model to quantify the physical transport process. Since the temperature has a controlling effect on the lake hydrodynamics, particularly the vertical transport processes, the modeling of the temperature has been an integral part of the modeling of the physical transport process. Thus, the term "hydrothermal model" is applied to describe the lake physical transport model.

The following section (section 2.2) is a review of the hydrothermal models used in the current dynamic lake eutrophication models. This is not intended to be an exhaustive literature review, but rather a representative sampling of existing model structures.

2.2 Hydrothermal Models Currently Used in Eutrophication Models

2.2.1 Fully-Mixed, 1 Box Model

In this model, the lake is assumed to be equivalent to a homogeneous, continuously stirred tank reactor (CSTR). Figure 2.2 is the schematization of this model. Flow into the reactor causes an instantaneous change in the lake, and the outflow has the same concentration and properties as that of the lake. The 1-box model is a reasonable description of small shallow lakes, e.g., those 3-5 m in depth. Jørgensen (1976) used the CSTR model in conjunction with a phosphorus model for shallow lakes.

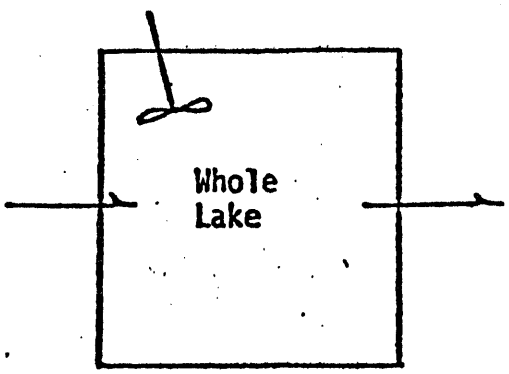

Figure 2.2: The Schematic Representation of a Fully Mixed, 1-box Model

For a typical lake in the temperate region, with medium depth, which undergoes the stratification/fully-mixed cycle, the application of a 1-box model over the whole year is questionable. A fully-mixed, 1-box model clearly cannot simulate a phytoplankton bloom which only occurs during the stratification period. Moreover, when sediment resuspension occurs, the descriptive 1-box model becomes insufficient. Although the shallow lake is fully mixed, the amount of wind induced kinetic energy reaching the sediment has to be computed from the knowledge of wind speed and lake water stability. Preliminary studies by Bloss and Harleman (1978) have shown that in shallow lakes, an appreciable portion of the wind induced turbulent kinetic energy may reach the bottom of the lake. Figure 2.3 is a plot of daily values of kinetic energy per unit area at the bottom of a lake having a uniform depth of 5 m and the same meteorology as Lake Anna (see section 2.3.4). During each month there are periods of calm conditions

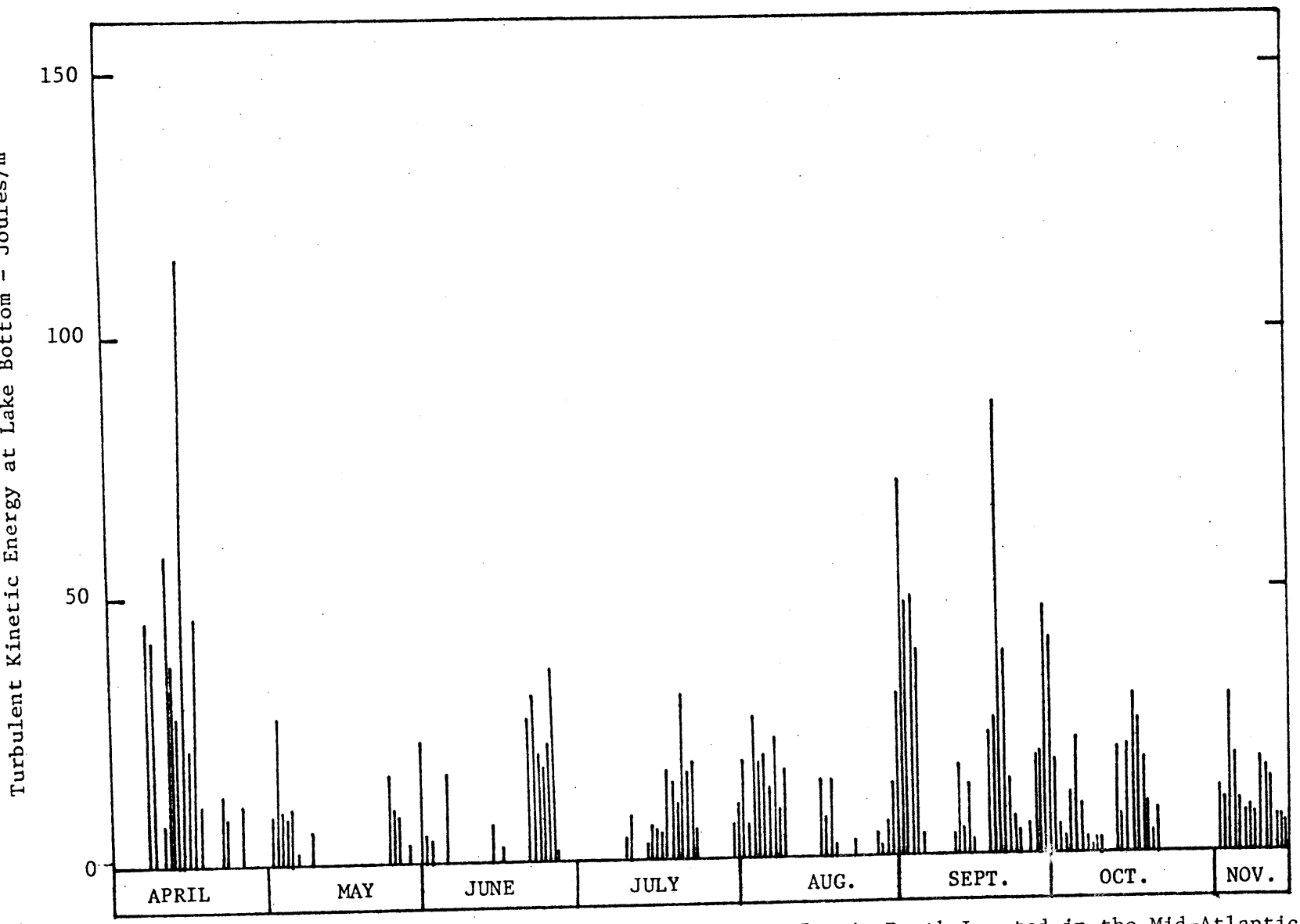

Figure 2.3: Turbulent Kinetic Energy at the Bottom of a Lake 5 m in Depth Located in the Mid-Atlantic States

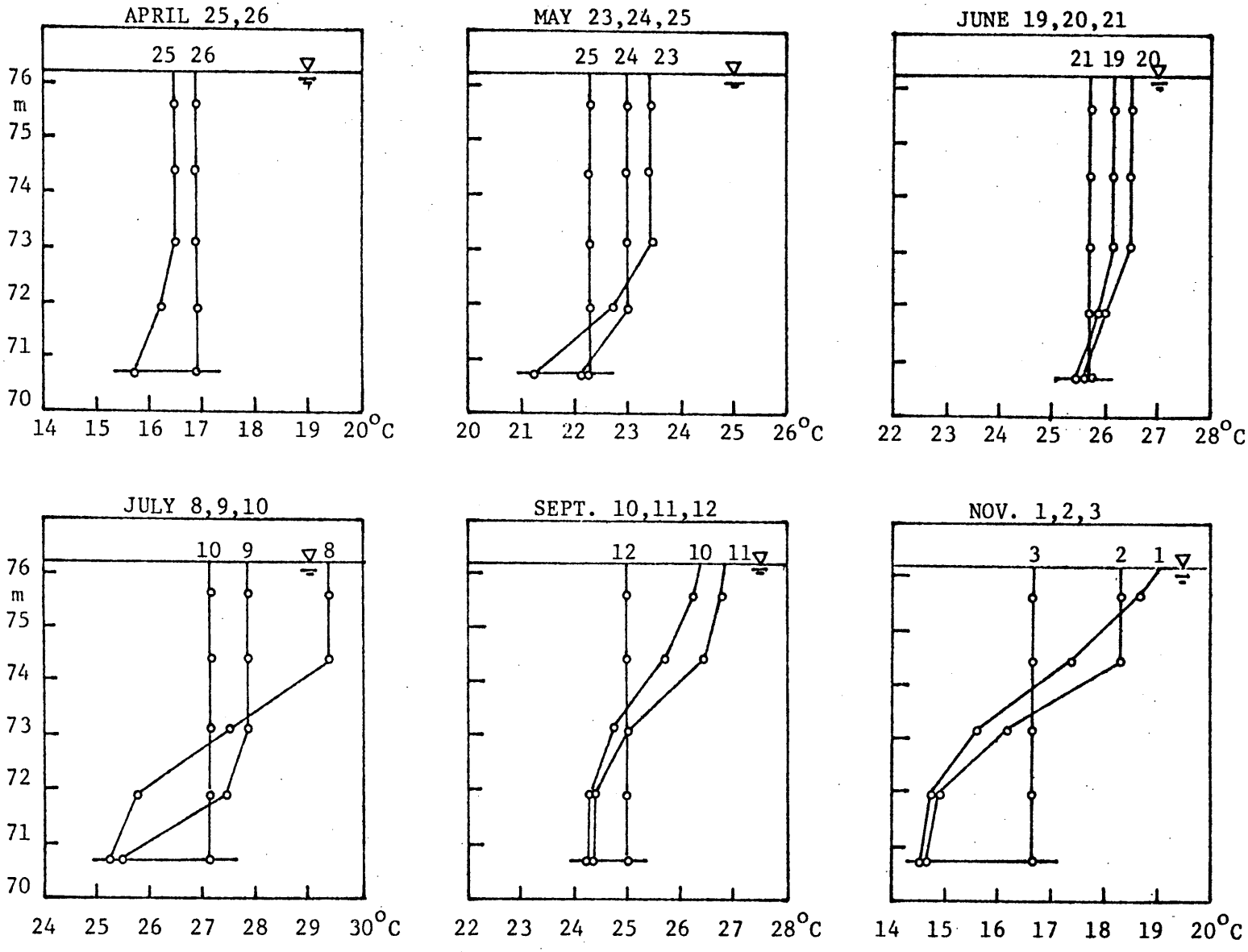

Figure 2.4: Simulated Temperature Variation of a Lake 5 m in Depth Located in the Mid-Atlantic States

(zero mixing energy at the bottom) interrupted by periods in which there is energy available for mixing and entraining bottom sediments. Figure 2.4 shows calculated vertical temperature profiles during selected 3-day periods. For example, during the period July 8-9-10, the July 8 profile shows a 4°C stratification resulting from the preceeding 12-day period of zero bottom energy. Beginning on July 9, mixing energy is available at the bottom and by July 10, the stratification is completely destroyed. An extensive study of the relationship between the sediment resuspension and wind energy in shallow lakes using Lake Balaton as the study case is currently being undertaken by Shanahan (1981).

2.2.2 Two-Layer Model

Snodgrass and O'Melia (1975), as well as DiToro and Matystik (1977) have utilized the two-layer model. This is the simplest possible model which captures the effective separation of the epilimnion and hypolimnion during the stratification period. According to this model, the lake is divided into two fully mixed layers separated by a thermocline located at a fixed depth (Figure 2.5). An empirical exhange coefficient K_{th} is used to characterize all the vertical transport mechanisms between these two layers.

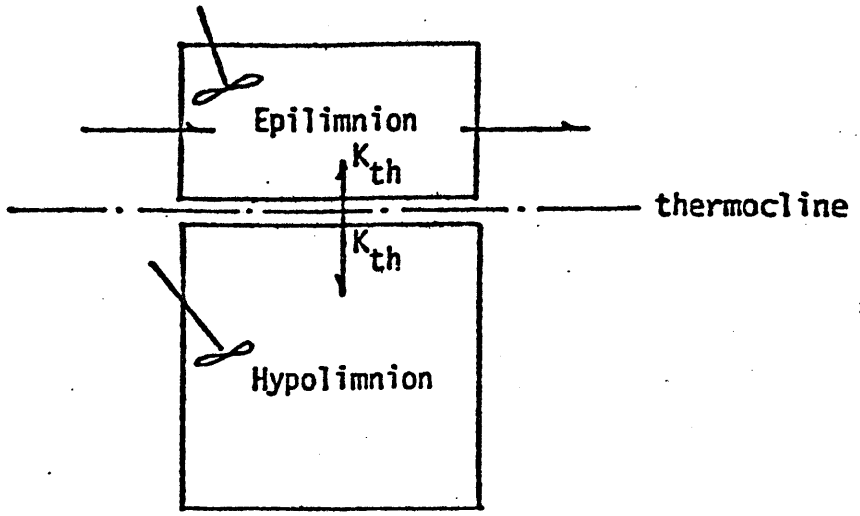

Figure 2.5: The Schematic Representation of a Two-Layer Model

The exchange coefficient K_{th} is obtained by considering the mass transport across the thermocline:

$$J = K_{th} \frac{C_e - C_h}{Z} \tag{2.1}$$

where J = mass flux across the thermocline per unit area; C_e = epilimnion concentration; C_h = hypolimnion concentration; Z = length scale. There are variations in the definition of the length scale, Z, used in Equation (2.1). It may be taken as the depth of the thermocline (Snodgrass , 1974), or it may be taken as the distance between the centers of gravity of the epilimnion and hypolimnion.

The exchange coefficient K_{th} defined by Equation (2.1) has a dimension of L^2/T. Sometimes the term exchange coefficient is used to define the quantity K_{th}/A, which has a dimension of L/T and is analogous to velocity (Snodgrass et al., 1975).

Snodgrass et al. (1975) assume that stratification occurs instantaneously at the end of the winter period and lasts for six months. A constant thermocline location is specified by averaging the thermocline locations from historical temperature profile data. In any given temperature profile, the location of the thermocline is defined as the depth with maximum temperature gradient. Alternatively, the constant thermocline location is calculated from an empirical relation which relates the location of the average summer thermocline to the lake mean depth. An exchange coefficient representing mixing between the upper and lower layers is determined from another empirical relationship based on the mean lake depth.

DiToro et al. (1977) also represents a stratified lake by two fully-mixed layers. It is assumed that all short wave radiation is absorbed in the

surface layer and that the epilimnion has a constant depth. Temperature measurements are used to calibrate an exchange coefficient K_{th} defined in the following manner. The variation of the exchange coefficient with time is shown in Figure 2.6. During the stratification period, a zero exchange coefficient is assumed and for the fully mixed period, a constant exchange coefficient of 10 m^2/day (800 times the heat molecular diffusivity) is postulated. The exchange coefficient during the transition period is linearly interpolated between 0 and 10 m^2/day.

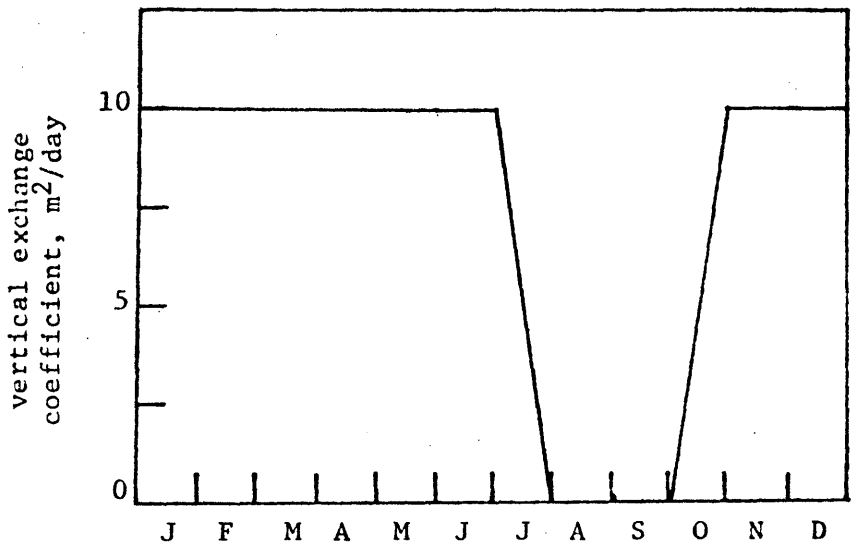

Figure 2.6: Vertical Exchange Coefficient Used by DiToro et al. (1977)

As a result of the assumption of a fixed thermocline location, the exchange coefficient must account for mixing at the thermocline location. Snodgrass's empirical formulation which relates the exchange coefficient with mean depth needs evaluation since the important factors which govern the thermocline depth and movement, such as extinction coefficient and wind speed, are not considered in the formulation. DiToro's formulation only allows a very crude representation of the annual fully-mixed/stratified cycle, so that a more realistic representation of the movement of the thermocline is needed.

The hydraulic and nutrient inflows and outflows are assumed to be confined to the epilimnion layer during the stratification period. This limits the ability of this type of model to predict lake responses due to flows entering or leaving the hypolimnion.

Treating the hypolimnion as a fully mixed layer is not in accord with observations that vertical gradients of biochemical properties are often significant within the hypolimnion. For example, a fully mixed layer assumption does not permit a representation of the anoxic region, which occurs only near the bottom of the lake. The anoxic condition in the water-sediment interface is closely associated with the sediment release of orthophosphate. In many lakes, particularly those with a long eutrophication history, this ortho-P released from the sediment under the anoxic condition becomes a significant fraction of the phosphorus input and a correct modeling of the nutrient source is consequently needed.

Since the hypolimnion should not be regarded as an isolated volume, it is always necessary to capture the effect of the boundary exchanges. The simplification of the hydrodynamic condition of the hypolimnion often

causes additional complexity in handling the boundary fluxes. To illustrate this point, let us consider the following simple diffusion problem in a semi-infinite flow field with specified boundary conditions.

Consider a case of the diffusion of ortho-P from sediment, into the rather quiescent hypolimnion of large depth. That is to say, during the period considered, the diffusion process does not bring about any appreciable change of the concentration at the top of the hypolimnion. We further assume that in the hypolimnion no chemical reaction takes place and no advection movement affects the transport of the ortho-P. At the time t = 0, the sediment-water interface becomes anoxic and it is assumed that from then on the concentration in the plane of water which is in contact with the sediment is uniformly equal to C_b. Although this example greatly simplifies the actual problem of the sediment return of ortho-P under the anoxic condition, some useful insights can still be gained.

Under these circumstances, the variation of the ortho-P concentration in time and space in the absence of reaction can be described by a diffusion equation,

$$\frac{\partial C}{\partial t} = E_h \frac{\partial^2 C}{\partial z^2} \tag{2.2}$$

with the following initial and boundary conditions

$$\begin{aligned} C &= C_o \qquad z > 0 \qquad t = 0 \\ C &= C_b \qquad z = 0 \qquad t > 0 \\ C &= C_o \qquad z = \infty \qquad t > 0 \end{aligned} \tag{2.3}$$

For this case the datum of the z axis is at the bottom of the lake. The solution to this problem is

$$C = C_o + (C_b - C_o)(1 - \text{erf} \frac{z}{2\sqrt{E_h t}}) \tag{2.4}$$

Thus the rate of the diffusion of sediment-released ortho-P into the hypolimnion per unit area at any time t is given by:

$$R = -E_h \frac{\partial C}{\partial z}\Big|_{z=0} = (C_b - C_o)\sqrt{\frac{E_h}{\pi t}} \tag{2.5}$$

and the total amount of ortho-P diffused into the water per unit area during the period T is

$$Q = \int_0^T R\, dt = 2(C_b - C_o)\sqrt{\frac{E_h}{\pi t}} \tag{2.6}$$

If we approximate the quiescent hypolimnion by a fully mixed layer with concentration C_o, then we need to specify an exchange coefficient between the hypolimnion and the sediment to account for this boundary flux. Under this circumstance, it is customary to express the boundary flux per unit area of the sediment-water interface as

$$R = k_L(C_b - C_o) \tag{2.7}$$

Comparing Equation (2.7) with Equation (2.5), we can see k_L equals $\sqrt{\frac{E_h}{\pi t}}$. The exchange coefficient is infinite at the beginning of the anoxic period and decreases with time, and the exchange coefficient k_L is proportional to the square root of the hypolimnion diffusivity E_h. This simple example clearly illustrates that when the hydrodynamic condition of the hypolimnion is simplified, an additional parameter k_L has to be introduced to account for the boundary value problems. Not only is k_L varying with time, the correct specification of k_L still depends on the knowledge of the actual hydrodynamic properties of the hypolimnion which

is characterized by the value E_h in this case.

2.2.3 Fully Mixed Epilimnion and One-Dimensional Vertical Diffusion Model in the Hypolimnion

This schematization was used by Imboden and Gachter (1978) in their dynamic lake model for trophic state prediction (Figure 2.7). The location of the thermocline separates the lake into two regions with distinctly different hydrodynamic properties. On top of the thermocline lies a completely mixed epilimnion whose thickness is allowed to vary with time and is specified as input data. Below the thermocline lies a stratified hypolimnion described by a one-dimensional, multi-layer diffusion equation. In this equation, the characterizing parameter for the vertical transport process is the diffusivity.

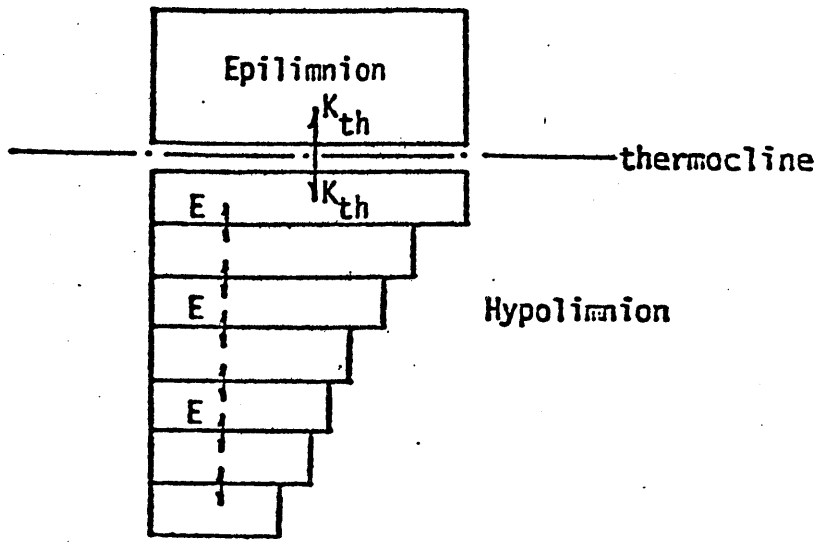

Figure 2.7: The Schematic Representation of a Fully Mixed Epilimnion and 1-D Vertical Diffusion Model in the Hypolimnion

Imboden and Emerson (1977) used natural radon to estimate vertical diffusivity in the hypolimnion. Radon is a better tracer than temperature for estimating the hypolimnion vertical diffusivity since the temperature profile is almost vertical in most of the hypolimnion. Unfortunately, no attempt was made to correlate the estimated vertical diffusivity with important influencing factors. Since the underlying principle is not identified, the extrapolation from isolated observations should be regarded as site specific information.

The exchange coefficient between the epilimnion and the first layer in the hypolimnion as well as the vertical diffusion coefficient between adjacent layers of the hypolimnion are tuned to fit field data. The exchange coefficient between the epilimnion and the first layer in the hypolimnion is primarily estimated from temperature profiles taken at bi-weekly intervals. The model does not have the capability to simulate the temperature; consequently, it cannot simulate the case with subsurface inflow.

This model ignores the absorption of solar radiation below the fully mixed layer. Bachman and Goldman (1965) have shown that in the metalimnion and hypolimnion (collectively defined as hypolimnion in Imboden's model) a large portion of the heat comes from the direct absorption of the short wave solar radiation. Using the terminology in Imboden's model, Bachman's finding indicates that in the upper region of the hypolimnion, the direct absorption of the short wave solar radiation is a significant portion of the heat increase. Therefore, the calibrated exchange coefficient has to account for this assumption in the model formulation as well.

In this model the epilimnion depth is defined at much more frequent

time intervals than in the two-layer models. This sampling period has to be evaluated in light of the current knowledge of the thermocline formation because of the possibility that the variations in the mixed layer depth occur at periods smaller than the sampling period.

The vertical exchange rates calculated by measuring the temperature increase rate of the hypolimnion water is a frequently employed method in the current water quality field sampling/analysis program and the frequency of sampling is usually one per two weeks or less. Therefore, Imboden's model represents a popular method of field data analysis and an evaluation of this will be informative. A model, similar to Imboden's, employing this schematization but having the added ability to account for the absorption of short wave solar radiation is developed in a later section (section 6.4). The comparison of this modified Imboden model with a more advanced dynamic hydrothermal model is also presented and discussed in detail in Chapter 6.

2.2.4 Multi-Layer, Vertical Diffusion Model

This mathematical model considers a lake as a horizontally homogeneous but vertically stratified water body (Figure 2.8). This is a good representation for small-to-medium size lakes where no obvious horizontal differences are observed. The ecological model developed by Chen and Orlob (1972) adopted the WRE model, which is a multi-layer vertical diffusion model, as the basic hydrothermal structure. A detailed description of the model development and application can be found in project reports of Water Resources Engineers, Inc., by Orlob and Selna (1967) and by Orlob and Roesner (1969). Other widely used multi-layer diffusion models are the MIT Reservoir model (Huber and Harleman, 1968; Ryan and Harleman, 1971) and the Cornell model (Sundaram, 1973).

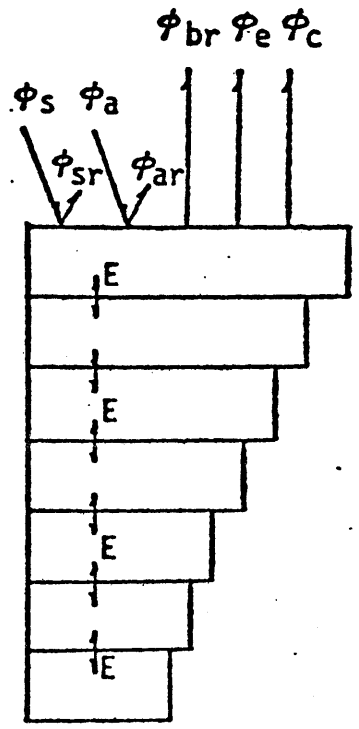

Figure 2.8: The Schematic Representation of a Multi-layer, Vertical Diffusion Model

These models include the effect of absorption and transmission of solar radiation, vertical advection due to inflow/outflow and vertical diffusion. Inflows are assumed to enter the water column at the elevation at which the density of the water column is equal to the density of the inflow after entrance mixing. Selective withdrawal at the outlet is included and velocities are computed from inflow and outflow rates. The vertical advective velocities are then computed from the continuity equation for each layer.

The basic equation for heat transport in the vertical direction is

$$\frac{\partial T}{\partial t} + \frac{1}{A}\frac{\partial}{\partial z}(Q_v T) = \frac{1}{A}\frac{\partial}{\partial z}\left[AE\frac{\partial T}{\partial z}\right] + \frac{Bu_i T_i}{A} - \frac{Bu_o T}{A} - \frac{1}{A\rho c}\frac{\partial(\Phi_z A)}{\partial z} \qquad (2.8)$$

where T is the water temperature at depth z, A = area of the lake, B = width of the lake, u_i = horizontal inflow velocity, T_i = temperature of the inflow, u_o = horizontal outflow velocity, Q_v = vertical flow rate, E = vertical turbulent diffusion coefficient, c = heat capacity of water and ρ = density of water.

The specification of spatial and temporal variations of the vertical turbulent diffusion coefficient has been a continuing problem for this type of hydrothermal model. There is no general agreement on how to relate the diffusion coefficient with environmental factors affecting vertical mixing. In applications to Fontana reservoir (TVA), the MIT model uses a constant eddy diffusivity of the order of 50 times the molecular diffusivity of heat. The WRE model uses a variable coefficient, which is considered to be a function of time and depth, to represent the stirring effect of the wind. In the earlier version of the WRE model, Orlob (1967) suggested the following formulation for the vertical eddy diffusivity:

$$E(z,t) = E_o(t)e^{-\delta z} \qquad z \leq z_T \qquad (2.9.a)$$

$$E(z,t) = E(z_T,t) \qquad z > z_T \qquad (2.9.b)$$

where $E_o(t)$ is the diffusion coefficient at the surface, z_T is the depth at which the thermocline is located and δ is a decay coefficient. The general form of this formulation is sketched in Figure 2.9. The values of $E_o(t)$ and $E(z_T,t)$ depend on the particular reservoir. z_T is computed from

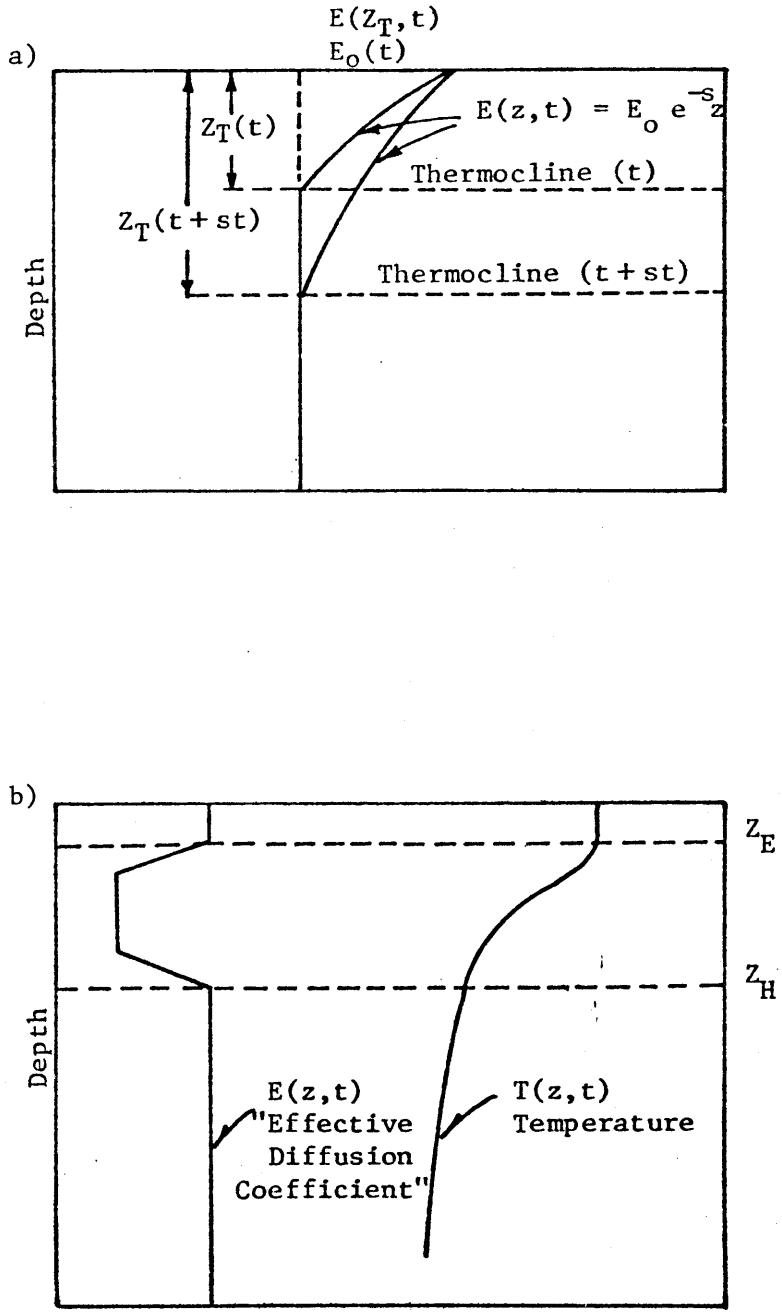

Figure 2.9: Definition Sketches for "Effective" Diffusion Coefficient vs. Depth

(a) After Orlob and Selna (1967)

(b) After Orlob and Roesner (1969)

the temperature profile and is defined as the depth at which the second derivative of temperature T with respect to z is zero. δ is uniquely determined by the ratio $E(z_T,t)/E_o(t)$ and the depth z_T. Reported values of E_o are of the order of one hundred to one thousand times the value of the heat molecular diffusivity (0.0125 m^3/day).

A modified formulation was later proposed (Orlob and Roesner, 1969) to describe the eddy diffusivity:

$$\begin{cases} E(z,t) = E_o(t)^{-z} & z < z_E \quad (2.10.a) \\ E(z,t) = b\ s^{-a} & z_E < z < z_H \quad (2.10.b) \\ E(z,t) = c & z_H < z \quad (2.10.c) \end{cases}$$

where s is the stability of the water column defined as $-\frac{1}{\rho}\frac{\Delta\rho}{\Delta z}$, z_E is the depth at which s equals 10^{-6} m^{-1} while z_H is the depth defined by $(b/c)^{1/a}$.

The following values were recommended for the parameters in equation (2.10):

$a = 0.7$

$b = 1.5 \times 10^{-8}\ m^{1.3}\ sec^{-1}$

$c = 2.5 \times 10^{-4}\ m^2\ sec^{-1}$

Furthermore, in the absence of better data from field observations in the lake or reservoir being considered, Orlob and Roesner (1969) suggested setting $E_o = c$ and $\delta = 0$. Both forms of the "effective" eddy diffusivity as represented by equation (2.9) and equation (2.10), are shown in Figure 2.9

Orlob noted that equation (2.10) is only applicable to reservoirs

where the vertical advection is the dominant vertical heat transport process. When vertical advection dominates the diffusion, a correct description of diffusivity is not necessary. Later studies on vertical heat transport mechanisms in lakes and reservoirs by Octavio, Jirka and Harleman (1977) demonstrated that in reservoirs the vertical temperature profile may be insensitive to the eddy diffusivity. Figure 2.10 shows the results of a sensitivity analysis of the MIT Reservoir Model (Ryan and Harleman, 1971) which is conceptually similar to Orlob's model. It shows that in the Fontana Reservoir where vertical advection dominates the vertical transport, an increase in the diffusivity by a factor of 100 causes very little change in the predicted temperature profiles (Octavio, 1977). Hence, Orlob's comment on the limitation of equation (2.10) implies that the formulation developed and tested in a reservoir may not be applicable to lakes where vertical diffusion is often the dominant transport process.

Octavio et al. (1977) proposed a dimensionless number, AE/Qd, that is proportional to the ratio of the rate of heat transport by vertical diffusion to the rate of heat transport by vertical advection. A is the horizontal cross-sectional area at the depth of the outlet d; Q is the average inflow/outflow rate and E is the vertical eddy diffusivity. In reservoirs that have appreciable inflows and outflows at different elevations, the vertical transport of heat by advection is often large enough to dominate the transport of heat by diffusion. In lakes, the opposite may be true, especially since inflows are relatively smaller and both inflows and outflows are usually confined to the surface of the lake. In Fontana reservoir, $\frac{AE}{Qd} = 7 \times 10^{-4}$ with E equal to the heat molecular diffusivity (0.0125 m^2/day), while $\frac{AE}{Qd} = 7 \times 10^{-2}$ with E equal to 100 times the molecular

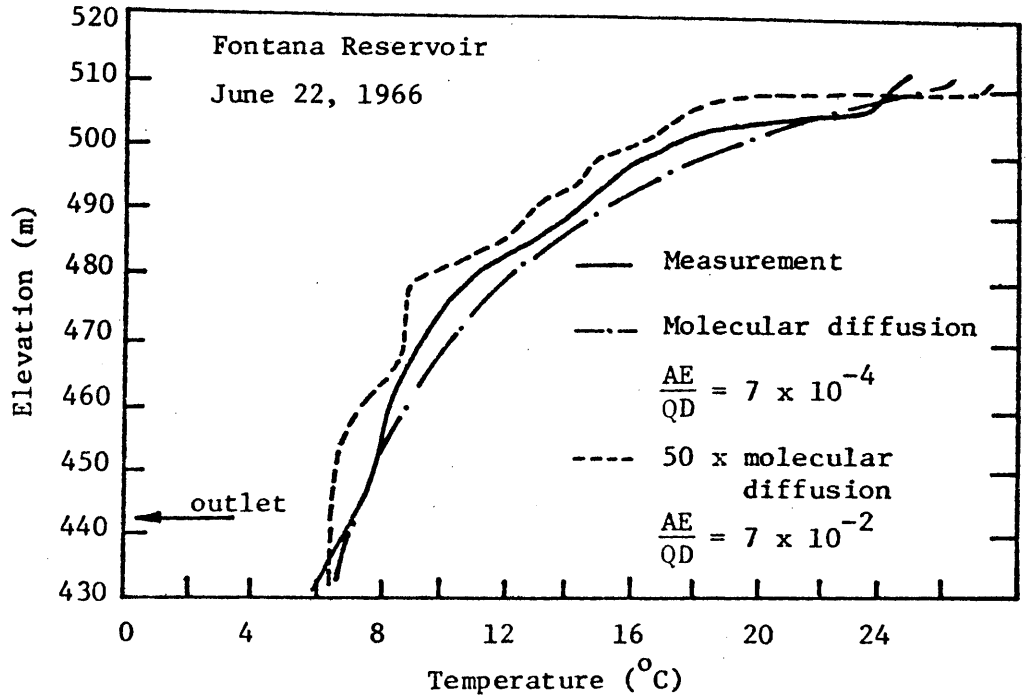

Figure 2.10: Sensitivity of Diffusion Coefficient in the Temperature Simulation for Fontana Reservoir

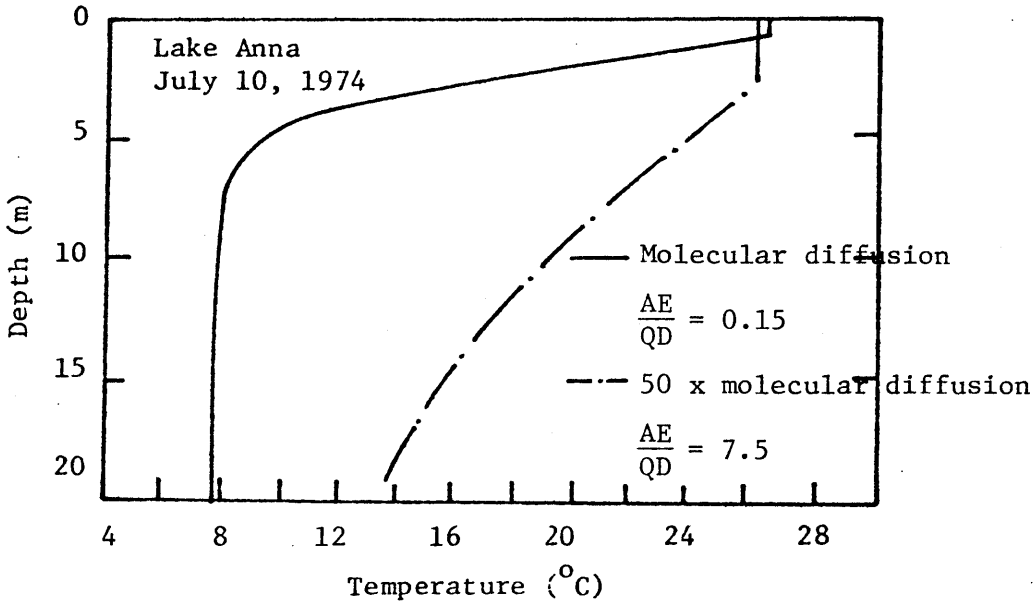

Figure 2.11: Sensitivity of Diffusion Coefficient in the Temperature Simulation for Lake Anna

diffusivity, indicating that in both cases shown in Figure 2.10 advection dominates diffusion. Whereas in a typical lake $\frac{AE}{Qd} \leq 1$ with E equal to the molecular diffusivity. From a similar sensitivity analysis for a typical lake having a negligible inflow a change from molecular diffusivity to 50 times this value produces a large change in the predicted temperature profile (Figure 2.11). With E equal to molecular diffusivity, $\frac{AE}{Qd} = 0.15$ while with E equal to 50 times molecular diffusivity, $\frac{AE}{Qd} = 7.5$; therefore, diffusion is important in both cases shown in Figure 2.11.

It is noteworthy to point out that each of the cited models employs the measured temperature profile for estimating the vertical diffusion coefficient. Although this approach of treating temperature as a tracer to calibrate the vertical diffusion coefficient is a reasonable approach, the necessity of using field data to calibrate the diffusion coefficient weakens the model's ability to simulate cases with different hydrologic, meteorologic or biological (affecting extinction coefficient) conditions and thus nullifies the model's role as a management tool. Moreover, it is of little value for the hypolimnion region where the thermal stratification is weak.

2.2.5 Summary

It is concluded that the hydrothermal models discussed above introduce varying degrees of uncertainty in the advection and mixing process that are important to the biochemical components.

The multi-layer, vertical diffusive model appears to be the most realistic hydrothermal structure currently employed in lake eutrophication models. It captures the thermal and biochemical stratification observed

in many lakes. However, the specification of the temporal and spatial variation of the vertical turbulent diffusion coefficients has been a continuing problem for this type of hydrothermal model. In lakes where the vertical diffusion dominates the vertical advective transport, the difficulty in determining the temporal and spatial variability of the diffusion coefficient becomes crucial.

A recent sensitivity analysis with the WRE model using Arcadia Lake as data base by Thornton and Lessen (1976) investigated the effect of changing the vertical eddy coefficient (E_o of equation 2.9) from 6.5×10^{-5} to 7.5×10^{-5} m^2 sec^{-1}. The results indicated changes in the algae concentration of over 100% and changes in the zooplankton concentration of over 40% for a large part of the annual cycle. Further, a slight increase in the transport across the thermocline, by decreasing from 0.75 to 0.675 of the parameter a in equation (2.10), which is the exponent relating the diffusion coefficient to the degree of stratification, led to large explosions in the surface algae and zooplankton densities. This sensitivity study further supports the importance of diffusivity in water quality modeling. Since current hydrothermal components of the eutrophication models are not totally satisfactory, an improvement of the present hydrothermal components is necessary to reliably simulate the eutrophication indices. The hydrothermal model to be used in this study is the modified wind mixing model (Bloss and Harleman, 1979) which is an improved version of an earlier wind mixing model (Octavio, 1977). A description of the model structure of the modified wind mixing model (WDMIX) will be given in the next section.

2.3 Wind Mixing Model

The WDMIX model uses an alternating heating-mixing algorithm to represent the interplay of the solar heating, surface cooling and wind-mixing effect.

The current WDMIX model is a further modification of the wind-mixing model (Octavio and Harleman, 1977) which in turn is a modification of the MIT Reservoir Model (Ryan and Harleman, 1971). The MIT Reservoir Model accounts for the surface heat exchange processes, internal absorption of solar radiation, advection due to through-flows, convective mixing and molecular diffusion as quantitatively as possible. The wind-mixing model modifies it by considering the wind induced turbulent transport. All the kinetic energy input caused by the wind action is assumed to be used for mixing. Bloss (1979) further subdivided the wind induced kinetic energy into dissipation, mixing and increase of kinetic energy in the mixing layer. A detailed treatment of the current model structure can be found in a series of MIT technical reports (Ryan and Harleman, 1971; Octavio and Harleman, 1977; Bloss and Harleman, 1979). Much of the information covered in this section is drawn from a recent paper by Harleman (1981) who documents the evolution of the MIT hydrothermal models. The model structure may be conveniently divided into three essential components: the 1-D heat conservation equation, the convective cooling and the wind mixing.

2.3.1 1-D Heat Conservation Equation

The basic equation for heat transport in the vertical direction is obtained by considering heat and mass flow through an internal control

volume taken as a horizontal layer of the water body. The model schematization is shown in Figure 2.12. The layer has a thickness Δz and a horizontal area A(z). Inflows enter the element at the upstream end and outflows leave through the downstream end. Short wave solar radiation is absorbed internally in the body of the lake and at the surface. The transmission of internal short wave solar radiation at elevation z is given by Dake and Harleman (1966):

$$\phi_z = \phi_{sn} (1 - \beta) e^{-\eta(z_s - z)} \tag{2.11}$$

where z_s = water surface elevation, ϕ_{sn} = net incident flux of short wave solar radiation (joules/m^2-day), β = fraction of ϕ_{sn} absorbed at the surface (approximately 0.4 to 0.5), η = extinction coefficient of water. The basic heat transport equation for an <u>internal element</u> is

$$\frac{\partial T}{\partial t} + \frac{1}{A}\frac{\partial}{\partial z}(Q_v T) = \frac{1}{A}\frac{\partial}{\partial z}\left[AD\frac{\partial T}{\partial z}\right] + \frac{Bu_i T_i}{A} - \frac{Bu_o T}{A} - \frac{1}{A\rho c}\frac{\partial(\phi_z A)}{\partial z} \tag{2.12}$$

where D is the heat molecular diffusivity. The equation is solved using an explicit finite difference scheme.

To satisfy the surface boundary condition, the governing equation for the <u>surface element</u> of thickness Δz_s includes (in addition to the terms in equation 2.12) the heat fluxes due to surface phenomena, i.e., direct solar radiation Φ_o, back radiation ϕ_{br}, evaporation ϕ_e, convection ϕ_c, atmospheric radiation ϕ_{an}, and the portion of the solar radiation which is absorbed at or near the surface $\beta\phi_{sn}$. Direct solar radiation (Φ_o) is usually available from meteorological stations or may be estimated by empirical formulas which express it as a function of the clear sky radiation and cloud cover.

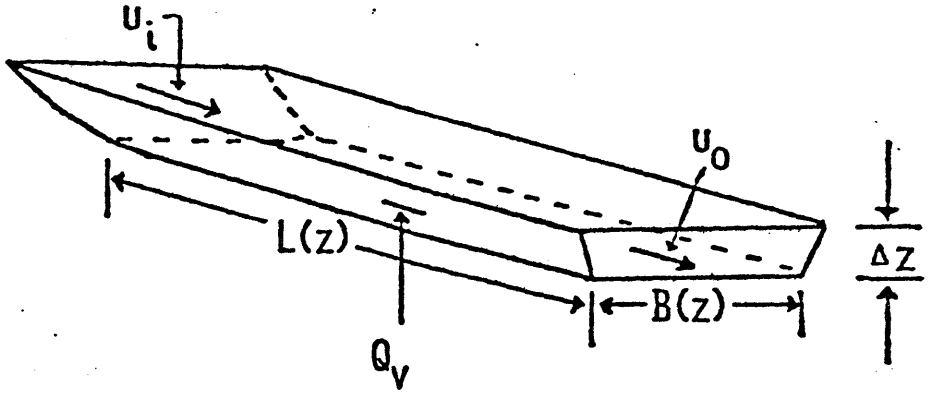

(a) CONTROL VOLUME SLICE

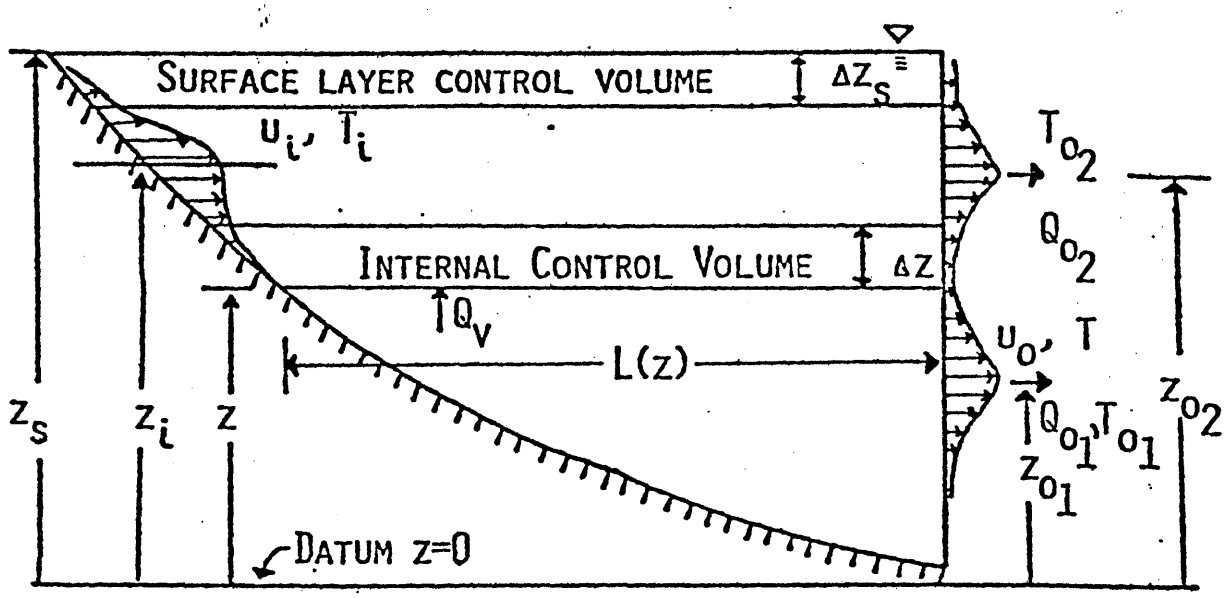

(b) SIDE ELEVATION

Figure 2.12: Schematization and Control Volume for Mathematical Model

Direct measurements of atmospheric radiation (Φ_a) and other heat fluxes generally are not available. Empirical formulas for estimating these fluxes are well developed and may be found in Ryan (1971) and Octavio (1977). The vertical flow rate Q_v is calculated from the following mass balance

$$\frac{\partial(Q_v)}{\partial z} = Bu_i - Bu_o \tag{2.13}$$

with

$$Q_v = 0 \qquad \text{at } z = 0 \tag{2.14}$$

The distribution of Bu_i and Bu_o which also appear in the so-called external heat source term in equation (2.12) as a result of the incorporation of the two-dimensional horizontal flows into a one-dimensional vertical scheme, is calculated from the continuity equation for each element in separate subroutines. With the notation in Figure 2.12,

$$Q_v(z,t) = B\int_0^z u_i(z,t)dz - B\int_0^z u_o(z,t)dz \tag{2.15}$$

Horizontal velocities are computed from inflow and outflow rates, assuming Gaussian velocity distributions about the entry and exit elevations. The height of the distribution is determined by the local density gradient. The distribution may be cut off by the surface (in the case of dam overflow or a surface outlet) or by the local bottom elevation (for a submerged outlet close to the bottom). Entrance mixing of inflows is accounted for by an entrainment factor, which specifies the additional flow entrained by a given inflow. The resulting mixed flow is assumed to spread with a Gaussian velocity distribution at a depth where the ambient density matches that of the mixed inflow. (See Ryan and Harleman, 1971.)

2.3.2 Convective Cooling

Since equation (2.12) does not account for turbulent transport caused by external energy inputs at the surface, two mixing algorithms are applied at the end of each computation time step. The first mixing algorithm is to eliminate any density instability in the water column: the model computes the density profile corresponding to the temperature profile obtained from equation (2.12). When there is a density instability, the adjacent layers of the unstable region are mixed downward until the stability of the water column is restored. During each mixing computation, it is assumed that the thermal energy is conserved, thus the temperature of the mixed layer is computed as the volume average temperature and the density corresponding to this new temperature is computed for checking the density stability of the water column. For example, if layer i with temperature T_i and volume V_i is mixed with layer i+1 with temperature T_{i+1} and volume V_{i+1}, the resulting mixed layer will have a volume of (V_i+V_{i+1}) and a temperature T_m defined as

$$T_m = \left(\frac{V_i T_i + V_{i+1} T_{i+1}}{(V_i + V_{i+1})}\right) . \qquad (2.16)$$

The density ρ_m corresponding to T_m is then computed from the equation of state which expresses the density of water as a function of temperature.

2.3.3 Wind Mixing

The second mixing algorithm takes into account the stirring effect induced by the wind. The wind mixing model is largely built on Kraus and Turner's (1967) model which computes the thickness of the ocean's upper mixed layer by balancing the turbulent kinetic energy and the

internal energy. This approach, which is based on energy considerations, overcomes the difficulty of specifying the temporal and spatial variations of eddy diffusivity encountered in the diffusion model.

The mixed layer concept can be summarized as follows. Surface wind shear acting as a stirring agent produces the turbulent kinetic energy (TKE) at a thin layer near the surface. This produced TKE is then transported downward and partially used to homogenize the fluid. At the density interface, the remaining TKE plus any that may be locally generated by interfacial shear, and minus that which is locally dissipated by viscosity or radiated into the quiescent layer by internal waves, is transformed into potential energy by entraining quiescent fluid below the interface into the mixed layer. This entrainment, in addition to the previously considered convective cooling and vertical advection, determines the thickness of the mixed layer. The rate of increase of the mixed layer thickness h during the time interval dt is defined as the entrainment velocity u_e. That is, $u_e = \frac{dh}{dt}$.

The principle of the wind mixing algorithm is based on a series of turbulence entrainment experiments on stratified fluid. In 1955, Rouse and Dodu performed a classic mixing experiment across a density interface. In this experiment, turbulence was generated in the upper layer of a two-layer stratified fluid by means of an oscillating grid. They found that turbulence produced a well-mixed upper layer separated from the undisturbed lower layer by a sharp interface. In later similar grid experiments by Turner (1968), salt or heat was used to create the density difference. Turner found that the entrainment velocity u_e when normalized by the characteristic scaling velocity u_ℓ, is inversely proportional to the Richardson

number Ri:

$$\frac{u_e}{u_\ell} \propto Ri^{-1} \tag{2.17}$$

with Ri defined as

$$Ri = \frac{\delta \Delta\rho g \ell}{\rho u^2} \tag{2.18}$$

where g is the gravity acceleration, $\frac{\Delta\rho}{\rho}$ is the relative density difference across the interface and ℓ is the characteristic length scale.

In other experiments, illustrated in Figure 2.13, turbulence in the upper mixed layer was generated by means of (1) a moving screen at the water surface (Kato and Philips, 1969), (2) oppositely directed ejecting jets (Moore and Long, 1971), and (3) wind shear at the surface (Wu, 1973). Data from these experiments all support the Ri^{-1} entrainment law observed by Turner (1968).

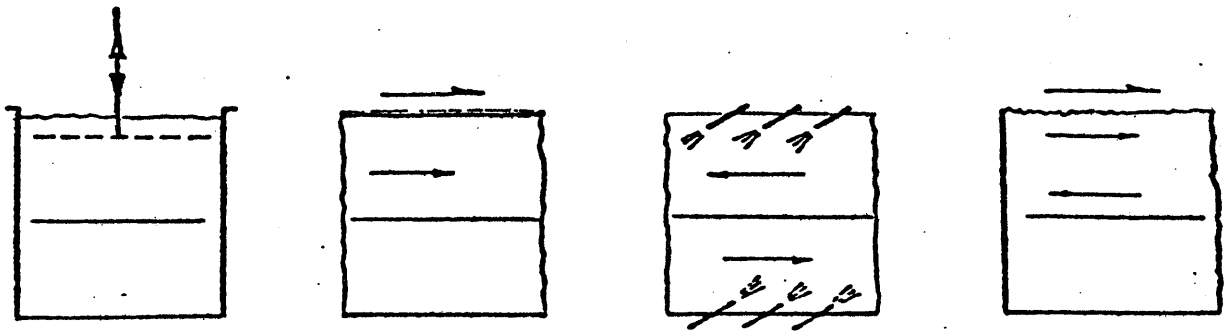

Figure 2.13: Turbulent Entrainment Experiments Using Mechanical Turbulence Generation

The physical interpolation of the Ri^{-1} law as an energy ratio can be illustrated by considering an idealized form of stratification shown in Figure 2.14, in which a mixed layer depth h is bounded by an interface of negligible thickness across which there is a density increase $\Delta\rho$. The quiescent layer beneath the mixed layer has a density gradient Γ. In accordance with the physical mechanisms discussed previously, turbulence in the mixed layer produced by wind shear at the surface, causes the mixed layer depth to increase by an amount dh during a time interval dt and the quotient $u_e = dh/dt$ is the entrainment velocity.

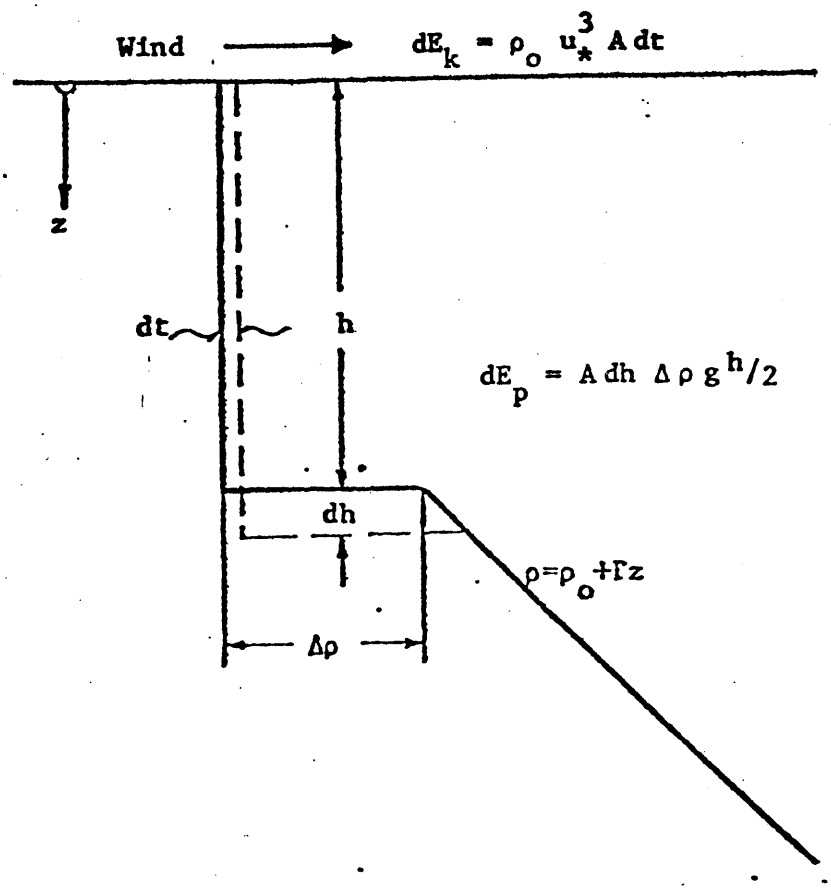

Figure 2.14: Idealized Representation of Turbulent Entrainment at a Density Interface

The change in potential energy E_p of the mixed layer due to the entrainment of the fluid element of thickness dh is

$$dE_p = A\ dh\ \Delta\rho\ g\ h/2 \tag{2.19}$$

where A is the interfacial surface area. The input of turbulent kinetic energy at the surface during the time interval dt is

$$dE_k = \tau_o u_s A\ dt \tag{2.20}$$

where τ_o is the surface wind shear stress and u_s is the wind induced water surface velocity. Replacing τ_o by the friction velocity $\tau_o = \rho_o u_*^2$ and assuming that the drift velocity $u_s \tilde{\sim} u_*$, equation (2.20) becomes

$$dE_k = \rho_o u_*^3 A\ dt \tag{2.21}$$

Using the thickness of the fully mixed layer as the characteristic length scale and u_* as the characteristic velocity scale,

$$Ri = \frac{\Delta\rho g h}{\rho_o\ u_*^2} \tag{2.22}$$

The ratio of the change in potential energy of the mixed layer to the change in turbulent kinetic energy due to wind shear during the time interval dt is given by

$$\frac{dE_p}{dE_k} = \frac{1}{2}\frac{dh}{dt}\frac{\Delta\rho g h}{\rho_o\ u_*^3} \tag{2.23}$$

Making use of the Richardson number defined by equation (2.22) and the definition of the entrainment velocity, $u_e = dh/dt$,

$$\frac{dE_p}{dE_k} = \frac{1}{2}\frac{u_e}{u_*} Ri \tag{2.24}$$

If the change in TKE is completely utilized in changing the potential energy of the mixed layer, the ratio $dE_p/dE_k = 1$ and equation (2.24) becomes

$$\frac{u_e}{u_*} = 2\ Ri^{-1} \tag{2.25}$$

This dependence of the entrainment rate on the Ri^{-1} has been observed in grid mixing experiments by Turner (1968) and others (see equation 2.17). This led to the earlier wind mixing rule used in the MIT wind mixing model (Octavio and Harleman, 1977), in which all the TKE input at the surface is used for entrainment. However, experiments by Kantha et al. (1977) covering a wide range of Richardson numbers indicated that the exponent of -1 is only appropriate for Ri in the range of 100. This observation, coupled with the fact that the MIT wind mixing model described above tended to overpredict the thickness of the wind-mixed layer resulted in a modification introduced by Bloss and Harleman (1979). This modification was based on a parameterization of the total TKE balance at the density interface given by Zeman and Tennekes (1977). Their studies indicated that transient storage and dissipation of TKE, within the mixed layer, are important in various parts of the Richardson number domain. If the stratification is weak (i.e., low Ri), input of TKE at the surface is mainly used to increase the TKE of the growing mixed layer and the buoyancy flux (entrainment) across the interface is relatively small. On the other hand, in a strongly stratified system (i.e., high Ri), dissipation of TKE in the mixed layer becomes important. This results in a reduction in the entrainment across the highly stable interface. Bloss and Harleman (1979) accounted for these two effects by assuming that

$$\frac{dE_p}{dE_k} = f(Ri) \tag{2.26}$$

where the Richardson number function is represented by

$$f(Ri) = 0.057\ Ri\ \left(\frac{29.5 - Ri^{1/2}}{14.2 + Ri}\right) \tag{2.27}$$

This function, shown in Figure 2.15, indicates that when Ri = 1 only 10% of the TKE input is available for increasing the potential energy of the mixed layer by entrainment. When Ri = 100, all of the TKE is available and at Ri = 800 only 10% is available.

Following the computation of the internal heat transfer (see section 2.3.1) and the convective cooling (see section 2.3.2), the wind mixing rule given by equation (2.27) is applied to redistribute the temperature profile. After the completion of the heating and mixing computation, the surface heat flux is recomputed using the slightly changed temperature of the wind mixed layer. The sequential heating and mixing steps are continued until there is no significant change in the surface heat flux from one iteration to the next. The computer program also checks to insure that the resultant density profile is stable at the end of each time step.

2.3.4 Verification of the Wind Mixing Model

Lake Anna, located in central Virginia, has a surface area of 9,600 acres, a volume of 10.6×10^9 ft^3, an average depth of 25 ft and a maximum depth of 70 ft. The lake receives an average annual inflow of about 270 cfs. The dimensionless number, $\frac{AE}{QD}$, has a value of 0.15, with E equal to molecular diffusion, which makes it an ideal lake for verifying the correct specification of the diffusivity (see section 2.2.4).

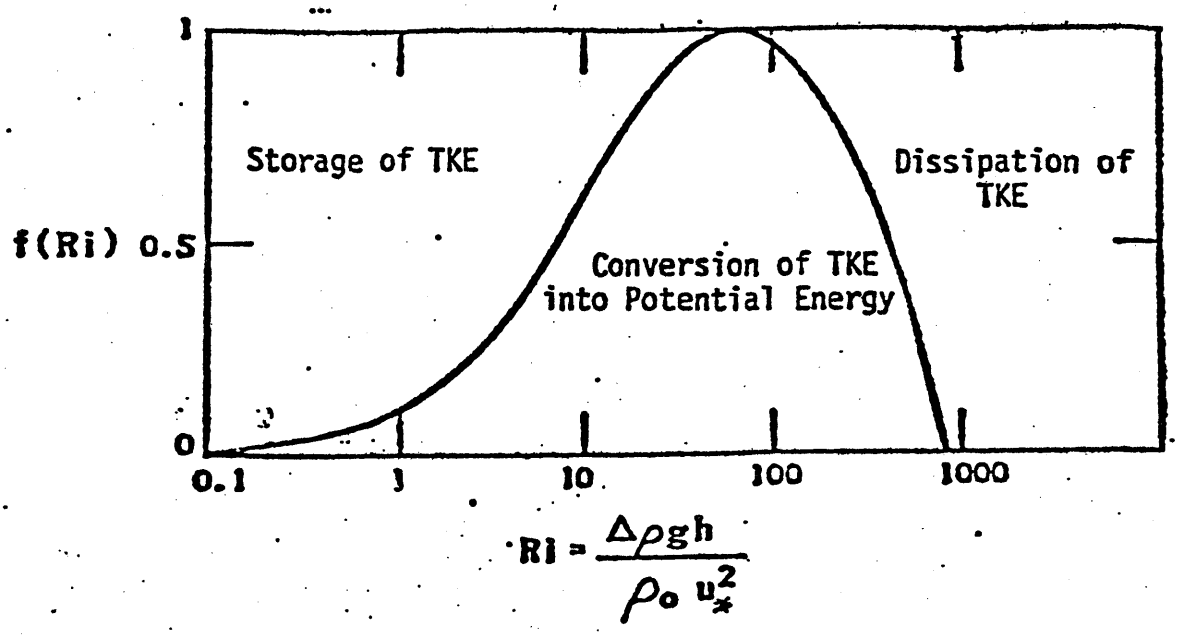

Figure 2.15: Dependence of the Conversion of TKE into Potential Energy on the Richardson Number

Synoptic temperature surveys have been conducted at about two-month intervals since 1974. A meteorological station at Lake Anna measures air and dew point temperatures, wind speed and short wave solar radiation. Daily water release rates were available for a one-year period.

When a time step of one day is used, the input requirements of the model include daily averaged values of the air temperature, relative humidity, wind speed, cloud cover, and total daily short wave solar radiation. Because cloud cover is not measured, it is calculated indirectly through a comparison of the measured daily short wave radiation and the known values for clear skies. Vapor pressure and wind speed values are corrected from those measured at 15 meters to corresponding values at 2 meters, based on the assumption of logarithmic profiles.

The surface solar absorption fraction, β, (see equation 2.11) is set equal to 0.5. Based on Secchi disk measurements, the extinction coefficient for short wave solar radiation, η, is taken as 0.5 m^{-1}. A vertical grid spacing, Δz = 0.5 m, is used.

A comparison of the modified wind mixing model (Bloss and Harleman, 1979) and the earlier version (Octavio and Harleman, 1977) with field data from Lake Anna is shown in Figure 2.16. The temperature simulation started on April 6, 1974, when the lake was well mixed at 11°C. An element thickness Δz = 0.5 m and a time step of 1 day were chosen. The bold lines correspond to the modified wind mixing model in which the Richardson number function is given by equation (2.27), while the thin lines correspond to the original version in which f(Ri) = 1. The diffusion model is also shown for comparison (dashed lines) and the field data from a number of vertical transects on the lake is represented by circles.

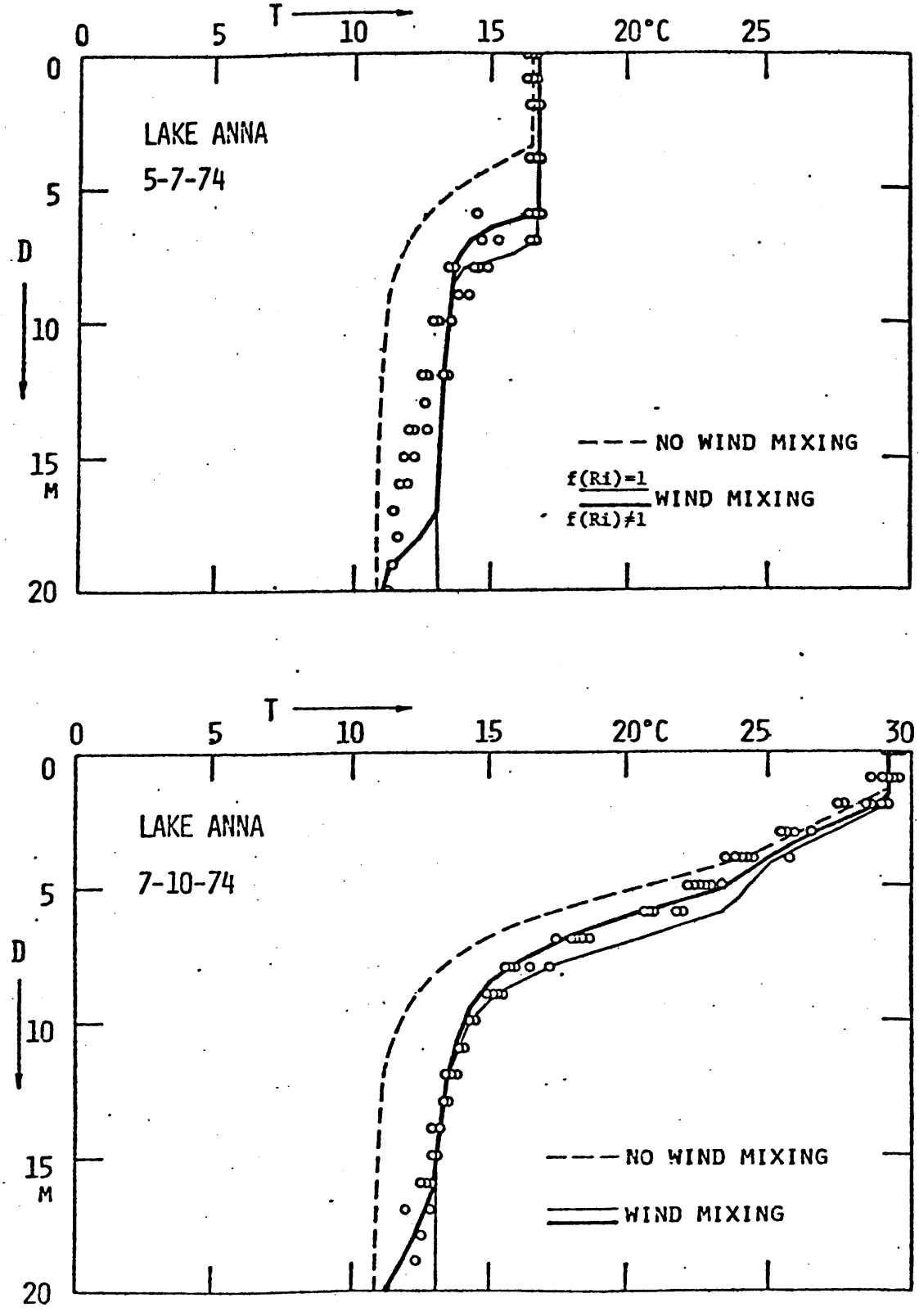

Figure 2.16: Temperature Simulations for Lake Anna, Virginia

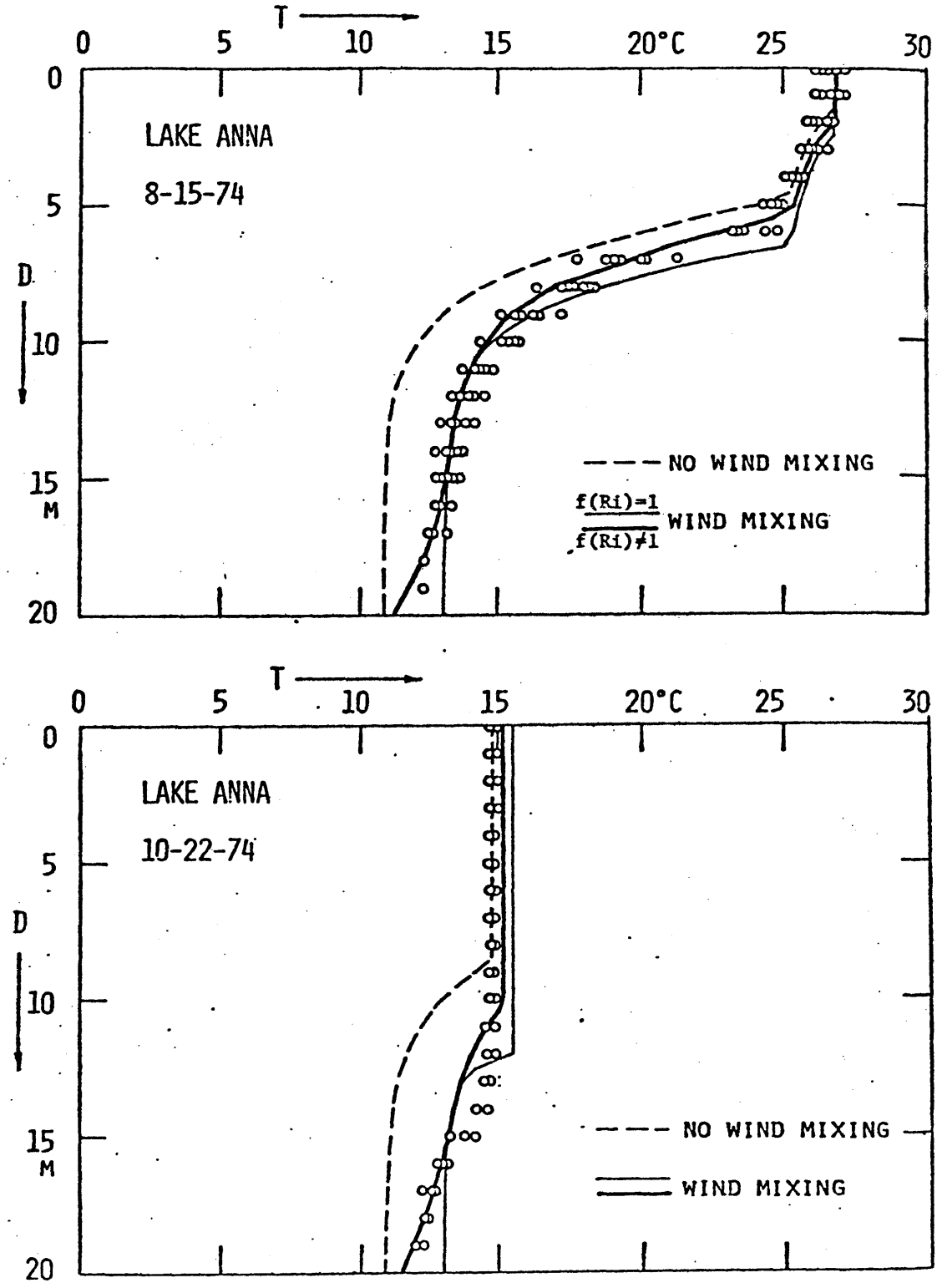

Figure 2.16: Continued

All three models used the molecular diffusivity of heat throughout the lake depth. The inclusion of the wind mixing algorithm has a very significant influence on the temperature profile, giving the modified wind mixing model the best overall agreement with the data.

Inasmuch as the eddy diffusivity in the diffusion model cannot be determined a priori, it may be asked whether it is possible to find a constant value of diffusivity which will reasonably reproduce the measured temperature profile which has been so well reproduced by the WDMIX model. The predicted temperature profile using an eddy diffusivity of 0.625 m^2/day (or 50 times the heat molecular diffusivity) is shown in Figure 2.17 as Curve B; Curve A is the profile using the molecular diffusivity. A comparison of Curve A and Curve B shows that increasing the diffusivity to 50 times the molecular value (Curve A in Figure 2.17) increases the temperature of the hypolimnion but does not result in an increase in the thickness of the epilimnion or upper mixed layer. A further increase of diffusivity will continue to increase the temperature below the mixed layer as Curve C illustrates. Hence, a constant value of diffusivity will not be able to reproduce the actual temperature profile.

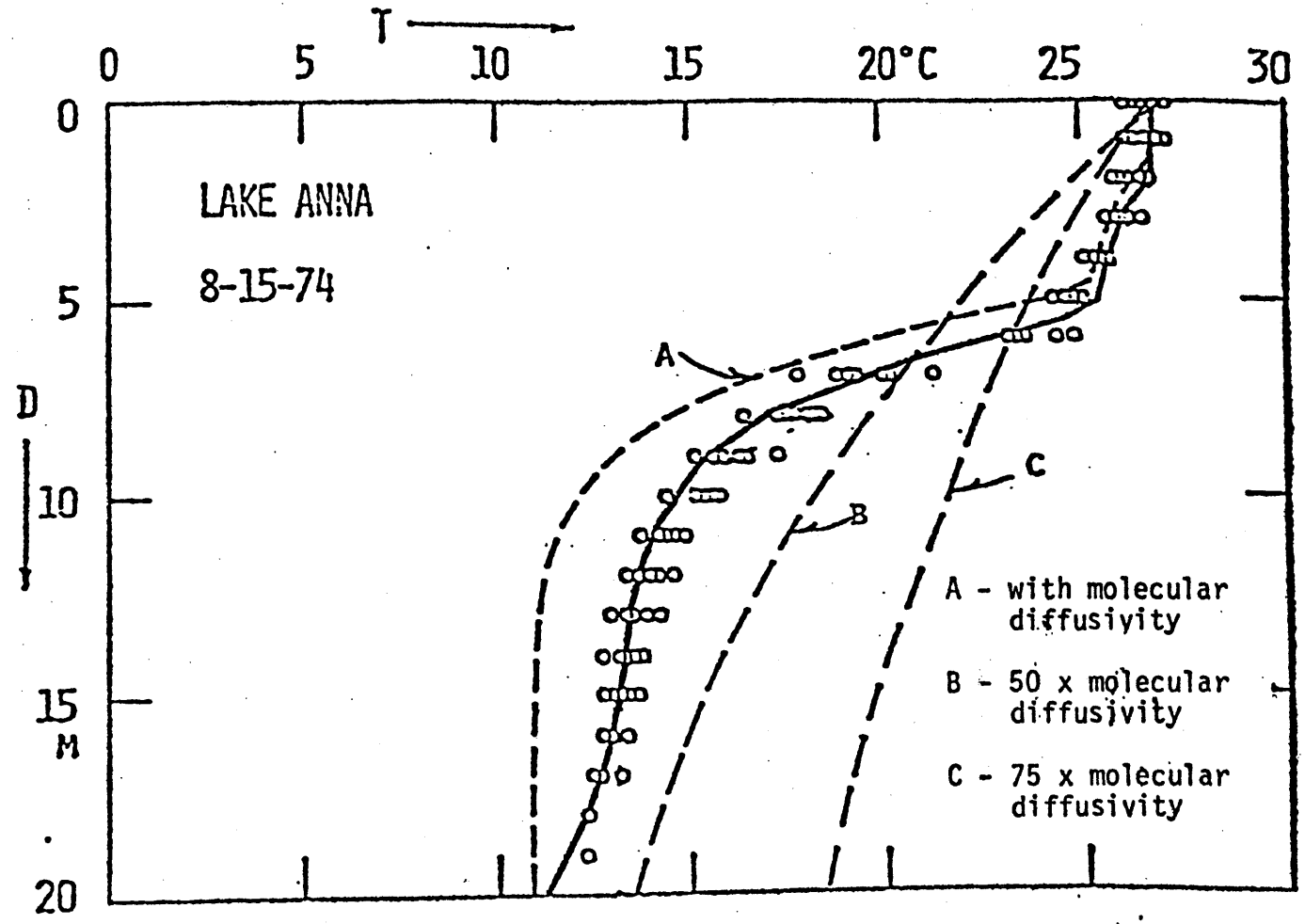

Figure 2.17: Temperature Simulation for Lake Anna, Virginia by the MIT Reservoir Model (Ryan and Harleman, 1971) Using Different Diffusivities

Chapter 3

PHOSPHORUS-CYCLE

3.1 Definition of Phosphorus Compartments

This chapter is concerned with the kinetics of the P cycle, which is mostly influenced by biogenic processes. The results of experiments, however, cannot be fully interpreted without a knowledge of the phosphorus terminology. Moreover, the important parameters in all lake eutrophication models are calibrated against field data which are also compared to the model predictions to test their goodness-of-fit. The data plays such an important role in the structure and the verification of the model that it seems logical to first review the state-of-the-art of P measurement and the state variables of lake eutrophication models.

The cycling of phosphorus in lakes is influenced by biogenic processes. Earlier studies of the redistribution of phosphorus in the ocean environment among three different forms (particulate phosphorus, soluble organic phosphorus and soluble inorganic phosphorus) have laid most of the ground work of our present understanding of the phosphorus cycle. The identification of phosphorus as the key element in causing lake eutrophication problems (National Academy of Sciences, 1969) has led to investigations of the phosphorus cycle in lakes. Basically, there is no difference between the phosphorus cycle in oceans and lakes; therefore, we may draw inferences from both oceanographic and limnologic studies.

3.1.1 Analytically Separable Compartments

The term "analytically separable P compartments" was introduced by Rigler (1973) to refer to the different forms of P measurable by current

chemical analytical techniques.

The measurement of P in a water sample usually involves three steps:

(1) the separation of P into different fractions;

(2) the transformation of the P fraction of interest into ortho-P by acid digestion;

(3) the application of the molybdate blue method to measure ortho-P.

Various separation methods, digestion acids, and molybdate blue methods have been used; Olsen (1966) counted about 100 variations.

3.1.1.1 The Molybdate Blue Method

The molybdate blue method was first developed by Osmond in 1887 to measure the ortho-P concentration in laboratory solutions. Ortho-P reacts with ammonium molybdate under acidic conditions to form ammonium phosphomolybdate:

$$PO_4^{-3} + 12\ (NH_4)_2MoO_4 + 24\ H^+ \rightarrow (NH_4)_3PO_4 \cdot 12MoO_3 + 21\ NH_4^+ + 12\ H_2O \qquad (3.1)$$

The molybdenum contained in ammonium phosphomoloybdate can readily be reduced to produce a blue-colored compound whose concentration may be measured colorimetrically. This forms the basis of the molybdate blue method. Deniges (1921) and Atkins (1923) modified the method to make it sensitive enough to measure the P content in natural water. Other modified methods differ in their use of additive, reducing agent or method of solvent extraction, but are based upon the same principles (Levine, 1975).

3.1.1.2 The Terminology of the Analytically Separable P Compartments

The terminology for the analytically separable P compartments is

based on the analytical separable method, the most commonly used being that developed by Strickland and Parson (1960). Figure 3.1 is a schematic diagram which illustrates this analytical procedure.

The total P content in the water is called total P(TP). The water sample is filtered, usually with a 0.45 μm membrane filter, and is separated into filterable and non-filterable portions. The amount of P in the non-filterable portion is called particulate P(PP); the amount of P in the filterable portion of the sample is called soluble P(SP). The amount of P measured in the filterable portion without the process of acid digestion is called soluble reactive P(SRP). The difference between SP and SRP is called soluble unreactive P (SUP).

There have been several improvements on the molybdate blue method since the early 1920's. Several filter sizes have been used to separate the particulate P and the dissolved P, sometimes a centrifuge is used in place of the filter. All these different methods certainly create a terminological chaos which was well documented by Olsen (1966).

PP is also referred to as suspended P (sus.P) or sestonic P. SRP is often referred to as soluble inorganic P (SIP), following the terminology of Ohle (1938). SP has another quite popular name: total dissolved P (TDP).

3.1.1.3 Possible Errors in the Measurement of Phosphorus

(a) The Presence of As:

P is not the only compound which reacts with molybdate. Si, Ge and As all react with molybdate under acidic conditions to form compounds which can readily be reduced to blue colored compounds. The optimal pH

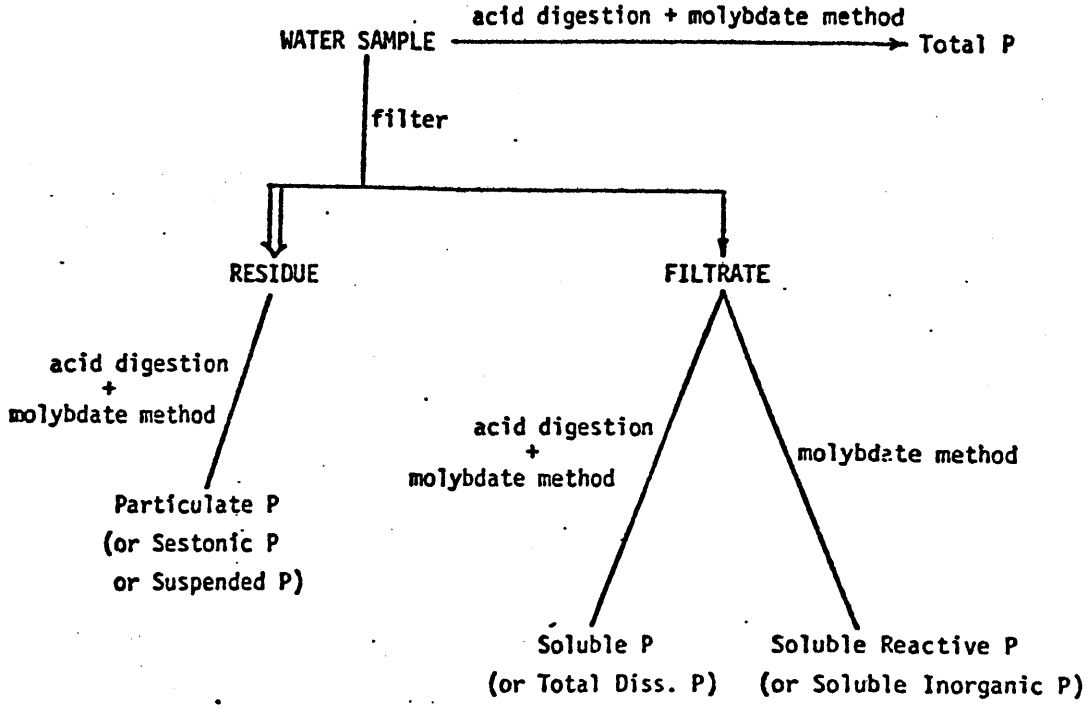

Figure 3.1: Schematic Representation of Phosphorus Analysis Method Developed by Stickland and Parson and the Terminology of the Analytically Separable P Compartments

for the reaction of Ge and Si are higher than that for the corresponding reaction of As. Molybdoarsenic acid is formed and reduced at a slower rate than molybdophorphoric. Chamberlain and Shapiro (1969) extracted the molybdophosphate into isobutyl alcohol to minimize the As interference and reported that the concentration in As is high enough to cause significant interference (Rigler, 1973).

(b) The Analysis of Anoxic Water Sample:

The iron concentration in a lake is often much higher than the ortho-P concentration, especially in the anoxic hypolimnion (Hutchinson, 1975). In handling the water sample taken from the anoxic layer, it is very difficult to keep the sample anoxic, particularly during the filtering process where there is no practical method of preventing the oxidation of water. Ferrous ion becomes ferric ion in the oxygenated water and forms precipitate with OH^- and PO_4^{-3} (Stumn and Morgan, 1970). Phosphorus in the water will be either precipitated with ferric ion as $Fe(PO_4)$ or be adsorbed onto the surface of the newly formed ferric precipitate. Consequently, oxygenation of the anoxic water sample will cause an overestimation of the PP at the expense of SP.

The occurrence of possible error during the measurement process of phosphorus is indicated by arrows in Figure 3.2. In the presence of As, there will be an overestimation of total P, while during the analysis of anoxic water, the measurement of total P is correct but there is a possibility of overestimating the particulate P with a corresponding underestimation of SP and SRP.

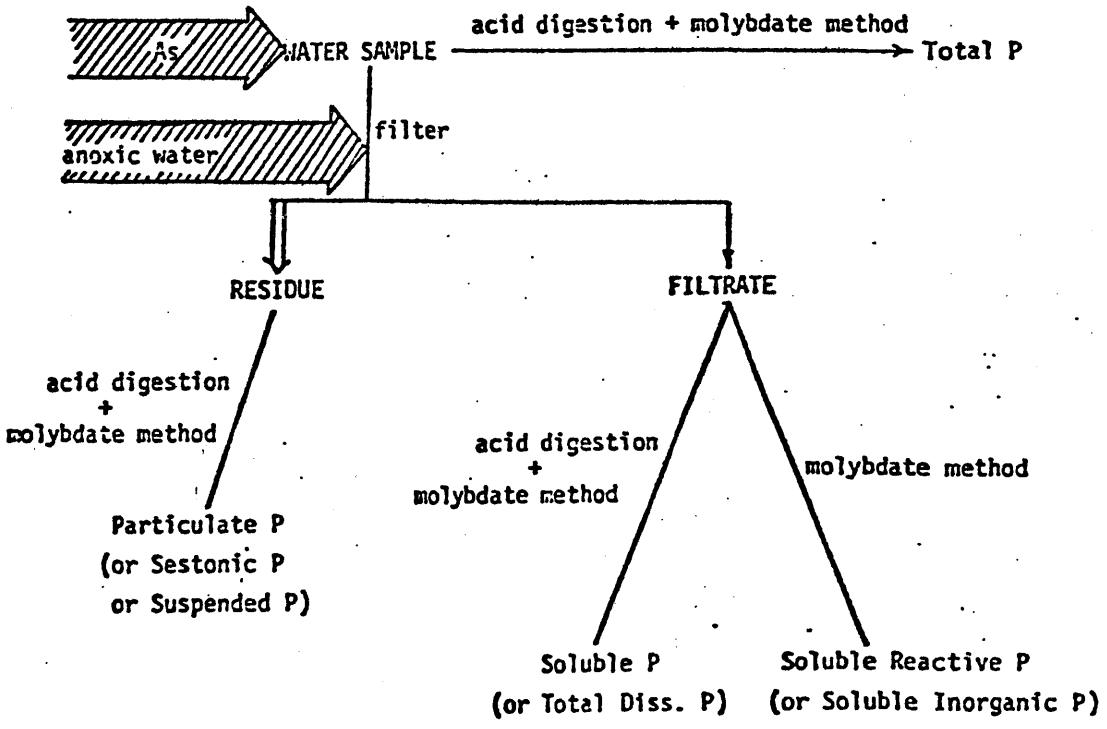

Figure 3.2: Possible Errors in the Measurement of Phosphorus

3.1.2 Biologically Separable P Compartments

A general summary of the major biological pathways of the P cycle in an aquatic environment is shown in Figure 3.3 where P is cycled among 7 biologically separable compartments - ortho-P, dissolved organic-P, bacteria-P, detritus-P, phytoplankton-P, zooplankton-P and fish-P. The use of radiophosphorus ^{32}P has been the most successful approach to study the cycling of phosphorus in a natural aquatic system where several processes are taking place simultaneously. Recent advances in our understanding of the P dynamics in lakes may be represented by works of Rigler (1964), Chamberlain (1968) and Lean (1973 a,b).

3.1.2.1 Ortho-P and the Biological Pathways of its Regeneration

Ortho-P is the nucleus of this biological P cycle. Almost all phytoplankton can take up only ortho-P for their needs (except for a few marine phytoplankton which have phosphatases bound to the surface of the cell enabling them to hydrolyze phosphorus esters). Bacteria may also compete with phytoplankton for the uptake of ortho-P. Rhee (1972) has demonstrated the importance of bacteria competition by showing that the growth of Scenedesmus algae was severely affected by the presence of Pseudomonas bacteria (Wetzel, 1975).

The extremely small ortho-P concentration must be rapidly and continuously replenished in order to sustain the growth of phytoplankton for any extended period. The turnover time of epilimnetic ortho-P has been measured in open lake water, artificial ponds, temperature oligotrophic to extreme eutrophic lakes, and bog lakes (Chamberlain, 1968; Confer, 1969; Rigler, 1964). Regardless of the trophic state of the water

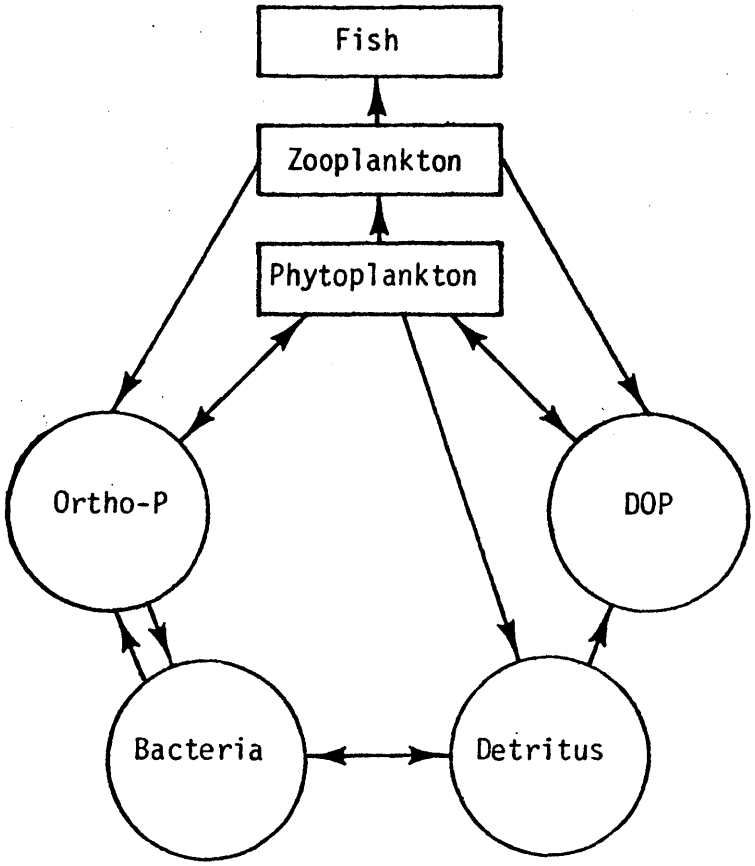

Figure 3.3: Major Biological Pathways in the Phosphorus Cycle of the Sea (Parson and Takahashi, 1977)

body, the turnover time is generally between 1 to 8 minutes during the summer stratification (Rigler, 1973).

Ortho-P may be regenerated from several sources: (1) the excretion by phytoplankton and bacteria, (2) the excretion by zooplankton, (3) autolysis of phytoplankton and zooplankton, (4) hydrolysis of dissolved organic phosphorus. Each has been stressed by one scientist or another as the most important source of ortho-P, but no systematic analysis of the relative importance of each mechanism has been, or is, possible (Rigler, 1973).

(A) The Excretion by Phytoplankton and Bacteria

Overbeck (1963) found that a bacterial suspension releases phosphate and makes this phosphorus available to phytoplankton. The most important evidence for this is probably the radioisotope experiment study by Lean (1973 a,b) on the movement of phosphorus between its biologically important forms in lake water. Lean (1973 a,b) took water samples from the epilimnion of Heart Lake (a small eutrophic lake) during the period of June to August and analyzed them using the following procedures:

(a) Addition of $^{32}PO_4$ to the water sample;

(b) Filtration with 0.45 um Millipore filters;

(c) Separation of the different compounds in the filtrate by using Sephadex gel filtration chromatography.

The fraction retained by the 0.45 μm filter is the particulate P and that unretained contains dissolved P. The dissolved P is further separated into 3 components: ortho-P, colloidal P and an unidentified phosphorus compound XP. Figure 3.4 reproduces his experimental result.

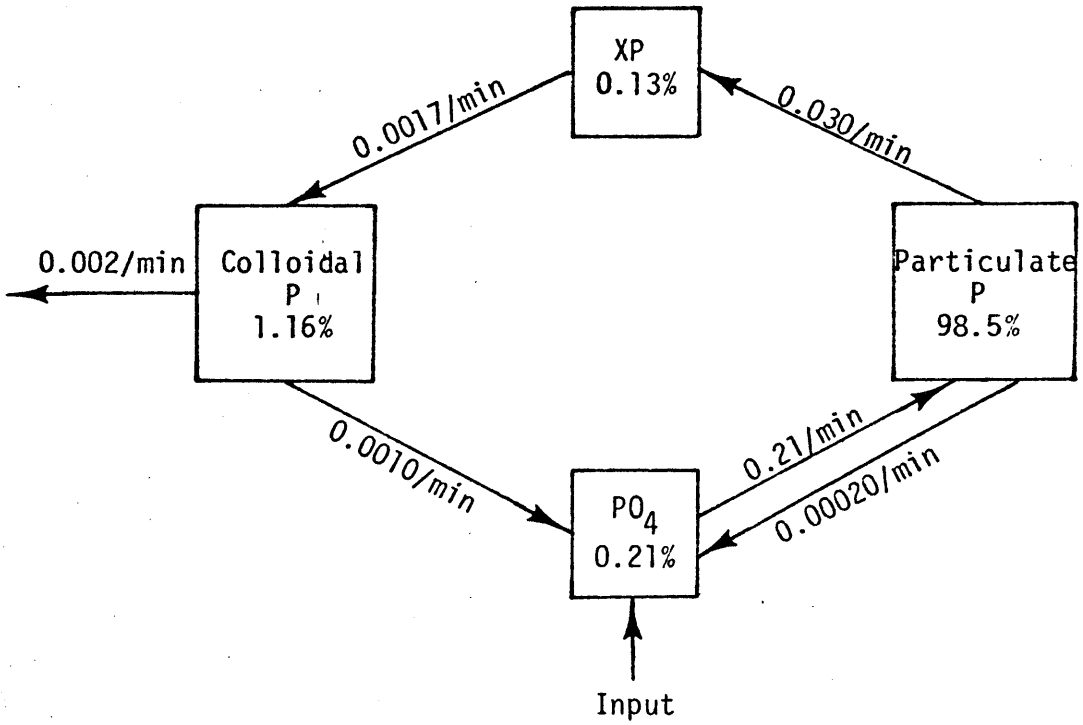

P MOVEMENT WITHIN EPILIMNETIC ZONE OF WATER
LEAN (1973)

Figure 3.4: Phosphorus Movement within Epilimnetic Zone of Water (Lean, 1973)

The significance of the colloidal P in the P cycling will be discussed in a later section.

Lean interpreted the particulate pool as a composite of phytoplankton and bacteria. From a steady state mass balance calculation, he estimated that the direct release of ortho-P from the particulate pool is the most important factor in causing the rapid turnover of the ortho-P pool.

(A) The Excretion by Zooplankton

Several scientists have studied the excretion of ortho-P by zooplankton. Gardiner (1937) demonstrated that significant quantities of inorganic phosphate are excreted by marine zooplankton. Rigler (1961) estimated the phosphorus release rates of Daphnia magna to be 0.033 μg-P mg^{-1} hr^{-1}. He also examined the forms of the released phosphorus and found no significant difference between the amounts of SRP and the total soluble P. Rigler (1961) therefore concluded that Daphnia released only inorganic phosphate. Although many others have studied the phosphorus release by zooplankton, the reported literature values are off by 2.5 orders of magnitude. Peters (1972) reviewed the various experimental methods and suggested that non-uniform labelling may have caused an underprediction, whereas re-uptake of the released phosphorus may have caused an overestimation. Peters (1972) carefully designed his experimental method to avoid the two possible sources of error. From studying the fully labelled Daphnia rosea, he then proposed an empirical formula to relate the phosphorus excretion rate per unit animal dry weight to animal dry weight, temperature, food cell concentration and food phosphorus content. He further compared excretion products with $^{32}PO_4$ using anion exchange, gel filtration, and uptake kinetics. These

studies showed that about 90% of the released soluble P is ortho-phosphate.

(C) Autolysis of Phytoplankton and Zooplankton

Hooper (1973) well documented several laboratory studies which follow the breakdown of plankton. Hoffman (1956) found that 20 to 25% of the inorganic phosphorus and 30 to 40% of the organic phosphorus is liberated by phytoplankton shortly after death, while between 80 and 90% is liberated within 24 hours. Marshall and Orr (1955) found a complete breakdown of phosphorus of dead marine copepod within 2 days. The rapid decomposition led these scientists to conclude that autolysis, rather than bacterial action or the action of free enzymes, was the most important regenerative process. Golterman (1960) reconfirmed the importance of autolysis by showing that during a few hours of autolysis, 50% of the particulate phosphate was returned to solution.

(D) Hydrolysis of Dissolved Organic Phosphorus

Dissolved organic phosphorus is readily hydrolyzed either by alkaline sea water or by phosphatases which are hydolytic enzymes present in many bacteria. The chemical reactions and hydrolysis rates of several phosphorus compounds that are commonly used in large scale operations can be found in Shen and Morgan (1973). The current state of the art on the hydrolysis of dissolved organic phosphorus, particularly its role in the P cycle of the natural aquatic environment, is reflected in Hooper's (1973) comment:

> Despite the wealth of data on the quantity of dissolved organic phosphorus in marine and freshwater systems, only fragmentary and isolated efforts have been made toward

> the identification of these compounds. More important, little or no effort has gone toward linking these organic fractions with the metabolic activities of bacterial and plant cells from which many of these materials must arise. Other than suggestions that the dissolved organic phosphorus represents the more refractory compounds that decompose slowly and that they are frequently liberated by bacterial cells, there are few guides to their role in the biochemical cycles of either marine or freshwater systems.

Lean (1973 a,b) separated the dissolved P of lake water into three fractions: ortho-P, colloidal P and XP (see Figure 3.4). He demonstrated that most of the P in the soluble P compartment is colloidal P which has a molecular weight larger than 10^7. This colloidal material was later identified as electron-opaque, non-rigid fibrils of approximately 3 to 10 nm in diameter (Leppard, Massalski and Lean, 1977). The behavior and contact relation of the fibrils and their aggregates suggest a role in contact cation exchange. An investigation of the chemistry of this material in underway. No enzyme has yet been found to hydrolyze this colloidal material (Burnison, personal communication) so that it may be considered a biologically inactive substance that may eventually aggregate and settle out.

3.1.2.2 Other Biological Pathways in the P Cycle

Since all living organisms contain phoshorus, P is incorporated into the biomass of each trophic level through the food chain: phytoplankton - zooplankton - fish. Each trophic level grazes on the next lower trophic level and is grazed on by the next higher trophic level.

The non-living particulates are collectively referred to as detritus, which can be further divided into inorganic detritus and organic detritus, depending on its origin. The definition of detritus by its origin not

only gives no information on its chemical properties but also may be misleading; for example SiO_2 and $CaCO_3$ are sometimes referred to as organic detritus. The detritus compartment in the P cycle only refers to the organic detritus, which consists of dead organisms and fecal pellets. Although in the natural aquatic environment most particulate matter may be detrital material(Wetzel, 1975), the rapid liberation of phosphate from dying cells by autolysis of phytoplankton and zooplankton causes the phosphorus content of detritus to be low (Golterman, 1973). Marshall and Orr (1955) found that Calanus produced pellets at the rate of one every 5 to 6 minutes. However, they believed that the phosphorus content is low. Thus the role of detritus in the phosphorus cycle is not clear.

3.1.3 Difficulties in Relating the Biologically Separable P Compartments to the Analytically Separable P Compartments

It is conventional to assume that ortho-P is measured as SRP and phytoplankton-P as PP. However, under many circumstances these assumptions may be invalid. The recognition of these circumstances is important for the modeller and the critic of the models. The following sections will elaborate further on these points.

3.1.3.1 Ortho-P from SRP

There has been an increased awareness of the fact that SRP (SIP) is not ortho-P since the early sixties. Rigler (1973) has excellently presented the historical developments which lead to this conviction. Kuenzler and Ketchum (1962), using radioisotope of P (^{32}P) to study the P uptake of Phaeodactylum tricornutum, found that the maximum possible ortho-P in the solution calculated from the ratio of ^{32}P in the solution

to ^{32}P in cells was 4% of the chemically determined SRP. Rigler (1966, 1968) found the same difference in lake water; he reported that the values of SRP from chemical analysis were 10 to 100 times higher than those maximum possible ortho-P values obtained from radioisotope analysis. He suggested that the gross overestimation of ortho-P by the chemical analysis could be due to any or all of the three causes:

(a) The damage of the algae cell during the filtration process;

(b) The hydrolysis of other forms of P to ortho-P by acid in the molybdate reagent;

(c) The presence of As which reacts with molybdate under acidic conditions and subsequently interferes with the colorimetric determination.

Although the first possibility lacks convincing evidence (King, 1970; Lean, 1976), the second and third possibilities have been confirmed. The second cause is the inherent limitation of the molybdate blue method which perhaps contributes most of the overestimation. In order to have a better estimation of the ortho-P concentration, several researchers have tried physical and biochemical methods to separate ortho-P from other soluble-P. Examples of these methods are: ion exchange, Sephadex gel filtration and radiobioassay.

Rigler (1968) used a column of hydrous zirconium oxide (HZO) to extract the orthophosphate from the lake water and measured the P in the eluate of the column and the P in the water sample which was without the extraction process. The result showed that the SRP measured from the column eluate was 11-66% of the SRP measured from the unextracted water sample. Lean (1973a,b) demonstrated that most of the P in the soluble P

compartments is associated with a high molecular weight colloid (with molecular weight as high as 10^7). Stainton (1980) subsequently showed that this colloidal P are hydrolyzed by the molybdate reagent of five popular molybdate blue methods.

Levine (1975), using Rigler's bioassay, measured the ortho-P content in the epilimnion and the hypolimnion of L227 (a very eutrophic lake) and L302S (an oligotrophic lake) and found that the values of ortho-P were extremely low (less than 0.1 μg/ℓ). Rigler's bioassay measures the maximum possible ortho-P; therefore, the true ortho-P in these lakes could only be lower than those measured.

3.1.3.2 Phytoplankton-P from PP

The size distribution of particulate matters in the water is summarized in Figure 3.5. Bacteria is at the lowest end of the spectrum with an upper limit of approximately 0.2 μm; phytoplankton varies from 0.2 μm to 1000 μm; zooplankton varies from less than 100 μm to larger than 2000 μm and detritus, which represents the dead organism or the decomposed dead organism, covers the whole size distribution. Although the exact limits of the size distribution of each of these biologically separable particulate matter are unknown, the overlapping is clear.

The demarcation line between the particulate matter and the dissolved matter is undoubtedly an artificial one. The general practice is to use a 0.45 μm filter to separate TDP from PP. Particles trapped by this size filter may include phytoplankton, zooplankton and detritus. Bacteria are often embedded in the detritus and cannot be distinguished from it by the conventional method of filter separation. Moreover, if the

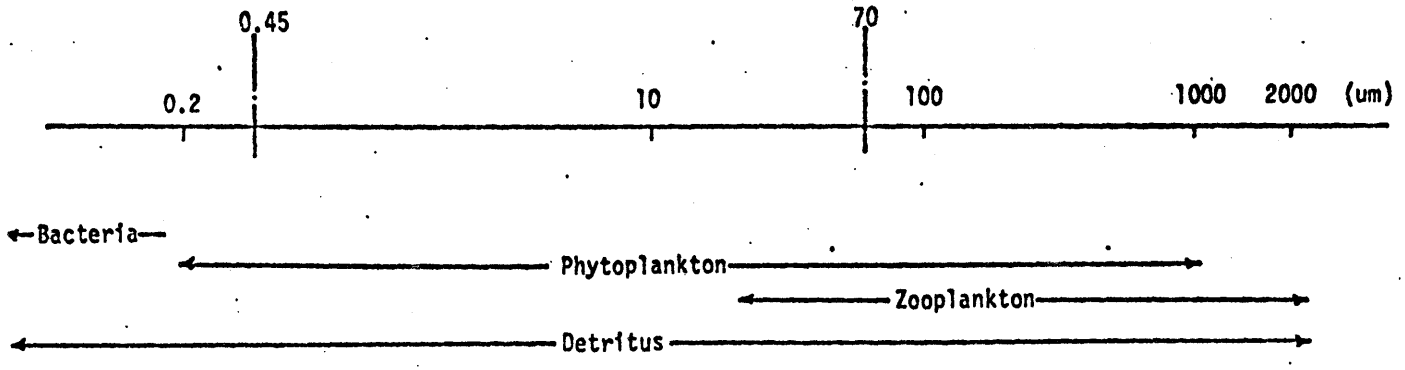

Figure 3.5: Size Distribution of Particulate Matter in Lake Water

pore of the filter becomes clogged, which is not uncommon during the filtration process, then the smaller particles such as bacteria will also be retained and will be measured as particulate P.

The separation of zooplankton from phytoplankton is difficult. Often, a filter size of 70 μm is used to separate the two; but as seen from Figure 3.5, a small zooplankton will not be screened by this filter. Consequently, the measured particulate P may include some small zooplankton.

The presence of zooplankton makes the data interpretation difficult. Zooplankton-P is an important fraction of the total P in the water column. If phytoplankton/zooplankton population exhibits the classic predator-prey oscillation, then there are periods when zooplankton bound P is the major fraction of total P. Yet, it is never clear whether the measured total P includes zooplankton-P. Zooplankton exhibits pronounced non-uniform distribution. A 50 ml or a 100 ml sample, which is normally used for the determination of total-P in lake water, does not adequately sample zooplankton. Chamberlain (1968) demonstrated that the temporal fluctuations in the total P in the trophogenic zone are due to the variance of particulate matters larger than 70 μm. He showed that the inclusion of one extra Daphnia, containing 0.19 μg-P in a 50 ml water sample would increase the total P of the sample by 4 μg/l. Multiple samples provide some guidelines on judging the presence of large zooplankton; however, the difficulty of separating small zooplankton from net phytoplankton (>50 μm) always casts doubt on the interpretation of the measured total-P.

Practically all the dynamic phytoplankton models assume that the measured TP does not include zooplankton bound P. A correct judgement is based on the knowledge of the employed method for data collection. It

is important to realize the variability introduced by inadequate sampling.

3.2 Review of the Structure of P Model of Some Existing Lake Eutrophication Models

A representative group of phosphorus models of varying degrees of complexity are reviewed in this section. The focus is on the nutrient cycling concept and on the relationship between model state variables and field measurement. A listing of the reviewed models follows (the formulation of phytoplankton growth will be described and discussed in Chapter 4):

(1) Snodgrass and O'Melia (1975): Cycling of soluble phosphorus (OP) and particulate phosphorus including plankton (PP).

(2) Imboden and Gachter (1978): Phosphorus cycle similar to Snodgrass and O'Melia with modifications in the transformation rate process and sediment exchange formulations.

(3) Jørgensen (1976, 1978): Cycling of soluble and detritus phosphorus with additional state variables for plankton, fish and sediment exchange.

(4) Chen and Orlob (1972): Inclusion of competitive species of plankton and fish in addition to consideration of nitrogen and carbon cycling.

(5) Thomann and DiToro (1975): Similar to Chen and Orlob structure with differences in linkages and transformation rates employed.

(6) Richey (1977): Complex biochemical model including explicit representation of bacterial transformation processes.

3.2.1 Snodgrass and O'Melia (1975)

The biochemical model, shown schematically in Figure 3.6 includes two state variables for phosphorus: [OP] which combines PO_4 and soluble organic phosphorus and [PP] which combines living particulate phosphorus (phytoplankton and zooplankton) and non-living particulate phosphorus.

A linear relationship is used to represent the production of [PP] from [OP]. This is a considerable simplification because of the aggregation of living and nonliving forms in [PP], and the very different natures of various forms of soluble phosphorus. Each of the components in [PP] possesses distinctly different physiological characteristics and it is questionable whether all these components can be lumped together. The model also assumes that the euphotic zone coincides with the epilimnion layer. Therefore, a net assimilation (increase in PP) occurs in the epilimnion and a net decomposition occurs in the hypolimnion. This demarcation is somewhat arbitrary. The lowest limit of the euphotic zone is the level at which the light intensity is 1% of that at the surface. This depth has been reported to vary between 10 m in turbid inshore temperature water to 100 m in clear water. The variability of this depth with turbidity is important and the depth of the euphotic zone should not be artificially fixed by the location of the thermocline.

Snodgrass and O'Melia assume a first order decomposition of [PP] to [OP], a valid approximation that has been verified in both pure and mixed cultures of plankton and bacteria. However, the use of a six-month constant rate coefficient is questionable since the rate of decomposition is temperature dependent. Moreover, there is no mechanism in the model to

SUMMER - TWO-LAYER STRATIFICATION

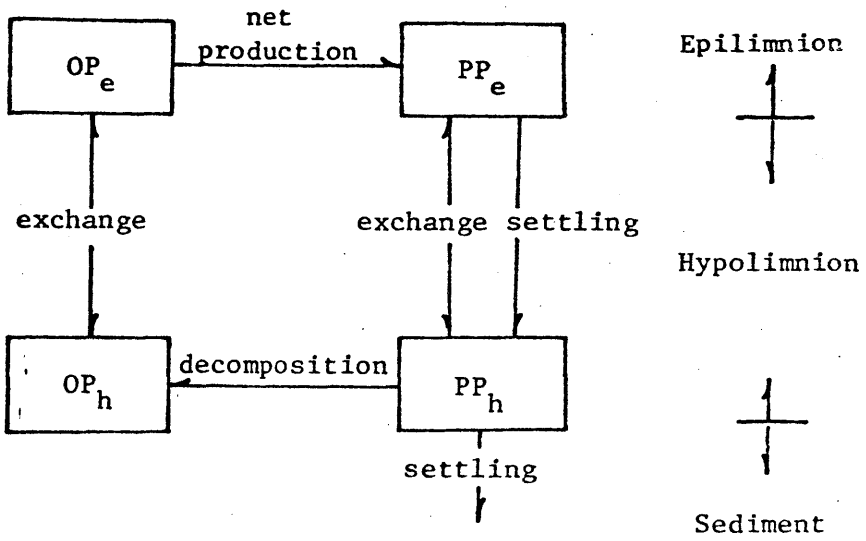

WINTER - FULLY MIXED

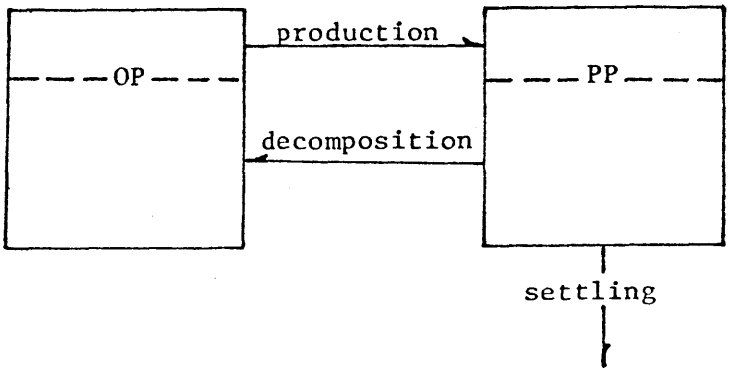

Figure 3-6: Schematic of Snodgrass and O'Melia (1974) Phosphorus Model

allow for sediment-water exchange of phosphorus. This limits the applicability of the model to lakes in which the effect of the littoral zone on the phosphorus cycle is of minor importance.

3.2.2 Imboden and Gachter (1978)

As shown in Figure 3.7, this model treats phosphorus in two compartments, [PP] and [OP] as in the Snodgrass and O'Melia model. Two major modifications are:

(a) The [PP] production rate is assumed to be phytoplankton growth rate which in turn is related to the [OP] concentration by Monod's kinetics; the self shadowing effect of the particulate phosphorus is included.

(b) The return of orthophosphorus from the sediment to the overlaying water is included.

The definitions of [OP] and [PP] differ slighlty from those in Snodgrass and O'Melia's model. [OP] represents only the concentration of orthophosphate and [PP] represents the concentration of particulate phosphorus incorporated in plankton. The model also assumes constant decomposition rate coefficients and an equality between the euphotic zone and the epilimnion. There are some difficulties in the choice of the total flux from the sediment and vertical diffusion coefficients since the effects of these parameters are linked.

Since the model does not explicitly account for the temperature effect, the production rate at optimal light and nutrient condition is left as a calibrated parameter. Its value varies by a factor of 4 to 5.5 over the year in the three applied cases (Alpnachersee, Greifensee and Lake

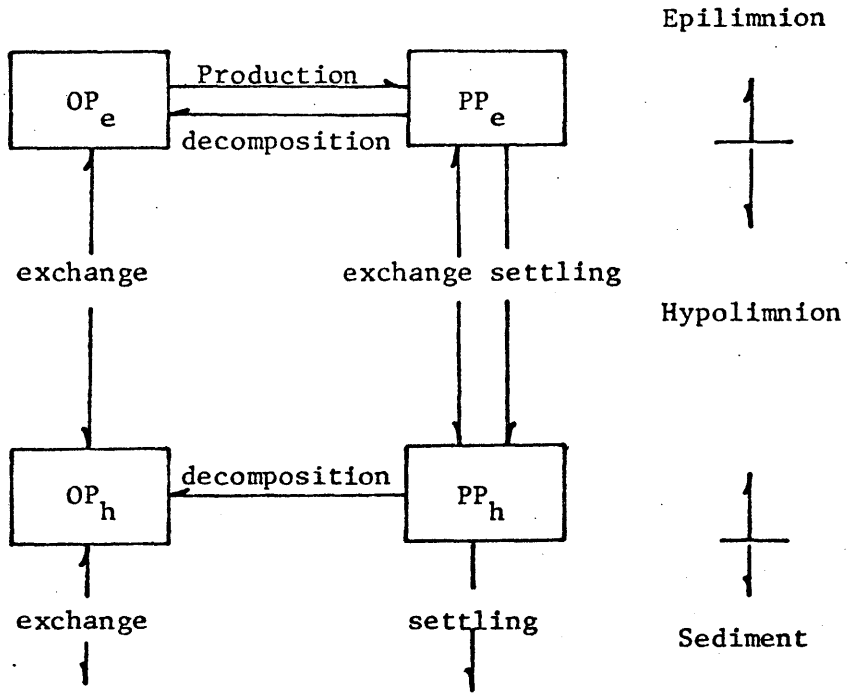

Figure 3-7: Schematic of Imboden and Gachter (1978) Phosphorus Model

Washington). In this model, there are more than 19 parameters calibrated using monthly field measurements. Table 3.1 shows the relationship between state variables (S) and field measurements (M), when the model was applied to Lake Alpnachersee and Greifensee.

Table 3.1

Model State Variables vs. Field Measurements
Application to Lakes Alpnachersee and Greifensee (Imboden et al.,1978)

M \ S	PO_4	Phyto-P
PO_4	1	-

Monthly measurements; PO_4 data were available at depths 0 m, 25 m, 32 m for Lake Alpnachersee and at depths 0 m, 5 m, 10 m, 20 m, 30 m for Lake Greifensee

3.2.3 Chen and Orlob (1972)

The phosphorus cycle in the Chen and Orlob model, shown in Figure 3.8, is considerably more complex than the previous models discussed. It includes two algal, one zooplankton and three fish species.

The orthophosphorus-algae interrelationship is basically similar to Imboden's formulation. Two major differences are:

(1) The uptake rate of ortho-P is affected jointly by three nutrients - nitrogen, phosphorus and carbon. The previous models assumed that phosphorus was the only limiting nutrient.

(2) The model explicitly simulates the competition of two algal species. The inclusion of two algal species is more satisfactory than the usual simplification that regards plankton as a single entity. This model is able to simulate the seasonal succession of phytoplankton, a common phenomenon observed in natural environments.

The model assumes that detritus is produced through the grazing inefficiency and mortality of fish and zooplankton; and that ortho-P is regenerated through respiration of all living organisms considered in the model. Phytoplankton, zooplankton and fish obtain their energy from aerobic respiration, that is, the oxidation of organic compounds by oxygen. Phosphorus in cells exists mainly as phospholipid (an essential component in plasma membrane), nucleic acid (RNA, DNA) and high energy compounds (ADP, ATP). None of these phosphorus containing compounds serve as the organic fuel of the phytoplankton respiration process. There is no evidence that phosphate is released during the phytoplankton respiration process. Perhaps the

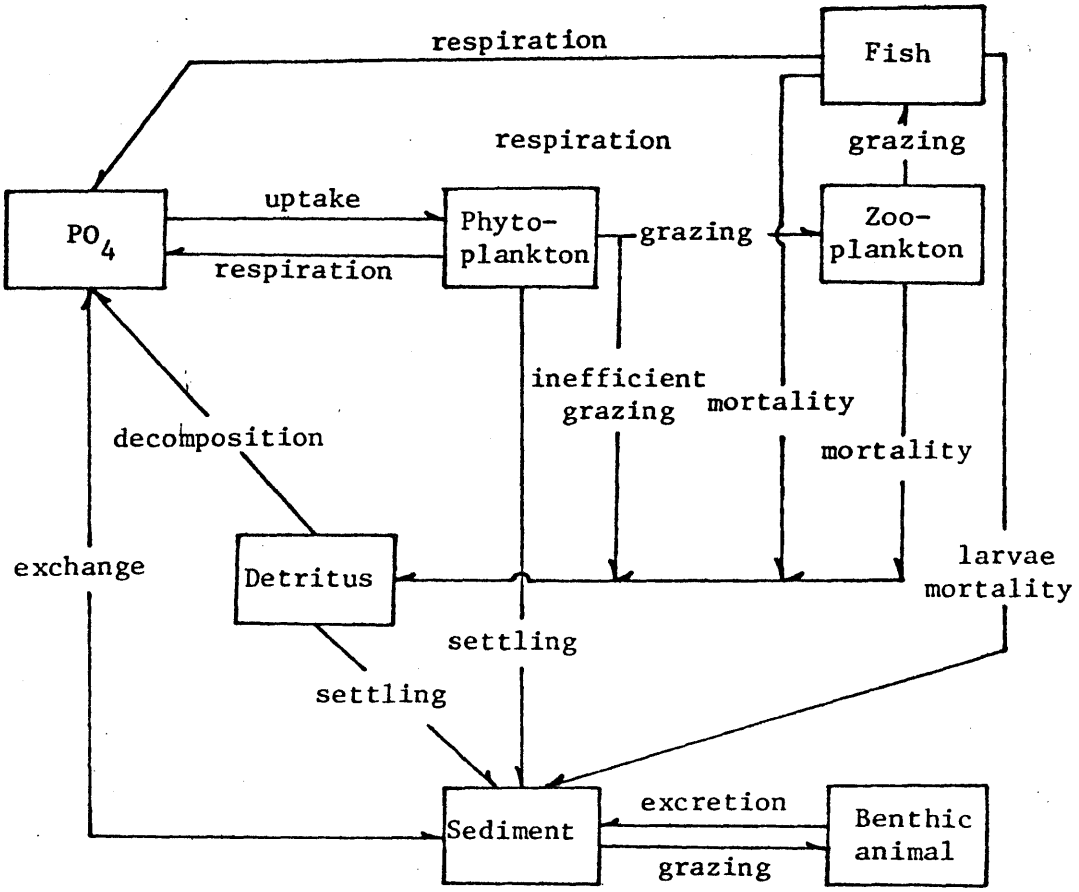

Figure 3-8: Chen and Orlob (1972)

respiration process in this model is loosely defined to include other biological activity such as excretion and lysis. If this is so, the term should be clearly redefined in the model since respiration is a very well studied process and the careless use of the term will lead to erroneous citation of literature values and findings.

When this 36-parameter model was applied to Lake Washington, the following relationship exists between state variables (S) and field measurements (M):

Table 3.2

Model State Variables vs. Field Measurements
Application to Lake Washington (Chen and Orlob, 1972)

M \ S	PO_4	Phyto-1	Phyto-2	Zoo.	Fish-1	Fish-2	Detritus
PO_4	1						
Chlo-a		k•c	k•(1-c)				

where k = the ratio of chlorophyll-a to phytoplankton biomass, c = the ratio of phytoplankton-1 to total phytoplankton with total phytoplankton defined as the sum of phytoplankton-1 and phytoplankton-2; bimonthly data averaged over the year 1962 and 1963 were used, 1 data point every 10 m.

Data are only available at 10 meter intervals. Secchi depths were in the order of 1 m for Lake Washington during July and August of 1962 and 1963 (Edmonson, 1972). The corresponding extinction coefficients may be estimated by (Ford, 1977):

$$\eta = \frac{1.9}{d_s} \tag{3.2}$$

where η is the extinction coefficient and d_s is the depth of disappearance of the secchi disk.

A secchi depth of 1 m gives an extinction coefficient of 1.9 m^{-1} which leads to an euphotic zone of 3 meters. One data point taken at 10 meter intervals hardly contains enough information to verify the important model parameters.

3.2.4 Thomann and DiToro (1975)

The diagram of the phosphorus cycle in Figure 3.9 shows the growth of phytoplankton as a function of light, temperature and two nutrients (P and N). The various constants are considered to be averages over the natural population. The food chain in this model is photoplankton - herbivorous zooplankton - carnivorous zooplankton - upper trophic level #1 - upper trophic level #2. Grazing rates and respiration rates for trophic levels higher than phytoplankton are linearly proportional to the temperature.

Phosphorus, other than that incorporated into plankton and higher trophic levels, is divided into two compartments - inorganic P and non-living organic P. Non-living organic P is produced from inefficient grazing and mortality of zooplankton and fish and is decomposed to inorganic P. The parallel of this non-living organic P in Chen and Orlob's (1972) model is detritus P. In Chen and Orlob's model, however, detritus is considered as particulate matter subjected to settling loss, while the non-living organic P in this model is considered to be dissolved substance

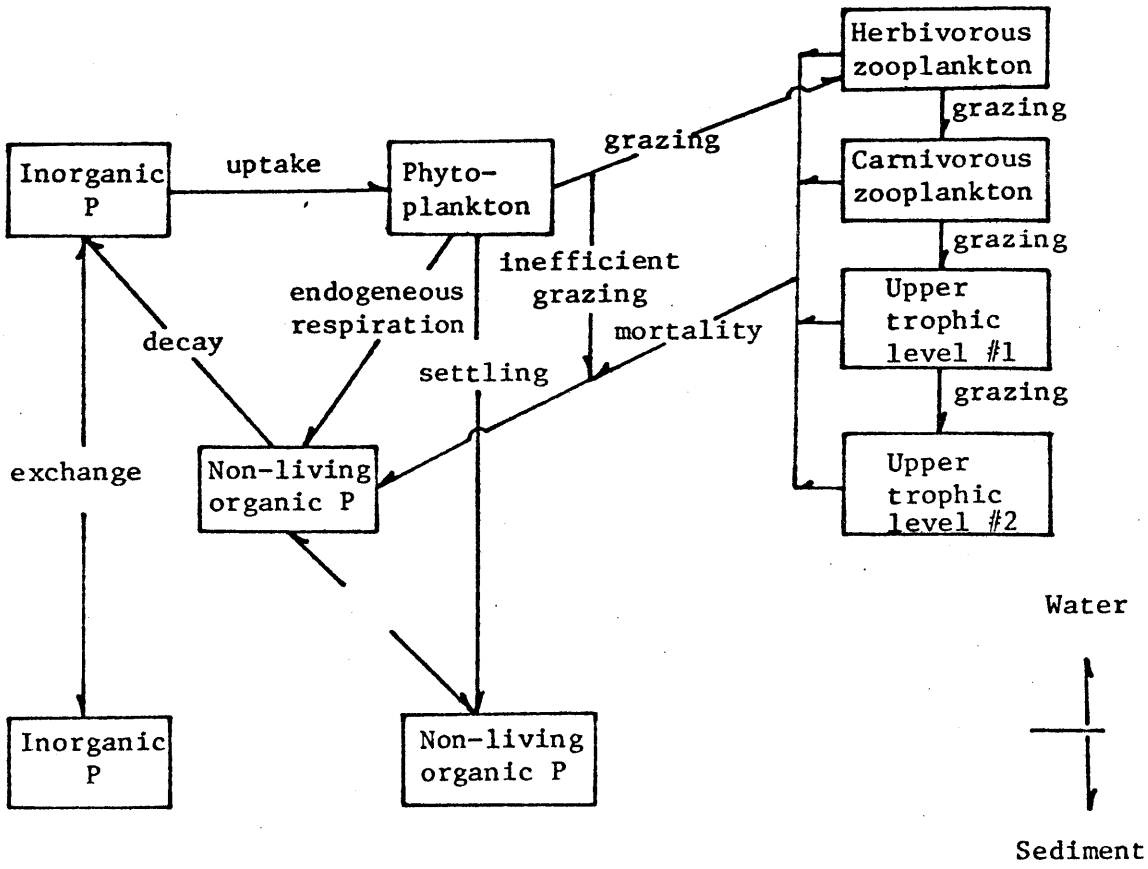

Figure 3-9: Schematic of Thomann, DiToro et al (1975) Biochemical Model

Note: Only the phosphorus cycle is shown in this diagram, other nutrients (C&N) are also included in the model.

subject to no settling loss but interchanged with the sediment through physical transport processes.

Inorganic P is also considered to interchange separately with the same form of phosphorus in the sediment. There is no interaction between sediment non-living P and sediment inorganic P, even though high bacterial activity is expected in the sediment.

There are 42 parameters in this model. When the model was applied to Lake Ontario, the following relationship existed between model state variables and field measurements.

Table 3.3

Model State Variables vs. Field Measurements
Application to Lake Ontario (Thomann and DiToro, 1975)

M \ S	PO_4	Phyto.	Zoo-H	Zoo-C	Troph.-1	Troph.-2	Non-living P
PO_4	1						
Chlo-a		k					
Zoo				k_1c	$k_1(1-c)$		

*where k = the ratio of chlorophyll-a to phytoplankton biomass, k_1 = the ratio of zooplankton carbon to zooplankton biomass, c = the ratio of herbivorous zooplankton to total zooplankton which consists of both herbivorous zooplankton and carnivorous zooplankton; Bi-weekly to monthly data were used (averaged over the years 1967, 1968, 1969, 1970), averaged over the upper 17 m depths.

3.2.5 Jørgensen (1976, 1978)

Figure 3.10 is the schematic diagram of Jørgensen's model (1976, 1978), which is also very similar to Chen and Orlob's (1972). Differences may be summarized as follows:

(1) The exchange of soluble P between sediment and water takes into account the concentration dependence of the decomposition rate and the model distinguishes between exchangeable and unexchangeable phosphorus.

(2) Mortality of phytoplankton is also a source of detritus.

(3) Soluble P is regenerated through zooplankton respiration and detritus decomposition and is exchanged with the sediment.

(4) Soluble P replaces the role of PO_4 in Chen and Orlob's model.

As defined in section 3.1, soluble P refers to the total amount of P contained in the fitrate passing through a 0.45 μm filter. Lean (1973 a,b) subdivided soluble P into colloidal P, XP and PO_4 and showed that colloidal P was the major fraction of the soluble P in lake water taken from the summer euphotic zone (see section 3.2). The concentration of colloidal P remains fairly constant throughout the year in both hard and soft waters. Uptake of phosphorus from this form is negligible (Schindler and Fee, 1975). Since colloidal P has chemical characteristics distinctively different from that of PO_4's it should not be lumped with PO_4 as a single identity.

It should be noted here that the uptake of soluble P by phytoplankton is actually formulated as the uptake rate of ortho-P by phytoplankton. In all the models previously reviewed, the uptake rate is formulated as phytoplankton growth rate.

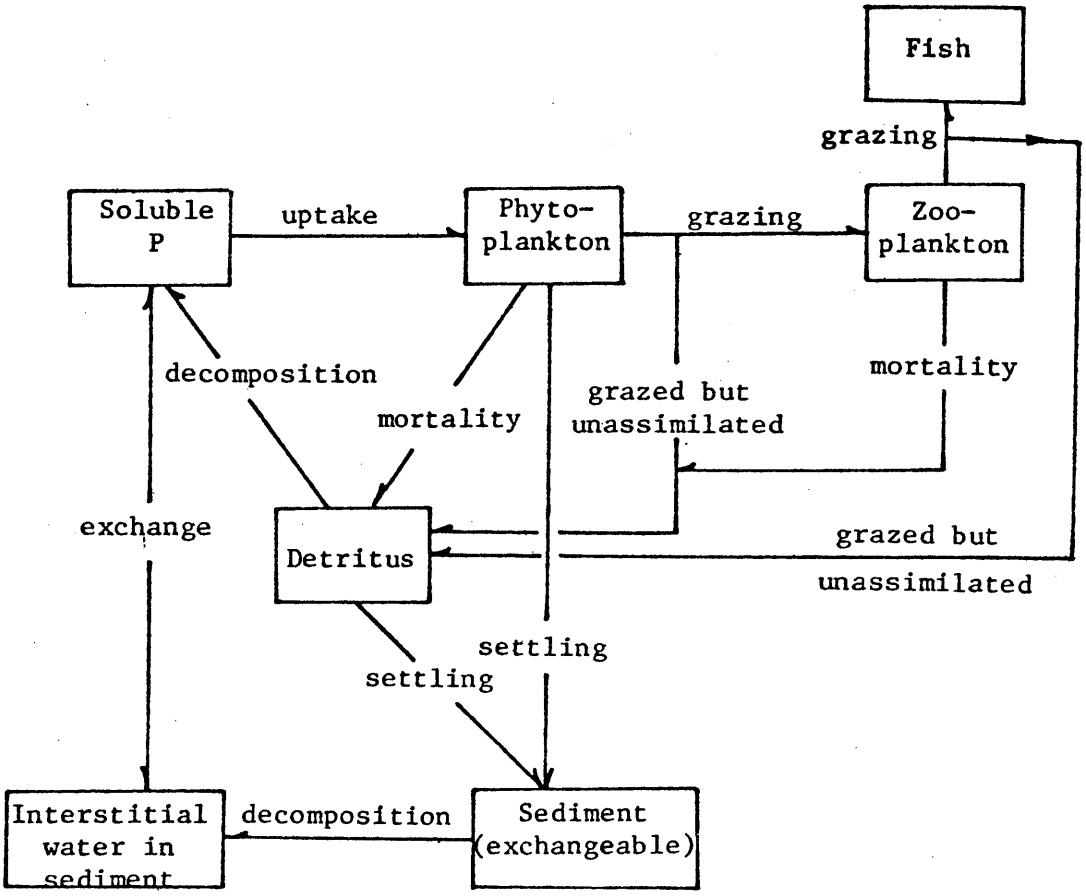

Figure 3.10: Schematic of Jorgensen (1976, 1978) Biochemical Model

Note: Only the phosphorus cycle is shown in this diagram, other nutrients (C & N) are also included in the model.

This model has been applied to three lakes (Jørgensen and Harleman, 1978). When this 45-parameter model is applied to Glumso Lake the relationship between state variables and field measurement shown in Table 3.4 exists.

Table 3.4

Model State Variables vs. Field Measurements
Application to Glumso Lake (Jørgensen, 1976)

S / M	PO_4	Phyto.	Zoo.	Fish	Detritus
Solu. P	1				
Chlo-a or Cell No.		k_1 or k_2			

*where k_1 = the ratio of chlorophyll-a to phytoplankton biomass, k_2 = the ratio of phytoplankton cell number to biomass; Biweekly to monthly measurements were used (averaged over the years 1972, 1973, 1974, 1975).

3.2.6 Richey (1977)

This model presents an excellent example of how to use a conceptual phosphorus model in conjunction with a short term, extensive field measurement program to test a series of hypotheses. The purpose of this model is to test the proposed relationship between primary production rate (measured as increase of particulate organic C in units of mg C/ m^3/hr) and phosphorus flux (measured as μg P/l/hr).

The schematic diagram shown in Figure 3.11 consists of 9 compartments: dissolved inorganic P, dissolved organic P, phytoplankton P, polyphosphate, bacteria particulate P, zooplankton particulate P, detrital particulate P, settleable particulate P and ferric phosphate.

Bacteria competes with phytoplankton for the uptake of ortho-P, and in addition, uses dissolved organic P as substrate. The uptake of ortho-P by phytoplankton is considered in a rather complicated manner:

(a) The uptake of ortho-P by phytoplankton = 1/40 (by weight) of the net carbon uptake rate by phytoplankton;

(b) If the amount of ortho-P present is not sufficient to supply the ortho-P required in (a), phytoplankton will produce the exoenzyme alkaline phosphatase to catalyze the hydrolysis of dissolved organic P;

(c) If there are excessive amounts of P inside phytoplankton, the excessive P will be converted to polyphosphate which will later supply the phosphorus needed for (a) when the external ortho-P is insufficient. It is not clear how condition (c) could exist if the uptake of ortho-P is modeled in the manner described in (a). Moreover, it is unclear how cases (b) and (c) could be measured and identified in this field study. As part of the metabolic process, phytoplankton excretes dissolved organic P which may

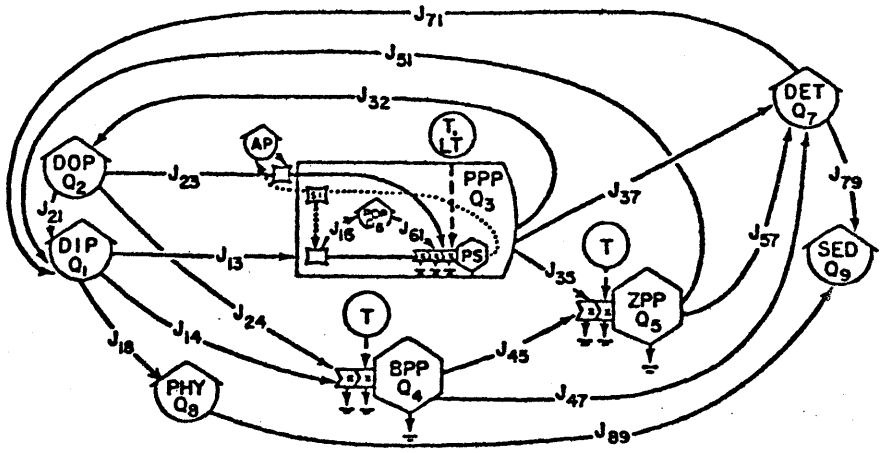

DIP (Q_1) = dissolved inorganic phosphorus
DOP (Q_2) = dissolved organic phosphorus
PPP (Q_3) = phytoplankton particulate phosphorus
BPP (Q_4) = bacteria particulate phosphorus
ZPP (Q_5) = zooplankton particulate phosphorus
POP (Q_6) = polyphosphate
DET (Q_7) = detrital phosphorus
PHY (Q_8) = ferric phosphate
SED (Q_9) = sediment phosphorus
AP = alkaline phosphatase
T = temperature
LT = light
J_{13} = phytoplankton uptake of DIP
J_{14} = bacteria uptake of DIP
J_{16} = polyphosphate formation
J_{18} = precipitation of phosphate
J_{21} = release of phosphate via condensation
J_{23} = phytoplankton uptake of DOP
J_{24} = bacteria uptake of DOP
J_{32} = phytoplankton excretion of DOP
J_{35} = zooplankton grazing of phytoplankton
J_{37} = phytoplankton death
J_{45} = zooplankton grazing of bacteria
J_{47} = bacteria death
J_{51} = zooplankton excretion of DIP
J_{57} = zooplankton death
J_{61} = polyphosphate utilization
J_{71} = autolysis of DIP
J_{79} = loss of DET to sediments
J_{84} = loss of precipitated DIP to sediments

Figure 3.11: Schematic of Richey (1977) P Model

release dissolved inorganic P.

Zooplankton grazes on bacteria and phytoplankton, and in turn excretes phosphate. Detritus P is formed from dead phytoplankton, bacteria and zooplankton. Within several hours after death, 25 to 75% of the phosphate will be released through lysis. The regeneration rate of ortho-P from detrital P is 0.7 hr^{-1}, or 16.8 day^{-1}. The remaining cell P, mostly slow-degrading nucleic acids, settles out of the water column. The model also considers the precipitation of ortho-P with iron, either through $FePO_4$ formation or through physical adsorption on to other iron precipitates.

This model was tested against the phosphorus cycle in Castle Lake. The discrepancies existing between the predicted phosphate uptake and the model prediction (Figure 3.12) indicate the need for accurate and sensitive analyses for the different phosphorus pools and for a further understanding of the interchange mechanisms.

The ability to test this complex model is further limited by the availability of data. However, the model does serve the purpose of indicating future directions for field measurements directed at the disaggregation of state variables now commonly lumped together.

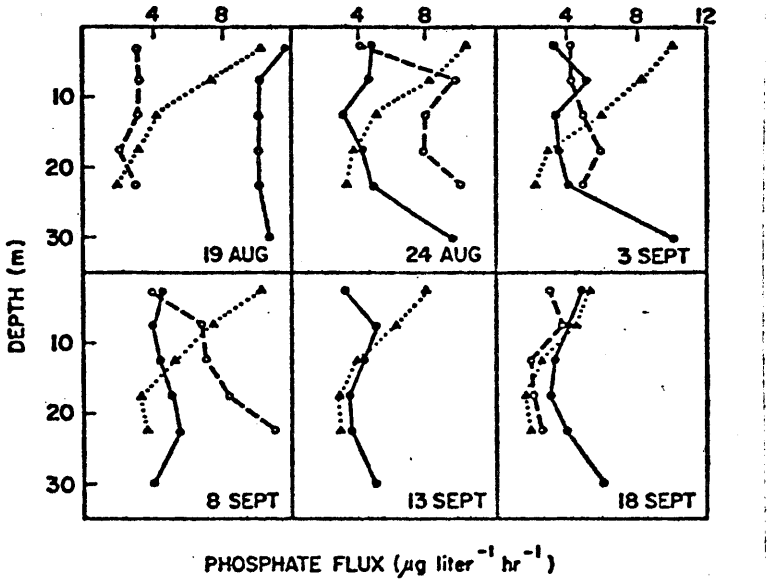

Figure 3.12: Comparison of Model Prediction and Measurement of P Uptake Rate (Richey, 1977)

3.3 Summary and Conclusions

3.3.1 Summary of P Models

3.3.1.1 Approaches in Presentation of P Models

The review of existing phosphorus models in section 3.2 indicates that two general approaches have been used in the presentation of the phosphorus cycle. In the first approach used by Snodgrass and O'Melia, and Imboden and Gachter, the cycle is presented in terms of the analytically separable forms of phosphorus, i.e., ortho-P and particulate-P. The second approach, as used by Chen and Orlob, Thomann et al., Jørgensen, and Richey, represents the phosphorus cycle as a life cycle of various trophic levels (ortho-P, detritus-P, bacteria-P, phytoplankton-P, zooplankton-P and fish-P).

3.3.1.2 The Comparison of the Two Approaches

The first approach is a natural consequence of the available existing field data for lakes, most of which are given in terms of concentrations of total-P, particulate-P, dissolved organic P and soluble reactive P (see section 3.1). The existence of these data allows models constructed by this approach to be calibrated and verified against field measurements. Imboden (1978), however, did not fully utilize the available data and compared only soluble reactive P with his model's ortho-P state variable (see Table 3.1). In order to express the reaction rates between the different P compartments, which might bear no biological meaning because of the lumped nature of the compartments, a large number of calibrated parameters is necessary. For example, even the simple structure of Imboden's model requires more than 19 parameters.

The second approach is derived from an understanding of basic interactions in laboratory pure culture studies. This approach is more theoretically pleasing since it follows the sequence of the natural food web structure. It allows the rates in the model to be related to the rates measured from laboratory studies. However, since the natural system is a composite of species, the direct extrapolation of the pure culture study results to the model formulation is not possible. The current approach with the exception of Richey's, is still to calibrate numerous model parameters with scanty field data. Therefore, the major difficulty of the second approach is in the limitations of the available data. For example, in Chen and Orlob's model, the particulate P was a composite of phosphorus contained in phytoplankton-1, phytoplankton-2, and detritus. When the model was applied to Lake Washington, complete model verification was not possible since there was no measurement of the size of each subparticulate phosphorus compartment (see Table 3.2). This fine division is only meaningful, however, if the reaction rates between each phosphorus compartment is known. At this stage when rates are still calibrated by field data, it seems premature to discuss the importance of each unmeasured compartment in the P cycling.

The uncertainty about the reaction rates can be illustrated by comparing the detritus decomposition rate (or decay rate of non-living organic-P in Thomann and DiToro's model) used in the different models. Chen and Orlob used a rate of 0.001 day^{-1} for Lake Washington, Thomann and DiToro 0.007 day^{-1} for Lake Ontario and Jørgensen 0.1 day^{-1} for Lake Glumso. These calibrated values differ by a factor of 100 and are much lower than the value of 20 day^{-1} estimated by Richey (1977) from field radio tracer

measurements. An overall factor of uncertainty of 2000 for the same reaction rate (0.001 day^{-1} in Chen and Orlob's vs. 20 day^{-1} in Richey's) certainly cannot be explained by the difference in aquatic systems; it is more a reflection of the lack of data.

The vast difference in the decomposition rate certainly leads to extremely different conclusions about the importance of the ortho-P regenerated through the internal cycling made possible by the detritus pool. The detritus pool (or the non-living organic pool in Thomann and DiToro's model) channels the regeneration of ortho-P through the mortality and inefficient grazing of zooplankton and fish (see Figures 3.8, 3.9, 3.10 and 3.11). To illustrate, consider a detrital particle settling at a rate of 0.2 m/day (Chen and Orlob, 1972). It will reach the bottom of a 10 m deep lake in 50 days and will still retain 95% of its original P content if it has been decomposed at a rate of 0.001 day^{-1}, but it will retain less than 1% if its original P content if it has been decomposed at a rate of 0.1 day^{-1}. Undoubtedly, with a rate of 0.001 day, the simulation result will indicate that little of the ortho-P is regenerated through the mortality and inefficient grazing of higher trophic levels, while with a rate of 0.1 day^{-1}, the opposite conclusion results. Therefore, we may conclude that if we have the correct knowledge of all the reaction rates between those biologically meaningful phosphorus compartments, the second approach is preferable. However, if we do not have correct knowledge of these reaction rates and have to rely on field data to calibrate important rate parameters, then we should consider the first approach.

Imboden et al. (1978) assumed that the particulate-P compartment is phytoplankton-P. This assumption allows us to view the P cycle presented in the first approach as a subset of the P-cycle of the second approach, i.e., the first approach simply stops at phytoplankton without including higher trophic levels. In the two approaches, all the reviewed models assumed that the total P measured excludes phosphorus contained in trophic levels higher than phytoplankton. The two approaches, therefore, differ in their representation of the mechanism through which total-P is lost from the lake. Figure 3.13 illustrates these differences. In the first approach, total-P is lost only through the settling of phytoplankton while in the second approach, total-P may be lost through the zooplankton grazing on phytoplankton and the settling of phytoplankton and detritus. Moreover, total-P may be gained from the respiration/mortality of any higher trophic levels (zooplankton and fish).

The settling rate in the first approach has to be time varying in order to account for the loss of total-P due to the storage of P in zooplankton and fish. There are cases, however, that cannot be modeled by the first approach even with a variable settling rate. Let us consider a classic predator-prey (zooplankton-phytoplankton) system as described by the Lotka-Volterra equation:

$$\frac{d(xp)}{dt} = (xp)[a - \alpha(zp)] \tag{3.3}$$

$$\frac{d(zp)}{dt} = (zp)[-b + \beta(xp)] \tag{3.4}$$

where xp and zp are the phytoplankton-P and zooplankton-P concentrations, respectively; a,β and α,b are the growth and death rates of phytoplankton,

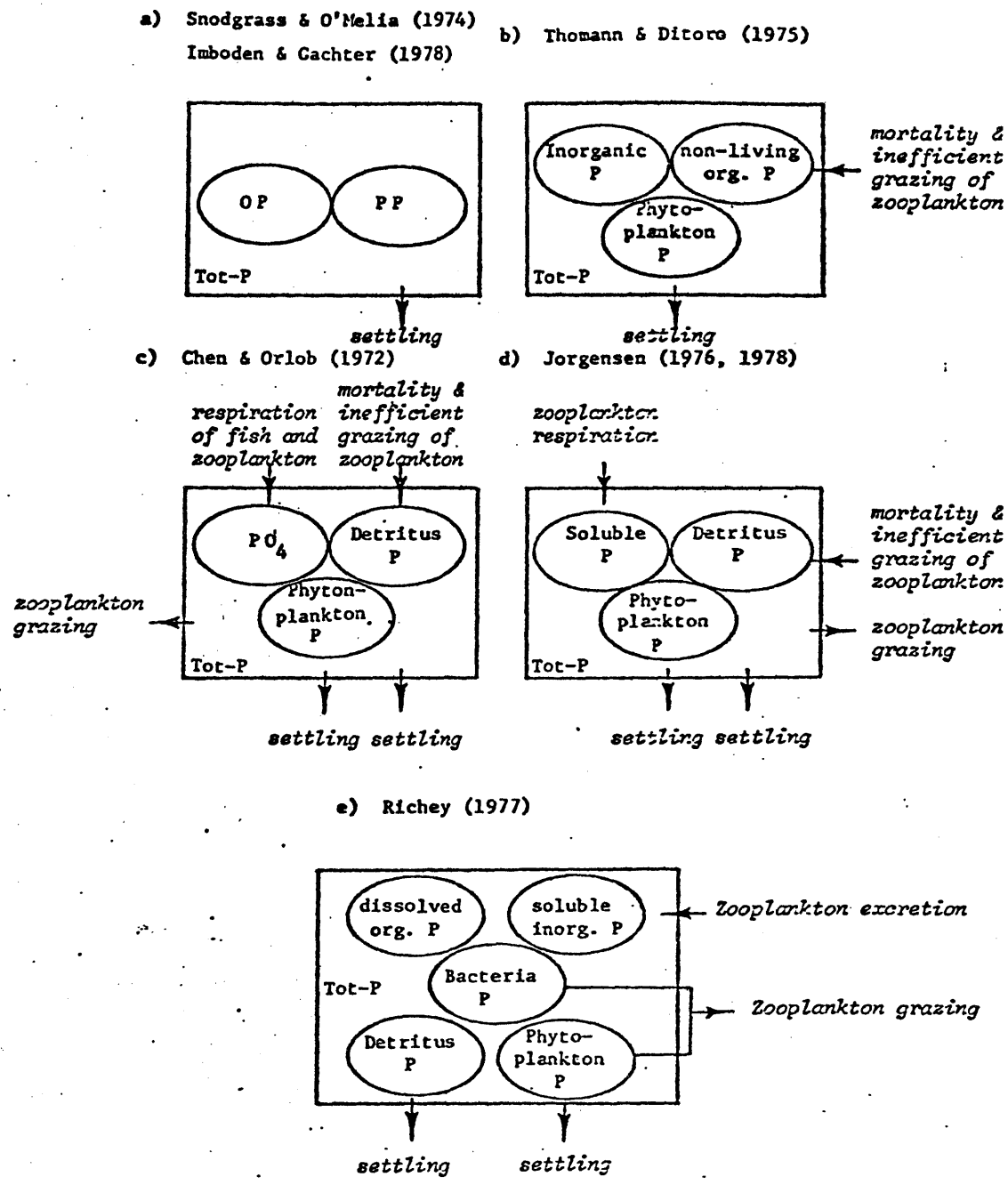

Figure 3.13: Presentations of Sources and Sinks of Total P (TP) in the Reviewed Models

zooplankton respectively. It is assumed that there is no external phosphorus supply; all the phosphorus released during the death of zooplankton is used for phytoplankton growth, that is a equals b; and phosphorus released during the death of phytoplankton is used for zooplankton growth, that is α equals β. If the initial concentrations of xp and zp are not the equilibrium concentrations (i.e., $\frac{b}{\beta}$ and $\frac{a}{\alpha}$), then the concentration of phytoplankton-P and zooplankton-P oscillates about the equilibrium concentration as illustrated in Figure 3.14.

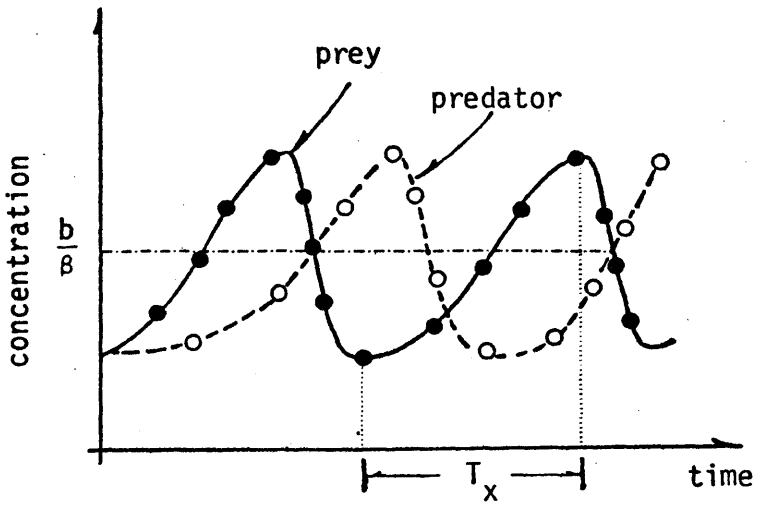

Figure 3.14: Oscillation of Predator-Prey Population as Described by the Lotka-Volterra Equation

Since the zooplankton-P is not measured as part of total P, the phytoplankton-P represents the total-P concentration. During the period T_x, there is an increase of total-P which cannot be modeled correctly by the first approach. The first approach has no means of accounting for this increase of total-P other than by treating it as an external source.

3.3.2 Evaluation of the Necessary Number of State Variables in a P Model

The major P biological pathways as of our current understanding have been incorporated in a P cycle shown previously in Figure 3.3. This P cycle is partially captured by each of the reviewed models. At this point, if we do not consider the option of representing each trophic level with multi-species, the maximum number of state variables may be as many as 7, which is the number of biologically separable P compartments in the P cycle shown in Figure 3.3 (ortho-P, soluble organic-P, detritus, bacteria, phytoplankton, zooplankton, fish). On the other hand, the smallest number of state variables is 2, as in Imboden and Gachter's (1978) and Snodgrass and O'Melia's (1975)models which only consider the movement of P between ortho-P and phytoplankton-P. Therefore, the number of state variables in a P model may lie between 2 and 7. As discussed previously, if all the reaction rates are known, an extensive model is preferable since it will allow an examination of all the important processes. At this moment, however, most of the reaction rates are still uncertain. The availability of data has to be considered in choosing a model, but there seems to be no clear indication which would be the best choice. However, an attempt will be made to decide on the necessary number of state variables by evaluating the maximum possible 7 variables using criteria such as the objective of the model, the limitation of the model and the simplification desired.

3.3.2.1 State Variables Not Included in the Total P Measurement

Fish. If the P model is to predict the effect of P input to the fish production or if the model is to consider the effect of trace metals

on humans from the consumption of fish, then the inclusion of fish as a state variable is necessary. However, if the objective of the model is to predict the duration and magnitude of the phytoplankton bloom, then the inclusion of fish may not be necessary.

Three of the reviewed models contain fish as a state variable. Fish, the highest trophic level considered, acts as (1) a sink for zooplankton through the grazing activity, (2) a source of detritus (or non-living organic P) through the mortality or inefficient grazing, and (3) a source of inorganic P through respiration. These roles of fish in the P cycle affect its choice as state variable in the P model, as seen in the next paragraphs.

It should be recalled that there are usually not enough zooplankton data to verify the zooplankton related parameter values. DiToro (1979), using Lake Ontario as a case study, investigated the reliability of the model parameters and found that the mortality rates of zooplankton are subject to coefficients of variation of 130% (carnivorous zooplankton) to 1600% (herbivorous zooplankton). The loss of zooplankton due to fish grazing is only 12% of the loss due to zooplankton mortality, i.e., 0.015 day^{-1} vs. 0.125 day^{-1} (Jørgensen, 1976). Since the mortality is subject to a high percentage of error, it seems hardly possible that the accuracy of the model's prediction can be increased by including a fish grazing factor which is only 12% of the mortality value.

The mortality of fish is considered as a source term for the detritus pool in Chen and Orlob's model (1972), and for the non-living organic P in Thomann and DiToro's model (1975). However, the calibrated mortality rate used was zero, which suggests that it is not necessary to include

fish as a source term.

Chen and Orlob (1972) also considered the fish respiration as a source of the ortho-P. The rate used in the model's application to Lake Washington is 0.001 day^{-1}. Since the duration of phytoplankton bloom is in the order of weeks to a month, a 0.001 day^{-1} rate is of little significance to the regeneration of ortho-P. In summary, unless the purpose of the model is to explicitly consider the fish population variation, the inclusion of fish as a state variable is not necessary.

Zooplankton. Zooplankton, being the principal predator of phytoplankton, are expected to have significant influence on the control of phytoplankton population. The classic predator-prey oscillation was observed by Shiao (1976), who showed a periodic growth of the phytoplankton and zooplankton, with zooplankton chasing the phytoplankton. As discussed previously (section 3.3.1), however, the zooplankton grazing effect may be lumped with the actual phytoplankton settling rate into what may be collectively termed the equivalent settling rate. There is a limitation, though to the use of this equivalent settling rate, which may be seen from a total P budget. When there is a significant increase of total-P which cannot be accounted for by an external source or sediment return, the inclusion of zooplankton as state variable is absolutely necessary. When the total-P budget shows a decrease or balance, the choice of incorporating zooplankton as model state variable or employing a variable settling rate is left to the discretion of the modeler.

3.3.2.2 State Variables Included in the Total P Measurement

The total P content in water, separated into three different components by conventional chemical analytical methods (see section 3.1), may be represented as a sum of five model state variables. The relationship between analytically separable P compartments (whose terminology follows that of Strickland and Parsons (1960)) and model state variables is shown in Table 3.5. SRP is often considered to correspond to state variable ortho-P, SUP represents the sum of soluble unreactive P and bacteria P; and PP represents the sum of phytoplankton P and detritus P.

Table 3.5

The Relationship Between Analytically Separable P Compartments and P Model State Variables

$$\begin{pmatrix} \text{SRP} \\ \text{SUP} \\ \text{PP} \end{pmatrix} = \begin{pmatrix} 1 & 0 & 0 & 0 & 0 \\ 0 & 1 & 1 & 0 & 0 \\ 0 & 0 & 0 & 1 & 1 \end{pmatrix} \times \begin{pmatrix} PO_4 \\ \text{soluble org. P} \\ \text{bacteria P} \\ \text{phytoplankton-P} \\ \text{detritus P} \end{pmatrix}$$

Phytoplankton P and Detritus P. Phytoplankton P is the center of the modeling objective and therefore certainly cannot be omitted; the question is whether the inclusion of detritus is necessary. The inclusion of detritus as a state variable is meaningful if the mortality rate of phytoplankton and other sources of detritus and the decomposition rate of detritus are confidently known.

We will first review our knowledge of the phytoplankton mortality rate. Although literature on phytoplankton physiology is extensive, the attention has been on the nutrient uptake and growth rate of phytoplankton. Canter and Lund's (1943) study on a number of English lakes is one of the few in the literature on phytoplankton mortality. They observed that after the depletion of nutrients, phytoplankton are physiologically incapacitated

and transformed into inactive cells which are highly sensitive to predation by native microflora. Their observation suggests that mortality of phytoplankton occurs after the cells enter the stationary phase. The active grazing of phytoplankton by zooplankton (Peters, 1972, estimated that 20% of the phytoplankton is grazed daily by zooplankton) keeps the phytoplankton in their logarithmic growth phase and thus reduces their susceptibility to the parasitic fungus infection.

Aside from phytoplankton, other sources of detritus are the particulates excreted by zooplankton becasue of ineffective grazing. Since more than 90% of the phosphorus excreted by zooplankton is ortho-P (see Section 3.2), less than 10% of the excreted P is retained in the particulate matter. In other words, the regeneration of ortho-P through direct zooplankton excretion is an order of magnitude larger than that through decomposition of the excreted particulate matter.

Finally, we may evaluate the necessity of including detritus as state variable in light of observations which indicate that detritus decomposes rapidly (Section 3.2). Richey (1977) estimated the detritus decomposition rate to be in the order of 2- day^{-1} which is far greater than its rate of supply. To illustrate this, consider the network of two consecutive first order reactions (or two stage reactions) shown in Figure 3.15.

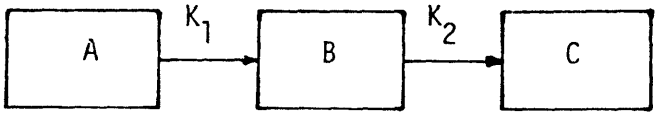

Figure 3.15: A Schematic Representation of a 2-Stage 1st Order Reaction

A represents the detritus source, B the detritus and C the ortho-P. Assuming that the initial concentration of A is A_o, and the initial concentrations of B and C are both 0, the solution to this problem is

$$A = A_o \exp(-k_1 t) \tag{3.4}$$

$$B = A_o \frac{k_1}{k_2 - k_1} [\exp(-k_1 t) - \exp(-k_2 t)] \tag{3.5}$$

$$C = A_o [1 - \exp(-k_1 t) - \frac{k_1}{k_2 - k_1} \exp(-k_1 t) + \frac{k_1}{k_2 - k_1} \exp(-k_2 t)] \tag{3.6}$$

If $k_2 >> k_1$ then the solution of C may be expressed as

$$C = A_o [1 - \exp(-k_1 t)] \tag{3.7}$$

Equation (3.7) is the solution for a single first order (or one stage) reaction shown in Figure 3.16 with initial concentrations for A and C of A_o and 0, respectively. This simple calculation demonstrates that if detritus is decomposed at a rate more rapid than its rate of supply (i.e., $k_2 >> k_1$), the omission of this variable by using the presentation given in Figure 3.16, which directly relates the source detritus to the regeneration of ortho-P, is acceptable.

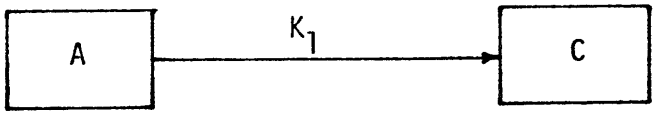

Figure 3.16: Schematic Representation of a 2-stage, 1st Order Reaction

Bacteria and Soluble Organic P. The omission or the misrepresentation of bacteria and soluble organic P in the reviewed models reflects the poor understanding of their roles in the aquatic P cycle. None of the models, except Richey's (1977), includes bacteria as a state variable. Soluble organic P is presented in many different ways ranging from as an inactive substance, as suggested by its omission in the Imboden et al. and Chen et al. models, to an active substance, as suggested by its being considered the same as ortho-P in Snodgrass and O'Melia's and Jørgensen's models.

The principal role of bacteria is often considered as a decompser of the organic material to release ortho-P. However, Rhee (1972) has shown the competition between bacteria and phytoplankton in the uptake of ortho-P. Since bacteria acts both as supplier and consumer of ortho-P, the difficulty of assessing its role from results of conventional chemical analysis is evident. The uptake of bacteria in natural aquatic environments may be quantified by comparing the uptake of ortho-P in an untreated water sample with the uptake rate in a corresponding antibiotic treated water sample. Although the use of antibiotics inhibits the bacterial uptake, this method still has inherent difficulties. The blue-green algae uptake of ortho-P is also inhibited by antibiotics. Therefore, the difference between the uptake rate of the treated and untreated water sample should not be attributed to bacterial uptake alone (Kuenzler and Greer, 1980). In his study of the ecology of the bacteria of Castle Lake in California, Jassaby (1973) demonstrated that the death rate of bacteria was almost as great as the growth rate, suggesting a steady state population. If the autolysis is rapid, then the ortho-P generated by bacteria through

autolysis is almost enough to sustain bacterial growth (Richey, 1977).

There are few guides in assessing the role of soluble organic P in the biological cycle of either marine or freshwater systems, other than that soluble organic P is decomposed slowly and may be liberated by microorganisms. Solorzano and Strickland (1968) suggested that the organic phosphorus isolated from seawater is mainly nucleic acid because little of the dissolved organic phosphorus in seawater is easily hydrolyzed by phosphate ester enzyme. Moreover, no enzyme has been found to hydrolyze the colloidal P, identified as the major fraction of the soluble P of lake water (see section 3.1).

A proper assessment of the roles of bacteria and soluble organic P cannot be made until more information is available on the identification of these components in aquatic systems and on their link with the metabolic activities of living organisms. Thus, within the limit of current knowledge and available data, it is best to treat the measured SUP as a single variable, unless the model is developed for a field study which employs the measurement method to identify these components. Whether to include SUP as a state variable may be judged from a simple mass balance on the SUP. If the difference between the external supply of SUP and the variations of the in-lake SUP is significant compared to the phytoplankton bound P, then the inclusion of SUP as state variable is necessary.

In conclusion, we recommend that the number of state variables in a P model be between 2 and 4, with ortho-P and phytoplankton-P as necessary state variables. There is, however, no substitute for a modeler's knowledge of the system being analyzed in deciding the inclusion of other state variables.

Chapter IV

PHYTOPLANKTON GROWTH MODELING

4.1 Introduction

A living cell functions like an extremely complicated non-linear system with a series of reversible and irreversible reactions and various control mechanisms. Scientists are just beginning to identify the pathways and some control mechanisms of the biological processes; consequently, we appreciate the reluctance of the biologist to accept a quantitative representation of such complicated processes as growth. However, in managing an aquatic system where the complexities are beyond human intuition, a model which bookkeeps the important processes becomes a necessary tool.

The first advantage of having a quantitative representation is that it calls for a clearer definition of the terminology. The second advantage of a quantitative representation is that it forces a more rigorous examination of the conditions under which the validity of each qualitative description holds. Ultimately, it will allow us to be in a better position to predict the outcome of many man-induced impacts on the natural aquatic system. It might be too ambitious to speak in terms of the ultimate goal, however, the need for a quantitative representation undoubtedly will stimulate a systematic organization of fragments of qualitative information. It is in this spirit that we attempt the modeling of phytoplankton dynamics.

A model is devised to represent a phenomenon by concentrating on the dominant processes and omitting its many secondary processes. The model then incorporates the simplifying assumptions that make the problem

tractable. Undoubtedly, the first danger might arise from the oversimplifications and this is especially hazardous when basic concepts are violated. Therefore, we will try to outline all the assumptions which are involved in each step of model construction.

4.2 Selecting a Model State Variable to Represent Phytoplankton

Phytoplankton has been measured in various units such as cell numbers, total cell volume and weight. In natural aquatic systems, cell number is a poor measure of the total biomass because phytoplankton differ greatly in sizes. Wetzel (1975) estimated that volumes of representative freshwater phytoplankton species range from 8 to 10^5 μm^3. Volume is also a poor measure of the biomass due to the high variation of internal air space. The use of wet weight is also not recommended because of the highly variable water content of phytoplankton. Organic dry weight, or the weight of phytoplankton determined by the loss in weight after ignition at 550°C, is the preferred general biomass criterion. In this research, the term biomass refers to the organic dry weight, unless otherwise defined.

Variation in phytoplankton biomass is a result of the mass fluxes exchanged between phytoplankton cells and their environment. In principle, to model the variation of phytoplankton biomass, we will have to gauge all mass fluxes into and out of the phytoplankton cell. This task can be considerably simplified if the mass flux balance is performed on an element which is a constant fraction of the biomass. Of all the chemical constituents in the phytoplankton cell, Wetzel (1975) reported that

carbon is probably the most invariant one:

> Perhaps the most satisfactory means of measuring the biomass of photosynthetic organisms is to oxidize the organic plant material back to carbon dioxide, from which it originated in photosynthetic reduction. The organic carbon content of plants is one of the least variable constituents, and all falls nearly without exception between the range of 40 to 60% of the ash-free dry weight. The average carbon content among algae is 53-55% of ash-free dry weight.

The major carbon fluxes into and out of a viable phytoplankton cell can be illustrated as shown in Figure 4.1 (the heterotrophic uptake of carbon is neglected here):

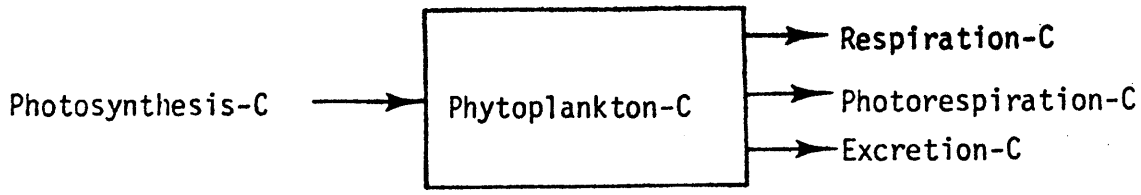

Figure 4.1: Carbon Fluxes into and out of a Viable Phytoplankton Cell

These exchanged mass fluxes are associated with identified phytoplankton metabolic processes. Sections 4.2.1 to 4.2.4 are brief reviews of the qualitative understanding of these processes.

4.2.1 Photosynthesis

Photosynthesis refers to the biological reaction of some autotrophs which convert light energy into chemical energy to assimilate cellular constituents from dissolved inorganic carbon (DIC). The biological importance of inorganic carbon fixation needs no reiteration. The photosynthesis reaction may be written as (Van Niel, 1932):

$$nCO_2 + 2nH_2A + h\nu \rightarrow nCH_2O + 2nA + nH_2O \qquad (4.1)$$

where H_2A refers to the reduced compound which serves as an electron donor in this reaction. In phytoplankton photosynthesis, the electron donor is H_2O.

To reduce 1 mole of CO_2 to CH_2O, 114 kcal of light energy are required. The energy content of a photon or quantum of light is inversely related to its wavelength, e.g., for 400 nm light, the energy content is 72 kcal/einstein but 41 kcal/einstein for 700 nm light (1 einstein = 1 mole of photons). Assuming a perfect energy transfer from a 700 nm quantum of light to chemical energy, it takes approximately 3 einsteins to supply 114 kcal chemical energy to ultimately produce 1 model of CH_2O from DIC.

Equation (4.1) is an oversimplification of the photosynthesis problem. Photosynthesis is in fact a series of many complicated reactions. It is, however, convenient to consider it as a combination of two phases: a light reaction and a biosynthesis reaction.

A. Light Reaction

In the light reaction the light energy is converted to chemical

energy. There are two types of light reactions, those producing O_2 and those not producing O_2. Those which produce O_2 are called non-cyclic reactions because the electron is transferred from the electron donor to the acceptor. Those which do not produce O_2 are called cyclic reactions because the electron returns to its original donor after the completion of the reaction.

The non-cyclic reaction may be summarized as:

$$2H_2O + 2ADP + P_i + 2NADP^+ + h\nu \rightarrow 2NADPH + 2H^+ + O_2 + 2ATP \qquad (4.2)$$

and the cyclic reaction as:

$$ADP + P_i \rightarrow ATP \qquad (4.3)$$

B. Biosynthesis

With sufficient supplies of NADPH and ATP from light reactions, CO_2 is reduced to glucose. There are two pathways which allow the reduction of CO_2 to glucose: the Calvin-Benson cycle (C3 cycle) and the Hatch-Slack pathway (C4 cycle). Most phytoplankton use the C3-cycle for carbon fixation, although the superposition of the C4 cycle under altered physiological states has been confirmed (Morris, 1981). The net reaction of this cycle can be summarized as:

$$6CO_2 + 12NADPH + 12H^+ + 18ATP \rightarrow \underset{\text{(glucose)}}{C_6H_{12}O_6} + 6H_2O + 12NADP^+ + 18ADP + 18P_i \qquad (4.4)$$

Following the synthesis of glucose is the synthesis of cell components which involves many complex reactions.

4.2.2 Excretion

The term excretion refers to the release of organic compounds by healthy phytoplankton cells; it should not be confused with the lysis of dead cells. Since excretion does not consume oxygen, unless these released organic compounds immediately stimulate heterotrophic respiration, this process cannot be detected by measuring the oxygen content of the water. Therefore, evidence of excretion came after the introduction of the C-14 method for photosynthesis measurement.

Fogg (1958) was the first to report evidence of excretion. He reported that up to 70% of the recently incorporated C-14 was released

outside the cell. The released organic compounds included metabolic intermediate compounds, which are of low molecular weight. Since Fogg's finding, there has been increasing evidence confirming the occurrence of phytoplankton excretion (Fogg et al., 1965; Hellebust, 1965, 1974).

Although the occurrence of excretion is well accepted, the rate of exretion is still debated. Sharp (1977) and Mague (1980), carefully examining laboratory procedures used by scientists who reported high excretion rates, suggested that evidence for excretion is marred by procedural artifacts. According to Mague et al. (1980), excretion is a normal cellular function but it is a small fraction of photosynthesis. In response to Sharp's article, Fogg (1977) re-examined his experimental procedures and rightly justified his earlier conclusion that extracellular products amount normally to between 7 and 50%, and occassionally up to 95% of the total carbon assimilated.

We would like to discuss this issue in light of the objectives of this study: the modeling of phytoplankton biomass and the interaction of biological-physical processes. It seems pointless that phytoplankton should synthesize their organic compound and then release it. However, no evidence exists suggesting that at a time scale much shorter than the duration of photosynthesis measurement there is an effective feedback mechanism which inhibits the synthesis of glucose or other metabolic intermediate compounds when a nutrient other than carbon is limiting the production of the metabolic end product. Therefore, DIC may still be taken up for glucose synthesis and oxygen production. As Fogg (1977) suggested, the high excretion of organic carbon and amino acid by

freshwater phytoplankton, which are often phosphorus limited, certainly leads one to hypothesize that phytoplankton cannot immediately sense the limiting factor on its metabolism end product. So, the photosynthetic process continues, producing more organic substance than is actually needed and excreting the excess outside the cell.

Sharp (1977) pointed out that the variation of light intensity is a prime reason for a high excretion rate. Culture grown under low light intensity show increased excretion when they are exposed to high light intensity (Watt and Fogg, 1966; Ignatiades and Fogg, 1973). Moreover, when phytoplankton are incubated at a light intensity lower than their preconditioned light intensity, they show higher excretion rates (Hellebust, 1965; Watt, 1966). Sharp called this variation of light "culture shock" and regarded it as a source of error. However, Mague et al. (1980) drew attention to another implication of this light shock effect:

> Perhaps most provocative is the suggestion that individual phytoplankton in turbulent, shallow, photic zone waters may experience considerable stress due to variations in light intensity and may release substantial portions of their photosynthetis when in situ.

4.2.3 Respiration

Like all eukaryotic cells, phytoplankton contain mitochondria in addition to chloroplasts. Respiration occurring in mitochondria is the oxidation of an energy source with an external electron acceptor (Brock, 1970). The energy sources are organic compounds synthesized during photosynthesis and the electron acceptor is oxygen. The key element of this pathway is the Kreb cycle (also called the citric cycle or tricarboxylic acid cycle). Most aerobic respiration results in complete

oxidation of the organic compound. For example, the respiration reaction using glucose ($C_6H_{12}O_6$) as the energy source may be written as:

$$C_6H_{12}O_6 + 36ADP + 36P_i + 36H^+ + 6O_2 \rightarrow 6CO_2 + 36ATP + 42H_2O \qquad (4.5)$$

4.2.4 Photorespiration

The occurrence of photorespiration for higher plants has been extensively studied (Hatch et al., 1971; Richardson, 1974; Tolbert, 1971). Phytoplankton also have this process (Tolbert,1974). Photorespiration differs from mitochondrial respiration in three ways: It does not occur in the dark, it does not produce ATP, and it does not utilize substrate of the tricarboxylic acid cycle (Kreb cycle).

Photorespiration can be considered as a short circuiting of photosynthesis (see Figure 4.2). Oxygen replaces CO_2 in the RuDP carboxylase reaction, the first reaction in the C3 cycle. Important things to remember are:

(1) It consumes oxygen and reduces the rate of CO_2 fixation,

(2) Two of its end products are sometimes released outside the cell: CO_2 and glycolate.

Factors Affecting Photorespiration

pH: The optimum pH of RuDP oxygenase, the enzyme which is responsible for this reaction, is around 9.3, while the optimum pH of RuDP carboxylase, the enzume which promotes CO_2 fixation, is around 7.8. At a pH above 8.3, the activity of RuDP carboxylase drops rapidly while the activity of RuDP oxygenase increases. The higher activity of RuDP oxygenase

gives photorespiration an advantage over photosynthesis at higher pH when both are competing for the use of RuDP (Tolbert, 1974).

Light: The increase of photorespiration rate with the increase of light intensity is postulated to be caused by the increased production of RuDP from photosynthesis. Moreover, the quality of light influences the photorespiration rate: Red and white light seem to stimulate it and blue light suppresses it (Becker et al., 1968; Lord et al., 1970).

O_2 and CO_2 Concentration: High O_2 concentration and low CO_2 concentration are favorable for photorespiration.

The high pH, low CO_2 concentration and high oxygen concentration are often observed in the lake surface water as a result of very active photosynthetic activity. This seems to suggest that as the photosynthesis reaction continues, it creates an environment which favors the occurrence of photorespiration.

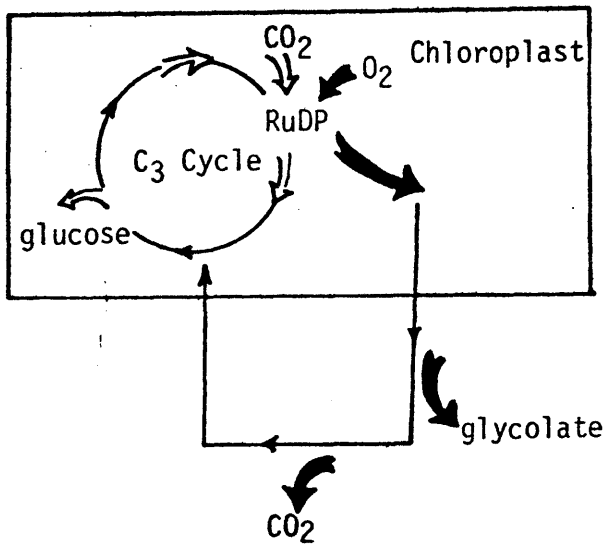

Figure 4.2: Photorespiration (➡) vs. Photosynthesis (⇨)

4.3 Formulation of Phytoplankton Growth

If the carbon/biomass ratio is constant, the net phytoplankton carbon increase will equal the phytoplankton growth rate. This assumption is either explicitly or implicitly employed by many modelers (Chen and Orlob, 1972; Thomann and DiToro, 1975; Imboden, 1978; Richey, 1977) in the formulation of the phytoplankton growth rate. The next step is to consider the functional expressions for the carbon fluxes in terms of the important environmental factors. Here, a second assumption, probably the most important one, is introduced. The effect of these environmental factors, such as light intensity (I), temperature (T) and the limiting nutrient are assumed independent of each other. This simplifying assumption is a consequence of the available literature which has studied the effect of each factor with the other factors held constant. Hence, a serious uncertainty exists concerning this assumption. Furthermore, it is assumed that the combined effect of these factors can be expressed as:

$$f(I)g(T)h(\text{limiting nutrient}) \tag{4.6}$$

An alternative approach is to express the combined effect as:

$$\min(f(I),g(T),h(\text{limiting nutrient})) \tag{4.7}$$

Graphical representations of the two formulations are given as Figure 4.3a and Figure 4.3b. The multiplicative formulation predicts a greater degree of limitation than the second type of formulation. A more important difference between the two formulations is that the multiplicative

a) $\mu = f(F_1)g(F_2)$

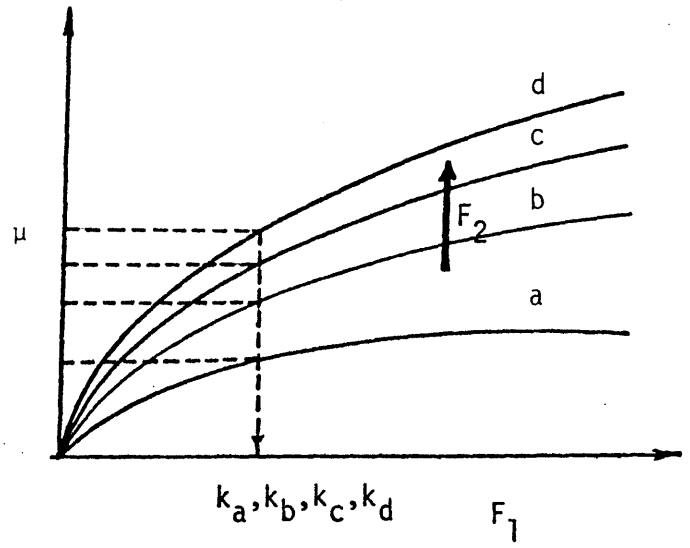

k_a, k_b, k_c, k_d are respectively the half saturation constant for function $f(F_1)$ for case a,b,c,d

b) $\mu = \min(f(F_1), g(F_2))$

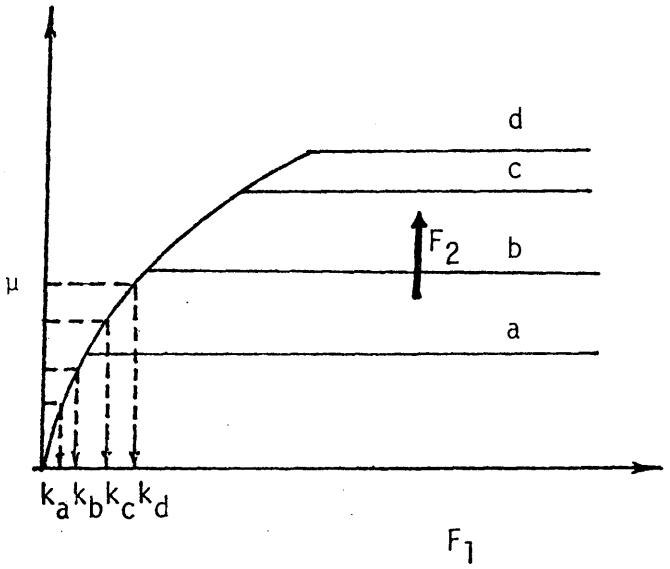

Figure 4.3: Graphic Representation of the Combined Effect of Multi-factors Upon Phytoplankton Growth

(a) the multiplication

(b) the minimum

formulation assumes that the parameter value for one factor can be determined independently of the others, while the second formulation suggests that the parameter value of one factor is a function of many others.

It is difficult to decide a priori what the optimum conditions are for all of the factors involved in phytoplankton growth. If the second formulation represents the true effect, then all the literature values have to be reexamined in terms of the second, third and fourth limiting factors which are often unrecorded. Since there is no clear indication which is a better formulation, our choice becomes that of convenience, and the multiplicative representation is assumed.

4.3.1 Effects of Light

In laboratory studies, many researchers have observed similar trends on the effect of light on photosynthesis. The photosynthetic rate increases linearly with light at low irradiance and reaches a maximum plateau at some higher irradiance. The length of this maximum plateau is variable. If the light intensity continues to increase after the maximum photosynthetic rate has been reached, the occurrence of photoinhibition, which is characterized by a significant decline in the photosynthetic rate, has been observed (Ryther, 1956; Steele, 1962).

One of the earliest characterizations of the photosynthetic response to light is the hyperbolic relationship which takes the form:

$$f(I) = \frac{I}{I+k_I} \tag{4.8}$$

where k_I is the half saturation constant. A graphical representation of

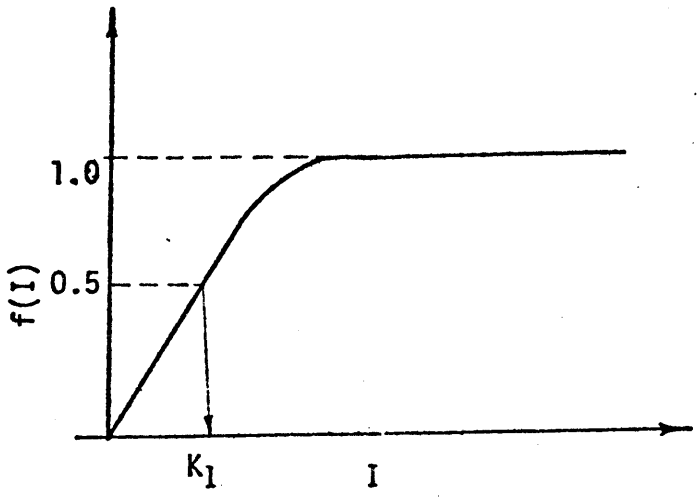

Figure 4.4: The Effect of Light Upon Photosynthesis - Hyperbolic Function

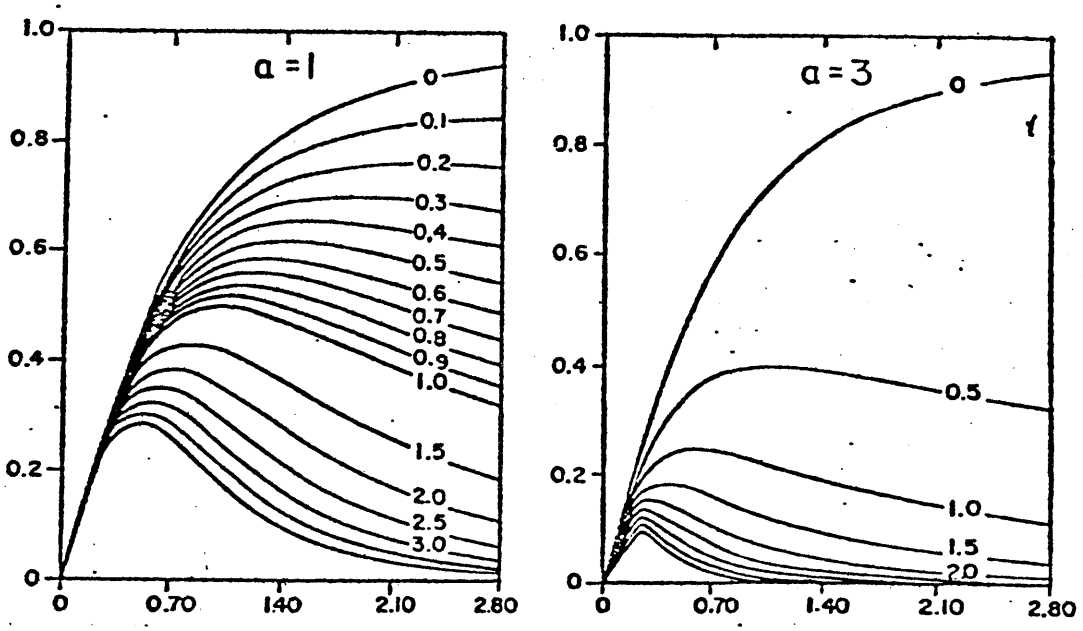

Figure 4.5: Graphic Representation of Vollenweider's Light Function (from Fee, 1969)

this formula is shown in Figure 4.4. The photosynthesis rate reaches half of the maximum value when the irradiance equals k_I. Among many modelers who have used this form of expression are Chen (1971), Jørgensen (1976) and Imboden et al. (1978).

Another expression for the photosynthetic response to light was proposed by Smith (1936):

$$f(I) = \frac{aI}{\sqrt{1+(aI)^2}} \tag{4.9}$$

where a is the parameter for this formulation. Smith's equation can also be written as:

$$f(I) = \frac{I}{\sqrt{I^2 + \frac{1}{a^2}}} \tag{4.10}$$

The hyperbolic expression and Smith's equation are identical at their limits of low and high irradiance:

for hyperbolic function, if $I \ll k_I$ $f(I) \propto I$

if $I \gg k_I$ $f(I) \sim 1$

for Smith's equation, if $I \ll \frac{1}{a}$ $f(I) \propto I$

if $I \gg \frac{1}{a}$ $f(I) \sim 1$

Both equations describe the linear increase of the photosynthetic rate at low irradiance and the leveling off of the photosynthetic rate at high irradiance.

Talling (1957) applied Smith's equation to some English lakes and

found the equation described well the photosynthetic activity of some freshwater algae. Vollenweider (1965) modified Smith's equation to allow varying types and degrees of photoinhibition by introducing two additional parameters n and a:

$$f(I) = \frac{(I/k_I)}{\sqrt{[1 + (I/k_I)^2][1 + (aI/k_I)^2]^n}} \tag{4.11}$$

The graphical presentation (Figure 4.5) of Vollenweider's formulation was given by Fee (1969).

An expression suggested by Steele (1962) which also has the ability to describe the effect of photoinhibition is often preferred:

$$f(I) = \frac{I}{I_{opt}} e^{(1-I/I_{opt})} \tag{4.12}$$

where I_{opt} is the irradiance corresponding to the occurrence of the maximum photosynthesis rate. This equation has only one parameter, but it predicts a decline of the photosynthetic rate for irradiance greater than the optimum irradiance. The depth and time integral of this equation was given by DiToro et al. (1971) and was employed by the Manhattan College group in their modelings of many aquatic environments (Thomann and DiToro, 1975).

Photosynthetic rates are often measured either by the ^{14}C method or the oxygen method. Depending on the method of measurement used by researchers, their reported values of photosyntehtic rate refer to either of the following:

(1) gross oxygen production rate, or

(2) net phytoplankton particulate carbon increase rate.

If it is assumed that all carbon fluxes defined in Figure 4.1 take place

in the course of measurement and that in ^{14}C measurement, the time to randomize the ^{14}C in the cell is much shorter than the duration of the measurement, then the measured rate may be expressed in terms of the carbon fluxes as follows:

$$\text{Net carbon increase rate} = X(k_p - r_e - r_p - r) = f(I) \tag{4.13}$$

$$\text{Gross oxygen production rate} = X\,k(k_p - r_p) = f(I) \tag{4.14}$$

where X = concentration of phytoplankton which is usually constant during the time course of measurement; k = mole of O_2 produced per mole of C fixed; k_p = gross carbon uptake rate; r_e = carbon excretion rate; r_p = photorespiration rate; r = respiration rate and f(I) = the light dependence function.

The light dependence functions may be grouped into two: those which consider photoinhibition and those which do not. Harris (1977) suggests that this difference is caused by the occurrence or absence of photorespiration, that is, the difference in the observed f(I) is due to the variation of the term r_p:

$$X(k_p - r_p) = f_1(I) \quad \text{if } r_p = 0 \tag{4.15}$$

$$= f_2(I) \quad \text{if } r_p \neq 0 \tag{4.16}$$

where: $f_1(I)$ is the light function which shows no photoinhibition and $f_2(I)$ is the light function which shows photoinhibition. Harris (1977) concedes that there is a time course of photorespiration; if the phytoplankton cell is not exposed to the light intensity for more than 10

minutes there will be no photorespiration. He suggests that the observed photoinhibition is due to the artifact of measuring the rate in a fixed-position bottle, where in reality, the photorespiration might not occur. Marra (1978, 1980) verified Harris' (1977) hypothesis by comparing the total photosyntehtic rate estimated from several fixed-position bottles with the rate estimated from a vertically transversing bottle, and found that the estimated rate from the transversing bottle is much higher than the rate estimated from the fixed-position bottle. Therefore, the formulation without photoinhibition (equation 4.8) is chosen for this model of phytoplankton growth.

4.3.2 The Effect of Temperature

The classic paper on the effect of temperature on phytoplankton growth rate (measured as cell division rate, biomass increase rate, net carbon increase rate, or photosynthetic rate) is probably the work of Eppley (1972). He extended the data on specific growth rate in cultures collected by Hoogenhout and Amesz (1965) to include that of marine phytoplankton. There was no apparent distinction between the specific growth rate and the response to temperature of phytoplankton in the marine and freshwater cultures, so that the data from the two were analyzed together. Figure 4.6 is the result of Eppley's compilation. Although it shows a great deal of fluctuation with respect to a given temperature, the maximum specific growth rate at any given temperature shows a trend of increasing with temperature until 40°C. Eppley (1972) suggested the following equation to describe the curve enveloping these data:

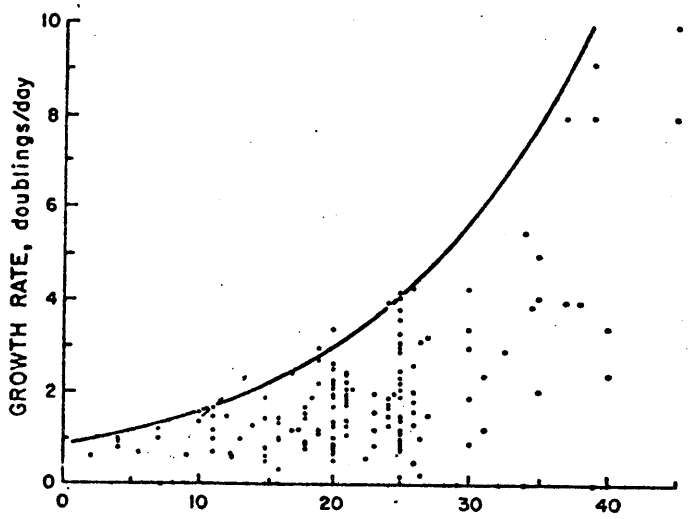

Figure 4.6: Temperature Effect upon Phytoplankton Growth Rate (from Eppley, 1972)

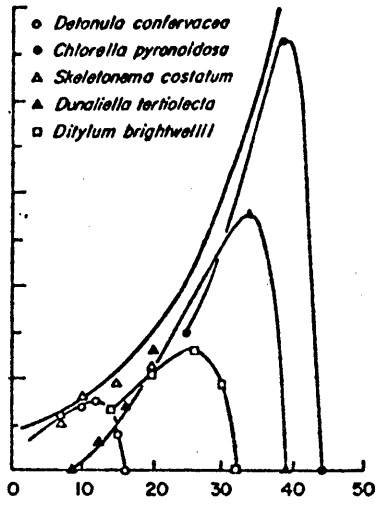

Figure 4.7: Growth vs. Temperature Curves for 5 Phytoplankton with Different Temperature Optima (from Eppley, 1972)

$$\log \mu = 0.0275T - 0.070 \tag{4.17}$$

where μ = growth rate in day^{-1}, T = temperature in °C. The equation can be rewritten as (Kremer and Nixon, 1978):

$$\mu = 0.8511\ e^{0.0633T} \tag{4.18}$$

Eppley explained the meaning of this equation by comparing growth rate vs. temperature curves for five phytoplankton species with different temperature optima (Figure 4.7). Each phytoplankton growth rate shows a gradual increase with temperature and an abrupt decline past the optimal temperature while the maximum growth rate of the whole at any temperature follows the curve expressed by equation (4.17). Therefore, equation (4.17) provides an upper limit for growth rate at any given temperature in a community with composite species and it does not intend to be species specific.

On the other hand, many researchers suggested that temperature is not a significant factor in affecting primary production. Goldman et al. (1976) conducted field and laboratory culture experiments for five marine phytoplankton species showing that the biomass production was essentially the same for the temperature range between 20° to 25°C. Rather, the effect of temperature is on the speciation. The species which grew optimally at a given temperature soon became dominant and utilized the resources of the environment extensively. Figure 4.8 reproduces Goldman's experimental result. The species vary with time but total particulate organic carbon (POC) remains fairly constant throughout the year.

Goldman's (1976) experimental result may be considered as a special

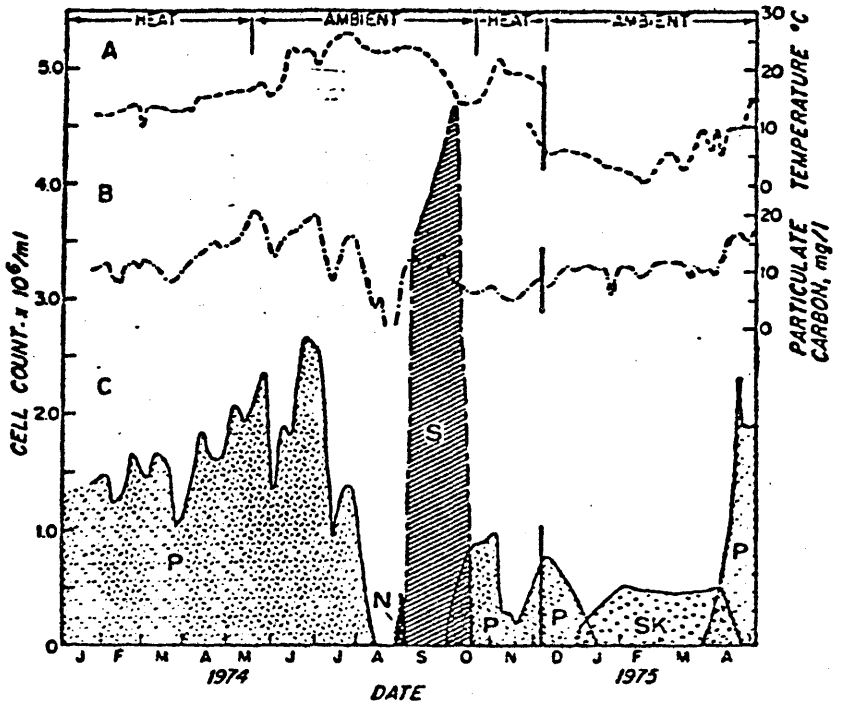

Figure 4.8: Summary of Phytoplankton Biomass Data Collected by Goldman (1976) in Outdoors Studies of Temperature Effect

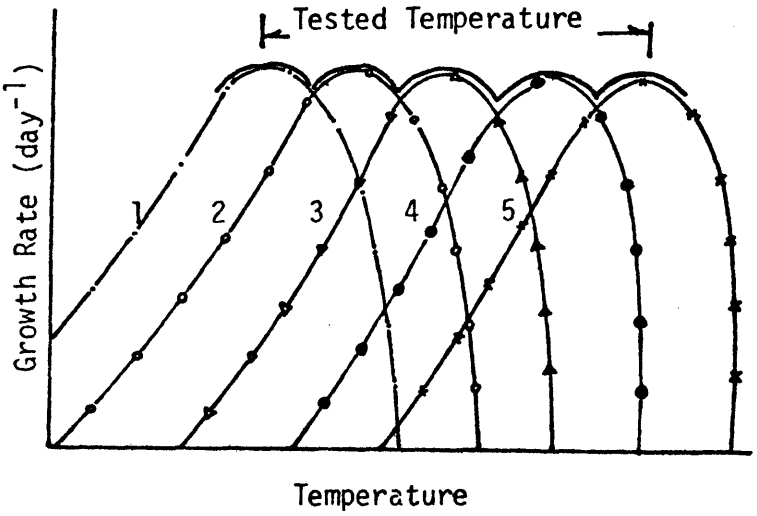

Figure 4.9: Possible Growth vs. Temperature Curves for the Phytoplankton Species in Goldman's studies.

case of Eppley's generalization. The five species might have growth vs. temperature curves shown in Figure 4.9 or the production of POC in Goldman's experiment was limited by factors other than temperature.

It is seen from Table 4.1 which summarizes formulations used to describe temperature effect on phytoplankton reactions that some models consider temperature effect while others do not. When temperature dependence is considered, two types of formulation are used:

$$(K_T)^{\Delta T} \tag{4.19}$$

$$\exp\left(-2.3\left|\frac{T-T_{opt}}{T_{div}}\right|\right) \tag{4.20}$$

Clearly, equations 4.19 and the equation proposed by Eppley (eq. 4.17) are subsets of equation 4.20; therefore, equation 4.20 is retained as the formulation to describe temperature effect in the present model.

4.3.3 The Effect of Limiting Nutrient

The growth of phytoplankton is controlled by the nutrient which is in shortest supply. Droop (1974) found that there is no multiplicative effect of phosphorus and vitamin B_{12} limitations on the growth of Monochrysis lutheri and Rhee (1978) shows that there is clearly no simultaneous limitation of growth by phosphorus and nitrogen. It is, therefore, assumed in this model that the growth of phytoplankton is controlled by one nutrient. We will consider a case of phosphorus limitation which is typical for most lakes in the temperate region (Golterman, 1975).

The effect of phosphorus on phytoplankton has been studied by many

Table 4.1

The Effect of Temperature on Phytoplankton Reactions

Model	Phytoplankton Reactions	Formulation	Comments
Chen and Orlob (1972)	growth, respiration	$(K_T)^{\Delta T}$	growth rate = C uptake rate = P uptake rate = N uptake rate respiration rate = rate of transformation of phytoplankton-P to PO_4 = rate of transformation of phytoplankton-N to NH_4 = rate of transformation of phytoplankton-C to CO_2
Thomann and DiToro (1975)	growth, endogeneous respiration	$(K_T)^{\Delta T}$	growth rate = same as Chen & Orlob's endogeneous respiration = rate of transformation of phytoplankton P, N or C to non-living P, N or C respectively
Richey (1977)	photosynthesis, death	no temperature dependence	photosynthesis = net C uptake rate death rate = rate of transformation of phytoplankton to detritus
Jørgensen (1976, 1978)	photosynthesis, respiration,	$\exp(-2.3\left\|\frac{T-T_{opt}}{T_{div}}\right\|)$	photosynthesis = C uptake rate respiration = rate of transformation of phytoplankton-C to CO_2
	mortality	no temperature dependence	growth = phytoplankton biomass increase rate mortality = rate of transformation of phytoplankton to detritus

*In both Snodgrass & O'Melia's (1973) and Imboden & Gachter's (1978) models, there is no explicit formulation which relates the temperature effect upon phytoplankton reactions.

researchers, mostly in chemostat studies whose results are reviewed briefly in section 4.3.3.1(A). The effect of phosphorus on photosynthetic rate of batch cultures is presented in section 4.3.3.1(B).

4.3.3.1 Effect of Phosphorus

(A) Chemostat Result

Chemostat, an historically important laboratory method for studying the relationship between phytoplankton growth and nutrients, is described in an excellent paper by Herbert (1956). This method schematized in Figure 4.10 is often referred to as steady-state continuous culture. Nutrient is continuously supplied to a chamber whose content is simultaneously withdrawn at the same rate of nutrient flow. The chamber is continuously stirred with light and temperature kept constant. After a sufficient time, the inoculated phytoplankton culture will reach a steady state condition. Mathematically, the chamber is considered as a fully mixed reactor where all constituents are uniformly distributed in space. The concentration variation of the constituents in this fully mixed chamber can be described by:

$$\frac{dX}{dt} = (\mu - D)X \tag{4.21}$$

$$\frac{dS}{dt} = -\rho X + D(S_i - S) \tag{4.22}$$

$$\frac{dQ}{dt} = \rho - \mu Q \tag{4.23}$$

where μ = growth rate; X = the organism concentration, S = the substrate concentration; Q = the intracellular nutrient content per organism;

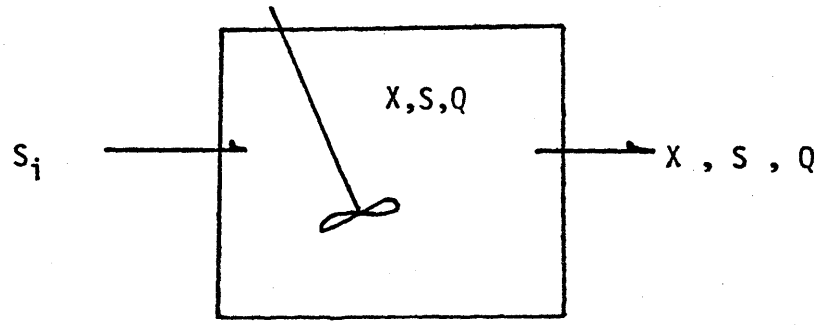

Figure 4.10: Schematic Representation of Chemostat

D = the dilution rate defined as the ratio of flow rate to chamber volume; ρ = uptake rate, and S_i refers to inflow substrate concentrations. At steady state, the relationships among the constituents are defined by

$$0 = \mu_\infty - D \tag{4.24}$$

$$0 = -\rho_\infty X_\infty + D(S_i - S_\infty) \tag{4.25}$$

$$0 = \rho_\infty - \mu_\infty Q_\infty \tag{4.26}$$

where the subscript $^\infty$ denotes the steady state condition. D and S_i are known conditions and the concentrations X_∞ and S_∞ can be measured so that the relationship among all these variables can be defined.

Many investigators have studied the effect of phosphorus on phytoplankton growth (measured as cell division rate). All observed a hyperbolic relationship between the growth rate and the cell phosphorus content (measured as P/cell) (Fuh, 1971; Rhee, 1973; Burmaster, 1978) as first observed by Droop in studying the effect of B_{12} upon phytoplankton growth (see section 4.3.3.2).

Goldman (1977) explicitly measured the phytoplankton biomass in terms of particulate carbon and also observed the similar hyperbolic relationship as other researchers:

$$\mu = \mu_{max} \frac{Q-q}{Q} \tag{4.27}$$

where μ = particulate carbon increase rate; μ_{max} = maximum particulate carbon increase rate; Q = phosphorus to carbon ratio in the cell; q = minimum phosphorus to carbon ratio below which there is no growth. This relationship suggests that:

(the net carbon increase rate = $\mu_{max} \frac{Q-q}{Q}$) or

$$(k_p - r - r_p - r_e) = \mu_{max} \frac{Q-q}{Q} \tag{4.28}$$

Usually, the light condition is kept at optimal intensity; that is, there is no photoinhibition ($r_p = 0$) so that equation (4.28) can be written as:

$$k_p - r - r_e = \mu_{max} \frac{Q-q}{Q} \tag{4.29}$$

The relationship derived from chemostat studies is often criticized as a poor representation of the dynamic condition. The criticism is well taken since a relationship at steady state does not have to hold for the transient conditions. In order to apply this relationship to describe the transient condition, we have to assume that the functional relationship is time independent.

(B) Batch Culture Result

Senft (1978) extended the study of phosphorus effect upon phytoplankton growth further by looking into the photosynthetic rate of a batch culture. Phytoplankton was inoculated in a flask to which other nutrients except phosphorus were supplied in excess. The flask was continuously illuminated and temperature was kept constant. The batch culture was harvested 48 to 192 hours after the inoculation and the photosynthetic rate was measured by the oxygen method. He found a hyperbolic relationship between the cell phosphorus content and the gross oxygen production rate at the optimal light intensity. Three biomass measurements were used for computing the cell phosphorus content: cell number, cell volume, and chlorophyll-a. All measures indicated significant correlation and although the ratio of phosphorus to chloropyll-a gave the best correlation, the P/C ratio is used for consistency. If we assume that the photosynthetic quotients were constant for all the experiments, Senft's result may be expressed in terms of carbon fluxes as follows:

$$k_p = \frac{\mu_{max}}{PQ} \frac{Q-q}{Q} \tag{4.30}$$

where PQ = photosynthetic quotient defined as the molar ratio of O_2/CO_2.

Since excretion does not consume oxygen, the oxygen method gives no information on the carbon excretion (see section 4.2.2). If the rates of both respiration and excretion are either independent of nutrient or linearly related to $(Q - q)/Q$, then during the transient, short-term process of carbon fixation, the following relationship may be assumed to exist:

$$k_p - r - r_e = k_1 \frac{\mu_{max}}{PQ} \frac{Q-q}{Q} = \frac{\mu'_{max}}{PQ} \frac{Q-q}{Q} \tag{4.31}$$

where k_1 is a constant and $\mu'_{max} = k_1 \mu_{max}$.

4.3.3.2 General Formulations

In defining the relationship between phytoplankton growth rate and phosphorus concentration as the limiting nutrient, two formulations have been proposed: constant P cell quota and variable P cell quota. The constant P cell quota formulation expresses phytoplankton growth rate as a hyperbolic function of external ortho-P concentration; the variable P cell quota formulation expresses phytoplankton growth rate as a hyperbolic function of internal P concentration. The hyperbolic relationship between substrate concentration and the growth rate of microorganism is often referred to as Monod theory.

Monod theory, the first mathematical expression for growth-nutrient relationship, was proposed by Monod in 1942 based on studies of the relationship between bacterial growth and the substrate concentration. According to Monod theory, the growth rate of bacteria is a hyperbolic

function of the limiting nutrient concentration and the production of bacteria biomass is related to the substrate consumed by a constant yield coefficient. Herbert et al. (1956) conducted chemostat tests in an attempt to obtain quantitative data to test the general validity of Monod's theory. The experimental results using Aerobacter cloacae as the bacteria specie were in general agreement with the theory. This theory, whose use in describing the bacteria growth-substrate relationship is widely accepted, has been extended to describe limiting nutrient effect upon phytoplankton growth rate.

There has been increasing evidence from chemostat studies, however, that the yield coefficient for phytoplankton varies with its growth rate and a simple empirical relationship exists between the rate of growth of a phytoplankton cell and the internal nutrient concentration or cell quota of a clearly limiting nutrient. A non-exhaustive list of these studies includes:

Monochrysis lutheri with B12 as the limiting nutrient (Droop, 1968)

Skeletonema costatum with B12 as the limiting nutrient (Droop, 1970)

Isochrysis galbana with nitrate as the limiting nutrient (Caperon, 1968)

M. lutheri and C. nana with nitrate as the limiting nutrient (Caperon and Meyer, 1972)

Thalassioseia pseudonana with silicon as the limiting nutrient (Paasche, 1973)

All these studies supported the theory proposed by Droop which states that the general growth rate of a phytoplankton cell is a hyperbolic

function of the cell quota of the limiting nutrient. The outside nutrient concentration only affects the growth rate indirectly.

It is the purpose of this section to discuss the nature of the two formulations and the feasibility of their application in modeling the phosphorus-limited phytoplankton growth in a large water body system.

(A) Monod's Theory

In studying bacterial cultures, Monod (1942) observed that at low substrate concentrations, the growth rate is a linear function of the substrate concentration. It increases with increase in substrate concentration up to a certain limit, after which the increase in nutrient no longer accelerates the growth rate and the cell remains at its maximum growth rate. The observed response to the external substrate concentration in terms of cell division rate is given for bacterial species in Figure 4.11. Monod commented: "Several mathematically different formulations could be made to fit the data. But it is convenient and logical to adopt a hyperbolic function." The suggested hyperbolic function takes the following form

$$\mu = \mu_m \frac{s}{k_s + s} \tag{4.32}$$

where μ = growth rate, μ_m = maximum growth rate, s = substrate concentration, k_s = half saturation constant.

Monod further introduced the concept of "growth yield", Y, defined as

$$Y = \frac{\text{amount of bacterial substance formed}}{\text{amount of limiting nutrient utilized}} = \frac{G}{\mu} \tag{4.33}$$

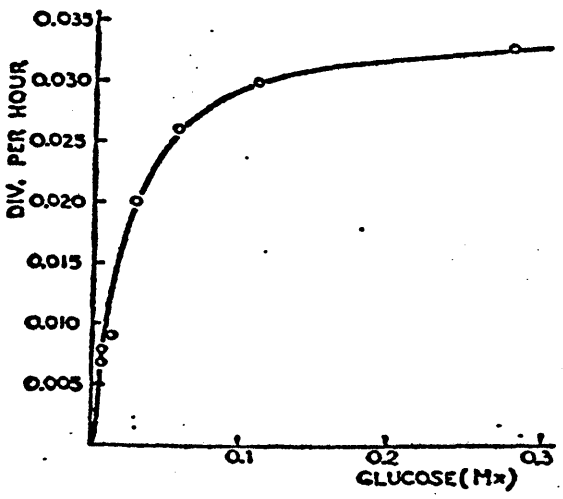

Figure 4.11: Bacteria Growth Rate as a Function of Substrate Concentration (from Monod, 1942)

Y was found to be fairly constant for bacteria with respect to organic source (see Table 4.2). So, if G is regarded as a measure of a "standard" cell concentration, 1/Y represents the amount of limiting nutrient used up in the formation of a "standard" cell.

Table 4.2

Total Growth of Purple Bacteria with Acetate as Limiting Factor [after Van Niel, 1944]

Acetate (mg/ml.)	0.5	1.0	2.0	3.0
Total Growth (mg/ml.)	0.18	0.36	0.70	1.12
K	0.36	0.36	0.35	0.37

(B) Droop's Theory

Droop (1968) studied the behavior of phytoplankton Monochrysis in the chemostat with limiting nutrient concentration of vitamin B12. Due to his inability to obtain kinetic data that fit the Monod equation, Droop searched for other formulations and found that a hyperbolic relationship existed between cell quota and dilution rate (see Figure 4.12). The relationship can be expressed as:

$$D = D_m \frac{Q-q}{Q} \qquad (4.34)$$

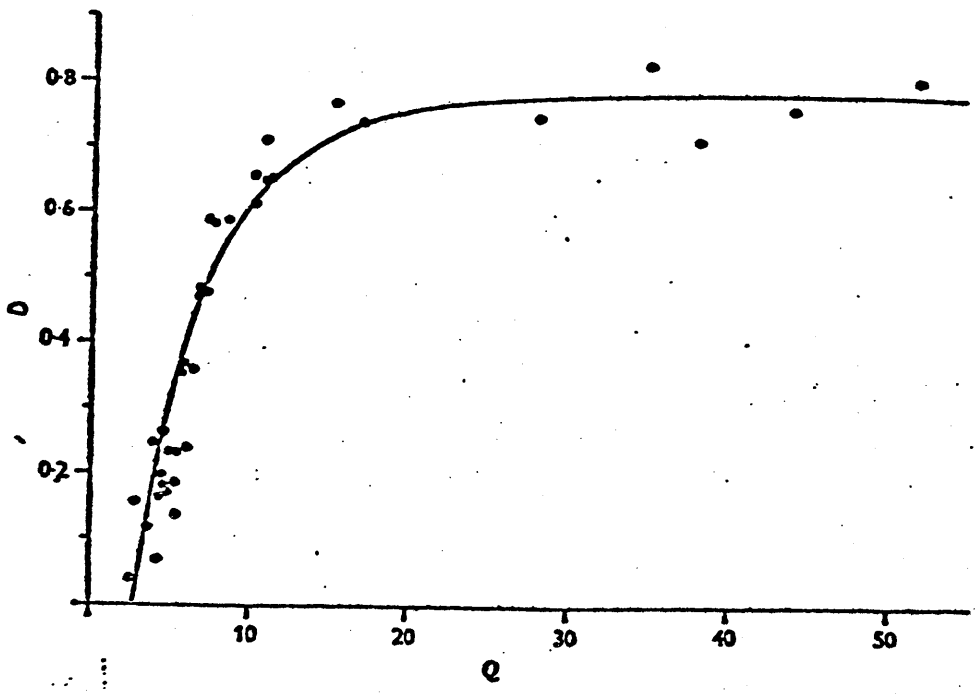

Figure 4.12: Relationship between Phytoplankton Growth Rate and Cell Quota (from Droop, 1968)

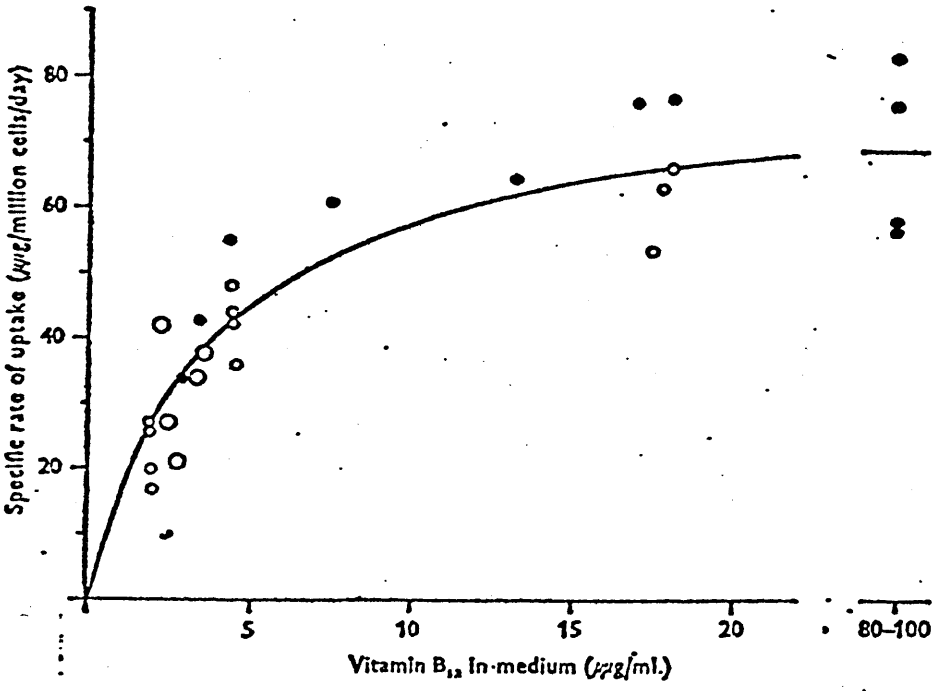

Figure 4.13: Specific Uptake Rate as a Function of External Substrate Concentration (from Droop, 1968)

where Q = cell quota and q = the minimum cell quota at which D = 0. Since at steady state the growth rate equals the dilution rate, the previous expression can be written as:

$$\mu = \mu_m \frac{Q-q}{Q} \tag{4.35}$$

At low Q, the growth rate of algae is proportional to Q and asymptotically reaches the maximum growth rate, μ_m, as Q becomes large.

The nutrient uptake rate under dynamic conditions was also studied. Figure 4.13 shows uptake rate against vitamin B12 concentration and it is seen that the functionality

$$\rho = \rho_m \frac{S}{K_\rho + S} \tag{4.36}$$

is suitable in describing the relationship, where ρ = uptake rate, ρ_m = maximum uptake rate, K_ρ = half saturation constant for uptake rate.

(C) Discussion

The phosphorus content in a phytoplankton cell may fluctuate widely because phytoplankton has the ability to accumulate intercellular phosphorus. Ketcham (1939) was one of the first to show that when grown with a supply of P, marine diatoms may accumulate an excess of phosphorus which subsequently enables them to grow in the absence of an external supply of P. Rodhe (1948) later demonstrated similar behavior in various freshwater phytoplankton. The ability of phytoplankton to accumulate phosphorus occurs even when they are grown at very low phosphorus concentration levels. Mackereth (1953) noticed that Asterionella formosa can take up

ortho-P from solutions containing 1 μg P ℓ^{-1} to accumulate as much as 7 μg P per 10^6 cells, which is more than 100 times the limiting P content. This high intercellular P concentration enables the phytoplankton to grow optimally after the depletion of ortho-P in the solution. Mackereth further demonstrated the same behavior of Asterionella in its natural environment of different phytoplankton species. Table 4.3 summarizes some reported values of phosphorus content of different phytoplankton species. The phosphorus content varies by a factor of 10 to 100 within the same species, in phytoplankton cells and it is doubtful that the constant P/biomass assumption applies.

Table 4.3

Species	Phosphorus Content, 10^7 μg-P/cell	Reference
Scenedesmus	9-90	Franzen, 1932
Asterionella	0.6-40	Lund, 1950
formosa	0.6-70	Mackereth, 1953
Chlorella	1-15	Alkholy, 1956
Phaeodactylum tricornutum	0.6-21	Kuenzler & Ketchum, 1962

The profound evidence of variable P content in phytoplankton cells, however, still cannot convince modelers of the necessity of using variable cell quota formulation to replace constant cell quota formulation in modeling phytoplankton growth in a P-limited aquatic system. The constant P cell quota formulation is still the most commonly used one. Five of the reviewed models use the constant P cell quota formulation: Chen and

Orlob (1972), Thomann and DiToro (1975), Snodgrass and O'Melia (1975), Richey (1977) and Imboden and Gachter (1978). Only one of the reviewed model uses variable P cell quota formulation: Jørgensen (1976).

The use of variable P cell quota formulation calls for modelling the phytoplankton growth in two sequential steps: the uptake of external ortho-P into the cell and the subsequent growth dependence on the internal P content. Therefore, additional formulations and parameters have to be introduced, and that is the main cause of many modelers' reluctance in accepting this formulation. For example, Kremer and Nixon (1978) suggest that the ability of phytoplankton to accumulate intracellular phosphorus only confers a strong advantage to species that have this ability in their competition with others. For a homogeneous species group without competition, Kremer and Nixon contend that:

> such complex schemes can be expected to follow closely the patterns of simple Monod kinetics, differing perhaps by short phase shifts in the reciprocal patterns of phytoplankton-nutrient oscillations. The additional programming complexity was not considered worth the possible improvement in the basic model.

Their statement, although unaccompanied by convincing evidence or a coherent quantitative description, reflects many modelers' opinion and will be discussed in the following paragraphs.

Burmaster (1978) showed that at cellular equilibrium the variable cell quota formulation can be expressed by an equivalent Monod function which replaces the growth rate as a function of external nutrient concentration. Cellular equilibrium is defined as the state at which the uptake of nutrient is balanced by cell division; that is,

$$\rho = \mu Q \tag{4.37}$$

Pairing equation (4.37) with the following two rate expressions:

$$\rho = \rho_m \frac{S}{K_\rho + S} \tag{4.38}$$

$$\mu = \mu_m \frac{Q-q}{Q} \tag{4.39}$$

it can be shown that:

$$\mu = \mu_m' \frac{S}{K_S + S} \tag{4.40}$$

where

$$\mu_m' = \mu_m \frac{\rho_m}{\rho_m + q\mu_m} \tag{4.41}$$

$$K_S = \frac{\mu_m \, q \, K_\rho}{\rho_m + \mu_m q} \tag{4.42}$$

Goldman (1977) confirmed that both external nutrient formulation and internal nutrient formulation can be simultaneously employed to represent experimental data from chemostat studies where the cell is at cellular equilibrium. Experiments were carried out over the entire growth rate region up to cell wash-out with marine Chrysophycea grown in a P-limited continuous culture. In discussing the relative utility of external nutrient formulation and internal nutrient formulation, Goldman emphasized that an important consideration in choosing the best equation to represent continuous culture data is the ease of collecting these data. The use of external nutrient formulation has serious draw-backs because of difficulties in measuring the residual limiting nutrient concentration over a wide range of dilution rates. This difficulty can be exemplified by the failure of many researchers to fit Monod theory to their data

(Caperon & Meyer, 1972; Droop, 1968, 1974; Fuhs, 1969). As Eppley and Regner (1974) pointed out, because the half saturation constant K_s for nutrient limited growth of marine phytoplankton is very small, the residual substrate concentration S will be undetectably low over a wide range of dilution rates D. Only as D approaches the washout rate does S increase to easily detectable levels. This region, however, is one of culture instability.

Equation (4.40) is based on the assumption of cellular equilibrium, that is $\rho = \mu Q$, a condition certainly satisfied in chemostat studies. Its applicability to dynamic situations, however, is open to question. The dynamic equation for cell quota follows a mass balance on the cell itself:

$$\frac{dQ}{dt} = \rho - \mu Q \tag{4.43}$$

By doing a perturbation analysis about the steady state values, DiToro (1980) showed that the time to reach cellular equilibrium (T_q) falls between 1/4 to one population doubling time under optimal conditions, i.e.,

$$\frac{1}{4} T_\mu < T_q < T_\mu \tag{4.44}$$

where $T_\mu = 1/\mu_m$. The result suggests that it is reasonable to assume that cells are at equilibrium since the internal cellular concentration can reach its equilibrium value more rapidly than the population can change significantly.

Even if the validity of the cellular equilibrium assumption is not

challenged, the difficulty of collecting data for function verification and parameter estimation for the external nutrient formulation as noted by Goldman (1977) in his laboratory experiments, is even more profound in the natural aquatic environment. Moreover, the determination of the concentration of ortho-P in natural water has been observed by many researchers to give little information on its capacity to sustain phytoplankton (Fogg, 1973; Schindler et al., 1972a). But perhaps the most important consideration is that the Monod formulation, which expresses the specific phytoplankton growth rate as a direct function of the external ortho-P concentration, will suffer from our inability to correctly measure the ortho-P concentration. The fact that the measured SIP may overestimate the true ortho-P concentration by as much as 100 times (see section 3.1) reflects our inability to detect the fluctuation of the the ortho-P concentration from the fluctuation of the measured SIP. Consequently, the measured SIP gives little information on the variation of the specific growth rate. A model containing a parameter directly obtainable from field measurement is preferable. The large discrepancy between the measured SIP and the ortho-P precludes the possibility of obtaining correct parameters needed for the Monod formulation.

Phytoplankton growth in its natural environment is often simultaneously limited by factors other than nutrient. If the growth rate and uptake rate are expressed as follows:

$$\mu = \mu_m \frac{Q-q}{Q} f(I)g(T) \tag{4.45}$$

$$\rho = \rho_m \frac{S}{K_\rho + S} \tag{4.38}$$

then at cellular equilibrium, equation (4.45) may be written as

$$\mu = \mu_m' \frac{S}{K_S' + S} f(I)g(T) \tag{4.46}$$

with

$$\mu_m' = \frac{\mu_m \rho_m}{\rho_m + \mu_m f(I)g(T)} \tag{4.47}$$

$$K_S' = \frac{\mu_m f(I)g(T)\ q\ K_\rho}{\rho_m + \mu_m f(I)g(T)q} \tag{4.48}$$

Therefore, the correct estimation of the parameters μ_m' and K_S' in the external nutrient formulation depends on the accurate knowledge of the functions f(I) and g(T). In contrast, the Droop equation, being dependent on the correct measurement of the more easily quantified parameters Q and μ, can be more readily verified.

So far we have only discussed the difficulty of obtaining the parameter values for the external nutrient formulation when compared with the internal nutrient formulation. However, the key issue is on the constant cell quota or variable cell quota. As DiToro (1980) rightly pointed out, cellular equilibrium, the necessary condition for using an external nutrient formulation in place of an internal nutrient formulation, does not mean constant cell quota. It only means that the cell achieves a new cell quota which is in equilibrium with its growth rate before the population size has changed significantly. In order to simulate the growth of phytoplankton it will be necessary to simulate the change of yield coefficient which is the inverse of the cell quota. Since the cell

quota is variable, it is impossible to know this quantity without explicitly including cell quota as a state variable and a variable cell quota formulation should be used.

4.3.4 Summary

In extracting information from the literature to model phytoplankton growth, it is imperative that the values obtained by comparable. This comparability can be difficult if not impossible because of the numerous criteria which have been used in evaluating the phytoplankton biomass. Often these criteria have not been used critically, making data interpretation difficult (Wetzel, 1975). Consequently, different terminologies compound difficulties in the modeling effort. Reviews of the terminology chaos can be found in Lund and Talling (1957), Strickland (1960), and Vollenweider (1969). For example, partly due to the different biomass measurements and partly due to the various interest of the scientists, growth has been reported in various units. Consequently, the method of measurement as well as the duration of measurement vary. Table 4.4 lists the commonly used terminology and methods in studying the effect of various environmental factors upon phytoplankton growth rate

Table 4.4

factor	definition of growth	method	duration
light	photosynthetic rate	^{14}C or oxygen method	2-6 hrs
nutrient	cell division rate	chemostat	day-weeks
temperature	biomass increase rate	chemostat, ^{14}C or oxygen method	hrs-weeks

Photosynthetic rate, cell division rate and biomass increase rate are closely related. However, they are not necessarily linearly related during the period of measurement. Therefore, assumptions have to be made in every step of the modeling construction in order to arrive at a consistent formulation. Table 4.5 summarizes the assumptions made in this modeling effort.

Table 4.5

Summary of Assumptions used for Phytoplankton Growth Formulation

Variable	Definition or Model Formulation	Assumption(s)
Growth rate	net carbon increase rate	carbon/biomass = constant
Combined environmental effect	f(I) g(T) h(limiting nutrient)	effects of environmental factors are separable
Light effect formulation	$\frac{I}{I+K_I}$	1. ^{14}C method measures the net carbon increase rate 2. All the fluxes take place during the course of measurement. 3. Photoinhibition is caused by photorespiration. 4. Photorespiration does not occur in the lake.
Temperature effect	0 or	-----
	$\exp(-2.3)\left\|\frac{T-T_{opt}}{T_{div}}\right\|$)	-----
Nutrient effect	$\frac{Q-q}{Q}$	If chemostate result is cited: 1. Phosphorus is the limiting nutrient 2. Stationary function 3. All carbon fluxes take place If photosynthesis result is cited: 1. Phosphorus is the limiting nutrient 2. All the carbon fluxes take place 3. Respiration and excretion are either independent of Q or linearly related to Q-q/Q.

Chapter 5

MODELING PHYTOPLANKTON CONCENTRATION IN L227

A CASE STUDY

5.1 Introduction

The simulation of phytoplankton concentration in lakes cannot be performed independently of the temperature simulation because thermal stratification affects the mixing process in the lake, which in turn affects the distribution of nutrients and phytoplankton, and temperature also affects biological reactions. Consequently, a lake phytoplankton model consists of two submodels: the hydrothermal and the biological model. Figure 5.1 is a schematic diagram illustrating the structure of a lake phytoplankton model and the linking between its two submodels. The hydrothermal model computes the vertical hydrologic transport processes and the temperature distribution. The wind mixing model, previously described in section 2.3, is the chosen hydrothermal model for this study (see discussion in section 2.2). The output of this model at each time step is the temperature profile and the depth of the FML. The biological model uses a reaction/mixing algorithm analogous to the heating/mixing algorithm of the hydrothermal model to compute the time varying vertical distribution of the model state variables. It first computes the variation of the concentration by solving the one-dimensional mass balance equations of the following general form (one for each biological state variable):

$$\frac{\partial C}{\partial t} = \frac{D}{A}\frac{\partial}{\partial z}\left(A\frac{\partial C}{\partial z}\right) + \frac{r_i}{\rho} + \frac{r_e}{\rho} \qquad (5.1)$$

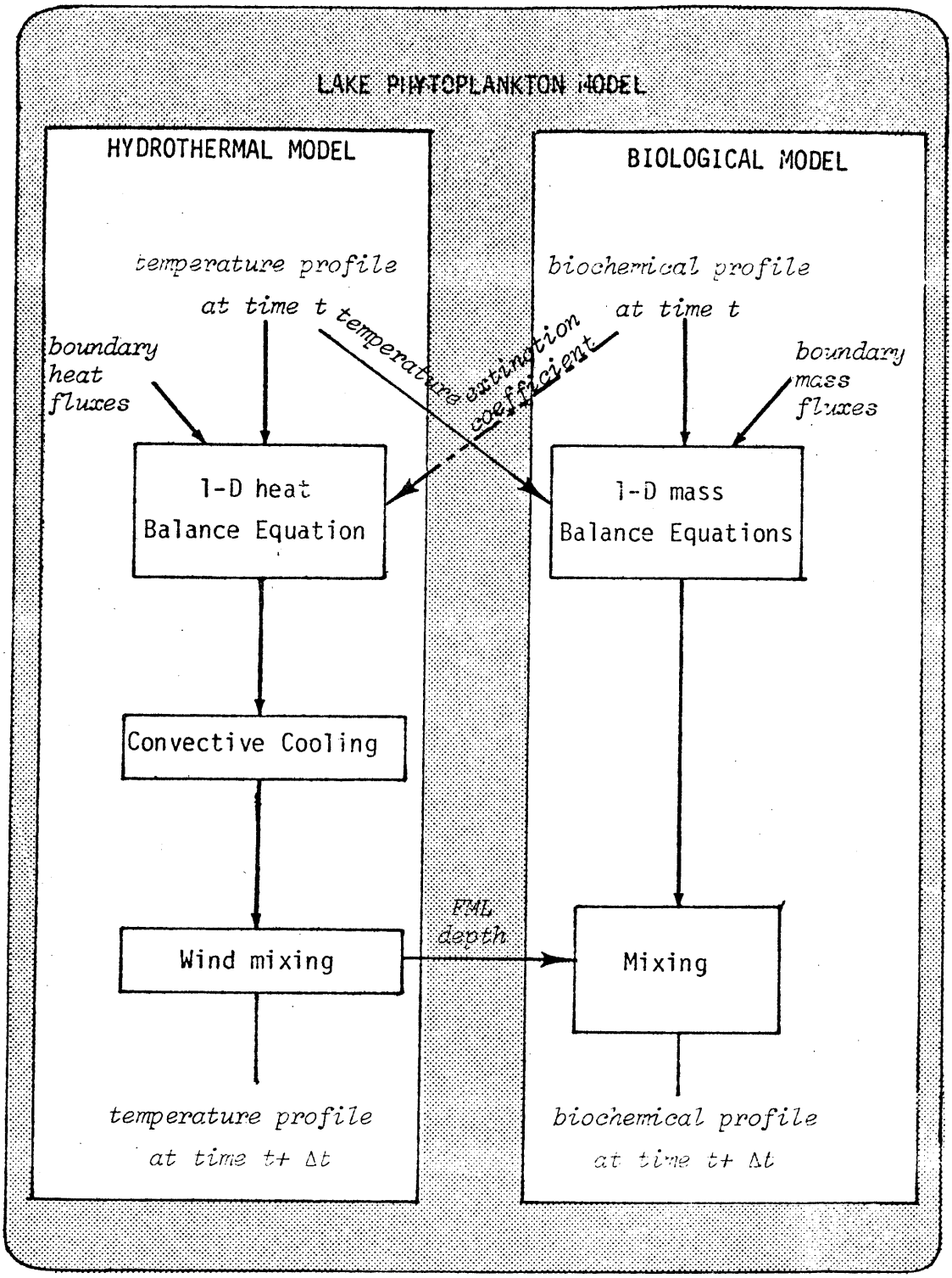

Figure 5.1: Schematic Diagram of Lake Phytoplankton Model

where C = the concentration of a biological variable (averaged over the horizontal plane); D = mass molecular diffusivity; r_i = the time rate of internal addition of mass of substance C per unit volume by transformation of reaction processes; r_e = the time rate of external addition of substance C per unit volume by addition across the lateral, free surface and bottom boundaries of the system; and ρ = the density of water. After the calculation of the 1-D mass balance equation, the biological model uses the mixed layer depth calculated from the temperature model to redistribute the mass in the water column. The concentration of the dissolved and suspended material affects temperature through its influence on the absorption of the solar radiation in the water column.

It is essential to realize that our ability to represent complex aquatic biological transformations by means of mathematical expressions is less well developed than the state of knowledge in the geophysical area. As a result, field data plays an important role in identifying the final biological model structure.

In the beginning of this research project, much effort was spent searching for available field data for model calibration and verification. Table 5.1 is a list of the data needed for this modeling effort. The availability and the frequency of data collection became an important consideration in our lake selection. The extensive coverage of the Canadian Experimental Lake Project in limnology journals, particularly the journal of the Fisheries Research Board of Canada, enabled us to learn about this project and to appreciate the advantages of the data collected by Schindler and colleagues.

The simulation of L227 phytoplankton is used as a case study to illustrate considerations on the number of model state variables and on the model formulations presented in Chapters 3 and 4.

Table 5.1

Lake Data Specification

Boundary Conditions

- Meteorological data - solar radiation
  relative humidity
  cloud cover
  wind speed
- Hydrologic data - precipitation
  inflow/outflow
  seepage
- Nutrient input*

In-lake Information

- Temperature
- Extinction Coefficient
- Phytoplankton
- Zooplankton
- Phosphorus
- Nitrogen
- Carbon
- Silicate
- pH
- Major Metal Ions

Lake Morphometry

*If the major input is through inflow, the temperature of the inflow and its chemical composition should be known.

5.1.1 The ELA Project

The Experimental Lake Project is a response to the International Joint Commission (IJC) recommendation for better understanding of the eutrophication problem. The site chosen for this project is now referred to as "ELA", the Experimental Lake Area. ELA is located approximately 170 miles east of Winnipeg, Manitoba, and 35 miles east-southeast of Kenora, Ontario. There are several factors which make ELA an ideal site for this case study:

(1) The area is unpopulated; therefore, it is essentially free of uncontrollable nutrient inputs such as sewage, fertilizer surface runoff and animal waste.

(2) The area is located on the Precambrian Shield and is free of groundwater influence.

(3) It has a high density of small stratified lakes. The lakes are close enough together to allow their responses to chemical manipulations to be compared without the influence of meteorologically induced variations. The small size of the lakes eases the task of chemical manipulation, and thermal stratification of these lakes makes them hydrothermally similar to many larger lakes.

To ensure the preservation of this ideal condition, in April 1968 the Fisheries Research Board of Canada concluded an argreement with the Ontario Department of Lands and Forest. This agreement, valid for a period of 20 years and including a renewal clause, enables the Fisheries Research Board of Canada to restrict the use of 17 drainage areas and to have exclusive use of 46 lakes in the ELA (Johnson et al., 1971).

L227 is a lake with extremely low carbon concentration where the task was set to understand the lake's short-term and long-term responses to enrichment by phosphorus and nitrogen. Since 1969 the lake has been artificially enriched with P and N and has also been regularly sampled. Like other lakes in ELA, L227 is generally free from nutrient input other than artificial fertilization. The artificial input of P, N is approximately 10 times the natural input (Schindler et al., 1971). This high level of control of the nutrient budget in itself is a tremendous advantage over many other field data. Most lake data sets contain water quality measurement without a simultaneous measurement of the nutrient input or hydrologic input. Also, the difficulty of obtaining a correct estimation of the nutrient input reduces the reliability of the conclusions drawn from studying lake responses. The importance of a correct nutrient input cannot be overstated. Moreover, the great number of publications on the observations of L227 experiment results provide detailed descriptions of this lake from various perspectives. Therefore, even though more than one lake was artificially fertilized in ELA, we have chosen L227 as our main source of data for model calibration and verification.

5.1.2 Characteristics of L227

L227 is a small circular lake (Figure 5.2) surrounded by tall jack pines, with a surface area of 5×10^4 m^2 and a volume of 2.2×10^5 m^3, which makes the mean depth to be 4.4 m. The deepest part of the lake is approximately 10 m. There is no stream flowing into the lake; surface runoff from the 49-hectare drainage area is the main source of inflow.

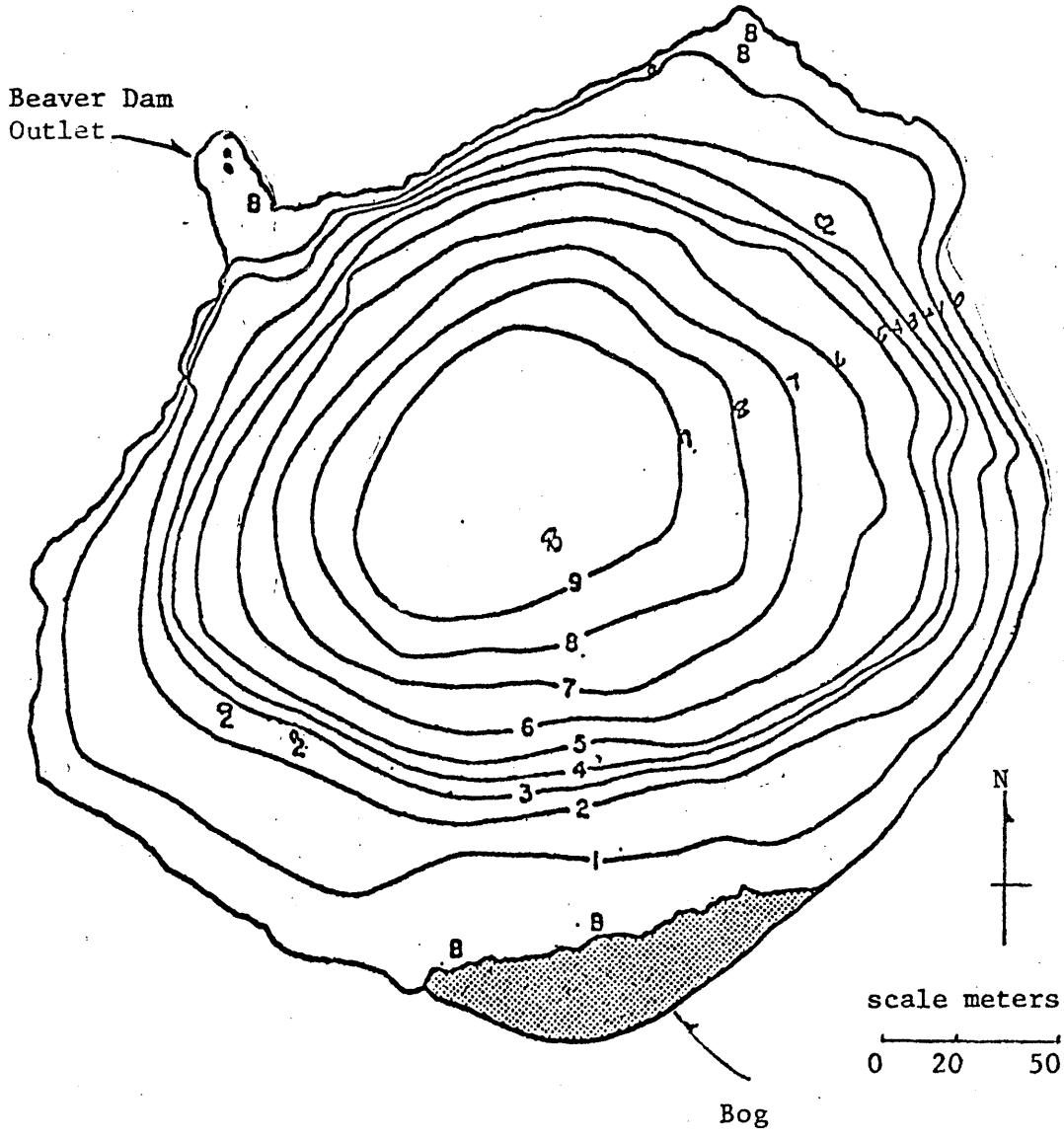

Figure 5.2 L227 Morphometry (from Johnson et al. 1971)

At the northwest corner of the lake there is a beaver dam outlet; the lake water flows over the beaver dam and into nearby lake 305 (Schindler et al., 1971).

The outflow generally shows higher values in April and May; however, the seasonal trend does show variation from year to year. The hydraulic retention time of L227 is estimated to be 1.4 - 2.9 years for the period 1970 to 1974 (Schindler, unpublished data). Ice covers the lake from November to April. During the ice-free season, the lake shows strong thermal stratification and becomes quickly stratified after the disappearance of the ice. For example, in 1969 the ice left the lake on the 24th of April; by midafternoon thermal stratification had become pronounced (Schindler et al., 1971). The spring mixing is incomplete. From May to October, the lake is stratified; in late October, the lake is fully mixed; the fully mixed period is usually short. Due to this monomictic nature and the short duration of the fully mixed period, the lower section of L227 is anoxic for most of the year. The anoxic layer extends from the bottom to approximately 4 meters from the surface.

The lake responds quickly to the addition of nutrients. A few weeks after the addition, "the lake was transformed to a teeming, green soup" (Schindler, 1974). Since then, the lake has become eutrophic. The summer chlorophyll-a concentration reached as high as 200 μg/ℓ. The extinction coefficient reached 2.8/m, coinciding with the occurrence of high chlorophyll-a concentrations.

There has been a continuous field sampling program since the beginning of nutrient addition in 1969. The frequency of field sampling

varied with the year. For example, the sampling of the ice-free period was made on a weekly basis from 1969 to 1971, and was made on a bi-weekly basis from 1972 to 1974. After 1974, sampling has been made every four weeks. The earliest year of our simulation is constrained by the availability of meteorological data. We were unable to obtain most of the meteorological data needed for lake hydrothermal simulation before the year 1973. Therefore, 1973 becomes our choice of the year for simulation.

Measurements were made at the deepest part of the lake at 1 m depth intervals. In the case of temperature measurement, a 0.25 m depth interval was used near the thermocline. Occassionally, one additional water sample was taken from 0.5 m depth.

5.2 Temperature Simulation

Temperature is used as the tracer to test the applicability of the MIT wind mixing model in describing the hydrodynamic transport process of L227. It is assumed that the density of the water in L227 is mainly governed by its temperature and since the extinction coefficient, which is influenced by the concentration of dissolved and suspended substances in the lake water has been measured at biweekly intervals, the temperature simulation may be commenced without a simultaneous computation of the biological variables.

The emphasis of this simulation is to predict the vertical temperature profile and the depth of the FML from given meteorological conditions. Measurements in lakes and reservoirs show that isotherms are horizontal except for cases with large through-flows such as the "run-of-the-river" reservoirs whose flow retention time is in the order of days. Since L227 has a flow retention time in the order of 2-3 years and the dominant forcing functions for lake temperature (such as solar radiation and atmospheric radiation) are uniform in the horizontal plane, it may be assumed that the temperature distribution is essentially one dimensional in the vertical direction with no significant differences in the horizontal plane. Therefore, the temperature measurement which was taken from only one station may be assumed to be representative of the whole lake temperature and may be used for comparison with the hydrothermal model output.

The amount of heat variation caused by inflow/outflow in L227 is small when compared with other heat sources; therefore, the inflow and outflow terms in equation (2.14) are neglected. Furthermore, since the

only outflow is the overflow from a beaver dam, the vertical advection velocity is also zero. That is, the 1-D heat balance equation (2.12) is now simplified to:

$$\frac{\partial T}{\partial t} = \frac{D}{A}\frac{\partial}{\partial z}\left(A\frac{\partial T}{\partial z}\right) - \frac{1}{A\rho c}\frac{\partial(\Phi_z A)}{\partial z} \qquad (5.2)$$

5.2.1 Input Data to the Hydrothermal Model

The simplified heat conservation equation (5.2) is approximated by considering heat flow through an internal control volume taken as a horizontal slice of the water body. L227 is divided into twenty horizontal slices each of 0.5 m thickness but of variable areas which conform to the actual bathymetric data listed in Table 5.2. Values at intermediate depths are linearly interpolated in the computer program.

Meteorological data for L227 were collected at the Rawson Lake meteorological station which was constructed in ELA in 1969; Rawson Lake is approximately two miles from L227. Short wave solar radiation is reported in the Annual Radiation Summary (Chapil, 1973) and other meteorological information, such as air temperature, relative humidity, wind speed and sunshine record, are reported in the Meteorological Records (Schindler and Beaty et al., 1976). Although wind speed and short wave solar radiation are also available on an hourly basis, only the daily average values are used.

The values of extinction coefficients at biweekly intervals are published in "Light Measurements in the Experimental Lake Area, 1969-73" (Reid et al., 1975). A linear interpolation on the biweekly measurements gives us the daily extinction coefficients.

Table 5.2

Lake 227 Areas

Depth (m)	0	1	2	3	4	5	6	7	8	9
Area ($10^4 m^2$)	5.00	4.17	3.30	2.85	2.60	2.31	1.81	1.30	0.888	0.510

*Area at 10 m depth is assumed to be the same as area at 9 m depth.

The period with all the necessary input data is from May 3 to October 29; the simulation period is chosen from May 15 to October 29 (135th to 302nd day).

Measurement of atmospheric longwave radiation is not available. Wunderlich's (1972) formula which modifies Swinbank's (1963) clear sky formula to include cloud effect is used for estimation:

$$\phi_a = 0.937 \times 10^{-5} \sigma T_a^6 (1.0 + 0.17 C^2) \quad (5.3)$$

where ϕ_a = atmospheric longwave radiation; σ = Stefan-Boltzmann constant = 1.171×10^{-6} kcal/m^2-day-K^4; T_a = air temperature in K; C = fraction of the sky covered by clouds (range 0 to 1).

Cloud cover in equation (5.3) may be estimated from the record of total clear sunshine hours:

$$C = 1 - \frac{S}{DL} \quad (5.4)$$

where S = total clear sunshine hours per day and DL = daytime hours per day. The daytime hours in ELA for the period from May to October range from 10.6 - 15.8 hours (Table 5.3) with an estimated mean of 13.9 hours. A sensitivity study of DL shows that there is no appreciable difference in the model's predicted temperature profile between a DL value of 11 and 15. Hence, a constant DL value of 14, which represents the mean estimated daytime hours and also the maximum recorded total clear sunshine hours (occurring on June 30, 1973), is specified for the whole simulation period.

The surface absorption coefficient of the incident solar radiation β, is set to 0.5 and measured wind speeds are multiplied by a factor of 0.7 to account for the sheltering and possible fetch limitation effect

on wind speed.

Table 5.3

Estimated Daytime Hours for ELA (49 42'N)
May to October

Month	May	June	July	Aug.	Sept.	Oct.
DL (hrs)	15.10	15.96	15.53	14.13	12.32	10.50

*DL = 4380 x f ÷ ND where DL = daytime hours of the month, f = the monthly percentage of daytime hours of the year, ND = the number of days in the month and 4380 represents the total annual daytime hours.

**The value of f is from Eagleson, P.S., "Dynamic Hydrology", 1976, McGraw-Hill.

5.2.2 Results of Simulation

The nine panels of Figure 5.3 are comparisons between model prediction and field data. In general, the wind mixing model satisfactorily simulates the vertical temperature distribution in L227. Starting October 15, the model tends to predict a slightly deeper fully mixed layer than field data suggest. This over prediction of the fully mixed layer in late fall could be due to our neglecting to include the effect of chemical species on water density.

For freshwater, the density change due to thermal expansion can be approximated by

$$\frac{d\rho}{dT} = - 0.0000126 \ (T-4) \qquad (5.5)$$

where ρ is in g/cm^3, T is in °C. The equation suggests that the density difference due to a temperature gradient becomes smaller as the temperature approaches 4°C. Thus, the density difference caused by chemical species becomes more important as the temperature approaches 4°C. L227 is a very eutrophic lake with a high concentration of suspended and dissolved substances, and with a pronounced gradient of these substances. The density of L227 as a function of temperature and chemical species was computed by Chen and Millero (1977) and Millero and Emmet (1976). The results of their computation is included in Table 5.4. For example, between depths 5 m and 8 m the density difference due to the temperature effect alone is 2.4×10^{-5} g/cm^3; when the effect of chemical species is included the density difference becomes 3.0×10^{-5} g/cm^3. This effect is negligible during the summer period of high stratification. The

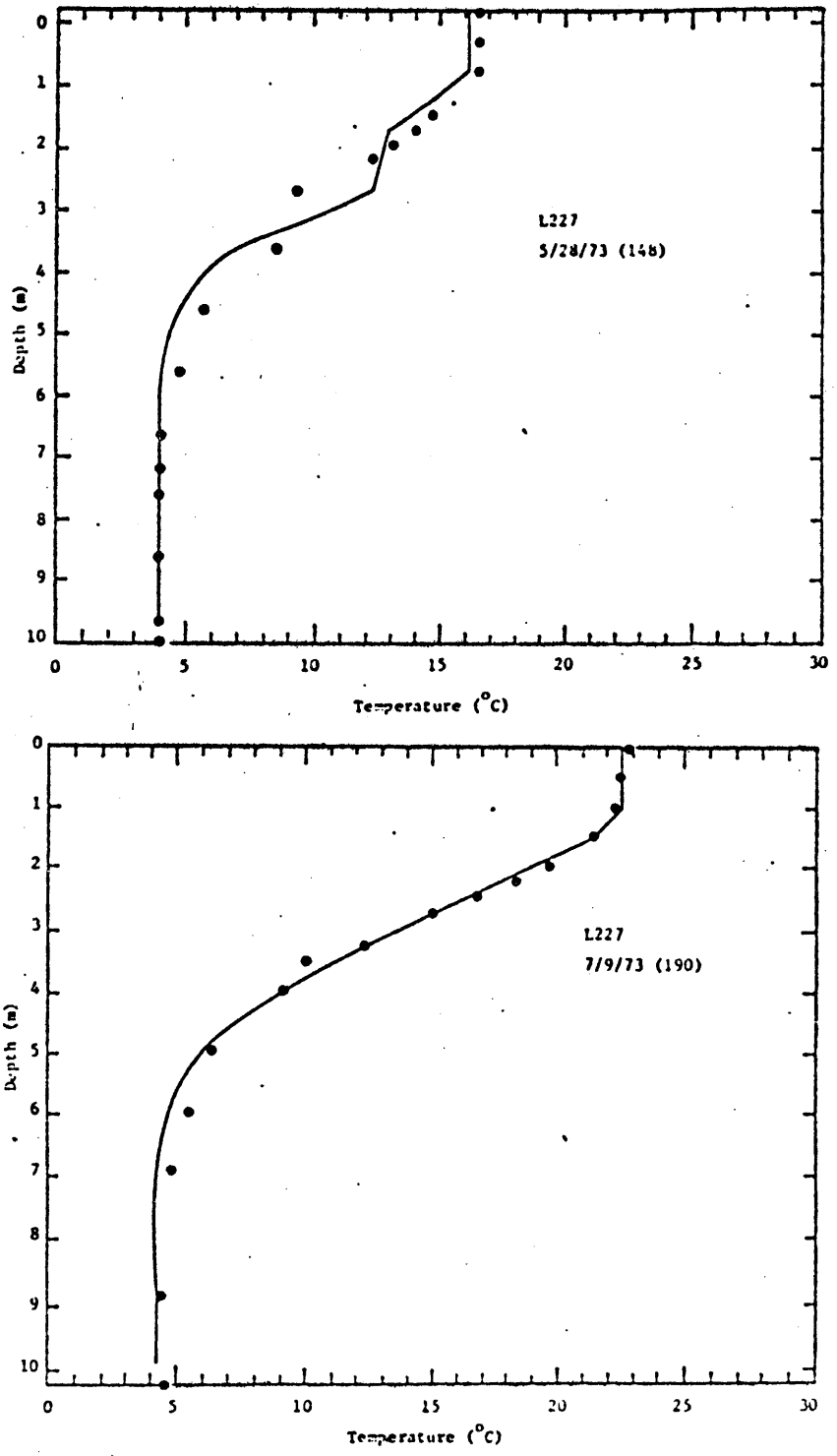

Figure 5.3: Temperature Simulation vs. Field Measurement

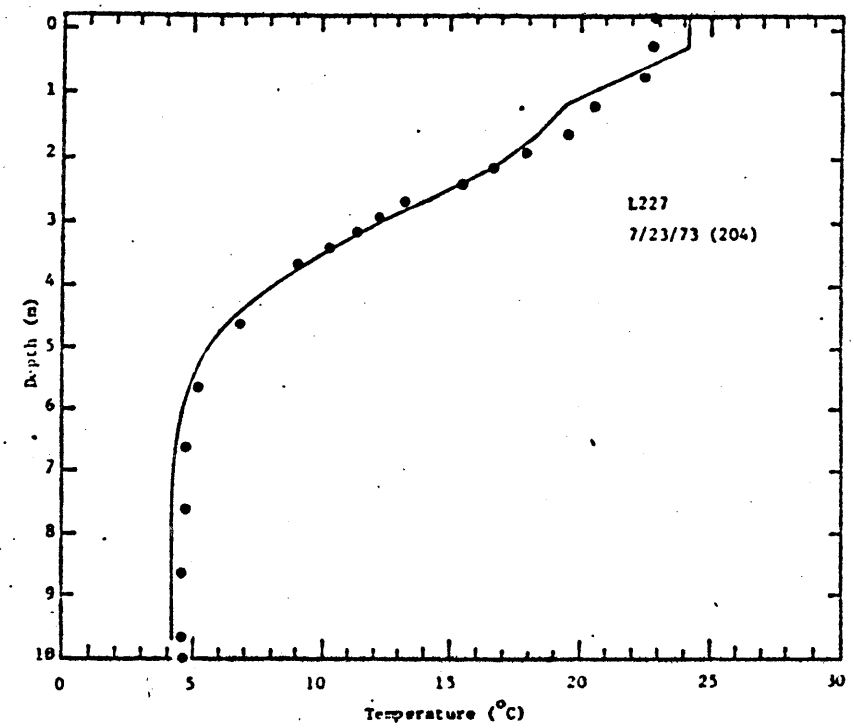

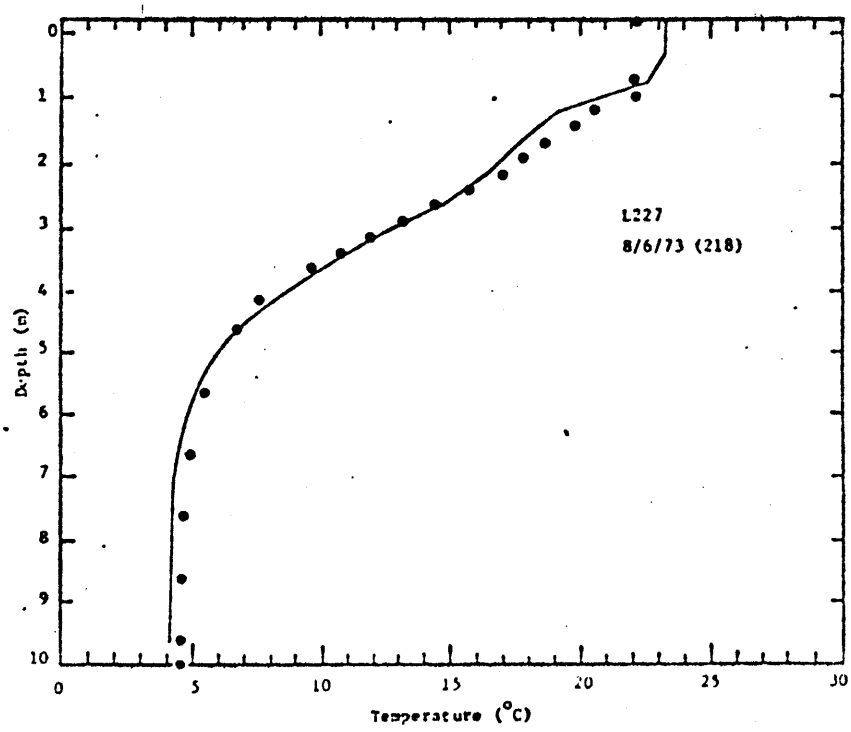

Figure 5.3: Continued

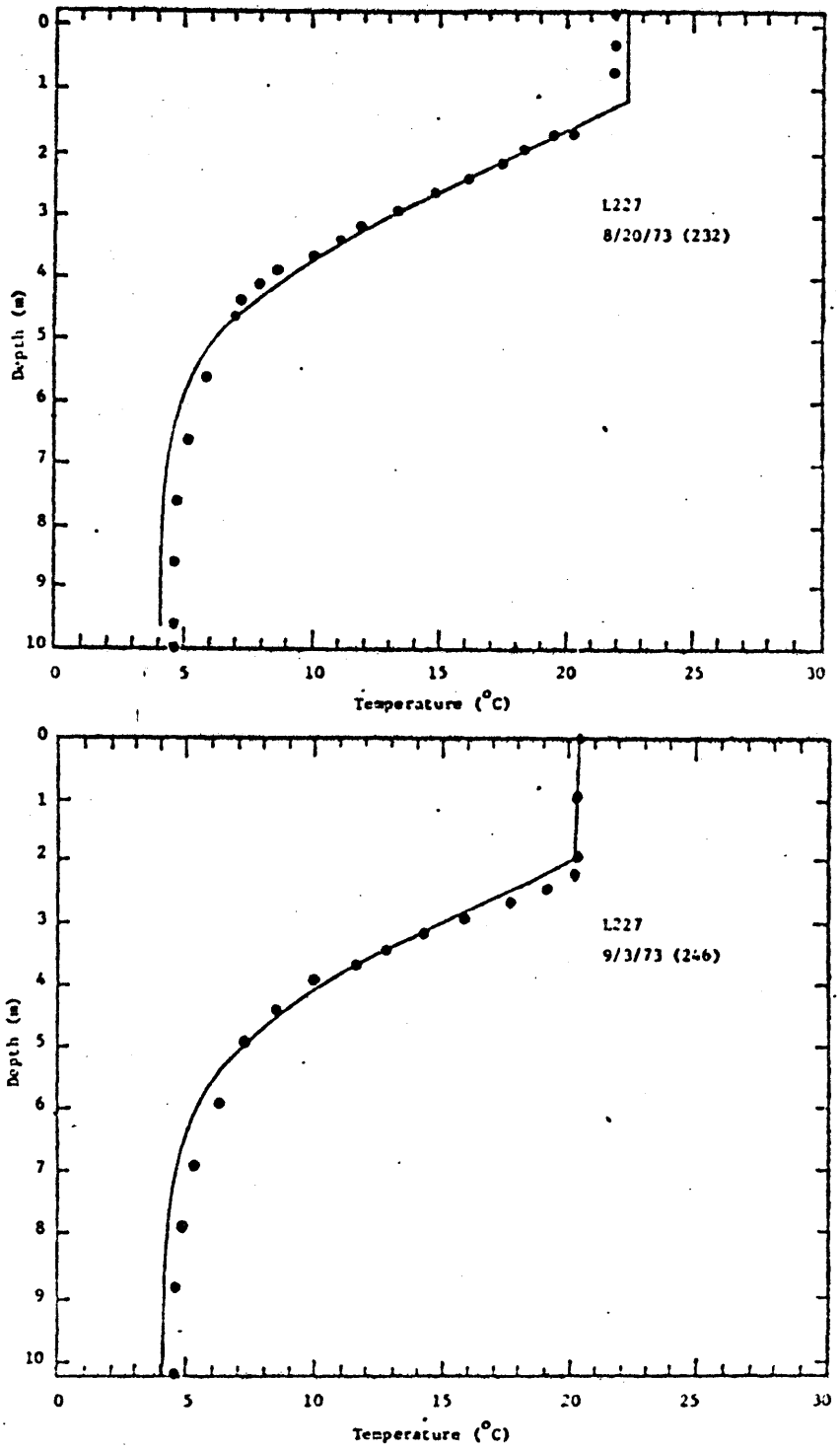

Figure 5.3: Continued

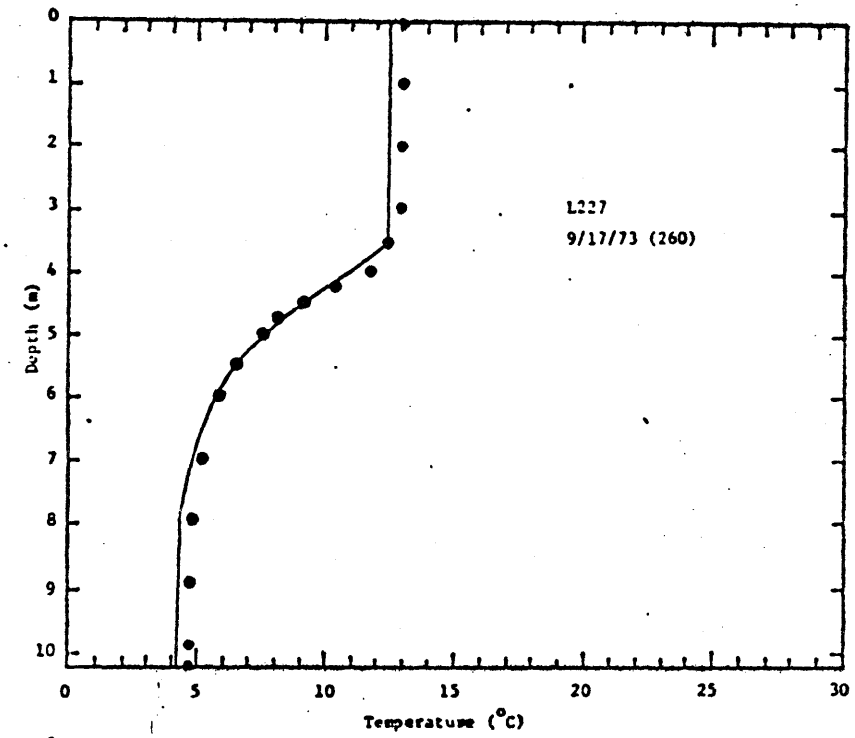

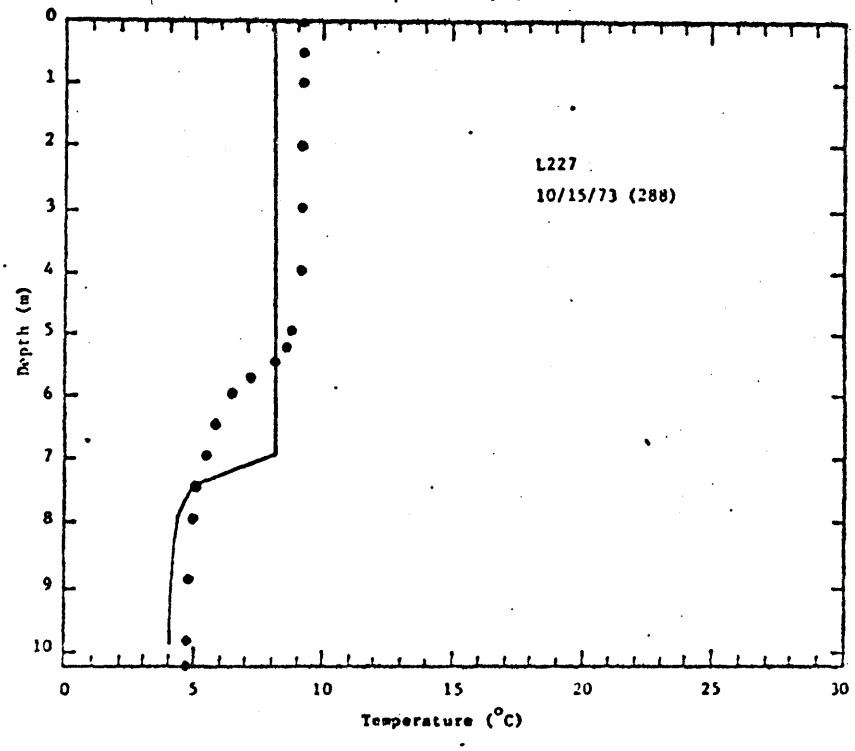

Figure 5.3: Continued

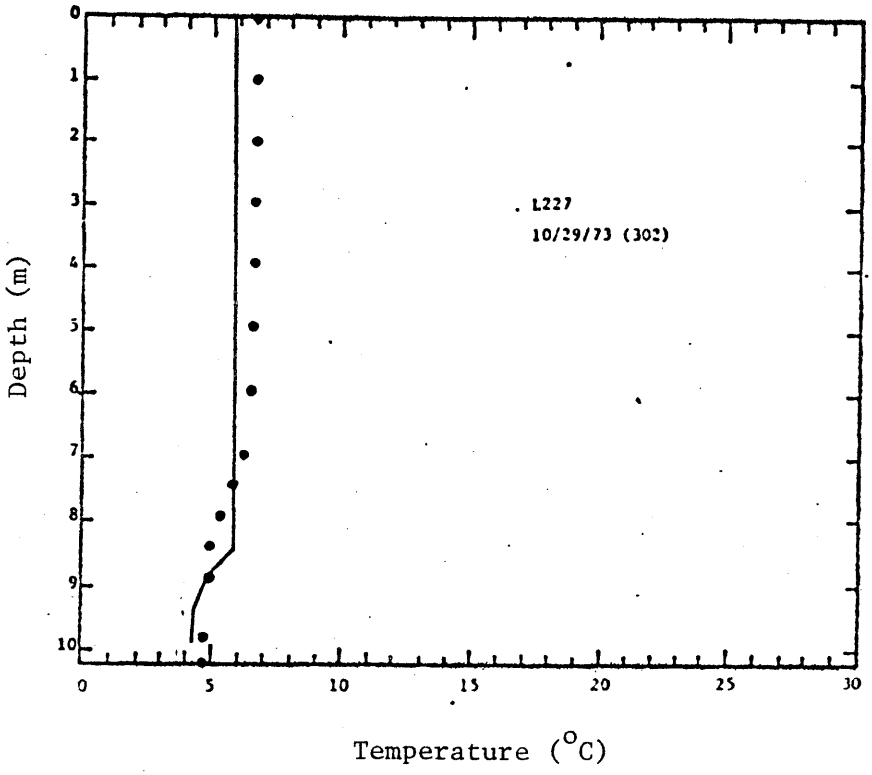

Figure 5.3: Continued

Table 5.4

Water Densities in L227 Due to Temperature, Dissolved Salt and Gas Concentrations, and Suspended Matter Measured on 5 August 1975 (Chen and Millero, 1977; Millero and Emmet, 1976)

Depth (m)	Temp. (°C)	Σ Salts ($mg/liter^{-1}$)	Σ Gases ($mmol/liter^{-1}$)	Density (g/cm^{-3}) due to		
				Temp.	Temp + Salts + Suspended Matter	Temp. + Salts + Gases + Suspended Matter
2	21.26	23.8	-	0.997936	0.997954	0.997955
4	8.56	42.0	0.150	0.999812	0.999846	0.999851
5	5.75	48.2	0.618	0.999947	0.999986	0.999989
6	4.70	53.8	0.975	0.999968	1.000011	1.000010
7	4.50	68.5	1.332	0.999970	1.000025	1.000019
8	4.29	82.0	1.770	0.999971	1.000037	1.000029
9	4.29	90.5	2.214	0.999971	1.000044	1.000032
10	4.29	100.0	2.748	0.999971	1.000052	1.000035

*This table is reproduced from Quay et al. 'vertical diffusion rates determined by tritium tracer experiments in the thermocline and hypolimnion of two lakes' Limnol. Oceanogr. 25(2), 1980, 201-218.

density of lake water for the period of this simulation cannot be computed due to lack of sufficient information on chemical species.

For most of the simulation period, L227 exhibits a very strong stratification pattern. Frequently, the maximum temperature gradient was 5°C/m and the Richardson number at the location of the thermocline was on the order of one thousand. At high Richardson numbers, dissipation of TKE in the mixed layer becomes important and the amount of energy available for entrainment is reduced (see section 2.3.3). Even without a full appreciation of the wind energy, the fully mixed layer of L227 still showed significant temporal variations (Figure 5.4).

The principal cause for the fully mixed layer variation in the summer period is the convective mixing induced by the fluctuation of meteorological conditions. Figure 5.5 shows the contribution to the fluctuations of the fully mixed layer by the convective cooling. The shallowness of the fully mixed layer causes the upper layer temperature to be sensitive to the meteorological condition. The time series plot of lake temperature for the upper 4 m is shown in Figure 5.6.

The general good agreement between the model predictions and the field measurements provides us with confidence in using the wind mixing model for interfacing with biological models.

The hydraulic retention time is approximately 2.6 years in 1973 and the value of the dimensionless number $\frac{AE}{QD}$ is 13 with E equal to the heat molecular diffusivity. This indicates that vertical diffusivity dominates the advection in the vertical transport (see section 2.2). Therefore, the output of the wind mixing model is sensitive to the specification of diffusivity. Temperature predictions for diffusivities, for all depths,

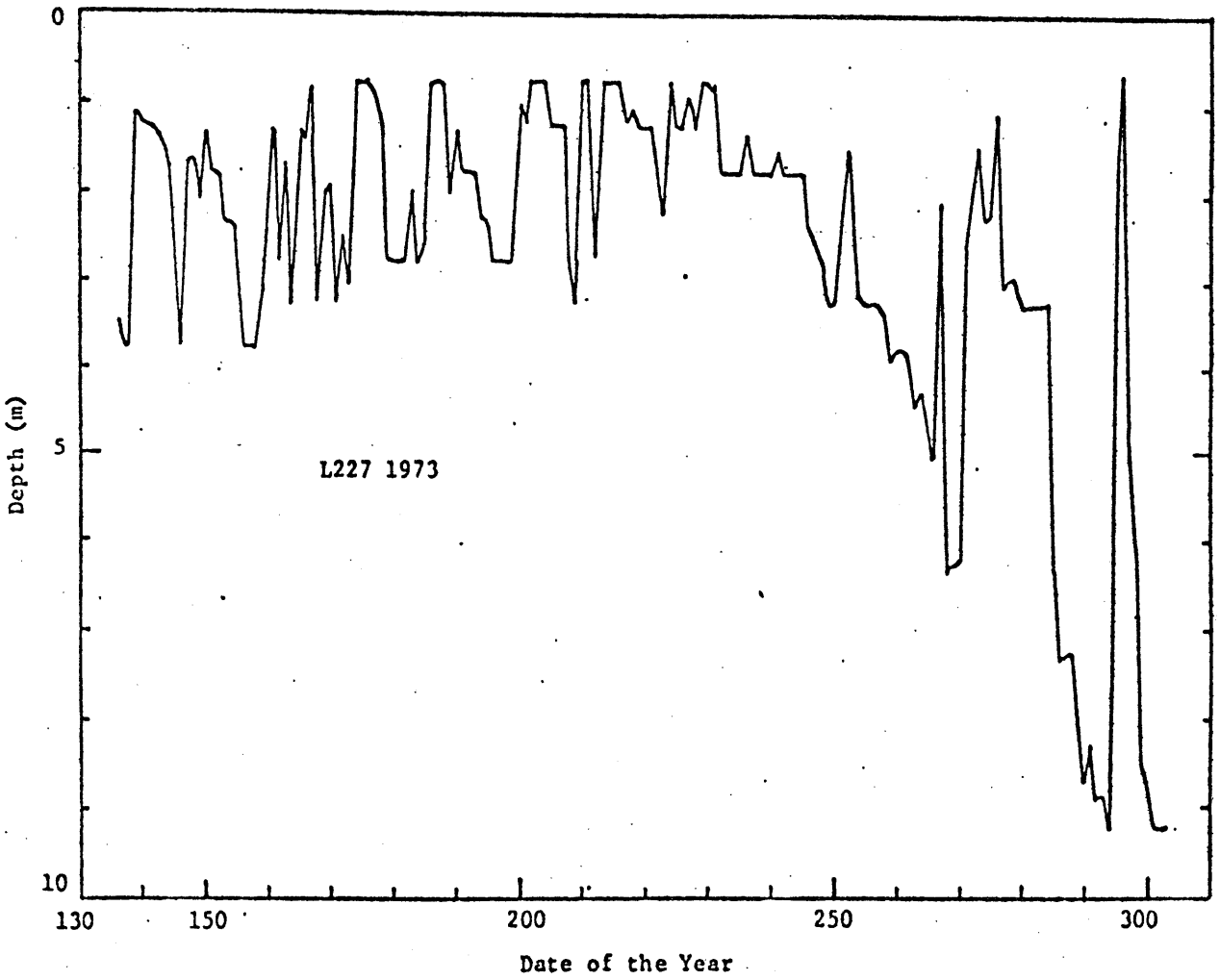

Figure 5.4: FML Variation with Time

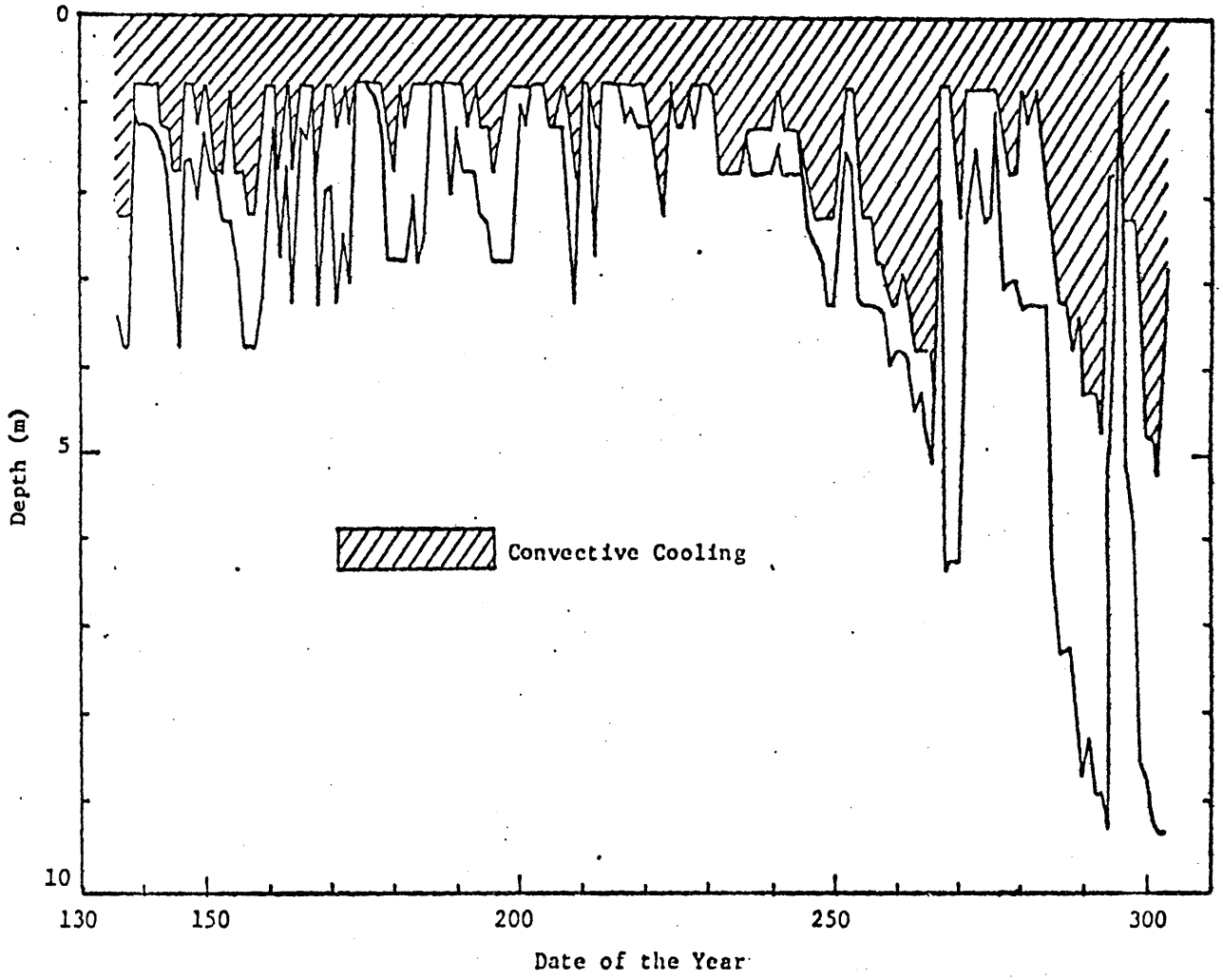

Figure 5.5: The Contribution of Convective Cooling to the FML Variation

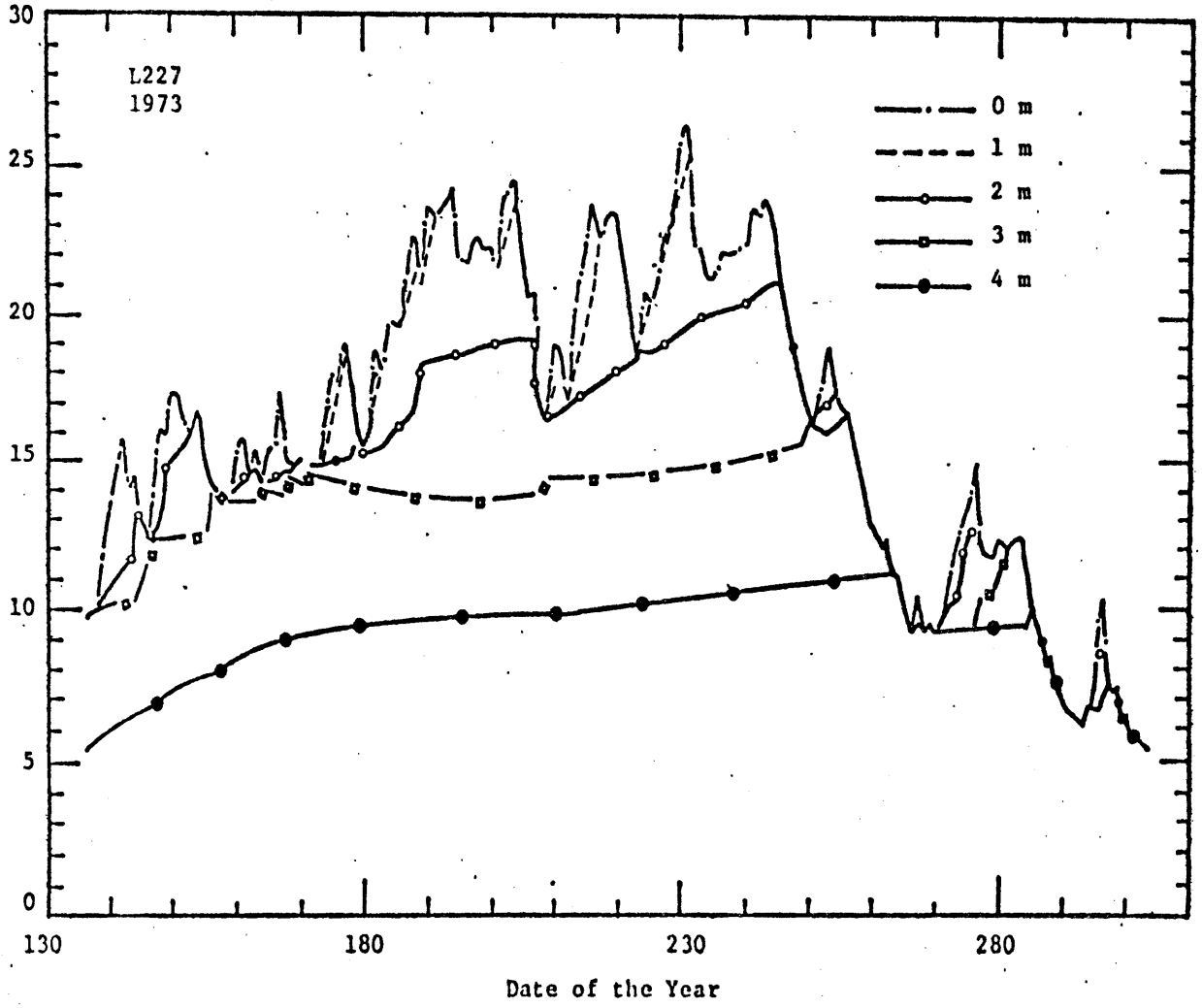

Figure 5.6: Time Series Plot of the Simulated Temperature for the Upper 4m

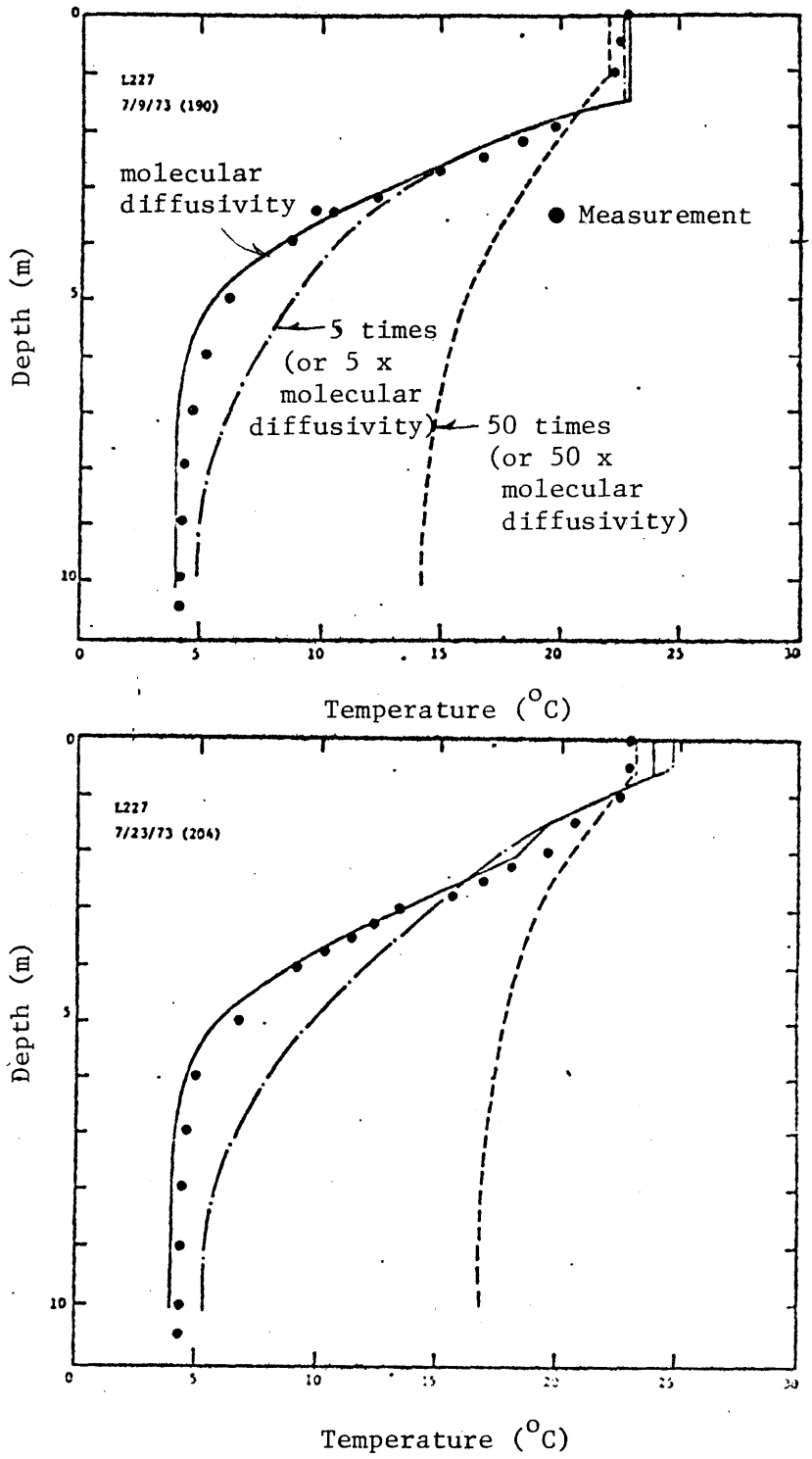

Figure 5.7: Sensitivity of the Temperature Prediction to the Value of Diffusivity (—— $\bar{\omega}$ molecular diffusivity; -·- $\bar{\omega}$ 5 x molecular diffusivity; --- $\bar{\omega}$ 50 x molecular diffusivity)

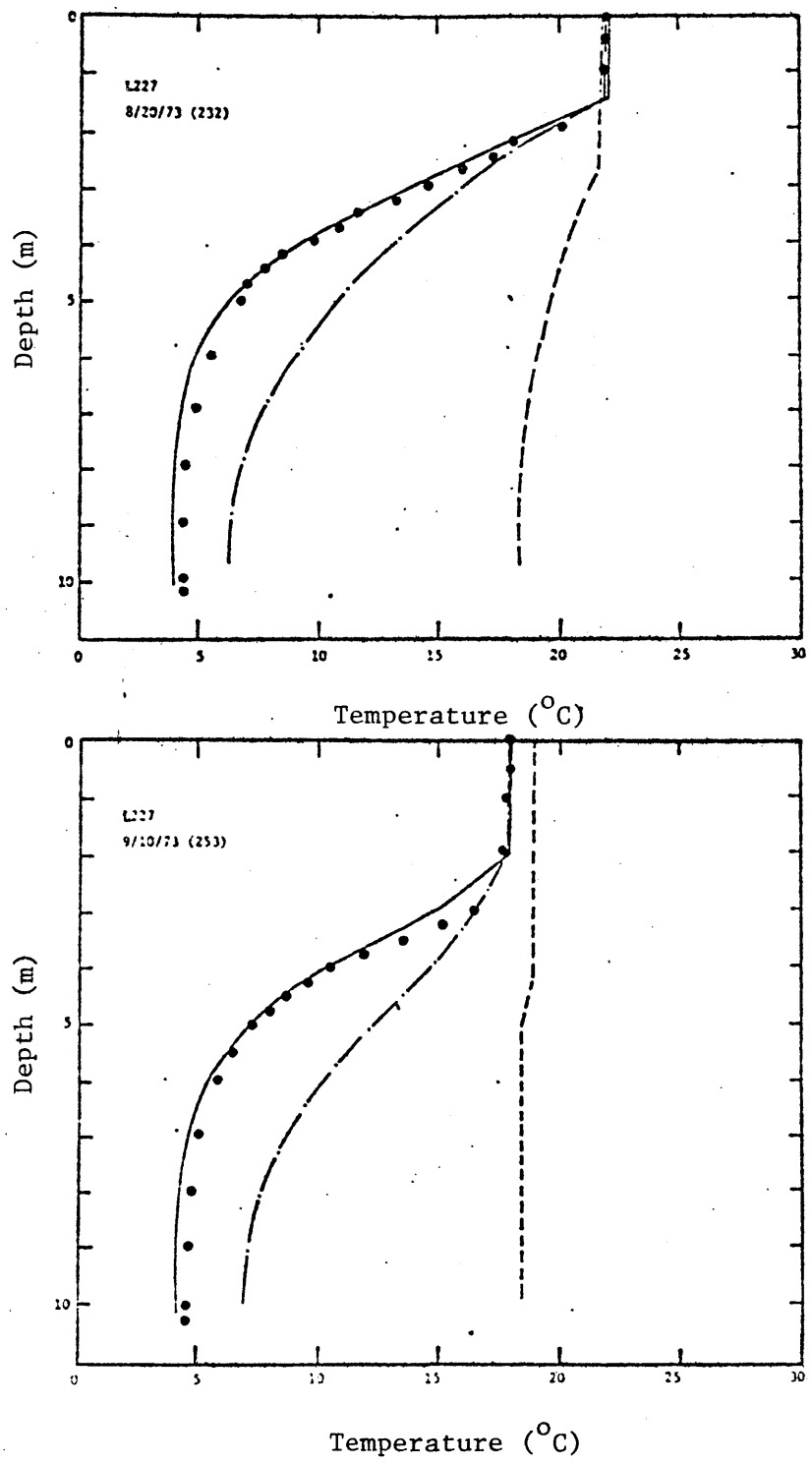

Figure 5.7: Continued

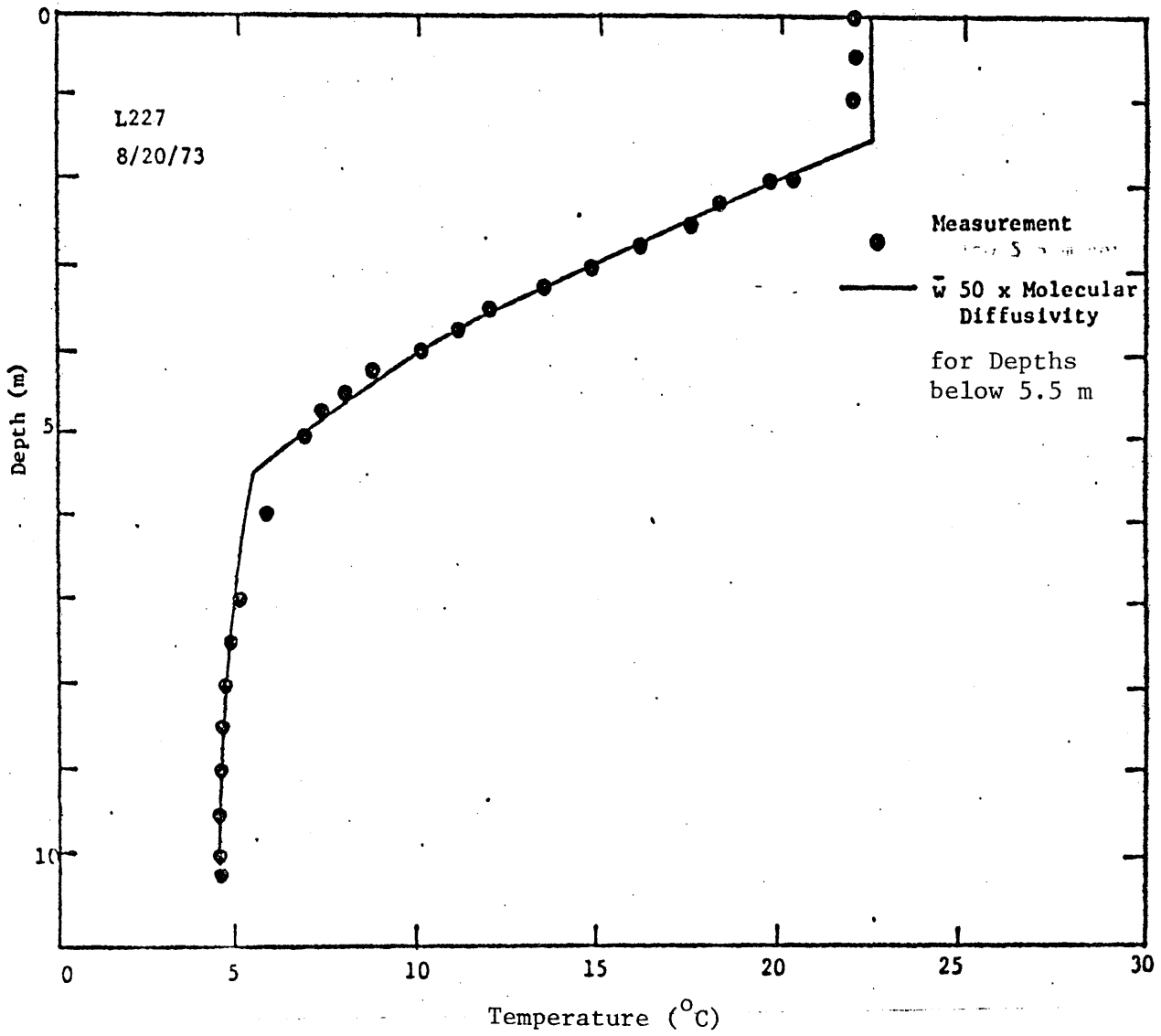

Figure 5.8: Sensitivity of the Temperature Prediction to the Diffusivity in the Hypolimnion

equal to the molecular diffusivity value, 5 times the molecular value and 50 times the molecular value are presented in the four panels of Figure 5.7. While the predicted surface temperatures show little difference in the three cases, the model with a higher diffusivity predicts a higher temperature for the subsurface region. For example, on the 204th day, the model with 5 times the molecular diffusivity overpredicts the temperature at the 5 m depth by 3°C and the model with 50 times the molecular diffusivity overpredicts by 10°C. However, if the diffusivity is increased only for depths below 5.5 m, the predicted temperature is similar to the field measurement (Figure 5.8). This is not unexpected, since the temperature gradient is very small for depths below 5.5 m and temperature becomes an inadequate tracer for estimating the diffusion rate in this region. The estimation of the hypolimnetic diffusivity should be the focus of future hydrodynamic research.

From these sensitivity analyses (Figures 5.7 and 5.8), it may be concluded that during the period when the FML has not extended to the 5.5 m depth, the diffusivity in the upper 5 m of L227 is of molecular level once the effects of convective cooling and wind mixing are considered. For the lower region where the temperature profile approaches the vertical, the temperature simulation result is inconclusive. However, information on the hypolimnion diffusivity of L227 may be found in a field tracer experiment by Quay (1977). In 1975, a thin layer of tritiated water was injected at a depth of 6.9 m in L227 and tritium profiles were collected from July 16 to August 28 in order to analyze the diffusivity in the hypolimnion. It was found that the vertical diffusivity in this region (6 m - 10 m depth) was extremely low and on the order of the molecular

diffusivity. Even though the hypolimnion diffusivity is affected by wind and inflow, the measured diffusivity from this considerably long duration field experiment (42 days) may be assumed to be representative of the diffusivity in this region of L227. Therefore, the MIT wind mixing model, which considers the diffusivity to be on the molecular level for the non-fully mixed layer, may be used to describe the vertical hydrodynamic transport process in L227.

5.3 Phytoplankton Modeling

5.3.1 Analysis of the Biological Field Data

On April 12, 1973, L227 was still covered by ice, but the next available measurement, which was taken 21 days after, indicated that the lake had been stratified (Figure 5.9). The significant chemical gradients on May 2 in the region below 4 m suggests that L227 was not likely to be fully mixed during the period of April 12 and May 2. Confined by the availability of meteorological data needed for temperature simulation, the phytoplankton simulation is limited to the period May 15 to October 29, which is the same as the temperature simulation period.

During the simulation period, biweekly measurements of TDP, PP and chlorophyll-a are available (Schindler, unpublished data). Ortho-P concentration measured during this period by Rigler bioassay (Levine, 1975) indicated levels below 0.1 µg/ℓ (Figure 5.10). Since ortho-P concentration is so low, the reported TDP value will be referred to as SUP in this report.

In 1973, L227 received 21 weekly additions of 1.14 kg PO_4-P and 14.97 kg NO_3-N during the period from May 22 to October 8 (ELA unpublished data). Nutrients were mixed with lake surface water and were placed in a boat with the drain plug of the boat in the transom removed. The boat then cruised around the lake to empty its nutrient content into the lake. The process was repeated 3 - 6 times taking 30 - 90 minutes altogether (Schindler et al., 1971). The phytoplankton standing crop was found to be governed by the amount of ortho-P added (Schindler and Fee, 1975). The epilimnion concentrations of PP and chlorophyll-a

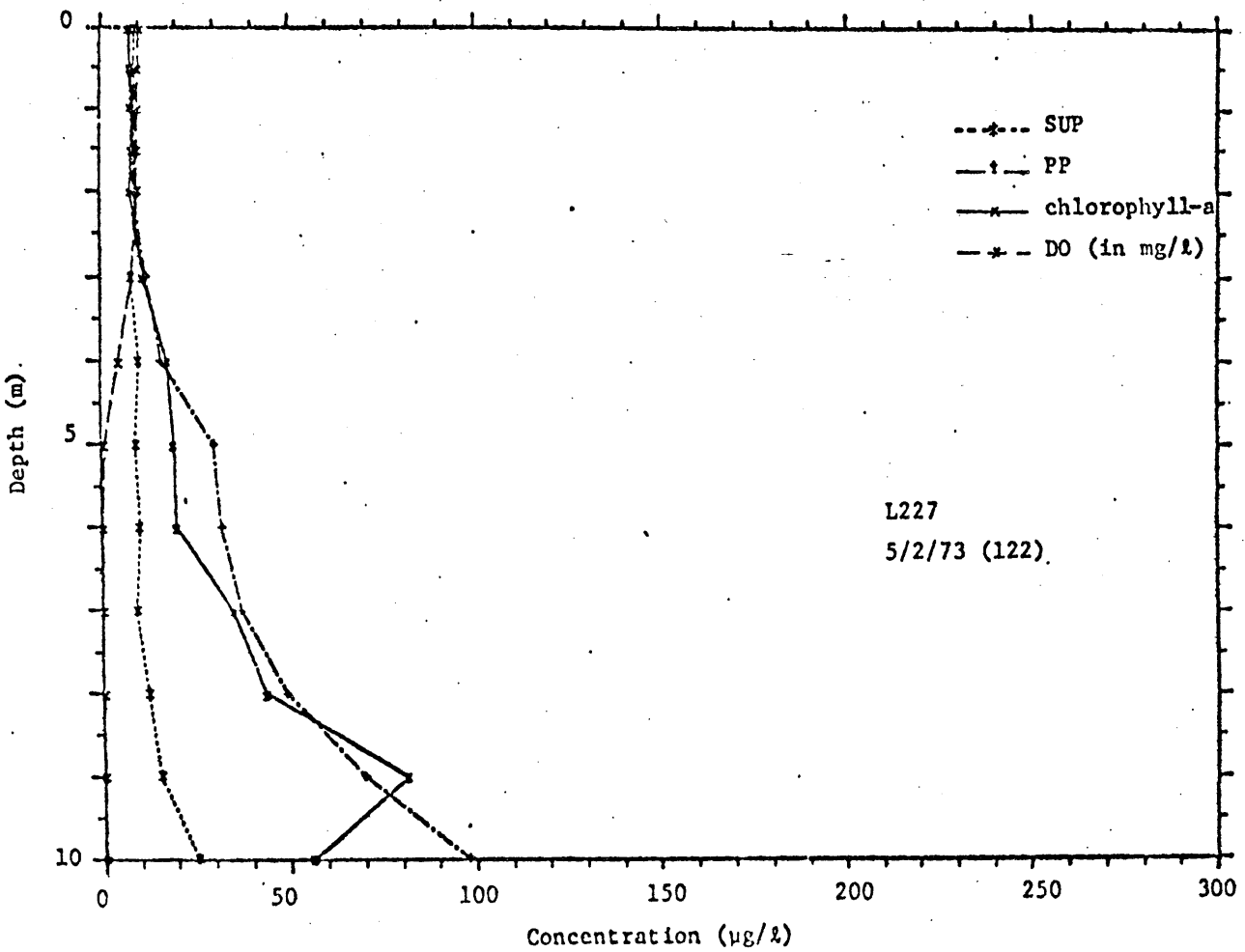

Figure 5.9: Chemical Profiles for L227 on May 2, 1973

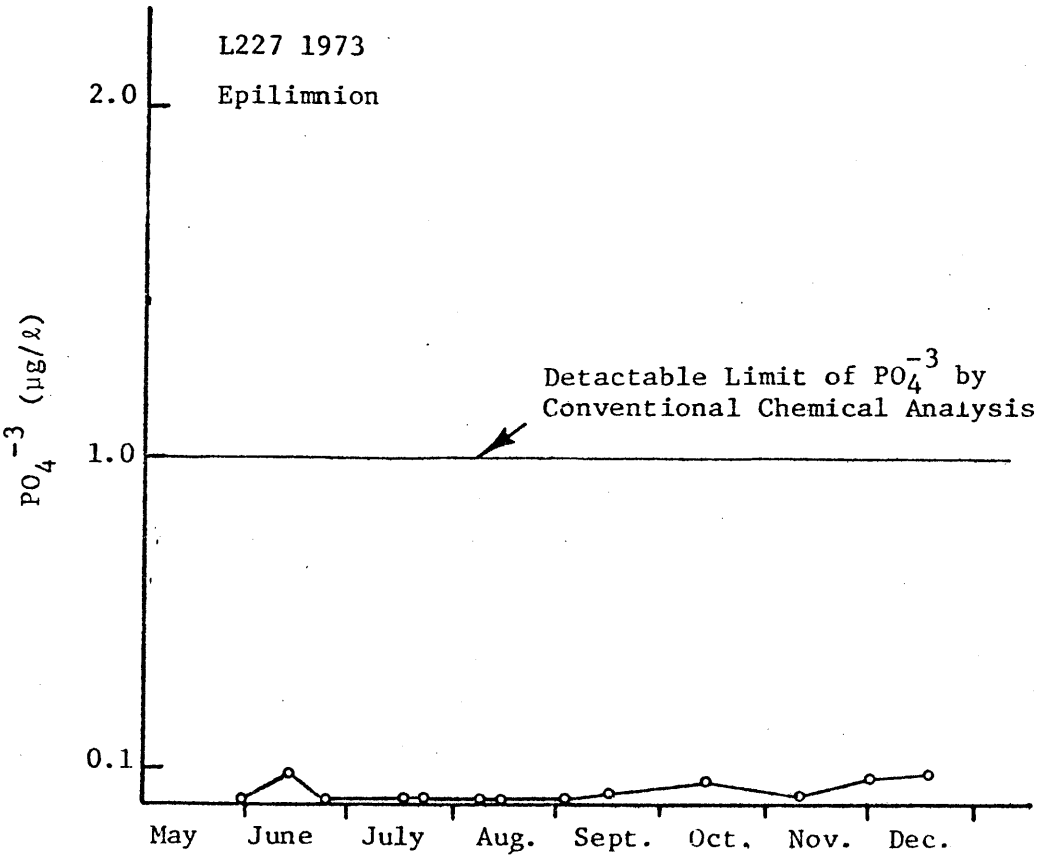

Figure 5.10: L227 Epilimnion Ortho-p Concentrations in 1973 (reproduced from Levine, 1975)

quickly responded to the addition of the nutrients while the SUP concentration remained fairly invariant.

Examples of the measurement of SUP, PP and chlorophyll-a are shown in the six panels of Figure 5.11 with the epilimnion depths indicated by arrows. The depth of the epilimnion is defined as the depth where the temperature gradient becomes greater than 1°C/m. Due to the shallowness of the epilimnion, only a few measurements were available in this region. The concentrations of SUP, PP and chlorophyll-a in the epilimnion so defined showed little gradient except for the 204th day and the 274th day. On the 204th day, the PP concentration at the surface was 132 μg/ℓ while the concentration of PP was 58 μg/ℓ at 1 m depth. On the 274th day, a high PP concentration of 154 μg/ℓ was recorded at 1 m depth which is 10 times the concentrations at the surface and the 3 m depth. Since the chlorophyll-a measurement at 1 m depth was similar to other chlorophyll-a measurements in the epilimnion, it is assumed that the value of 154 μg/ℓ is an error in recording and a value of 15.4 μg/ℓ is used instead. The volume weighted average of the epilimnion concentration obtained with the depth of the epilimnion previously defined will be used for comparison with the model's prediction of the FML biological and chemical concentrations.

Profiles of PP and chlorophyll-a shown in Figure 5.11 have two distinctive features: high hypolimnion concentrations of both PP and chlorophyll-a in the anoxic region of the lake.

The method used for chlorophyll-a measurement in ELA studies may measure substances which radiate fluorescence in addition to phytoplankton chlorophyll-a. Although the result is reported as chlorophyll-a, it is

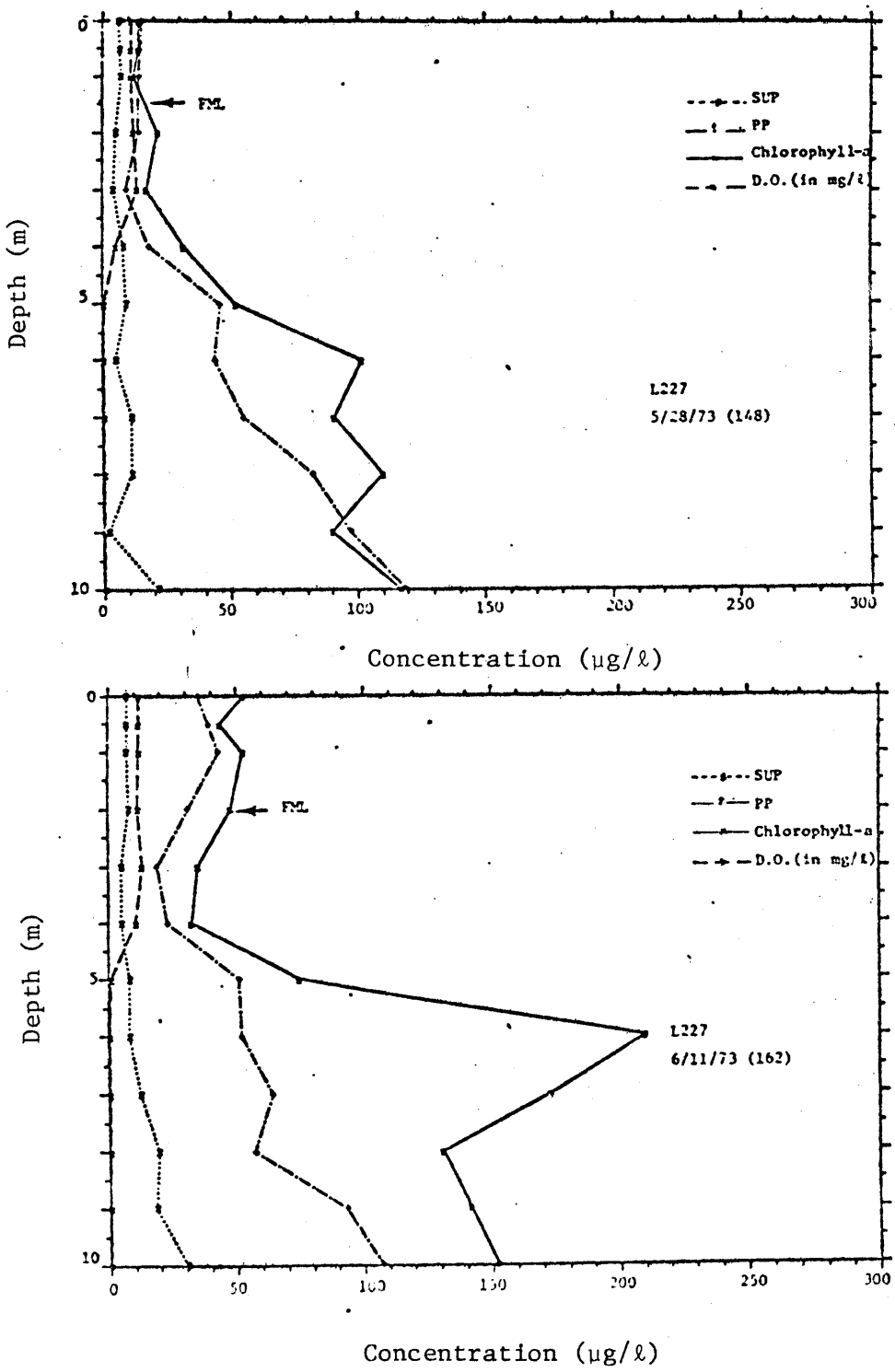

Figure 5.11: Examples of Chemical Measurements in 1973

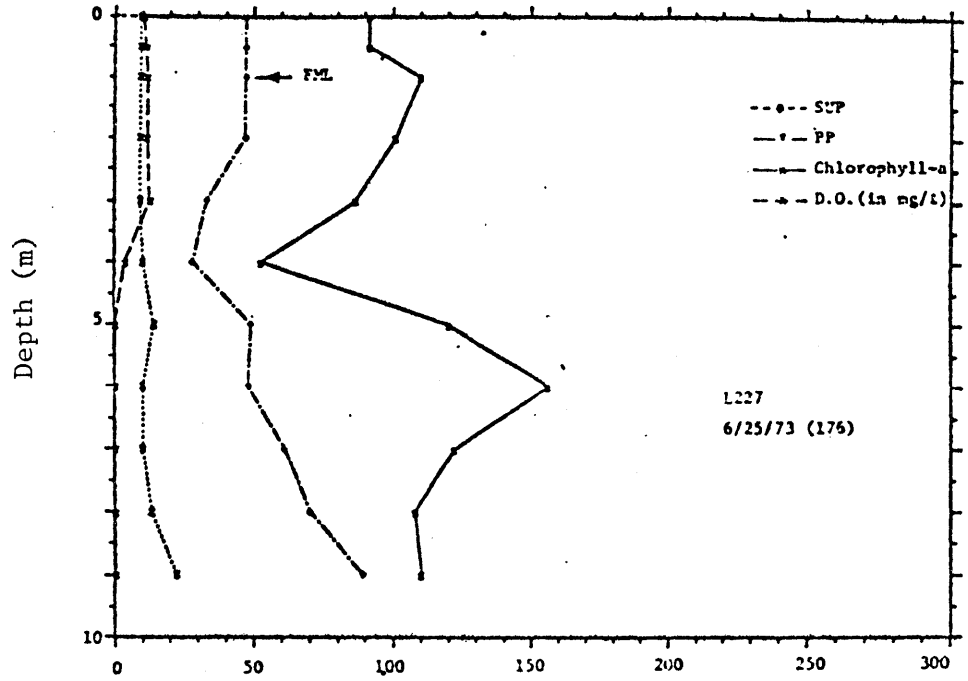

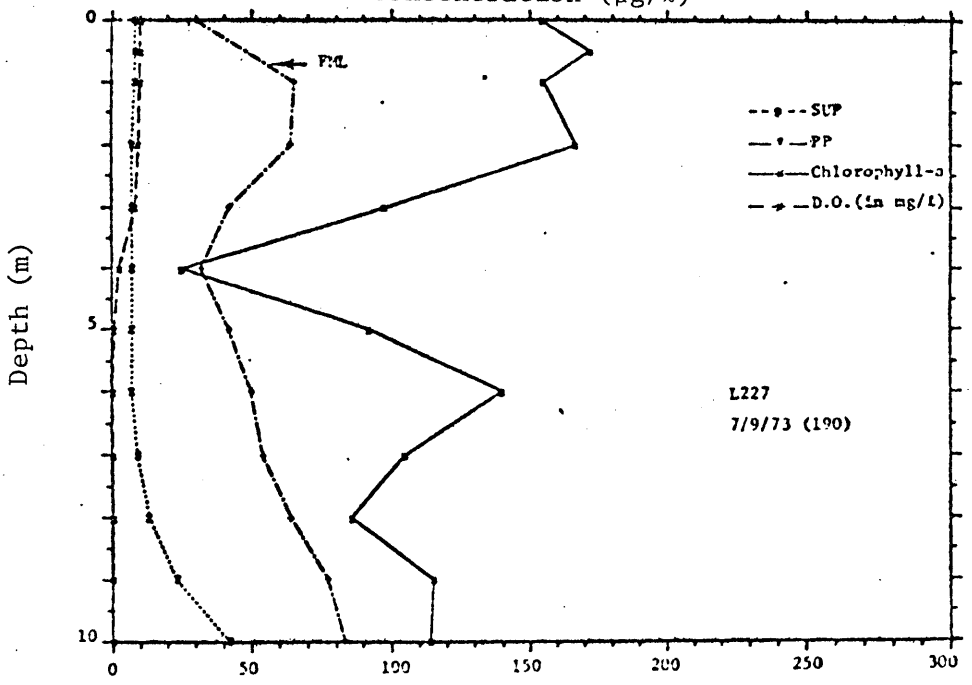

Figure 5.11: Continued

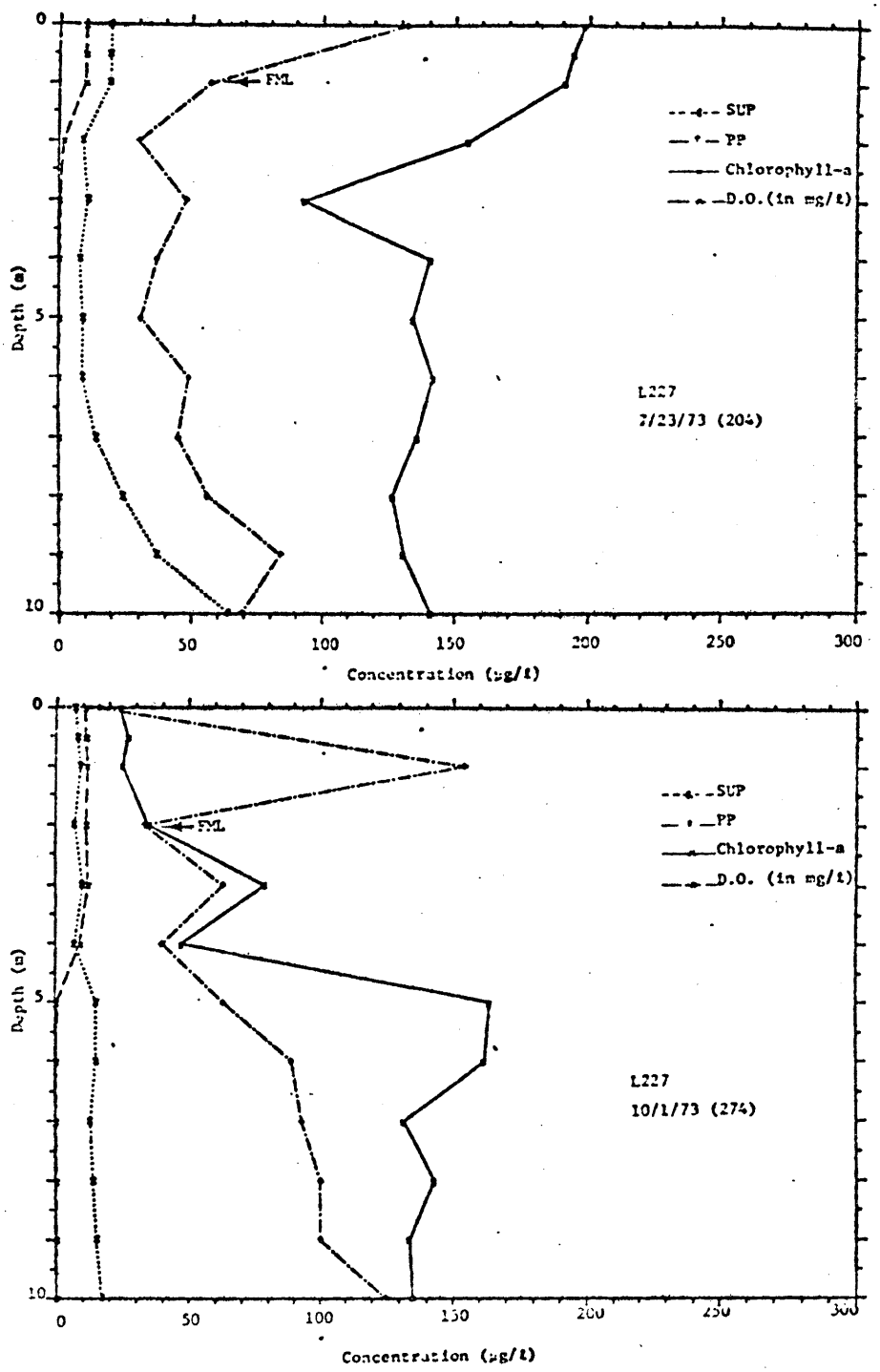

Figure 5.11: Continued

better to regard this measured result as chlorophyll, which includes bacteria chlorophylls as well as phytoplankton chlorophylls. Healey identified the pigment of bluish-green photosynthetic bacteria, which was frequently found in ELA lakes, as Chlorobium chlorophyll "650" from absorption spectra peaks in either methanol or acetone. His studies indicated that pigment concentration for these bacteria are similar to that measured by the Fluorometer from the standard fluorometer calibration procedure for chlorophyll-a (Fee, 1978). Since photosynthetic bacteria are obligated anaerobes, the photosynthetic bacteria peak usually occurs at the top of the anoxic layer. Hence, the abundant hypolimnion chlorophyll in L227 may very likely be bacteria chlorophylls.

Hypolimnion chlorophyll-a peaks have been observed in many other oligotrophic lakes in the ELA. These hypolimnion chlorophyll-a peaks are composed of specific phytoplankton species, mainly large colonial chrysophycean flagellate which do not occur in significant quantities in the water column above the hypolimnion peak. The location of these chlorophyll-a peaks were observed to be near low light levels (0.1% of the surface light) and near the depth where oxygen concentration is close to zero.

The similarity in the location of bacterial chlorophyll and the hypolimnion chlorophyll-a peak with respect to light conditions and oxygen concentration makes it difficult to judge from field measurement of chlorophyll profile which organism (bacteria or phytoplankton) is present. Whether this observed hypolimnetic chlorophyll peak is due to bacteria chlorophyll calls for an additional photosynthetic organism with characteristics greatly different from the phytoplankton of the upper

water column. Difficulties exist in modeling the growth of photosynthetic organisms at depths of low light intensity. Due to the high extinction coefficient, the light intensity at 6 m depth, which corresponds to the hypolimnion chlorophyll peak, is from 6×10^{-8} to 6×10^{-3} of the surface light value. If the data on the 135th day is not included, the range becomes 6×10^{-8} to 6×10^{-4} (Table 5.5). It is conceivable that organisms which thrive at such low light irradiance might have a pigment which has a high efficiency in absorbing light waves penetrating to the deeper region of the lake and the different penetrations of different wavelengths have to be considered. The conventional method of estimating light extinction gives no information on this aspect. Moreover, the hypolimnetic chlorophyll-a peaks may even be maintained heterotrophically (Fee et al., 1977).

The high hypolimnetic PP concentration may be due to two possible causes. Levine and Schindler (1980) showed that the rapid uptake of ortho-P by hypolimnion decomposers keeps the ortho-P concentration low in this region. The high concentration of hypolimnetic photosynthetic organisms, reflected by the high chlorophyll-a concentration, may be responsible for the high PP concentration in the hypolimnion. Whether this high PP is bound in the photosynthetic organism or non-photosynthetic organism in the hypolimnion, the major fraction of this PP is not phosphorus contained in the epilimnion phytoplankton. At this stage, the uptake of ortho-P by organisms other than epilimnion phytoplankton is not considered so that our phytoplankton model has no ability to simulate this high particulate P in the anoxic layer.

Table 5.5

Estimated Light Intensity at 6 m Depth - 1973
(As fraction of the surface irradiance)

Date:	5/14	5/28	6/11	6/25	7/8	7/23	8/8	8/20	9/3	9/17	10/1	10/15	10/29
	6×10^{-3}	1×10^{-4}	2×10^{-4}	5×10^{-7}	6×10^{-8}	3×10^{-7}	1×10^{-4}	2.6×10^{-5}	7×10^{-5}	2×10^{-4}	3×10^{-4}	9×10^{-4}	2×10^{-4}

Because of all the above reasons - possible measurement error, non-equivalence of PP and phytoplankton-P, absence of information on the penetration and amount of light which enters the deeper lake region and possible heterotrophic growth, our simulation is limited to fitting observed chlorophyll-a and PP concentrations of the upper layer region defined by whichever is of larger depth: the 4 m depth or the FML. 4 m represents the lower bound of the oxic layer for most of the period. The oxic layer, obtained from the bi-weekly chemistry measurement, is shown as the shaded region of Figure 5.12.

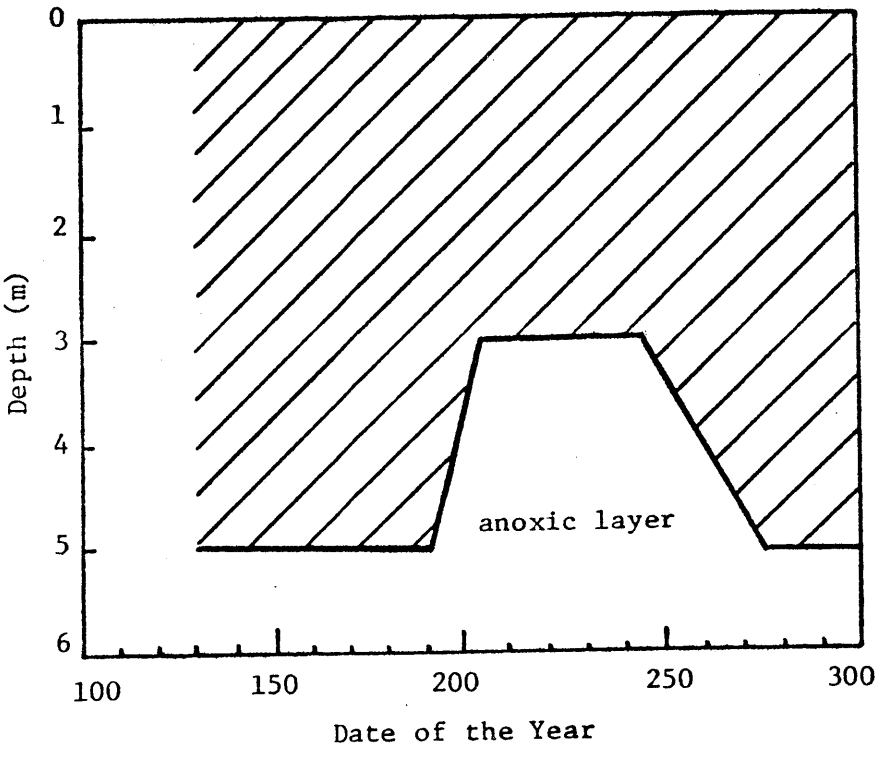

Figure 5.12: The Anoxic Layer

5.3.2 Phytoplankton Simulation - Level I

5.3.2.1 Simulation with the Minimum Number of State Variables - Model I

A. Model Description

In Chapter 3, the suggested optimal number of phosphorus state variables is between 2 to 4, with ortho-P and phytoplankton-P as the necessary variables. The other two state variables are SUP and zooplankton-P. As a rule, the simplest model will always be used unless data suggest otherwise. A logical starting point is to consider a measured variable as a possible state variable. Since zooplankton-P was not measured, this state variable is not presently considered.

Our main interest is the amount of phosphorus retained by phytoplankton, that is, phytoplankton-P in this case. Whether SUP should be included as a state variable depends on how it affects the dynamics between ortho-P and phytoplankton-P. Figure 5.11 shows that SUP remained fairly constant ($\sim$10 $\mu g/\ell$) for the whole period while PP in the upper layer fluctuated over the range 8 - 65 $\mu g/\ell$. Based on this, it is assumed that SUP represents a fraction of dissolved P which is not actively involved in the ortho-P - PP dynamics and contributes very little to the PP fluctuation. This assumption further reduces the number of P compartments to two: ortho-P and phytoplankton-P.

While the best way to model phytoplankton biomass variation is to model the phytoplankton organic carbon variation, the use of field measured particulate organic carbon (POC) to obtain information on phytoplankton biomass variation is exceedingly difficult for the following reason. The measured POC includes all particulate matter in

the water column since the separation of phytoplankton from detritus and zooplankton is not practical. While the separation of zooplankton and bacteria can be partially achieved by using filters, there is no practical way to separate detritus from living phytoplankton. Hobbie et al. (1972) measured the major C component in a small arctic pond for a typical summer day and found that the ratio of phytoplankton carbon to total particulate organic carbon is only 1/85. Saunders (1972) measured the ratio of phytoplankton carbon to total particulate organic carbon to be 1/3 in Frains Lake, Michigan, on July 22, 1968. Particulate organic detritus is generally 5 to 10 times greater than that of the living plankton (Wetzel, 1975). This evidence strongly suggests that the measured POC constituents are mostly particulate matter other than phytoplankton C. Thus the measured C variation will not be sensitive to the phytoplankton dynamics at all; the measured POC variation is very likely dominated by other kinetics. So we much choose an indicator which better reflects the phytoplankton dynamics.

Chlorophyll-a, being able to easily measure and correct for pigment degradation products, has often been used to estimate the composite phytoplankton population in a natural aquatic environment. Chlorophyll-a also varies appreciably. However, since chlorophyll-a is the dominant pigment which absorbs quantum and turns the light energy into chemical energy, we may regard the concentration of chlorophyll-a as the potential of phytoplankton to use light energy. In analysing their field data on primary production from lakes and reservoirs, Brylinsky and Mann (1973) found a very high correlation between chlorophyll-a and phytoplankton

biomass (r = 0.98). As Lund (1969) asserted:

> A convenient measure of the size of an algal population is the amount of chlorophyll-a present. Despite the fluctuations in the amount of chlorophyll-a per cell in different kinds of algae and under diverse environmental conditions, it does not seem that the more extreme variations recorded from laboratory experiments often arise under natural conditions.

Therefore, in this case study we choose chlorophyll-a data for calibrating biological model parameters.

Two measurements - chlorophyll-a and PP - represent phytoplankton. As discussed in Chapter 4, if the phosphorus content in phytoplankton is constant, then phytoplankton growth dependence on phosphorus may be expressed as a function of external ortho-P concentration and phytoplankton-P may be converted to phytoplankton biomass by a constant yield coefficient. However, if the phosphorus to phytoplankton biomass ratio is variable, the Droop formulation has to be used to account for this variable yield coefficient. The ratio of PP to chlorophyll-a in the upper 4 m of the lake, based on the record of routine chemical measurements, is plotted in Figure 5.13. It may be observed that the ratio PP/chlorophyll-a is neither constant with time nor depth. This variability of PP to chlorophyll-a ratio with time and space suggests a variable phosphorus cell quota and Droop formulation, which relates the phytoplankton growth to intracellular content of the limiting nutrient, should be used.

Model I consisting of three state variables -- ortho-P, phytoplankton-P and phytoplankton biomass -- is selected as the simplest biologically

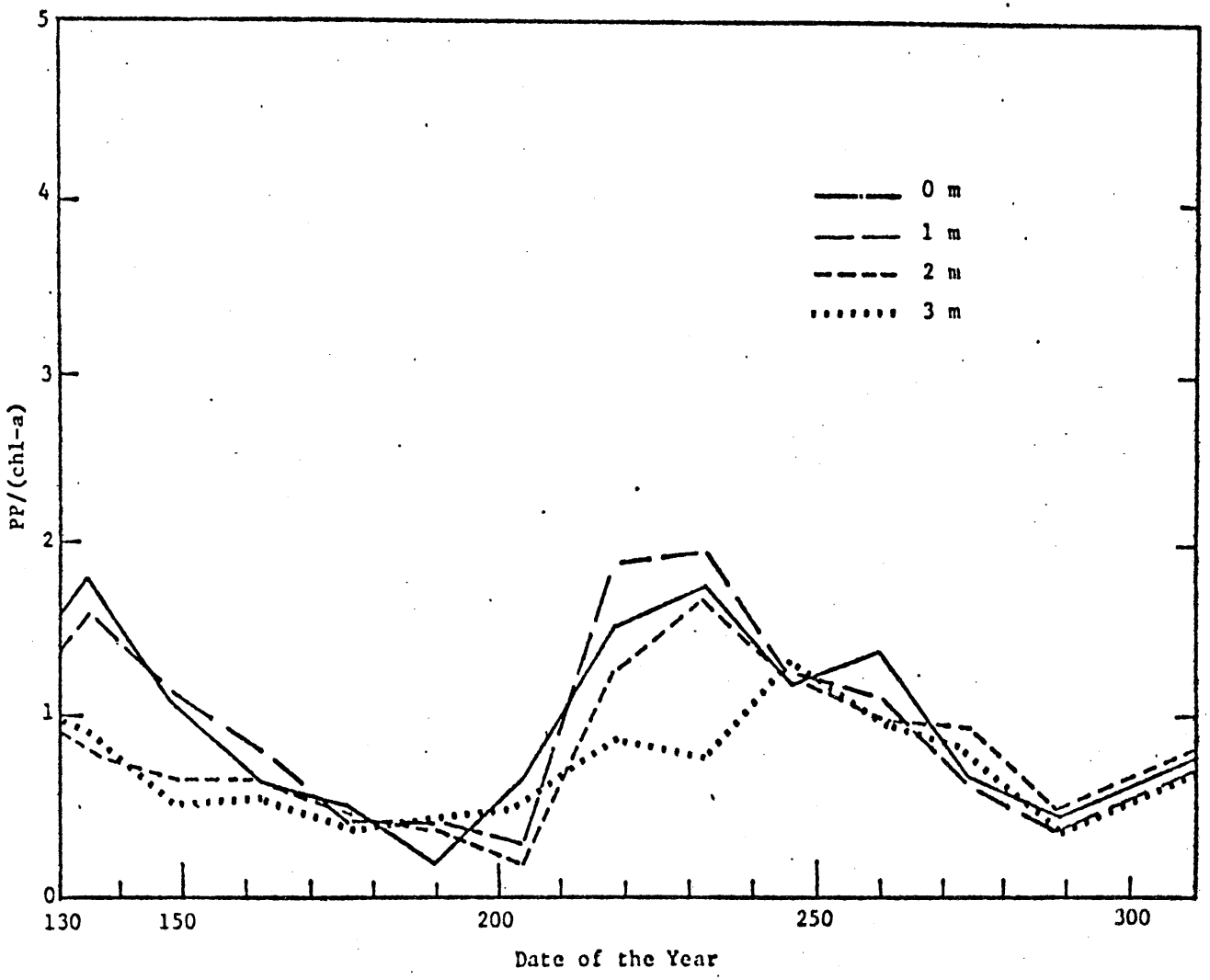

Figure 5.13: Measured PP/(chlorophyll-a) Ratio at Different Depths

plausible model with the ability to simulate the field measurements. The schematic representation of Model I and the relationship between model state variables and measurement are shown in Figure 5.14 and Table 5.6, respectively; the number of model state variables is the same as the number of field measurements. The 1-D mass balance equations for this biochemical model are shown in Table 5.7.

The formulation of the phosphorus cycle is an open matter flow loop with the sedimentation of phytoplankton-P carrying the phosphorus out of the lake system. If the sinking term represents a perfect vertical mass transport in the water column, then the mass change due to the sinking should be written as:

$$\frac{1}{A}\frac{\partial}{\partial z}[gA(xQ)] = (xQ)\frac{\partial g}{\partial z} + (xQ)\frac{g}{A}\frac{\partial A}{\partial z} + g\frac{\partial (xQ)}{\partial z} \qquad (5.6)$$

$$\qquad\qquad (1) \qquad\qquad (2) \qquad\qquad (3)$$

The first term represents the concentration change due to the vertical settling rate, the second represents the concentration change due to the variation of lake area and the third represents the change due to the variable phytoplankton-P concentration. However, it is more reasonable to assume that the contraction of area does not cause an increase in concentration since the settling phytoplankton is retained in the sides of the lake (see Figure 5.15) so that the second term may be neglected. The vertical concentration variation due to the sinking term is, therefore, written as

$$\frac{\partial}{\partial z}[g(xQ)] \qquad (5.7)$$

Use of equation (5.7) instead of equation (5.6) represents a loss of mass from the water column during the process of sinking

$$g(xQ)\,\frac{1}{A}\,\frac{\partial A}{\partial z}\,dz \tag{5.8}$$

MODEL I

.3 STATE VARIABLES

S - ORTHO-P, IN µG/L

X - PHYTOPLANKTON BIOMASS, IN µG/L

Q - PHOSPHORUS TO BIOMASS RATIO BY WEIGHT

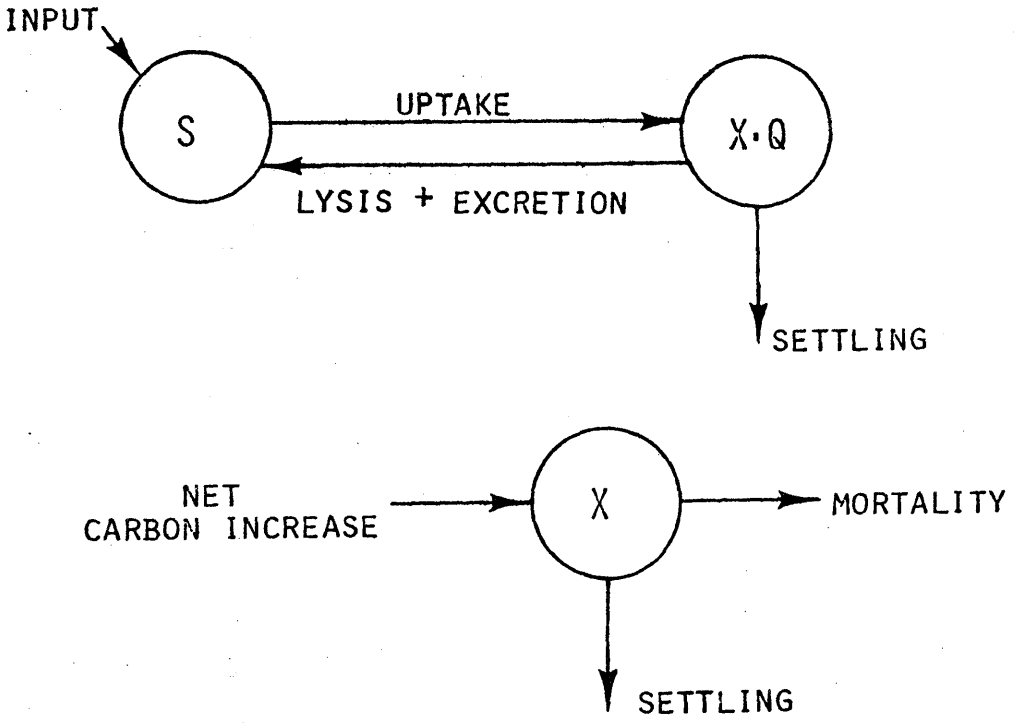

NET CARBON INCREASE = PHOTOSYNTHESIS - RESPIRATION
-PHOTORESPIRATION - EXCRETION

Figure 5.14: Schematic Diagram - Model I

Table 5.6

Model State Variables vs. Field Measurement

Model I

$$\begin{pmatrix} 1 & 0 & 0 \\ 0 & r & 0 \\ 0 & 0 & 1 \end{pmatrix} \begin{pmatrix} S \\ X \\ XQ \end{pmatrix} = \begin{pmatrix} \text{ortho-P} \\ \text{chlo-a} \\ PP \end{pmatrix}$$

r = chlorophyll-a/biomass ratio, assumed to be 0.01

Table 5.7

1-D Mass Balance Equations - Model I

1-D Mass Balance Equations:

$$\frac{\partial S}{\partial t} = \frac{\alpha}{A}\frac{\partial}{\partial z}\left(A\frac{\partial S}{\partial z}\right) + D(S_i - S) + i_S - \rho X + (k_1 + k_2)(XQ)$$

$$\frac{\partial X}{\partial t} = \frac{\alpha}{A}\frac{\partial}{\partial z}\left(A\frac{\partial X}{\partial z}\right) + D(X_i - X) + \mu X - k_2 X - \frac{\partial}{\partial z}(gX)$$

$$\frac{\partial (XQ)}{\partial t} = \frac{\alpha}{A}\frac{\partial}{\partial z} A\frac{\partial (XQ)}{\partial z} + D(X_i Q_i - XQ) + \rho X - (k_1 + k_2)(XQ) - \frac{\partial}{\partial z}(gXQ)$$

Rate Expressions:

$$\mu = \mu_m f(I)\, g(Q)\, h(T)$$

$$f(I) = \frac{I}{I+k_I}$$

$$g(Q) = \frac{Q-q}{Q}$$

$$h(T) = \exp\left(-2.3\left|\frac{T - T_{opt}}{T_{div}}\right|\right)$$

$$\rho = \rho_m \frac{S}{S+k_\rho}$$

Parameters to be Calibrated:

g, k_1, k_2, k_I, k_ρ, T_{opt}, T_{div}, ρ_m, μ_m, q

Constraints:

All variables are non-negative values
Q should have an upper bound which corresponds to the maximum phosphorus content in phytoplankton

Definitions:

S - ortho-P
Q - P/biomass ratio
I - light
μ - growth rate
D - dilution rate
g - settling rate
k_1 - ortho-P excretion rate
k_2 - mortality rate
X - phytoplankton
T - temperature
ρ - uptake rate
i_S - input of ortho-P
α - mass molecular diffusivity
A - lake area

*Subscript i denotes the inflow concentration

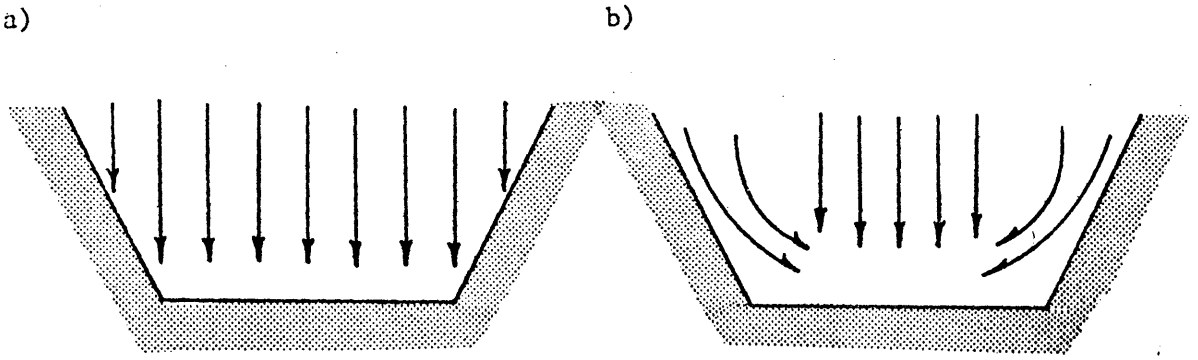

Figure 5.15: Schematic Representation of Settling

The regeneration rate of ortho-P through the processes of excretion and lysis should always be equal to or greater than the phytoplankton mortality. However, due to the rapid uptake of ortho-P by phytoplankton, it is assumed that ortho-P and phytoplankton are in kinetic equilibrium and the measurement of the concentration distributions of ortho-P and particulate-P provides no information in calibrating the kinetic rates involved. While the uptake rate may be estimated by the observation that phytoplankton-P can quickly take up the weekly added nutrient within hours, there is no information for calibrating the excretion rate. The phosphorus excretion rate is, therefore, purposely left uncalibrated.

The function f(I) describes the phytoplankton growth dependence on light. The light intensity I at a given depth z can be written as:

$$I = I_o\beta + I_o(1-\beta)\exp(-\eta z) \qquad \text{for } z \leq z_o \qquad (5.9.a)$$

$$I = I_o(1-\beta)\exp(-\eta z) \qquad \text{for } z \geq z_o \qquad (5.9.b)$$

where η is the extinction coefficient and z_o represents the depth of the layer which absorbs most of the longwave solar radiation.

In the process of photosynthesis, light energy is transformed into chemical energy. Figure 5.16 is a schematic representation of the photosynthetic reaction with the estimate of the reaction time for each step (Radmer and Kok, 1977). The overall reaction time for the photon absorption-oxygen production-CO_2 fixation is approximate 12 m sec. Since the mixing time scale is much longer than 12 m sec, we may assume that even inside the FML, phytoplankton responds to the light intensity which varies with the depth instead of responding to the depth averaged

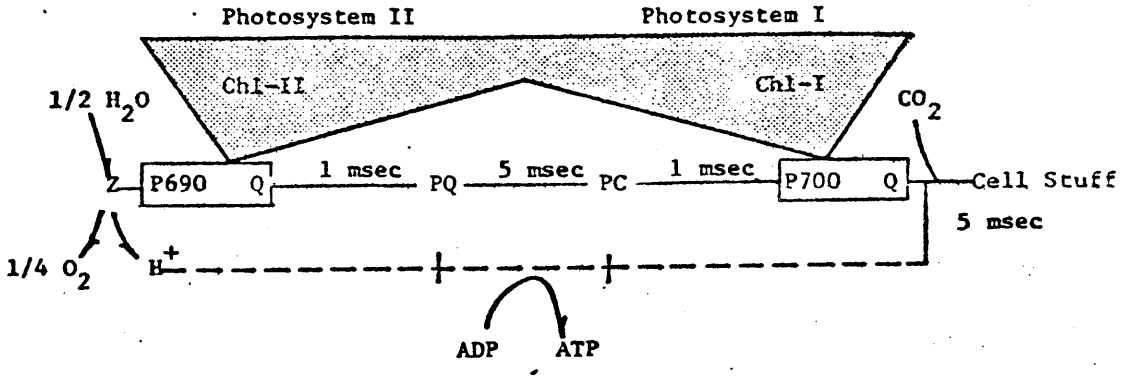

Figure 5.16: Timescale of a Photosynthetic Process

(redrawn from Radmey and Kok, 1977)

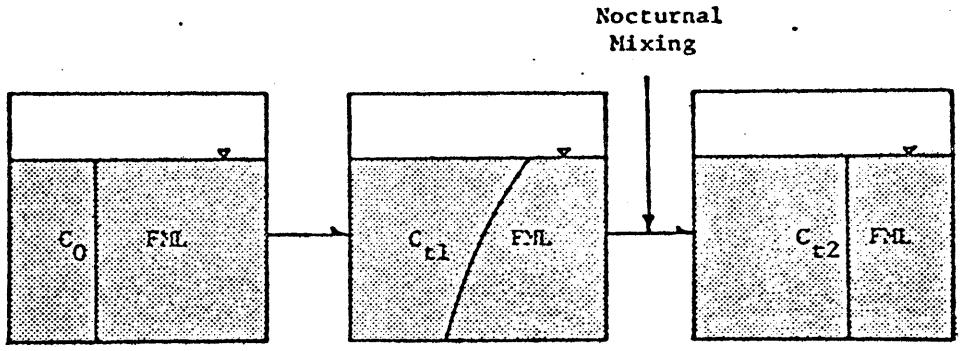

Figure 5.17: Schematic Representation of the Mixing Effect Upon Photosynthetic Organism

light intensity of the FML. That is, before the occurrence of the night time mixing event, phytoplankton may show a concentration gradient inside the FML as illustrated in Figure 5.17. Since the light has a typical diurnal variation and the function f(I) is non-linear, an estimation of the function f(I) based on the daily average light intensity is different from the estimation of f(I) based on light with diurnal variation. The diurnal light variation may be expressed as a half sinusoidal function with a period of 24 hours:

$$I(t) = A \sin(\frac{2\pi t}{24}) \tag{5.10}$$

where A, the amplitude of the sine function is related to the daily average light intensity, I_{avg}, by

$$A = \pi I_{avg} \tag{5.11}$$

The importance of preserving this diurnal variation in using the hyperbolic function to describe the light effect is illustrated in Figure 5.18. The equations used to compute curves I and II are:

$$\text{Curve I :} \quad f(I) = \frac{I_{avg}}{I_{avg} + K_I} \tag{5.12}$$

$$\text{Curve II:} \quad f'(I) = \frac{1}{24} \int_0^{12} \frac{A \sin \frac{\pi t}{12}}{A \sin \frac{\pi t}{12} + K_I} dt \tag{5.13}$$

Since the function $I/(I+K_I)$ is a concave function, according to Jensen's inequality (1905), Curve I which uses the daily average light intensity always predicts higher values than Curve II which computes the average value of the function over the day. The difference between the two varies with

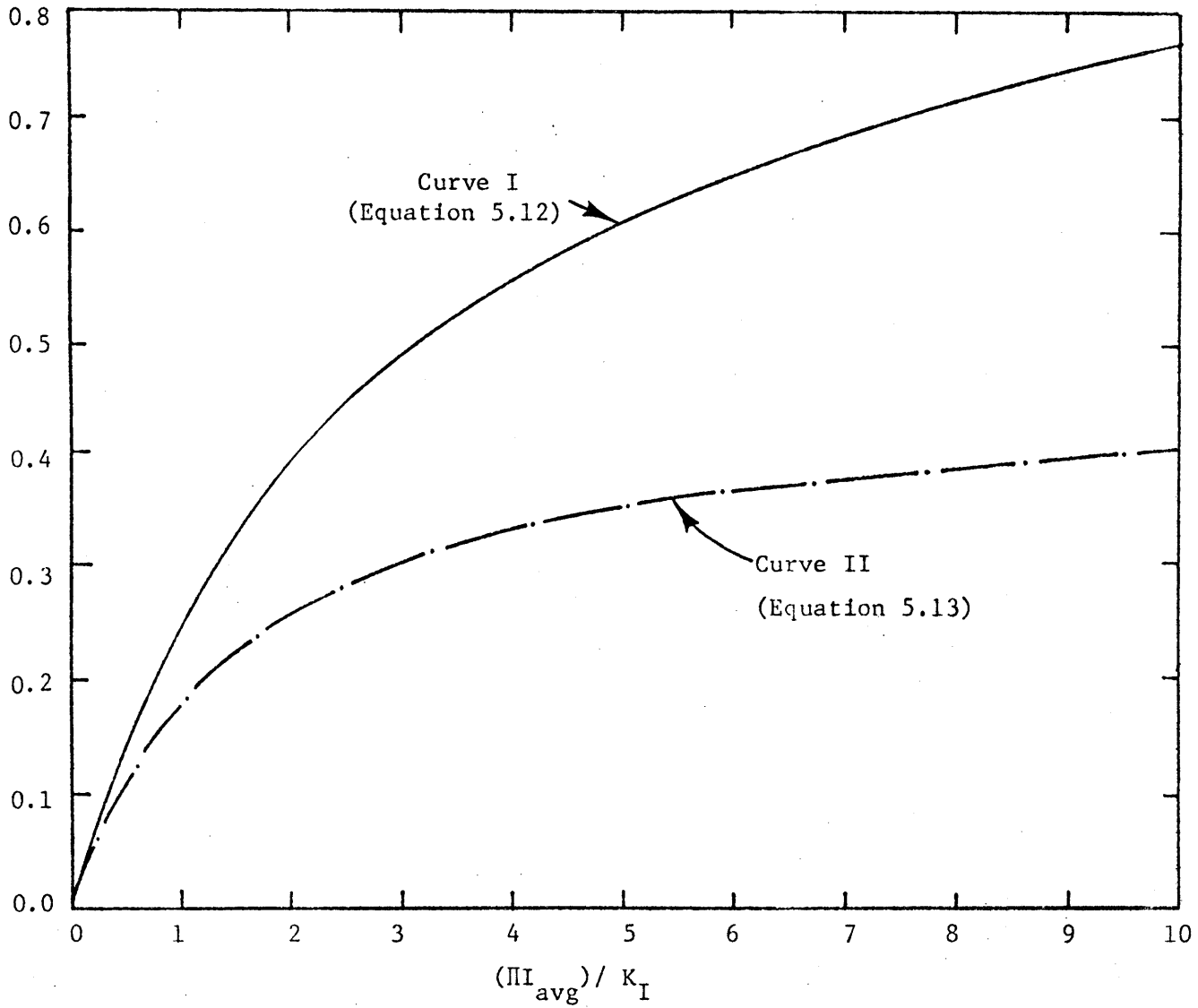

Figure 5.18: Comparison of the Light Effect by Using Daily Average Light Intensity with the One Using the Sinosoidal Light Intensity

I_{avg}/I_k, which is the ratio between the daily average and the half saturation coefficient. As the value of I_{avg}/I_k increases, the difference in the two curves increases to as much as 50%. Therefore, it is important for the model to preserve this diurnal light variation in computing the phytoplankton growth dependence on light.

B. Simulation Results and Analysis

The model solves the 1-D mass balance equations for the biological state variables using an explicit finite difference method similar to that used in the temperature model for solving the heat balance equation. However, the computation time step for the biological model is set to 0.1 day, or one tenth of the computation time step used in the temperature simulation. The light intensity at each computing time step within the day that is needed for computing f(I) is estimated using the sinusoidal function (equations (5.10) and (5.11)] and the measured daily average value of solar radiation. The initial concentrations of ortho-P, phytoplankton-P and phytoplankton biomass are obtained from the chemical measurement record using the measured particulate-P as phytoplankton-P and 100 times the measured chlorophyll-a as the phytoplankton biomass. Temperature needed for computing g(T) is obtained from the temperature model output while the quantity and schedule of ortho-P addition are available from ELA unpublished records.

The weekly addition of ortho-P is assumed to only increase the ortho-P concentration of the FML, that is, the increase of the ortho-P concentration, i_s, in the water column is computed as:

$$i_s = \frac{1140}{VOL_{FML}} \quad \text{for FML} \tag{5.14}$$

$$= 0 \quad \text{for non-FML} \tag{5.15}$$

where VOL_{FML} is the volume of the FML. The inflow concentrations of the biological variables are assumed to be negligible and the outflow is assumed to occur within the surface element.

At the end of one day, or after 10 computation time steps, the biological model uses the FML computed from the temperature model to redistribute the chemical state variables in the water column.

Our initial task was to simulate the magnitude and occurrence of the observed chlorophyll-a peak around the 204th day. From the formulation presented in Table 5.8, nine parameters (g, K_I, μ_m, q, T_{opt}, T_{div}, K_2, ρ_m, K_ρ) had to be specified before proceeding with the simulation. In the absence of any other information to identify these parameters, the only alternative was to calibrate these parameters with field measurements of ortho-P, particulate-P and chlorophyll-a.

The following procedures were taken in parameter calibration:

(1) Assigning reasonable values to all parameters using literature values as guidelines.

(2) Calibrating the settling rate, g, from measurements of particulate-P. During this step, the fitting between model predicted chlorophyll-a and field measurement was not necessary but it was important to ensure that the ortho-P concentration conformed to the field measurement that ortho-P disappeared within hours after the weekly nutrient addition and that there were no appreciable ortho-P concentrations at other times.

(3) Calibrating the values of K_I, μ_m, q, T_{opt}, T_{div} and k_2 from the chlorophyll-a measurement.

(4) Readjusting the values of ρ_m and k_ρ.

The concentration of PP is tied with the input of ortho-P and the settling rate. Since there was never an appreciable amount of ortho-P during the period of simulation, PP represented more than 99% of the total-P. In other words, the concentration of PP was, in fact, the concentration of total-P. In a water body with known hydrodynamic conditions and known input, the only parameter needed for simulating total-P concentration is the settling rate. Thus this calibration of settling rate may be perceived as an alternative approach to modeling the following:

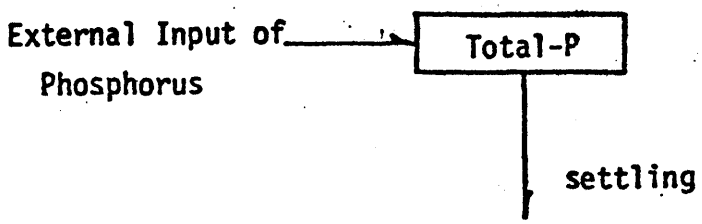

Figure 5.19: Calibrating the Settling Rate

The reason why the approach shown in Figure 5.19 is not taken is because the presence of ortho-P in the hypolimnion outside our modeling focus is allowed.

The field measurement of PP suggests that phosphorus added to the lake surface was effectively retained in the FML. The reduction of the PP concentration in the FML occurred only due to the dilution effect caused by the deepening of the FML which entrained the water below which had a lower PP concentration. For example, the model's predictions of the PP concentration on the 176th and 190th days using a settling rate of 0.05 m/day are shown in Figure 5.20. Comparison of the model predictions and the field measurements indicates that even with such a small settling rate, the model underpredicts the PP concentration by as much as 35% by the 190th day. A better fit is presented in the five panels of Figure 5.21 which shows the model simulation results with a zero settling rate together with the field measurements. The good fit of model prediction to field measurement is evident up to the 190th day. On the 204th day, if the average of the field measured PP concentration at the surface and at the 1 m depth is used as the upper 1 m PP concentration (represented by the open circles), then the model only misses the data point at the 2m depth. Therefore, we may consider the overall fit of the model prediction to field measruement as satisfactory for a zero settling velocity.

After the 204th day, for zero settling velocity, the model predicts a continuous increase of PP concentration in the FML (Figure 5.22). The predicted PP concentration in the FML reaches a peak value of 140 μg/ℓ on the 240th day. After the 240th day, although the addition of ortho-P was

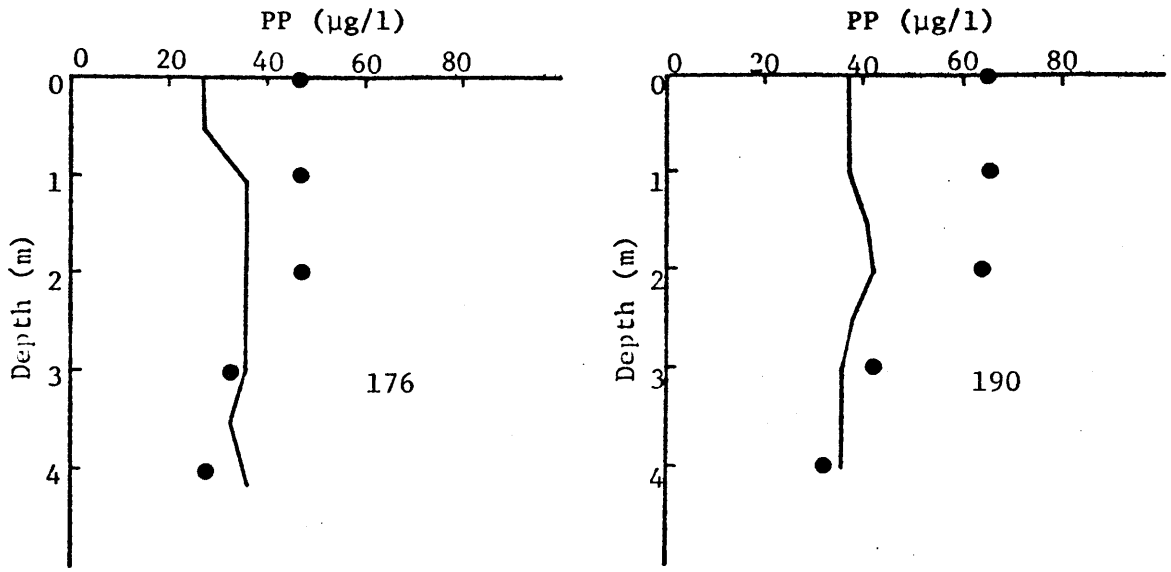

Figure 5.20: PP Profiles - Model I Simulation Results with Constant Settling Velocity (g = 0.05 m/day)

continued at the same rate of 1.14 kg-P/week, the increase in concentration due to the nutrient addition was offset by the deepening of the FML and the PP concentration in the FML began to decrease. Contrary to the model's prediction of the PP peak occurrence in the FML on the 240th day, the field measurement shows that in the FML the peak PP occurred around the 204th day after which the PP concentration reduced drastically. In order to simulate this observed decline after the 204th day, a non-trivial settling rate has to be employed for the period after the 204th day.

Chlorophyll-a, as a measurement of phytoplankton biomass,

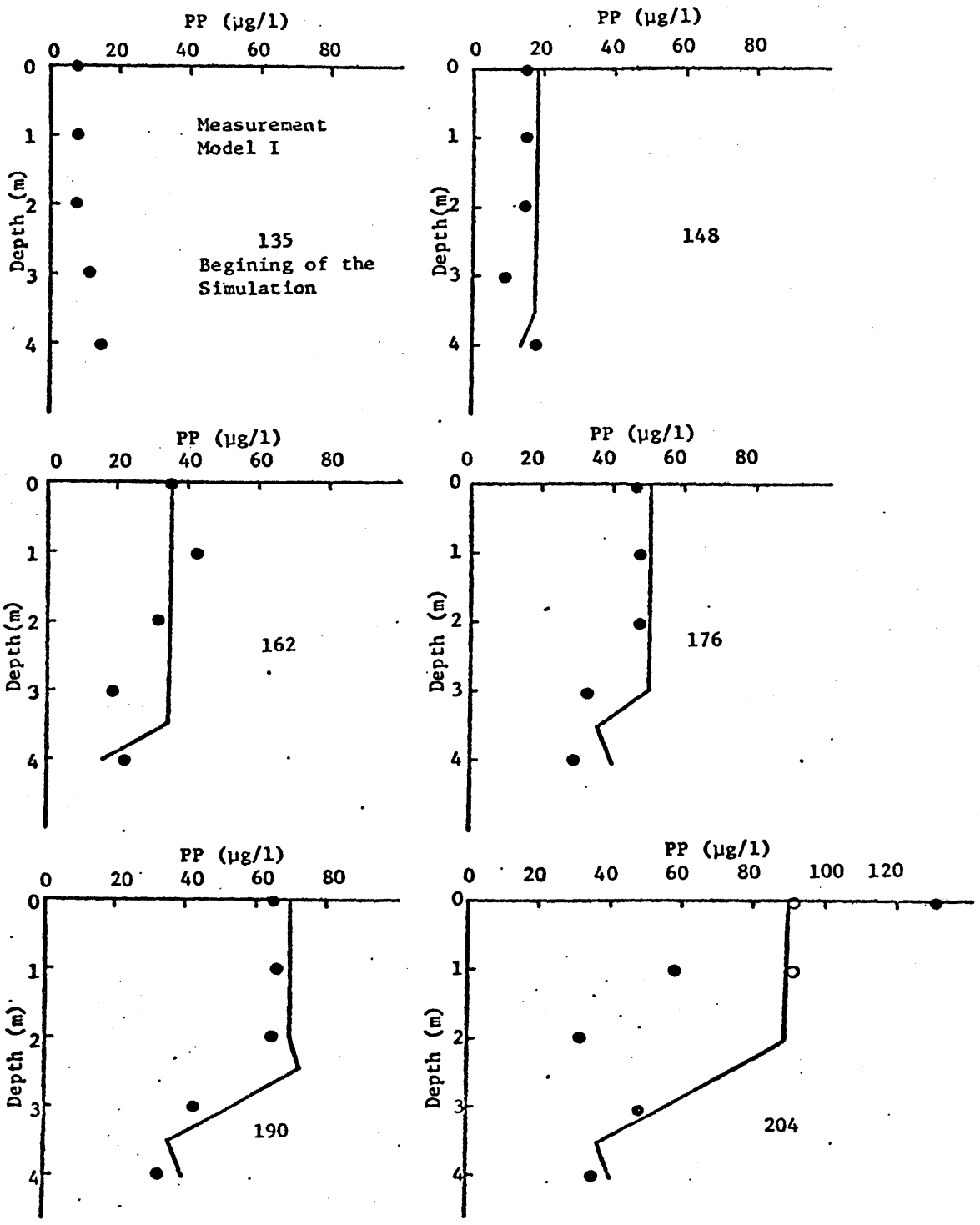

Figure 5.21: PP Profiles - Model I Simulation Results with Zero Settling Velocity

is the main state variable of the model. Since our present emphasis is to simulate the magnitude and the occurrence of the chlorophyll-a peak, as a first assumption, the phytoplankton mortality rate, k, is set to zero based on the argument that during the period of active growth, the mortality rate is negligible. Based on the assumption that PP are all bound in phytoplankton, the calibrated settling rate obtained from the PP simulation should also apply to chlorophyll-a. A convenient choice of the value for minimum cell quota, q, is 0.4 P/(chlorophyll-a) or 0.004 P/biomass by weight which is the value of the P/(chlorophyll-a) ratio at the chlorophyll-a peak. A phytoplankton growth rate of 1/day, a generally accepted value, is assumed.

After the assumption of these parameters, μ_m, q, k, there are three more parameters left to be calibrated, T_{opt}, T_{div}, and k_I. The calibration of these remaining three parameters proceeds with the simulation where the phytoplankton growth dependences on light and temperature are disregarded. That is, the phytoplankton is presently assumed to grow under optimal light and temperature conditions. The five panels of Figure 5.23 show model results (the bold curves) with the preliminary parameter values. The model predictions of chlorophyll-a concentration are high for the earlier three observations - the 148th, the 162nd and the 176th day - but are reasonable for the latter two observations - the 109th and the 204th. An examination of the temperature time series plot from the previous temperature simulation (Figure 5.6) indicates a trend of increase in the surface temperature from 10°C to 24°C during the period from the 135th day to the 204th day. The overprediction of the chlorophyll-a values for the earlier period may be corrected by introducing the

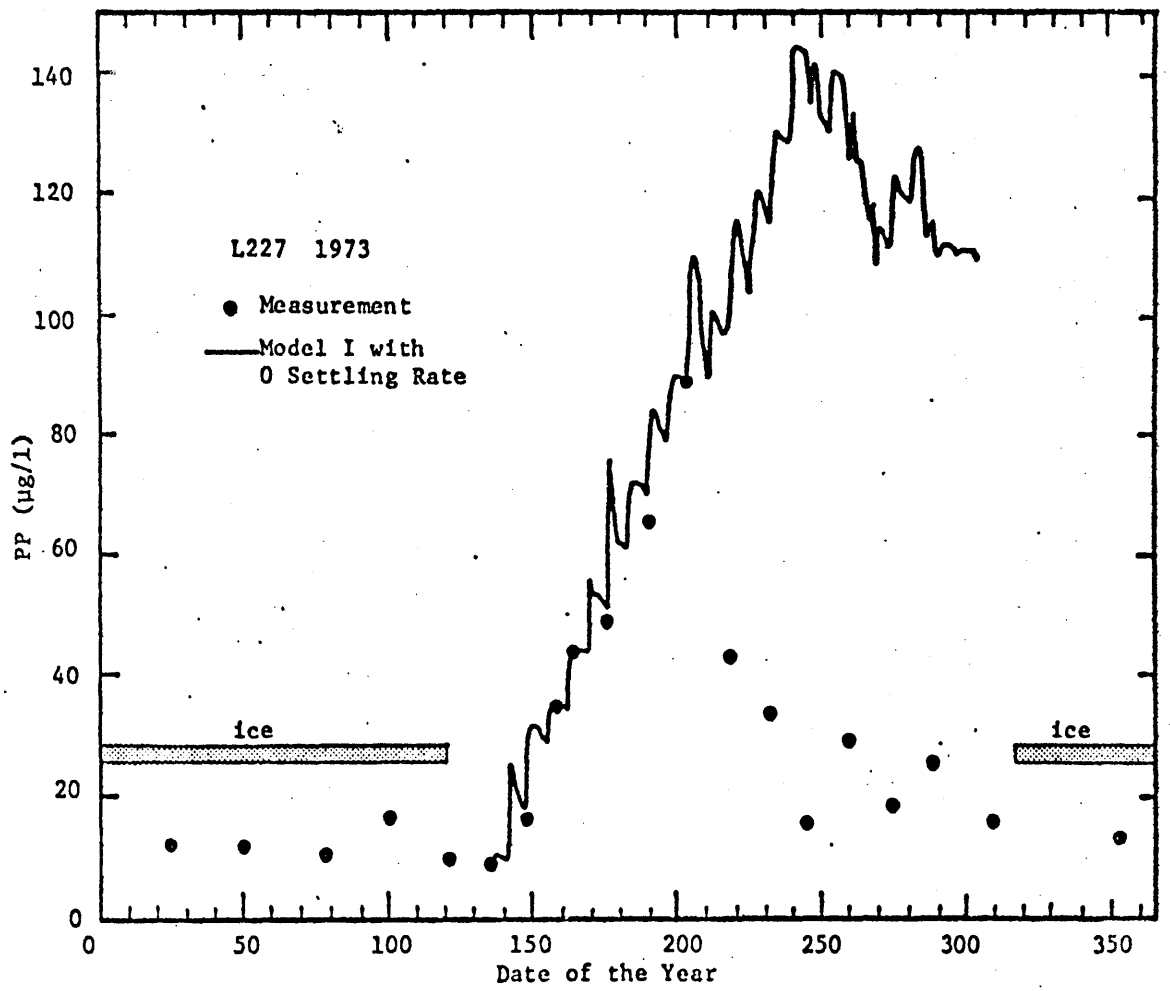

Figure 5.22: PP Time Series Plot - Model I Simulation Results with Zero Settling Velocity

temperature function with an optimal temperature value near the surface temperature during the later period. A value or 25°C which is higher than any of the surface temperatures is assumed. The other parameter in the temperature function, T_{div}, which regulates the sensitivity of the temperature dependence is left to be calibrated.

The model predictions with the addition of a temperature dependence function (equation 4.20) are shown as the dashed curves in Figure 5.23. T_{opt} equals 25°C and T_{div} equals 15°C. The introduction of these temperature parameters significantly reduces the chlorophyll-a predicted by the model for the 148th and 162nd days. The model currently overpredicts the chlorophyll-a concentration at the 3 m depth from the 162nd to the 190th day, and significantly overpredicts the chlorophyll-a concentration at the 4 m depth on the 190th day. A light dependence function will be a natural choice to eliminate these discrepancies. The daily average light intensities at the 3 m depth and 4 m depth are shown in Figure 5.24. Due to the high light extinction coefficient, the light intensity at the 3 m and 4 m depths are mostly less than 10 ly/day. Since the results in Figure 5.23 suggests that phytoplankton in the 3 m and 4 m depths suffer only a slight light limitation, a small value of k_I, the half saturation coefficient for the light function (equation 4.8) will be appropriate.

The model prediction with a k_I of 15 ly/day is shown in Figure 5.25. Except for the chlorophyll-a concentration at the 4 m depth on the 204th day, the field measurement of chlorophyll-a is now well depicted by the model. On the 204th day, the 4 m depth is anoxic, since there is no emphasis on fitting the chlorophyll-a measurement of the anoxic region (see section 5.3.1) the model prediction is regarded satisfactory and the

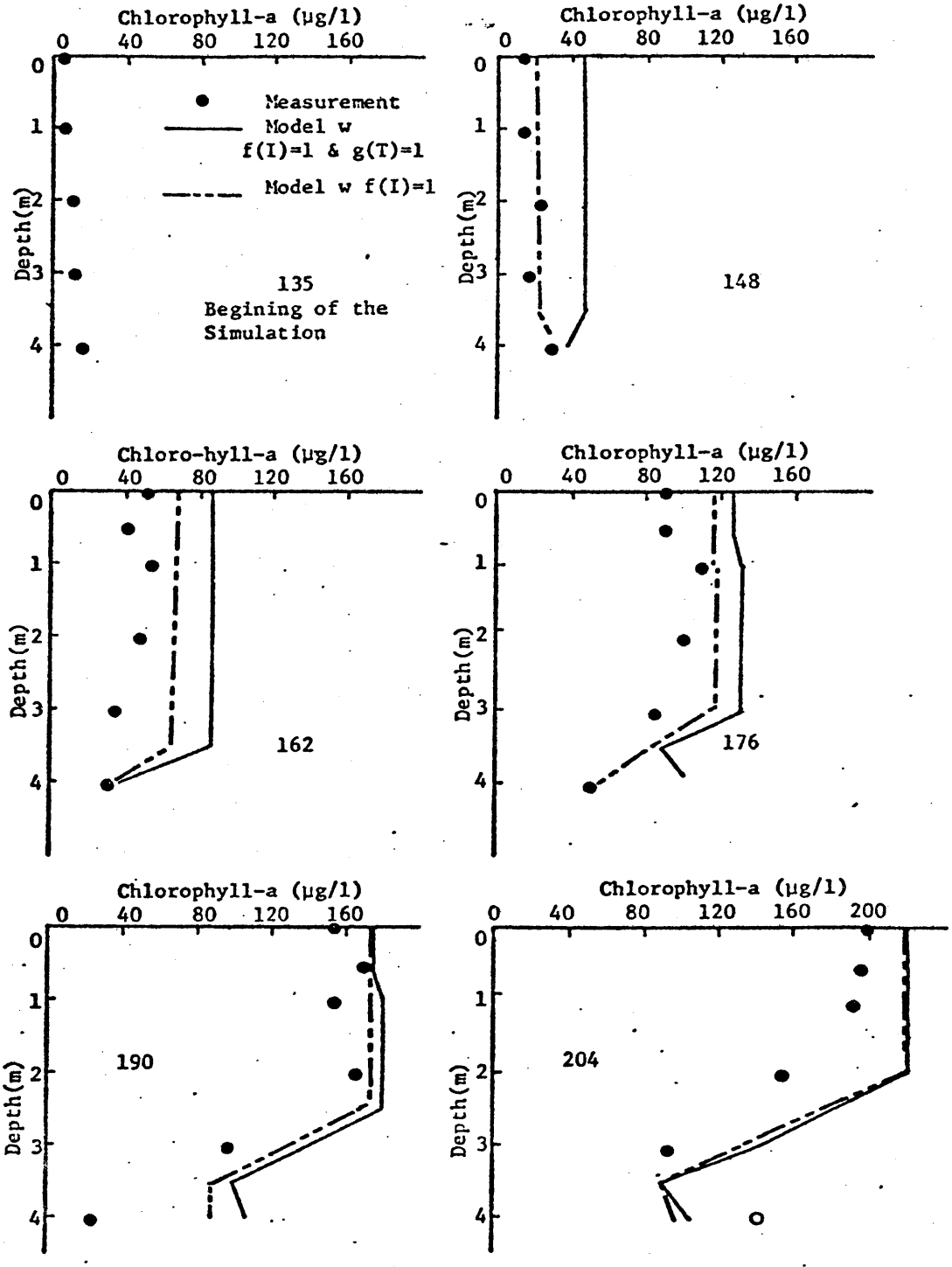

Figure 5.23: Calibration of Additional Biological Rate Constants with Chlorophyll-a Measurement (with zero settling rate)

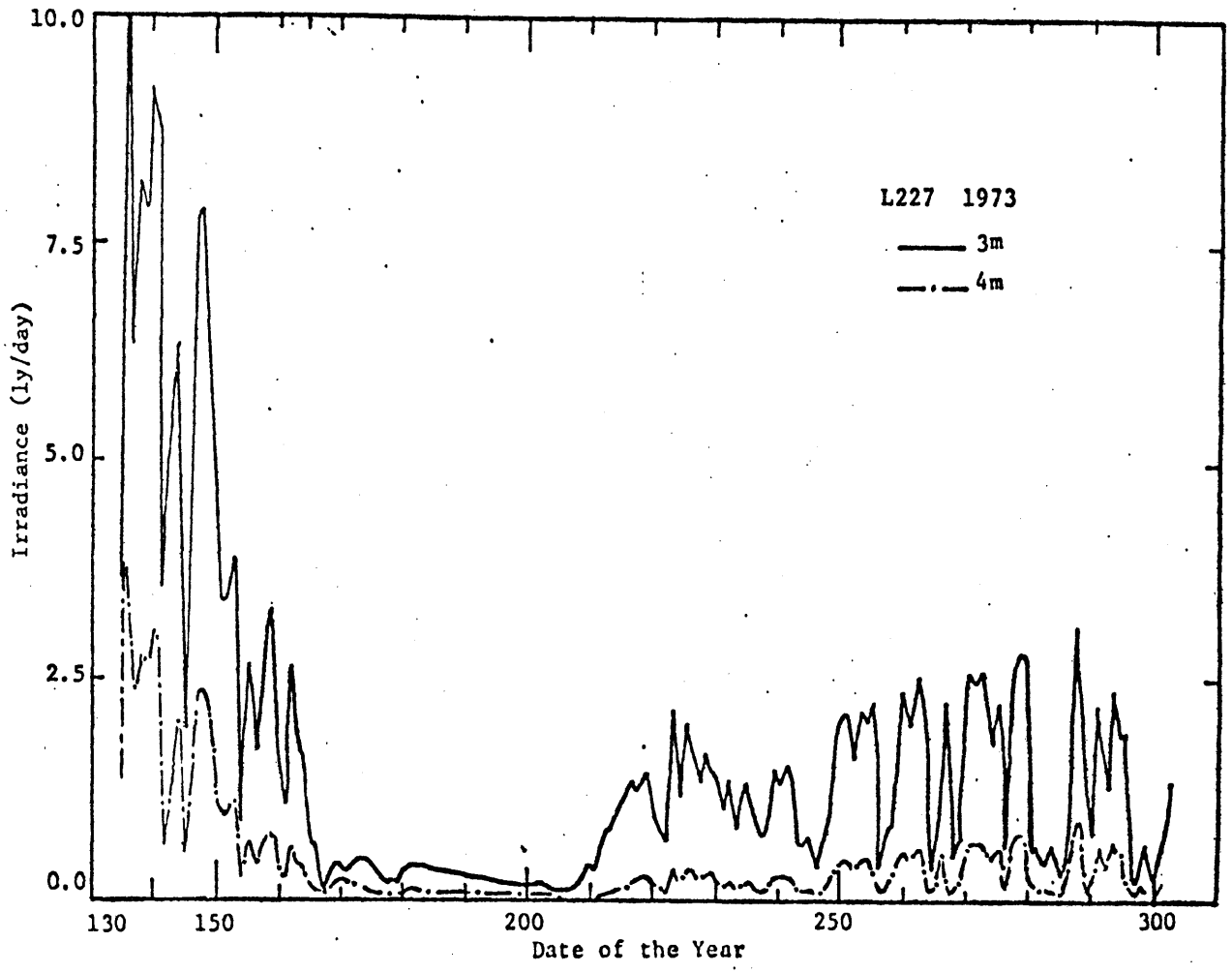

Figure 5.24: Daily Averaged Light Intensities at 3,4 m Lake Depths

task of calibrating the model parameters, μ_m, q, T_{opt}, T_{div}, k_I, is completed.

The model with these parameters predicts a continuing increase of chlorophyll-a concentration in the FML after the 204th day (Figure 5.26), a trend similar to that in the PP simulation. A maximum value of 350 μg/ℓ is predicted on the 245th day which is followed by a reduction mainly induced by the dilution effect brought about by the deepening of the FML. The field measurement, however, indicates a drastic decrease of chlorophyll-a after the 204th day. The present model's overprediction of the PP in the FML for the period after the 204th day is undoubtedly the main cause for this corresponding overprediction of the chlorophyll-a in the FML.

A combination of ρ_m = 0.3 μg-P/(μg-chlorophyll-a)/day and k_ρ = 20 μg/ℓ allows the added ortho-P to be taken up to a non-detectable amount within a day. However, it must be emphasized that this combination is not the only one which will produce the same effect. Moreover, a combination of these two values sets the lower bound of the nutrient uptake rate since the information on the exact time history of ortho-P from the moment of addition to the time of reaching non-detectable levels is not available. The set of coefficients used to produce the above effect is summarized in Table 5.8.

The next step is to simulate the observed sharp decline of the epilimnion PP and chlorophyll-a after the 204th day. The only parameter in the present model, Model I, which can exert the same loss effect on both PP and chlorophyll-a is the settling rate. Figure 5.27 shows the values of settling rate needed in order to simulate the observed PP

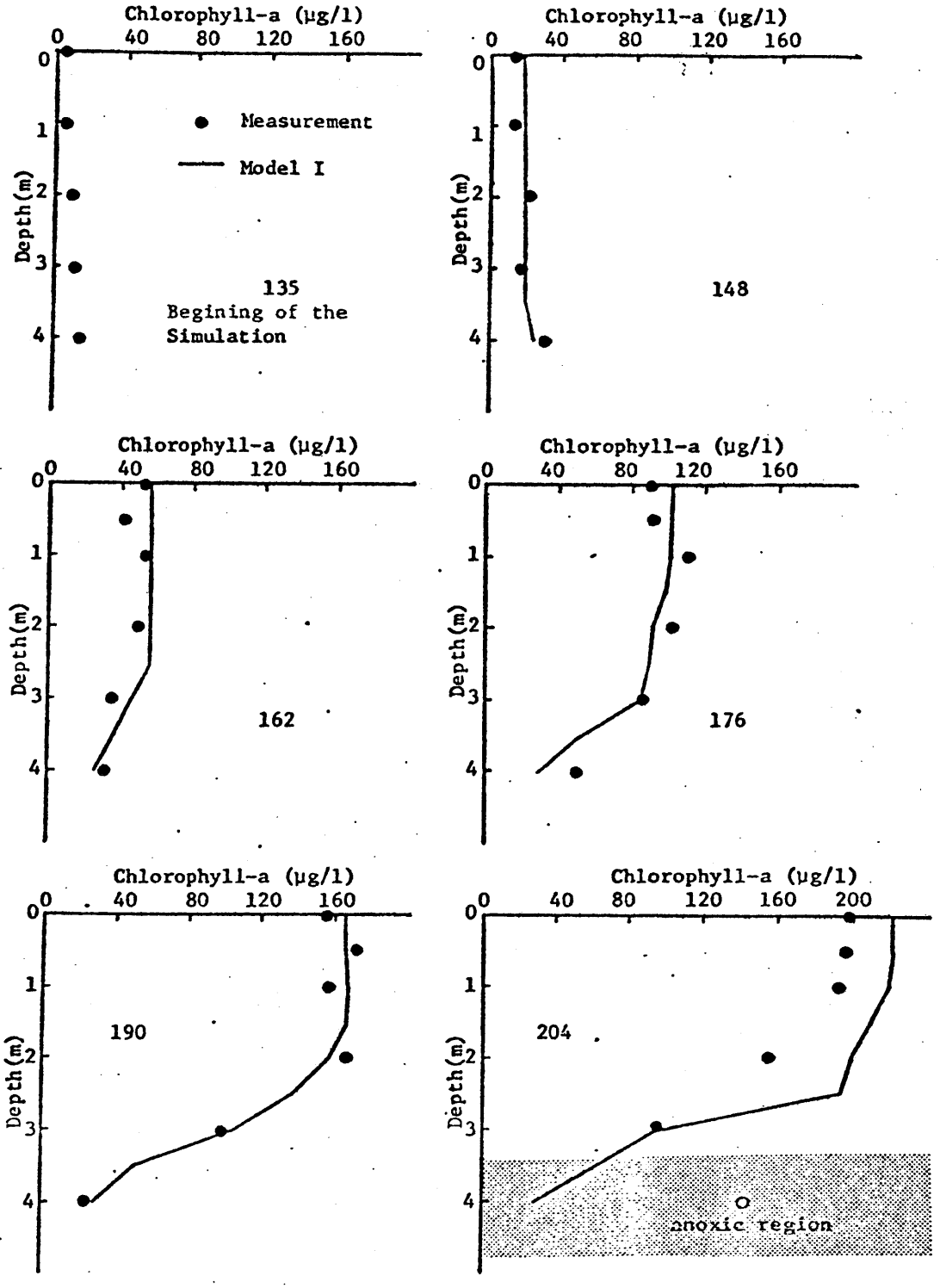

Figure 5.25: Chlorophyll-a Profiles - Model I Simulation Results With Zero Settling Rate

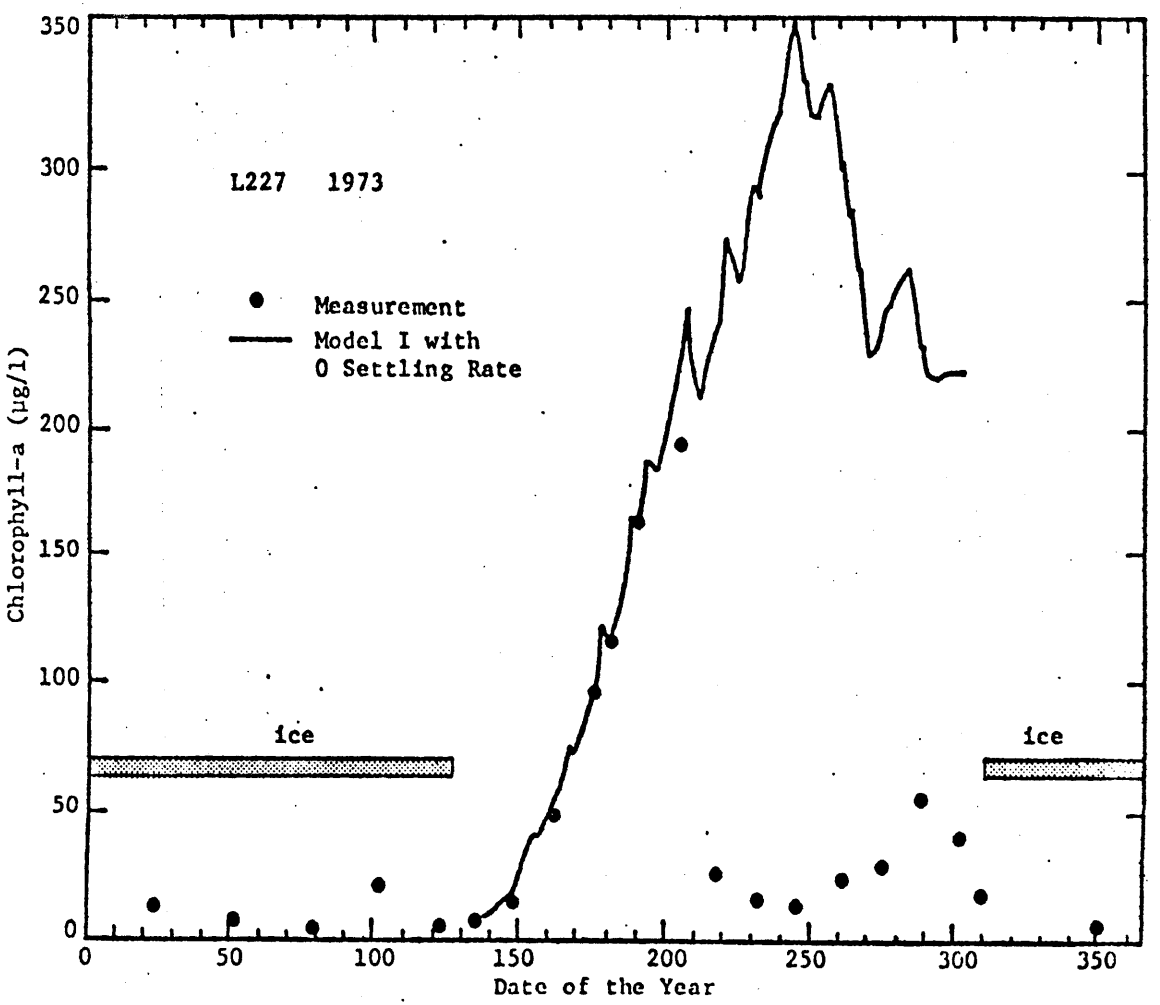

Figure 5.26: Chlorophyll-a Time Series Plot - Model I Simulation Results with Zero Settling Velocity

Table 5.8

Model Parameters - Model I

Parameter Values

Symbol	Definition	Unit	Value	Source
ρ_m	max. PO_4^{-3} uptake rate	$(g\text{-}P)(g\text{-phytoplankton})^{-1}$ day^{-1}	0.3	Calibration
K_ρ	Michaelis constant for PO_4 uptake by phytoplankton	$\mu g/\ell$	20.	Calibration
g	settling velocity	$m(day)^{-1}$	0.	Calibration
q	minimum. P cell quota	$(g\text{-}P)(g\text{-phytoplankton})^{-1}$ day^{-1}	0.004	Calibration
T_{opt}	optimum temperature for photosynthesis	C	25.	Calibration
T_{div}	temperature coefficient	C	15.	Calibration
m	maximum phytoplankton growth rate	day^{-1}	1.	Assumption
K_I	half saturation constant for light function	langley	15.	Calibration
k_2	phytoplankton mortality rate	day^{-1}	0	Assumption

*Initial concentrations of ortho-P, phytoplankton, phytoplankton-P are obtained from the chemistry measurement notebook.

concentration in the period after the 204th day (Figures 5.28 & 5.29). The settling rate varies from 0.01 m/day to 0.3 m/day. A time varying parameter reflects a definition of the model formulation which assumes a constant settling rate; therefore, a formulation which captures the variability of this parameter-settling be included in the present model.

A variable phytoplankton settling rate is not an uncommon phenomenon. Diurnal to seasonal variations of the phytoplankton settling rate has been observed (Burns and Rosa, 1980; Lannergren, 1979). The diurnal variation may not be considered since we are not modeling phytoplankton variation at that time scale. Seasonal variation may be associated with a change of phytoplankton species which has often been identified to be induced by a change of the FML depth.

When the FML depth is larger, settling becomes a less significant loss factor for phytoplankton when compared with the case with a smaller FML depth. Therefore, as thermal stratification progresses, the dominance of phytoplankton species with smaller settling velocities tends to be favored. Lund (1954, 1955) has shown that the diatom, which has a higher settling velocity than other phytoplankton but a better ability to adapt to low temperature conditions disappears almost completely from the lake when the lake becomes stratified.

Conversely, the deepening of the FML might give phytoplankton with higher settling velocities a better chance to compete with others. The applicability of the species variation induced by FML variation may be evaluated by examining the time series plot of the FML in Figure 5.4. Following the previously stated reasoning, the dominance of phytoplankton with a small settling rate should be favored in the period from the 204th

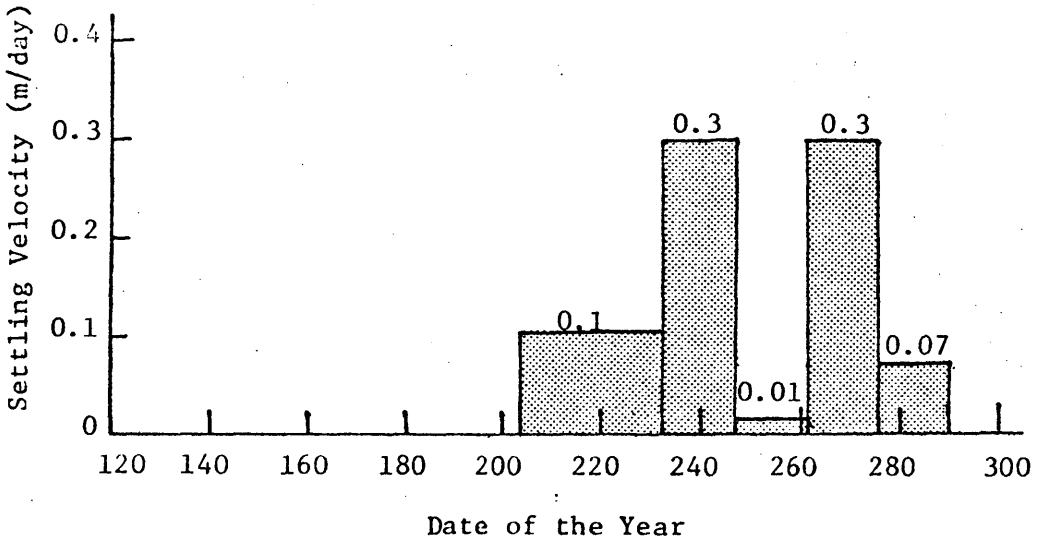

Figure 5.27: Settling Velocity Needed to Fit PP Measurement

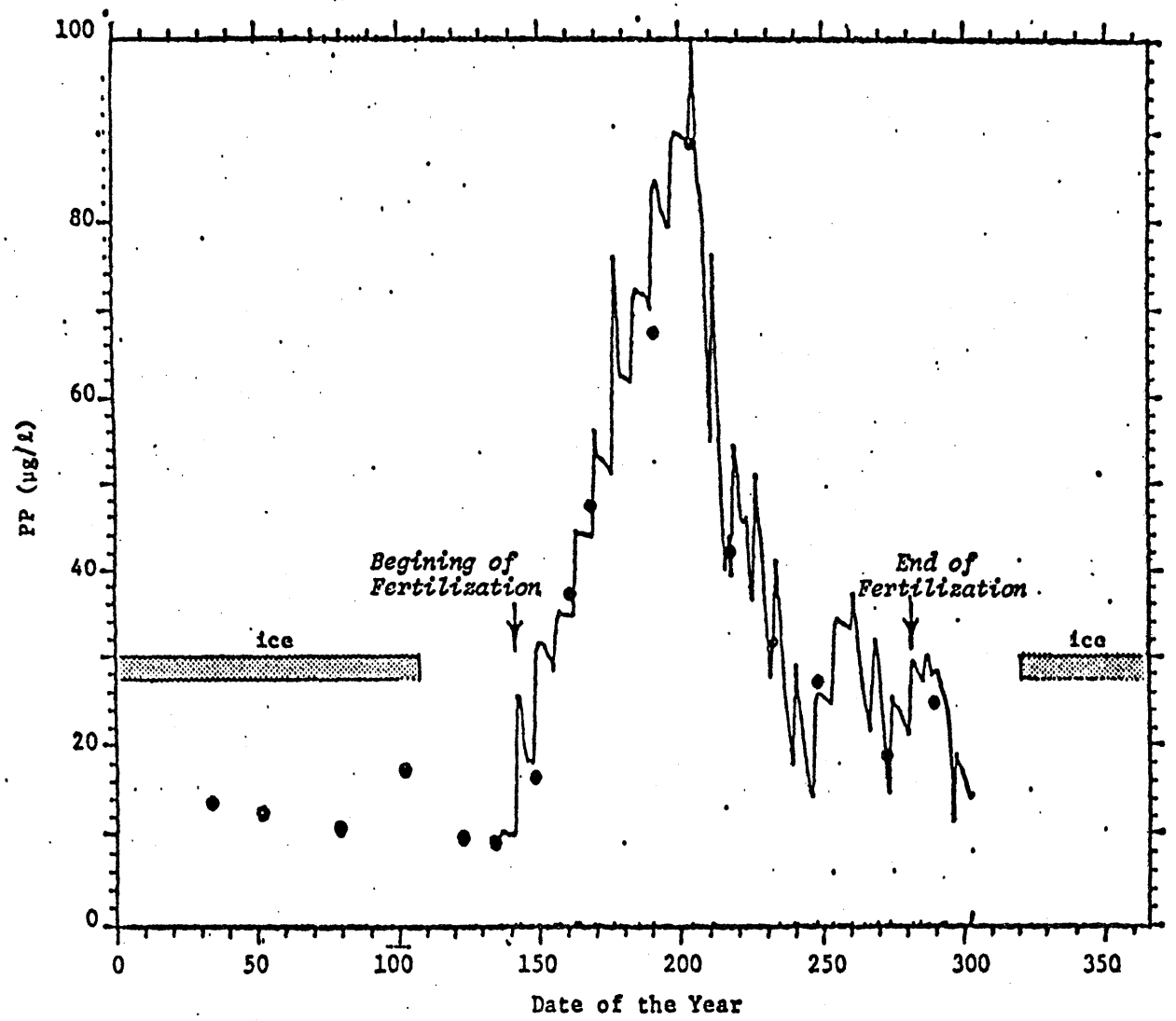

Figure 5.28: Chlorophyll-a and PP Concentration in the FML Obtained by Using a Variable Settling Velocity

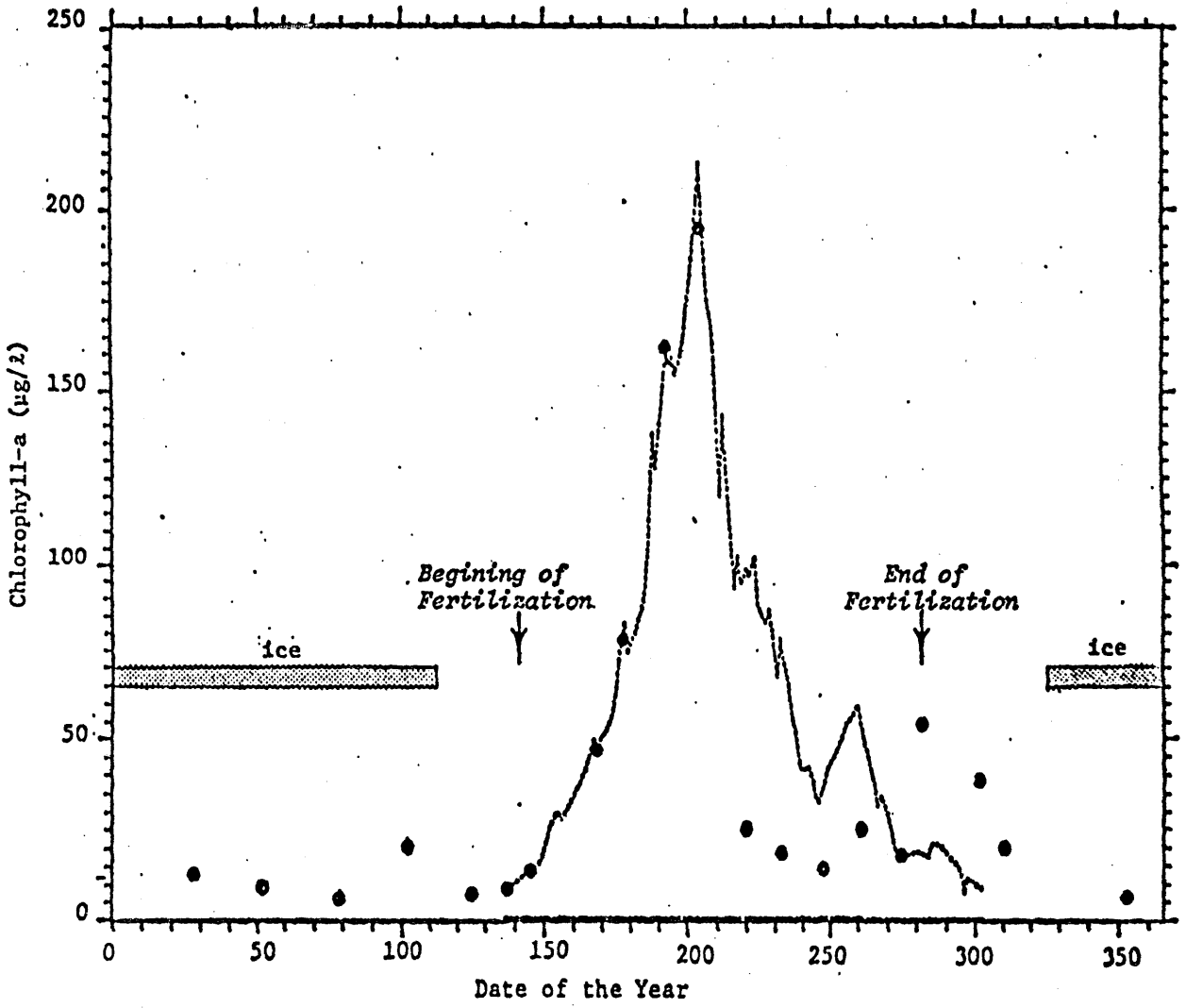

Figure 5.29: Comparison Between Ivlev and Holling Formulas

to the 240th day which is in fact the period with the smallest FML depths. Therefore, we may conclude that the inclusion of competition among species with various settling velocities will not lead to the desired result of having a species with a higher settling velocity dominating during the period immediately after the 204th day.

Other than the seasonal species succession caused by environmental factors, the phytoplankton settling rate may vary with its physiological state. Eppley et al. (1967) found that sinking rate was inversely related to the growth rate in cultures of Thalassiosira fluvuatillis. Titman and Kilham (1976) studied the settling rate of four freshwater phytoplankton species and found that on the average, cells at a stationary growth phase sink four times faster than cells in the log growth phase. The growth rate of phytoplankton is related to the limiting nutrient content of the cell. The plot of P/(chlorophyll-a) ratio vs. time (Figure 5.13) serves as a clear guideline for judging the success of including a formulation which expresses the settling rate as a function of the phytoplankton nutrient status. It is not possible to predict a high settling velocity for the period after the 218th day since the P/(chlorophyll-a) ratios are high for that period. Consequently, this formulation will not predict an increase of settling rate as Figure 5.27 suggests.

Since neither of the two possible formulations would allow a successful prediction of the change in the settling velocity, an alternative is to include an often encountered ecological phenomenon - the control of the population of a trophic level by the next higher trophic

level. The disappearance of the PP and chlorophyll-a from the water column may be caused by zooplankton grazing. A model which incorporates zooplankton as an additional state variable is discussed in the following section.

5.3.2.2 Simulation with Zooplankton as Additional Variable -- Model II

A. Model Description

The inclusion of zooplankton in the model introduces far more complexities. The elements which have been considered in modeling zooplankton dynamics include speciation (Thomann et.al., 1975), differentiation between egg, juvenile and adult (Kremer and Nixson, 1978), and selective feeding (Park et. al., 1974). The vertical migration of zooplankton compounds the difficulty (Bowers, 1978). While a detailed consideration of the zooplankton dynamics is important in its own right, the lack of information hardly justifies an elaborate approach in our present modeling attempt. Three fundamental processes of zooplankton are considered: growth, excretion and mortality. The description of each of these three processes are kept in the simplest possible form.

The classic model describing the predator-prey relationship is that of Lotka-Volterra (1925, 1926) which describes the specific predator grazing rate ρ_z as a linear function of the prey concentration X:

$$\rho_z = a\ X \tag{5.16}$$

where a = constant. However, many researchers have observed that there is an upper limit to the rate at which a predator can assimilate its food (Rigler, 1961b; Reeve, 1963; Kersting et. al., 1976). Therefore, a more realistic function must have the ability to simulate this asymptotic maximum. Two classic examples are those of Ivlev (1961) and Holling (1965):

$$\text{Ivlev:} \quad \rho_z = \rho_{z\ max}(1-e^{-cX}) \tag{5.17}$$

$$\text{Holling:} \quad \rho_z = \rho_{z\,max} \frac{X}{X + K_X} \tag{5.18}$$

The graphic representation of these curves is shown in Fig. 5.29. The two are similar and the Holling (1965) function is used in our model.

Peters (1973) has investigated the phosphorus excretion by zooplankton and observed that 90% of the phosphorus excreted by Daphnia is ortho-P. This finding permits the assumption that all excretion by zooplankton is ortho-P without suffering more than 10% error. The excretion rate is considered to be a constant fraction of the grazing rate:

$$e = c\,\rho_z\,Q\,z \tag{5.19}$$

where e = ortho-P excretion rate per zooplankton, ρ_z = specific grazing rate of zooplankton and c = fraction of ingested phosphorus which is excreted.

All sink terms for zooplankton and zooplankton - contained phosphorus are lumped into one parameter - mortality rate which represent the aggregated effect of zooplankton death, loss of zooplankton contained phosphorus by the settling of fecal pellets and fish grazing.

The mortality rate of zooplankton is assumed to be constant, an oversimplification since the zooplankton population is likely to be affected by the next higher trophic level, just as the phytoplankton population is controlled by zooplankton or by food limitation. However, since the present goal is to simulate the decline of the phytoplankton concentration after the 204th day and less emphasis is placed on

correctling simulating the phytoplankton concentration after the peak, a more realistic formulation of zooplankton mortality rate will not be considered. Instead, the variation of mortality will be considered in a sensitivity analysis. The effect of temperature on the zooplankton grazing rate is described using the same formulation as that describing the effect of temperature on photosynthesis. This model (Model II) is presented in Figure 5.30 and Tables 5.9 and 5.10.

The inclusion of zooplankton grazing followed by excretion of ortho-P and the assimilation of ortho-P by phytoplankton (grazing/excretion), will induce the following two effects:

(1) decrease in phytoplankton biomass

(2) increase in phosphorus cell quota

In the absence of zooplankton, the epilimnion chlorophyll-a concentration would be 242 μg/ℓ (Figure 5.26) while the data suggest that 90% of this population was lost in two weeks time. On the other hand, the PP simulation result (Figure 5.21) indicates that the amount of phosphorus in the water column was well accounted for by the phosphorus contained in phytoplankton up to the 204th day. Since zooplankton grazing causes a loss of phosphorus (see section 3.3.1.2), the result in Figure 5.21 suggests that the amount of zooplankton present must be still low on the 204th day. Therefore, the major consideration is to check the possibility of the current model in simulating a situation which has a low initial concentration of zooplankton but this small amount of zooplankton present could reduce 90% of the phytoplankton population in two weeks time.

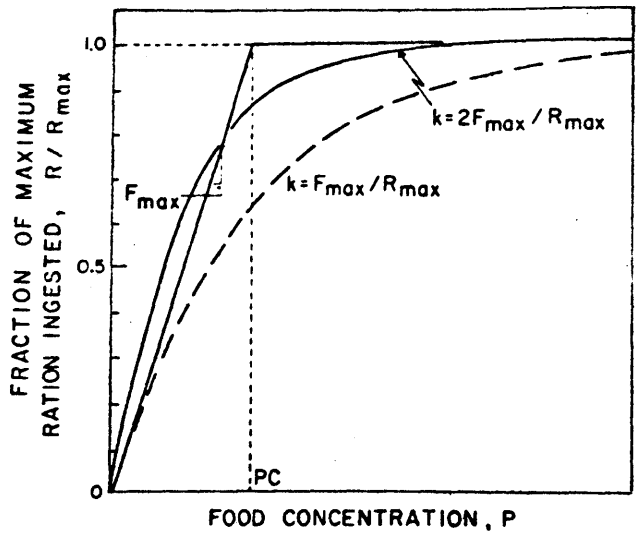

Figure 5.29. Empirically derived relationship between a maximum filtering rate and the appropriate exponent (k) in the Ivlev Eq. (18). Specifying $k=2F/R_{max}$ provides a more satisfactory fit to the initial maximum filtering rate below the critical food concentration (PC) where the maximum ration is predicted (from Kremer, J.M. and S.W. Nixon, 1978).

MODEL II

4 STATE VARIABLES

S - ORTHO-P, IN µG/L

X - PHYTOPLANKTON BIOMASS, IN µG/L

Q - PHOSOPHORUS TO BIOMASS RATIO BY WEIGHT

Z - ZOOPLANKTON BIOMASS, IN µG/L

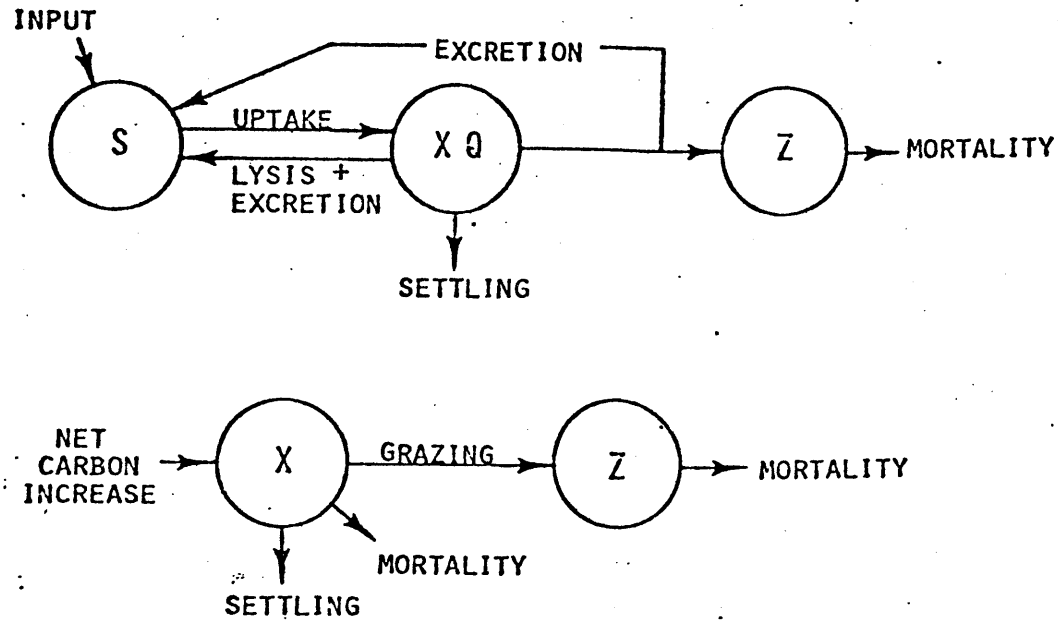

NET CARBON INCREASE = PHOTOSYNTHESIS - RESPIRATION
- PHOTORESPIRATION - EXCRETION

Figure 5.30: Schematic Diagram - Model II

Table 5.9

Model State Variables vs. Field Measurement

Model II

$$\begin{pmatrix} 1 & 0 & 0 & 0 \\ 0 & r & 0 & 0 \\ 0 & 0 & 1 & 0 \\ 0 & 0 & 0 & 1 \end{pmatrix} \begin{pmatrix} S \\ X \\ XQ \\ Z \end{pmatrix} = \begin{pmatrix} \text{ortho-P} \\ \text{chlo-a} \\ PP \\ - \end{pmatrix}$$

r = chlorophyll-a/biomass ratio assumed to be 0.01

Table 5.10

1-D Mass Balance Equations

Model II

1-D Mass Balance Equations:

$$\frac{\partial S}{\partial t} = \frac{\alpha}{A}\frac{\partial}{\partial z}\left(A\frac{\partial S}{\partial z}\right) + D(S_i - S) + i_S - \rho X + (k_1+k_2)(XQ) + \left(\frac{1}{f} - 1\right)\mu_z QZ$$

$$\frac{\partial X}{\partial t} = \frac{\alpha}{A}\frac{\partial}{\partial z}\left(A\frac{\partial X}{\partial z}\right) + D(X_i - X) + \mu X - k_2 X - \frac{\partial}{\partial z}(gX) - \frac{1}{f}\mu_z Z$$

$$\frac{\partial (XQ)}{\partial t} = \frac{\alpha}{A}\frac{\partial}{\partial z} A\frac{\partial (XQ)}{\partial z} + D(X_i Q_i - XQ) + \rho X - (k_1+k_2)(XQ) - \frac{\partial}{\partial z}(gXQ) - \frac{1}{f}\mu_z ZQ$$

$$\frac{\partial Z}{\partial t} = \frac{\alpha}{A}\frac{\partial}{\partial z}\left(A\frac{\partial Z}{\partial z}\right) + D(Z_i - Z) + (\mu_z - r_z)Z$$

Rate Expressions:

$$u_z = \mu_{zm}\frac{X}{X+k_X}\exp\left(-2.3\left|\frac{T-T_{zopt}}{T_{zdiv}}\right|\right)$$

$$r_z = r_{zm}\exp\left(-2.3\left|\frac{T-T_{zopt}}{T_{zdiv}}\right|\right)$$

u, ρ are the same as those defined in Table 5.8

Parameters to be Calibrated:

μ_{zm}, r_{zm}, k_x, f, T_{zopt}, T_{zmax}

and all the calibrated parameters listed in Table 5.8

Definitions:

Z - zooplankton

r_z - zooplankton mortality rate

μ_z - zooplankton growth rate which is a constant fraction (f) of the grazing rate ρ_z

f - efficiency of zooplankton grazing

α - mass molecular diffusivity

All other symbols are the same as those defined in Table 5.8

The epilimnion PP concentration in the absence of zooplankton is shown in Figure 5.22. When compared with the field data, the result in Figure 5.22 indicates that 50% of the phosphorus was lost in the subsequent two weeks. PP was lost at a smaller rate than chlorophyll-a there must be an increase of phytoplankton cell quota in this period. The second consideration is to check the possibility of the current model-Model II to increase phytoplankton P cell quota. Simple mathematical presentations will be helpful in appreciating the magnitude of these two effects. First, the effect of zooplankton grazing on phytoplankton population under the following conditions is considered:

- System: a fully mixed batch system
- Species: phytoplankton and zooplankton

then the temporal variation of the species can be described as:

$$\frac{dx}{dt} = \mu x - \frac{\mu_z}{f} \frac{x}{x + k_x} z \qquad (5.20)$$

$$\frac{dz}{dt} = (u_z - b)z \qquad (5.21)$$

where: x = phytoplankton concentration

z = zooplankton concentration

μ = phytoplankton growth rate

μ_z = zooplankton growth rate which is a constant fraction of the grazing rate (ρ_z)

b = zooplankton death rate

f = efficiency of grazing

k_x = half saturation constant

If the phytoplankton growth rate approaching zero and the phytoplankton concentration being much greater than the half saturation constant of the zooplankton grazing rate represent the situation where the phytoplankton have used up the resources in the environment and have reached their peak value, i.e.,

$$\mu \doteq 0 \tag{5.22}$$

$$\frac{x}{x + k_x} \doteq 1 \tag{5.23}$$

then the solution for the phytoplankton concentration in this case is:

$$x = x_o + \frac{\mu_z z_o}{f(\mu_z - b)} (1 - e^{(\mu_z - b)t}) \tag{5.24}$$

where x_o, z_o are the initial concentrations of phytoplankton and zooplankton. If it is assumed that (1) the zooplankton mass increase from grazing on phytoplankton is 0.24/day, (2) the net increase rate is 0.16/day, and (3) the initial concentration of zooplankton is one-tenth of that of the phytoplankton, then the concentration of phytoplankton will be reduced to one-tenth of its initial concentration in ten days. This case illustrates that if the phytoplankton population reaches its saturation value, it only takes ten days for the zooplankton, whose initial concentration is one-tenth of the phytoplankton concentration, to reduce the phytoplankton to one-tenth of its initial value.

For our second mathematical presentation, the effect of zooplankton grazing/excretion on phytoplankton cell quota is considered under the following simplified conditions:

- System: a fully mixed batch system
- Species: phytoplankton, zooplankton, phytoplankton-P (or phosphorus cell quota)
- No external source of ortho-P

then the temporal variation of these species can be described as:

$$\frac{dx}{dt} = \mu x - \frac{\mu_z}{f} z \tag{5.25}$$

$$\frac{dz}{dt} = \mu_z z \tag{5.26}$$

$$\frac{d(xQ)}{dt} = (\frac{1}{f} - 1)\mu_z zQ - \frac{\mu_z}{f} zQ \tag{5.27}$$

$$= - u_z zQ$$

The variation of the cellular phosphorus content Q may be readily obtained from Equations (5.25) and (5.27):

$$\frac{dQ}{dt} = \mu_z (\frac{1}{f} - 1) \frac{z}{x} Q - \mu Q \tag{5.28}$$

$$\text{If } \mu_z(\frac{1}{f} - 1)\frac{z}{x} \geq \mu \tag{5.29}$$

$$\text{then } \frac{dQ}{dt} \geq 0 \tag{5.30}$$

Equation (5.29) defines the condition under which the phytoplankton cell quota increases in the presence of zooplankton and Equation (5.28) defines the effect of zooplankton grazing/excretion on phosphorus cell quota.

This result appears perplexing at first glance because the optimal growth rate of phytoplankton is about one order of magnitude larger than the growth rate of zooplankton, that is, $\mu_{max} = 10\ (\mu_z)$. If f equals 0.5, i.e., 50% of the ingested nutrient is released as ortho-P, then a zooplankton population ten times the phytoplankton population size is needed to sustain a constant phytoplankton cell quota. But in a natural environment, a correct representation of ρ has to account for the reduced light effect, that is,

$$\mu = \mu_{max} f(I) \tag{5.31}$$

If the suboptimal light reduces the phytoplankton growth rate to one-twentieth of its maximum rate, i.e., $\mu = 0.05\ \mu_{max}$, then a zooplankton population that is half of the phytoplankton population size will be able to sustain a constant cell quota. This could explain the occurrence of the following three phenomena:

(1) absence of trace amounts of ortho-P in the environment

(2) a high phosphorus cell quota

(3) an appreciable photosynthetic activity, if the measurement is done by suspending a bottle at a depth near optimal light intensity.

However, the condition needed for a net phytoplankton growth is defined by:

$$\mu x > \frac{\mu}{f} z \qquad (5.32)$$

Comparing the condition needed for sustaining constant cell quota (Equation 5.29) with Equation (5.32), it may be seen that two conditions cannot be simultaneously satisfied in the absence of an external nutrient supply. That is, in the absence of an external nutrient supply, the grazing/excretion activity of zooplankton can only slow the rate of cell quota decrease in the period of net phytoplankton population growth. To sustain a constant cell quota or even to increase it, the net phytoplankton population must have a net decrease.

In the period from the 204th to the 218th day, phytoplankton in L227 decreased by 90%, therefore, we may conclude that the inclusion of zooplankton grazing/excretion will increase the P cell quota as reflected by the smaller reduction (50%) of the measured PP during this period.

B. Simulation Results and Analysis

The results of the Model II simulation is presented in Figure 5.31 and Figure 5.32. The inclusion of zooplankton successfully decreases the epilimnion chlorophyll-a and particulate P concentrations after the 204th day. No special emphasis is placed on simulating the chlorophyll-a and particulate-P concentrations after the 204th day so that the percentage error in model prediction is considerably higher for the post-204th day period. The dissolved oxygen concentration was near zero from 3 m and deeper for the period between the 204th day and the 260th day. Therefore, the concentration of zooplankton was specified to be be zero at depths below 3 m assuming that zooplankton is sensitive to the dissolved oxygen concentration in the environment. Table 5.11 summarizes the parameter values and initial concentrations used to produce the results shown in Figures 5.31 and 5.32. Parameters which are common to both Models I and II are kept the same, as shown in Table 5.8.

In Model I, the initial concentration of each state variable is provided by the field measurement while in MOdel II, the initial concentration of zooplankton has to be specified without the benefit of measurement. The initial concentration of zooplankton should, therefore, be considered as a paramter. The sensitivity of the Model II prediction to the variation of individual parameters (only those related to zooplankton) is presented in the four panels of Figure 5.33. Model prediction is sensitive to each of the following parameters: grazing rate (Figure 5.33a), initial concentration (Figure 5.33b) and optimal temperature for growth (Figure 5.33d).

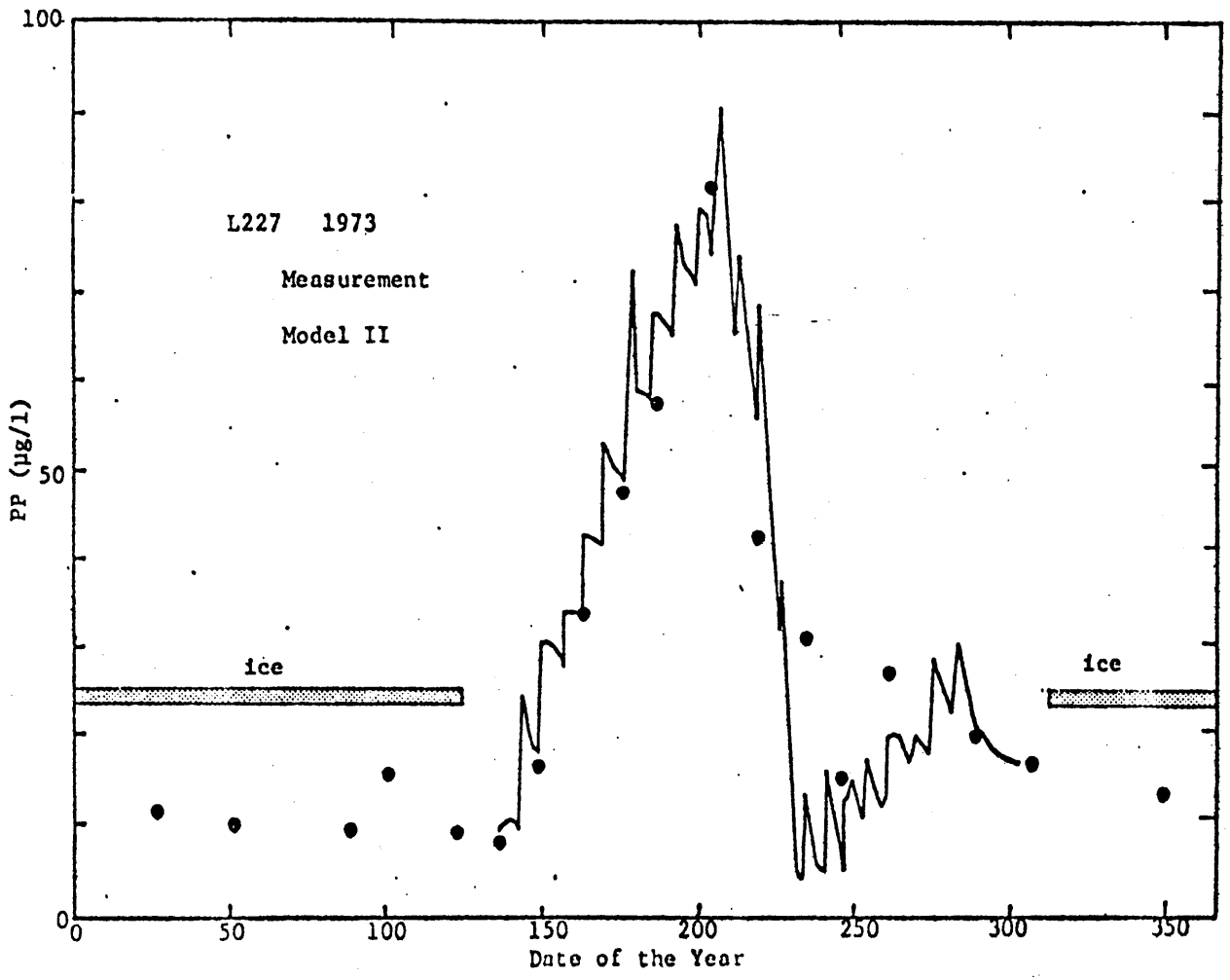

Figure 5.31: FML Concentrations of PP Model II Simulation Results

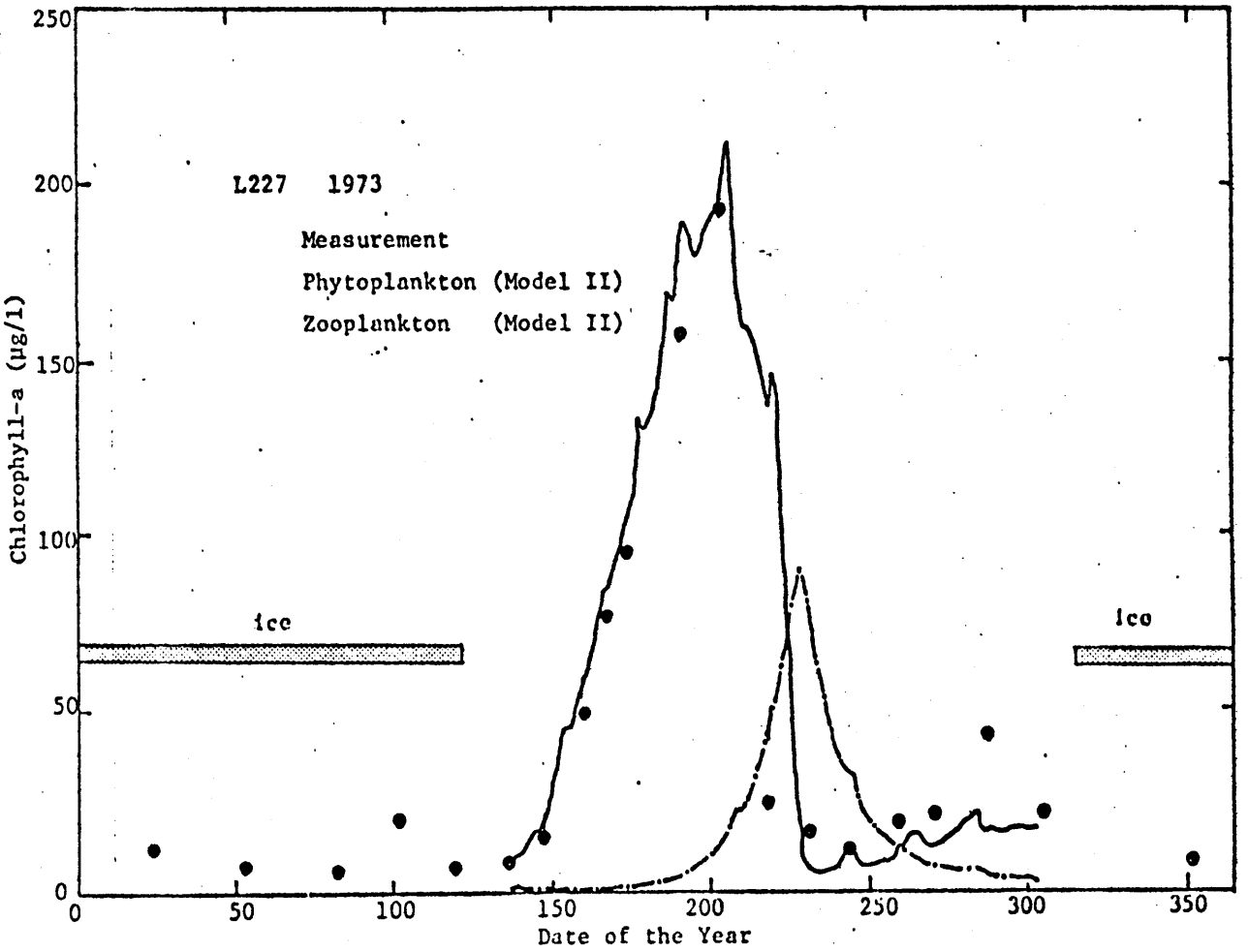

Figure 5.32: FML Concentration of Chlorophyll-a - Model II Simulation Results

Table 5.11

Parameter Values - Model II

Symbol	Definition	Unit	Value	Source
μ_{zm}	maximum specific zooplankton growth rate	day^{-1}	0.25	Calibration
r_{zm}	specific zooplankton respiration and mortality rate	day^{-1}	0.1	Calibration
T_{zopt}	optimum temperature for zooplankton growth	C	20	Calibration
T_{zdiv}	temperature coefficient for zooplankton growth	C	20	Calibration
K_x	half saturation coefficient for zooplankton grazing	µg/ℓ	100	Calibration
f_z	efficiency of zooplankton grazing	-	0.6	Chen & Orlob (1975)

Initial concentration for zooplankton: 100 µg/ℓ for the upper 3 meters
0 for the depth below 3 meters

A more subtle point is that the measurements of chlorophyll-a and particulate-P hardly serve as good indicators for a correct prediction of zooplankton concentration. Figure 5.33c is a comparison of the base run with a case with a different set of zooplankton parameters. The predicted phytoplankton concentration shows little variation by the zooplankton concentration differs by as much as twofold. Another important interpretation of Figure 5.33c is that there is more than one set of zooplankton parameters which will produce indiscernable results of phytoplankton concentration.

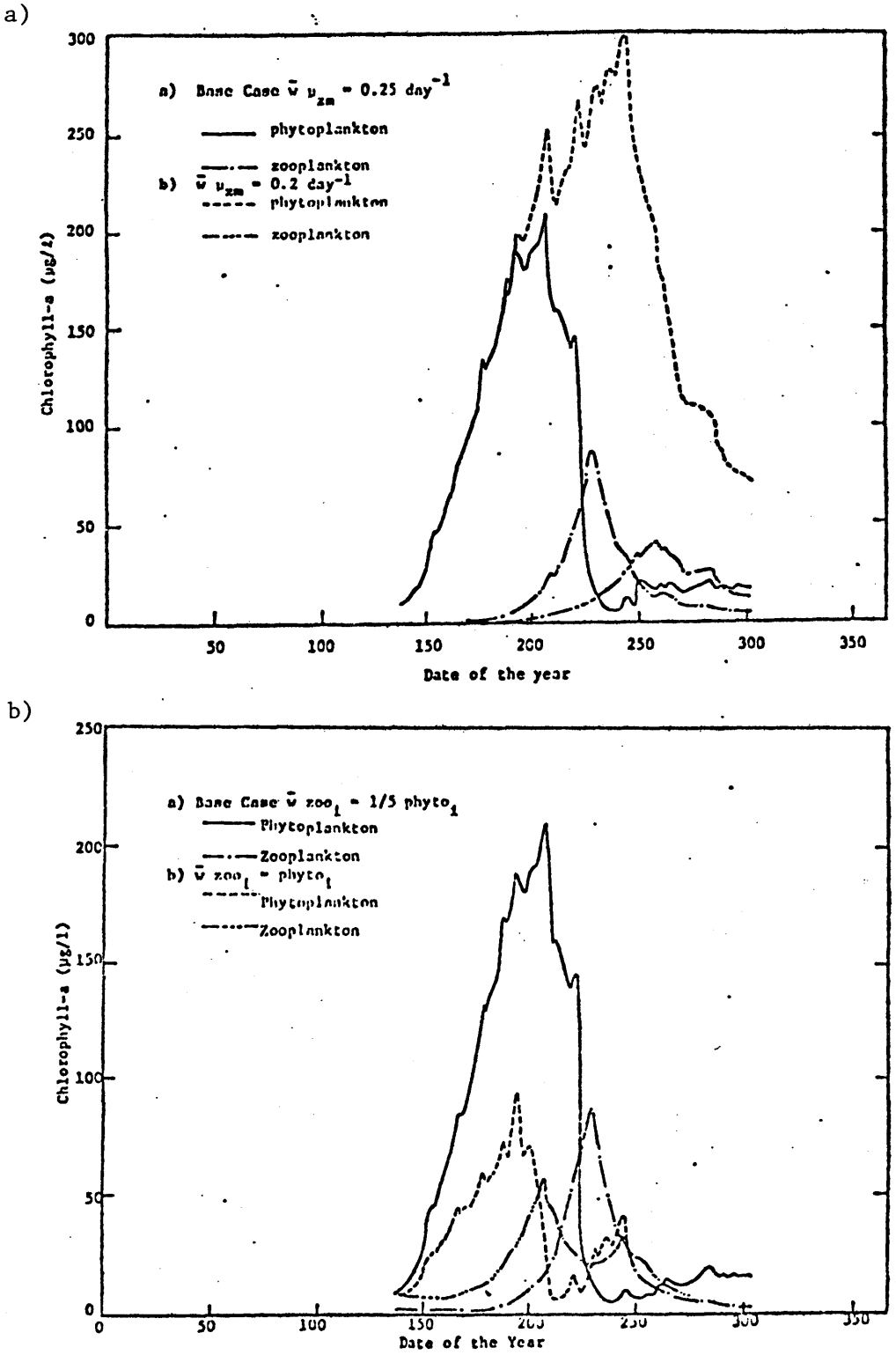

Figure 5.33: Sensitivity Studies on Zooplankton Parameters

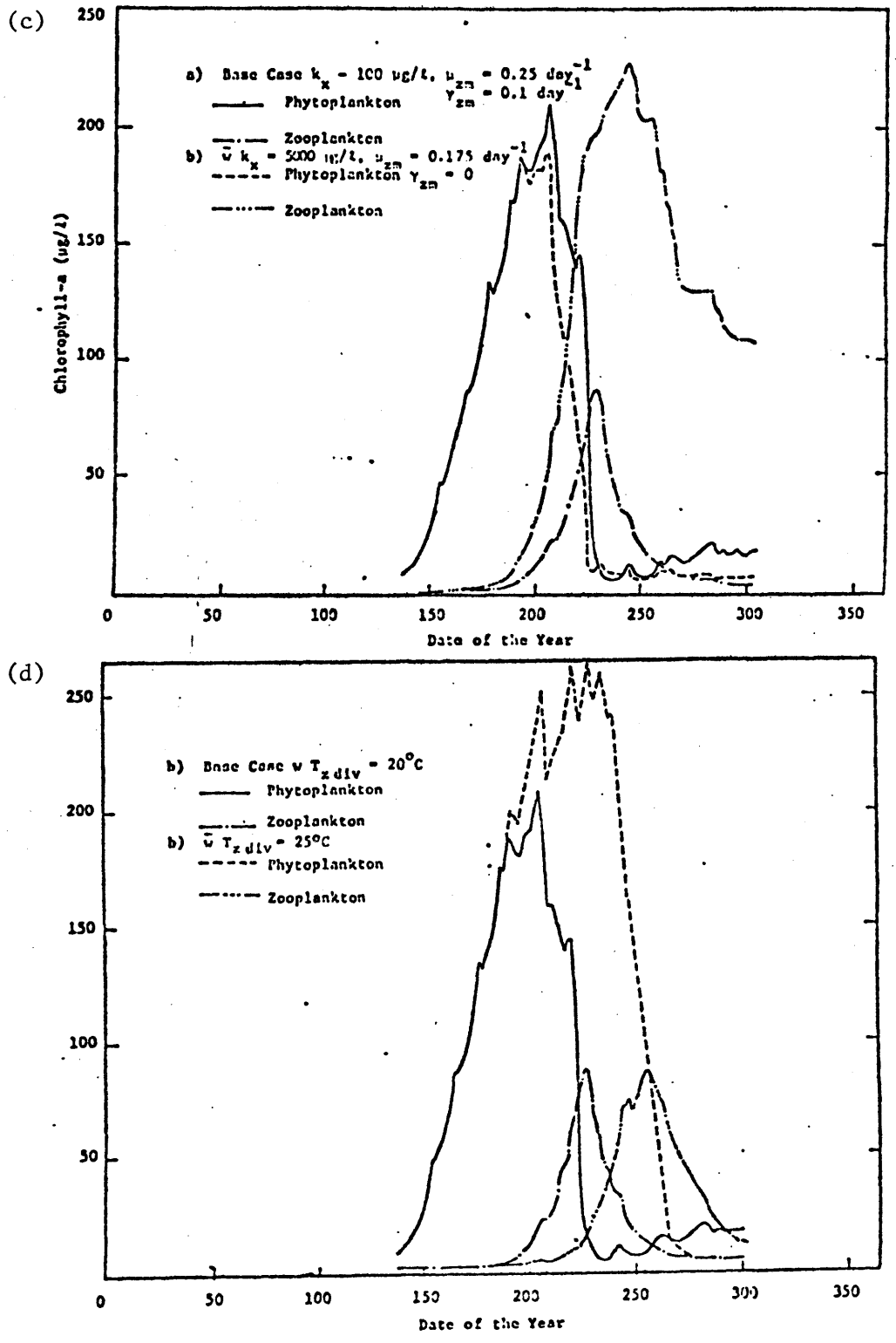

Figure 5.33: Continued

5.3.3 Model II vs. Corresponding Model Using Constant P Cell Quota Formulation - Level II

This section compares two phytoplankton models using two types of formulations to describe the effect of phosphorus upon phytoplankton growth rate:

(a) Variable cell quota formulation where the specific growth rate is a function of the cellular phosphorus content,

(b) Fixed cell quota formulation where the specific growth rate is a function of the external phosphorus concentration.

The comparison between the two formulations has been discussed in section 4.3.3. Model II, presented in section 5.3.2.2, which uses the variable cell quota formulation, will be compared to Model II', the corresponding model which uses constant cell quota formulation to describe the growth dependence on phosphorus. Model II' is presented in Figure 5.34 and Table 5.12 and the relationship between the model state variables and measurement is shown in Table 5.13. Model II' makes use of only two of the three measurements (ortho-P, particulate-P and chlorophyll-a). The state variable ortho-P should be compared with the field measurement of ortho-P. However, there are two possible ways of comparing the state variable particulate-P with the field measurement: one is to compare it with the measured PP and the other is to compare it with the measured chlorophyll-a concentration. Both ways will be considered here.

Model II' has been shown to be equally applicable as Model II if cellular equilibrium exists (section 4.3.3.2) with the corresponding growth rate μ'_{max} and half saturation constant k'_s computed as follows:

MODEL II'

.3 STATE VARIABLES

S - ORTHO-P

X - PHYTOPLANKTON BIOMASS RELATED TO PHYTOPLANKTON-P BY A CONSTANT RATIO 1/R'

Z - ZOOPLANKTON BIOMASS RELATED TO ZOOPLANKTON-P BY A CONSTANT RATIO 1/R'

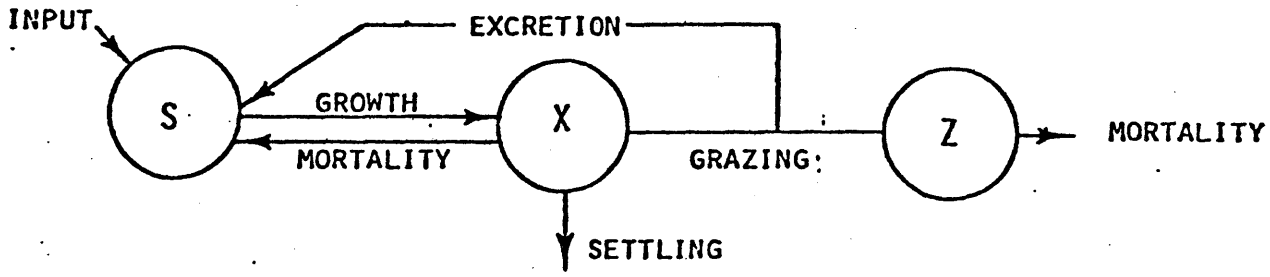

Figure 5.34: Schematic Diagram - Model II'

Table 5.12

1-D Mass Balance Equations

Model II'

1-D Mass Balance Equations:

$$\frac{\partial S}{\partial t} = \frac{\alpha}{A}\frac{\partial}{\partial z}\left(A\frac{\partial S}{\partial z}\right) + D(S_i - S) + i_S - \mu r'X + k_2 r'X + \left(\frac{1}{f} - 1\right)\mu_z Z\, r'$$

$$\frac{\partial X}{\partial t} = \frac{\alpha}{A}\frac{\partial}{\partial z}\left(A\frac{\partial X}{\partial z}\right) + D(X_i - X) + X - k_2 X - \frac{\partial}{\partial z}(gX) - \frac{1}{f}\mu_z z$$

$$\frac{\partial Z}{\partial t} = \frac{\alpha}{A}\frac{\partial}{\partial z}\left(A\frac{\partial Z}{\partial z}\right) + D(Z_i - Z) + (\mu_z - r_z)Z$$

Rate Expressions:

$$\mu = \mu_m' \frac{S}{S+k_S} f(I)\, h(T)$$

μ_z is the same as that defined in Table 5.10

Parameters to be Calibrated:

μ_m', k_s, r'

g, k_2, k_1, T_{opt}, T_{div}

$\mu_z m$, k_x, r_{zm}, T_{zopt}, T_{zdiv}

Definitions:

μ - phytoplankton growth rate also, ortho-P uptake rate

r' - phosphorus/biomass ratio by weight

All other symbols are the same as that defined in Tables 5.8 and 5.11

Table 5.13

Model State Variables vs. Field Measurement

Model II'

$$\begin{pmatrix} 1 & 0 & 0 \\ 0 & r & 0 \\ 0 & 0 & 1 \end{pmatrix} \begin{pmatrix} S \\ X \\ Z \end{pmatrix} = \begin{pmatrix} \text{ortho-P} \\ \text{chlo-a} \\ - \end{pmatrix}$$

or

$$\begin{pmatrix} 1 & 0 & 0 \\ 0 & r' & 0 \\ 0 & 0 & 1 \end{pmatrix} \begin{pmatrix} S \\ X \\ Z \end{pmatrix} = \begin{pmatrix} \text{ortho-P} \\ PP \\ - \end{pmatrix}$$

r = chlorophyll-a/biomass ratio

r' = phosphorus/biomass ratio

$$\mu'_{max} = \frac{\mu_{max}\rho_{max}}{\rho_{max} + q\mu_{max}} \tag{5.33}$$

$$k_s = \frac{q\mu_{max}k}{\rho_{max} + q\mu_{max}} \tag{5.34}$$

μ'_{max} is 1/day and k'_s is 0.24 μg/ℓ and the values of μ_{max}, ρ_{max}, k_ρ, and q are given in Table 5.8. The detectable limit of ortho-P by conventional chemical analysis is about 1 μg/ℓ (Stainton et al., 1977) and this low value of k_s suggests that according to constant cell quota formulation, ortho-P is not the limiting factor for the specific phytoplankton growth rate unless its concentration is below the detectable limit.

Figure 5.35 presents the simulation result for PP and ortho-P from Model II'. The concentrations of PP are similar in both cases to that predicted by Model II (see Figure 5.31). Model II' predicts intermittent intervals during which the ortho-P in the lake is in the order of 10 μg/ℓ. Before the 204th day, the duration of intervals with detectable ortho-P are short and may escape detection during the measurements taken at weekly or biweekly intervals. From the 240th to the 302nd day, Model II' predicts a continuous period of 60 days with ortho-P in the order of 20-40 μg/ℓ which is not in accord with the field observation. This is the period when the effect of zooplankton grazing/excretion becomes pronounced and phytoplankton are unable to reach cellular equilibrium. Moreover, the effect of zooplankton grazing/excretion could have significantly increased the phytoplankton P cell quota (see section 5.3.2.2). Therefore, the application of Model II' which is based on the assumptions of cellular equilibrium and constant cell quota fails.

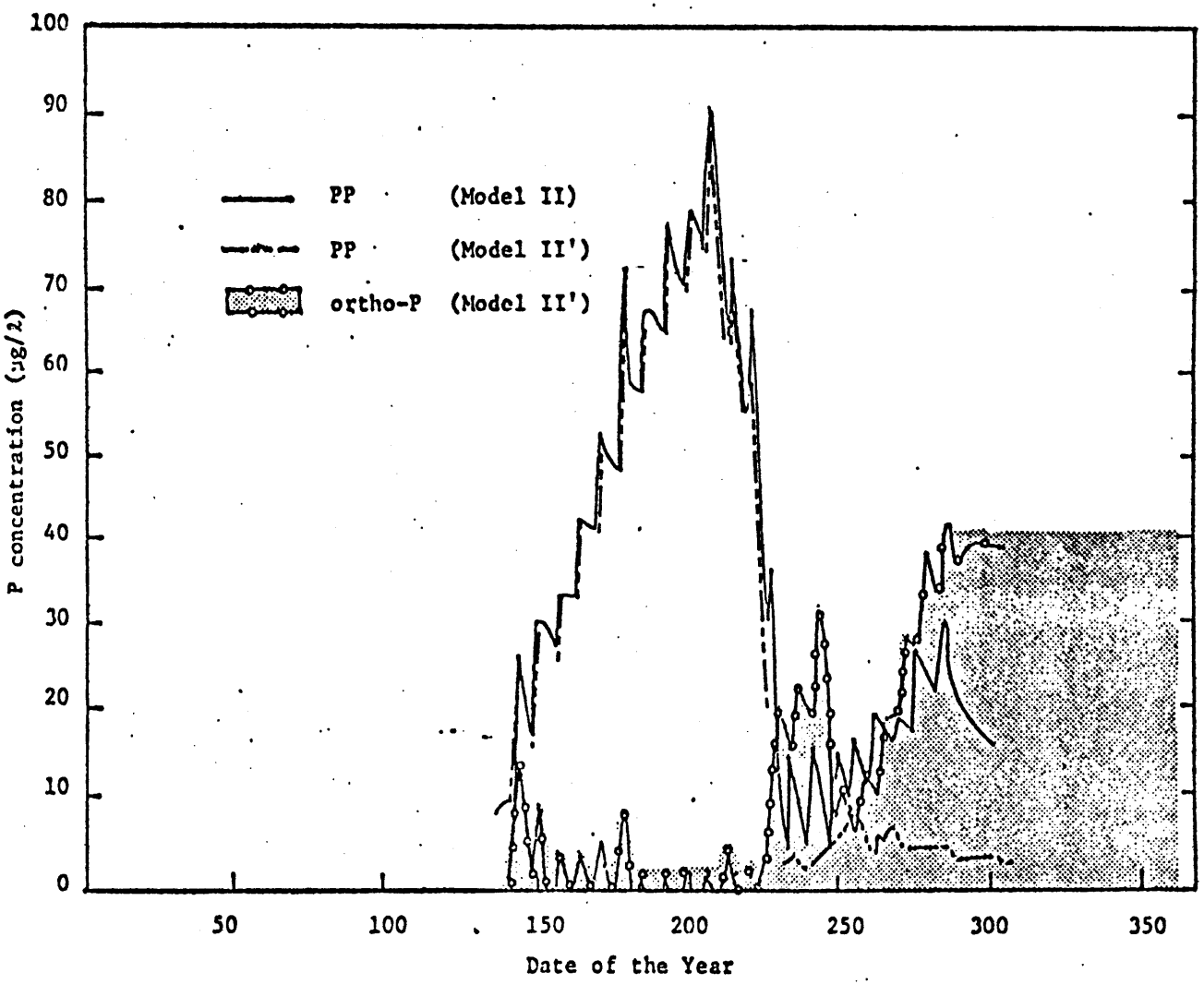

Figure 5.35: Comparison of the FML Phosphorus Concentration - Model II vs. Model II'

In many cases, the model state variable PP is not compared with the field measurement of PP. Instead, it is compared with the chlorophyll-a measurement. In order to make the comparison, a stoichiometric ratio between PP and chlorophyll-a will have to be assumed. It was shown in Section 5.3.2.1 that field data clearly suggest a variation of the PP/chlorophyll-a ratio so that we are faced with the difficulty of choosing this ratio. Since the emphasis is always placed on matching the peak value of the chlorophyll-a concentration which has a PP/chlorophyll-a value of 0.4 from Model II, this value is used for the stoichiometric ratio PP/chlorophyll-a. Fig. 5.36 compares the chlorophyll-a concentrations predicted by Models II and II'. The peak values are similar, with Model II' slightly overpredicting the concentration of chlorophyll-a on both sides of the peak. The value of PP/chlorophyll-a used in the Model II' simulation for comparison with the field measurement of chlorophyll-a is less than 40% of the value used by Thomann et. al. (1975). If Thomann's value of 1 for P/chlorophyll-a is used in this simulation, the peak chlorophyll-a concentration will only be around 80 µg/l instead of 200 µg/l.

These comparisons lead to the conclusion that it is not possible to find constant values of k_s and PP/chlorophyll-a for constant cell quota formulation which can produce identical results for all three measurements -- ortho-P, PP and chlorophyll-a concentration simultaneously. The two models predicted similar PP peak values but the ortho-P concentration are different in the off peak period with the most pronounced difference during the period with significant zooplankton grazing/excretion. The important point is that the value k_s for the constant cell quota formulation,

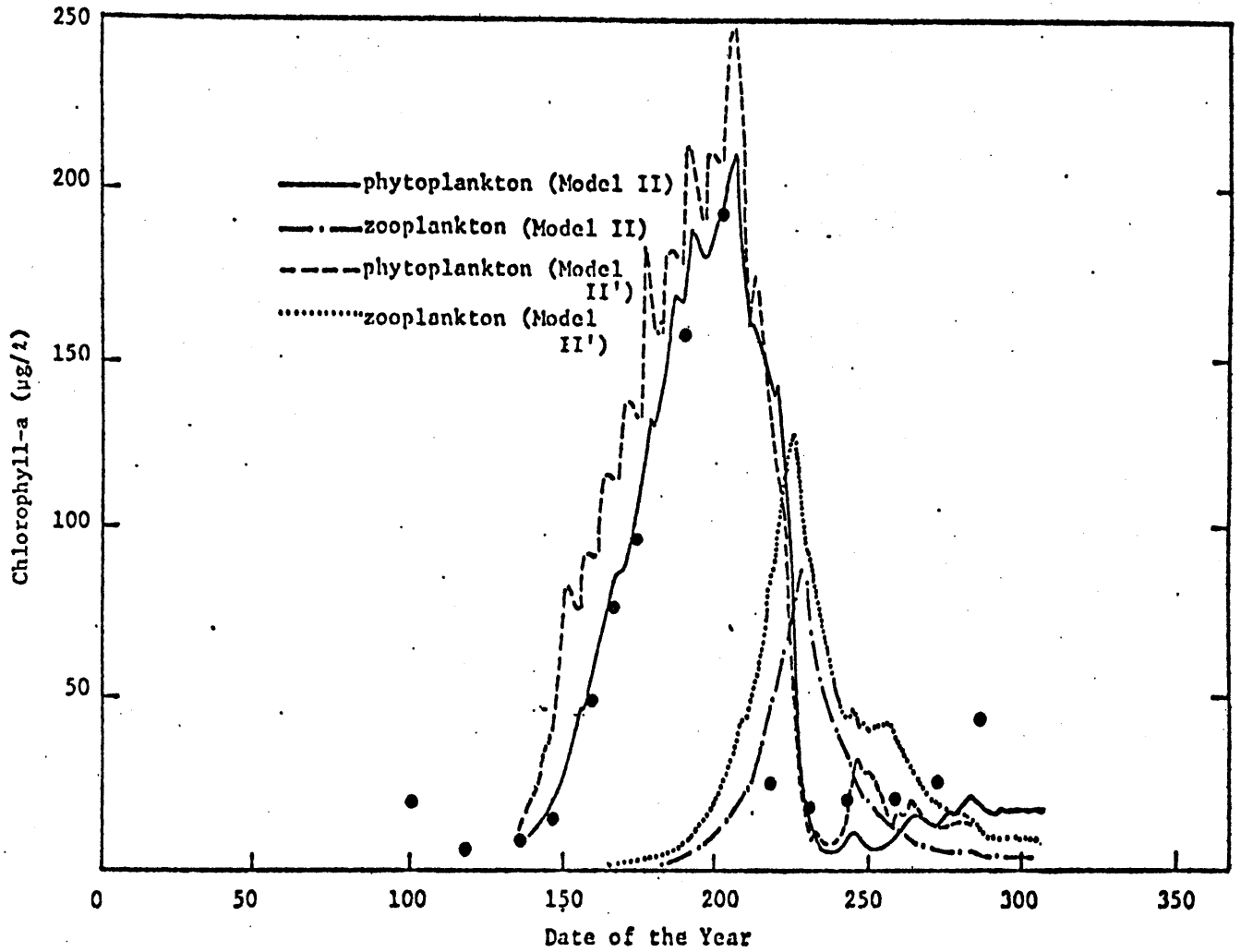

Figure 5.36: Comparison of the FML Chlorophyll-a Concentration - Model II vs. Model II'

calculated from the assumption of cellular equilibrium (0.24 μg/ℓ), is below the detectable limit by conventional chemical analysis of PO_4 (1 μg/ℓ). Also, in matching the observed chlorophyll-a peak value, a PP/chlo-a ratio which is less than 40% of that used by other modelers is used. This indicates that it is important to compare the PP/chlo-a ratio at the chlorophyll-a peak occurrence because this value alone would induce a significant difference in the chlorophyll-a prediction from the given phosphorus input.

5.3.4 Parameter Estimation and Function Evaluation from Primary Production Data -- Level III

Primary production usually refers to the rate at which phytoplankton assimilates organic carbon from the dissolved inorganic carbon (DIC). Since carbon is the major cellular constituent of the phytoplankton, primary production rate should closely reflect the increase of the phytoplankton biomass. Also, oxygen is produced in the phytoplankton's synthesis of the organic carbon from DIC and oxygen is one of the most important elements for many aquatic organisms. Therefore, it is hardly surprising that of all the phytoplankton activities, primary production has received most attention in the limnology studies.

While the specific properties of the primary production are of interest in their own right, study of the primary production has been exceedingly rewarding for other reasons. In modeling the multi-seasonal phytoplankton dynamics in a natural water body, inadequate field data do not allow us to verify our assumptions about the phytoplankton characteristics, such as the seasonal succession and spatial inhomogenity. The additional knowledge acquired from studying the primary production can be of tremendous importance in gaining insights into the phytoplankton characteristics. If we accept the assumption that the cellular C constituent is the least variable cellular constituent, that is ,the average C content among the algae is invariably 53 ± 5% , then primary production should be closely related to the increase of the phytoplankton. However, it is surprising that few have tried to relate the measurement of primary production to the parameter values in a biological model's expression for phytoplankton growth rate.

Depending on the formulation used for describing the growth rate, four to eight parameters have to be specified. Since there are no universal constants which permit direct substitutions, the values of these parameters have to be calibrated. Many modelers, due to the lack of information, are compelled to calibrate these parameters with a few field measurements of the net biomass variation, which is similar to the case presented in Section 5.3.2.

In our attempt to model phytoplankton dynamics in L227, we are fortunate to have primary production data from ELA. Since 1973, primary production in ELA has been measured with an incubator technique and published in "Phytoplankton Primary Production in the ELA Using an Incubator Technique -- 1973 Data" (Shearer and Fee, 1975). A detailed description of method of measurement, parameter estimation and functional evaluation is included in Appendix A. Only the results will be presented here.

Results of the incubation tests have been presented in tables and graphs. An example of the data presentation is given in Fig. 5.3.

For convenience in explanation, the following notation is introduced: U_{ij} = the measured carbon uptake rate for incubation session i under a given light intensity I_{ij}, in units of mg $C/m^3/hr$. The measured U_{ij} was obtained by applying liquid scintillation counting of C^{14} on the CO_2-free water sample (Schindler, 1972), therefore, it can be related to the carbon fluxes previously defined in Sections 4.2 and 4.3 by:

$$U_{ij} = kX_i[(k_p)_{ij} - r_{ij} - (r_p)_{ij}] \qquad (5.35)$$

where k is the carbon to biomass ratio and X_i represents the phytoplankton concentration during the incubation session i.

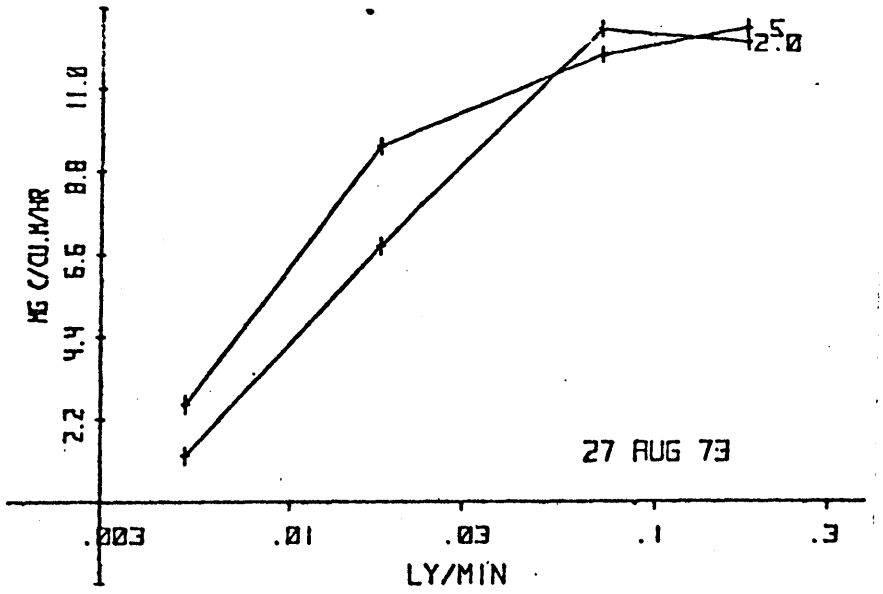

DATE	DEPTH	TIME	TEMP	I_1	P_1	I_2	P_2	I_3	P_3	I_4	P_4
27 Aug.	0.50	1259	21.5	0.1801	12.64	0.7918	11.93	0.0179	9.47	0.0051	2.58
	2.00	1259			12.26		12.63		6.83		1.23

Figure 5.37: Presentation of Primary Productivity Measurements - ELA (from Shearer and Fee, 1974)

5.3.4.1 Primary Productivity and Phytoplankton Growth

In our phytoplankton model, it is explicitly assumed that the phytoplankton growth rate is linearly related to the net carbon increase rate which is defined as [photosynthetic rate - respiration rate - photorespiration rate - excretion rate]. This assumption closely links the measured primary productivity to the model's definition of phytoplankton growth rate:

$$U_{ij} - kX_i(r_e)_{ij} = kX_i u_{ij} \tag{5.36}$$

where $(r_e)_{ij}$ and u_{ij} are the excretion and growth rates, respectively, during the incubation session i under a given light intensity I_{ij}. Phytoplankton growth rate in the model is assumed to be a function of light, temperature and cellular phosphorus content, that is, u_{ij} may be expressed as:

$$u_{ij} = u_m f(I_{ij}) g(T_i) h(Q_i) \tag{5.37}$$

with the assumption that in each incubation period, light is the only variable. Substituting Equation (5.36) into Equation (5.37):

$$U_{ij} - kX_i(r_e)_{ij} = kX_i u_m f(I_{ij}) g(T_i) h(Q_i) \tag{5.38}$$

5.3.4.2 The Light Function

Equation (5.38) may be rearranged into:

$$\frac{U_{ij} - kX_i(r_e)_{ij}}{kX_i u_m g(T_i) h(Q_i)} = f(I_{ij}) \tag{5.39}$$

The light function f(I) may be obtained from the ratio of the measured primary productivity, U_{ij}, to the maximum primary productivity measured during each incubation, $U_{i\ max}$, if either of the following two conditions exists:

(1) $kX_i(r_e)_{ij}$ is small compared to U_{ij}

(2) $(r_e)_{ij}$ is also a function of $f(I_{ij})$

For the year 1973, there are 18 incubations for the period May 28 to October 29 and for each incubation there are four pairs of $(U_{ij}/U_{max}, I_{ij})$, giving 72 pairs of data points altogether. The value of $U_{i\,max}$ is estimated from the incubation result for each incubation session i. If the light dependence function is stationary, these data points may be used to estimate parameter values needed for the light dependence function. Three functions of light dependence are considered: Smith function, hyperbolic function and Steele function. A non-linear regression package from the Troll system developed at MIT is used to find the best fitted parameter for each function. The regression package also provides information on the percentage of data variance explained by the best fitted parameter. From a comparison of the variance explained by each formulation may be obtained a basis for decision on which formulation fits the data best. Table 5.14 presents the regression result for the year 1973, where K_I is he best fitted parameter value for the light function in ly/day. The standard error of the estimation is also included (following the "±" sign); γ is the percentage of variance explained by the regression. Both the hyperbolic and Smith functions explain 80% of the data variance. The normalized standard error of the hyperbolic function is 10% which is lower than, although by a small margin, the normalized standard error of Smith's function. The K_I value obtained from this regression for the hyperbolic function is 13 ± 1.3, which agrees well with the value of 15 obtained by calibrating with the chlorophyll-a field measurements.

Rigorous application of the regression results should be confined to the condition under which the incubation experiments were conducted. The

Table 5.14

Regression of Specific Primary Productivity
as a Function of Light

Dependent variable: U_{ij}/U_{imax}

Independent variable: I_{ij}

Parameters: K

	Hyperbolic $\frac{I}{I+K_I}$	Smith $\frac{I}{\sqrt{K_I+I^2}}$	Steele $\frac{I}{K_I}\exp(1-I/K_I)$
K_I	12.9 ± 1.3	628 ± 100	130 ± 10
r	80%	80%	51%

ability of a proposed formulation to describe the incubation results is a necessary condition for accepting the formulation, but not a sufficient condition since the conditions under which the incubation tests were conducted form only a subset of the natural environment conditions. On the other hand, unless there is contradictory information, there is no reason to reject the use of the hyperbolic function to describe the photosynthesis dependence on light.

5.3.4.3 The Temperature and Nutrient Functions

The function $f(I_{ij})$ has a value between 0 to 1 and when it is equal to 1, the measured primary productivity $U_{i\ max}$ should be related to temperature and cell quota by:

$$U_{i\,max} - kX_i(r_e)_{i\ max} = kX_i u_m g(T_i)h(Q_i) \qquad (5.40)$$

$U_{i\ max}$ is a function of $g(T_i)h(Q_i)$ if either of the following conditions exists:

(1) $kX_i(r_e)_{i\ max}$ is neglibible compared to $U_{i\ max}$

(2) $(r_e)_{i\ max}$ is also a function of $g(T_i)h(Q_i)$

If either of the above conditions exists, then the functions g(T) and h(Q) may be obtained from the information on $U_{i\ max}$, T_i and Q_i provided that the two functions are stationary functions.

If the information on X_i, T_i and Q_i is available, the utility of the primary production data can immediately be extended to the evaluation of the validity of the functional representation of the temperature and nutrient effect on specific photosynthetic rate. Unfortunately, only T_i has been

recorded for these incubation measurements of the primary production rate. However, since there remains a significant gap between growth rate and photosynthetic rate, the additional knowledge acquired from analyzing the primary production data can be of tremendous importance in gaining insight into the phytoplankton behavior. It would be a meaningful task to attempt analyzing the dependence of the specific primary activity on nutrient and temperature, even with estimated values of X_i and Q_i.

From our previous simulation results (Section 5.2.2, it is seen that chlorophyll-a data fall on a rather smooth curve so that we may linearly interpolate the measurement of chlorophyll-a from the data to obtain the values for conditions in the incubation measurements. The time series plot of particulate-P, however, shows significant variations so that the value obtained from the model simulation result (i.e., Model I with varying settling rates after the 204th day) is used instead. The values of the estimated PP and chlorophyll-a are summarized in Table 5.15 along with the corresponding P cell quota (Q_i),temperature (T_i) and specific photosynthetic rate ($u_{i\ max}$) which is defined as $U_{i\ max}/X_i$. The same nonlinear regression package in the Troll system is used to estimate the best fitted parameters for the following three possible functions:

Function I : $u = a(1-q/Q)$

FunctionII : $u = a \exp\left(-2.3 \frac{T_{opt}-T}{T_{div}}\right)$

Function III : $u = a(1-q/Q) \exp\left(-2.3 \frac{T_{opt}-T}{T_{div}}\right)$

All these functions are based on our assumed dependence of growth rate on temperature and nutrient.

Table 5.15

Date	U_{max}	PP	Chlo-a	T	u_{max}	Q
151	72.	17.	21.	17.	3.4	0.8
158	115.	26.	38.	16.	3.0	0.68
166	130.	28.	60.	18.5	2.2	0.47
169	150.	37.	69.5	18.	2.1	0.53
183	180.	51.	125.	21.	1.44	0.41
197	300.	66.	180.	20.5	1.67	0.37
199	200.	80.	184.	20.5	1.09	0.44
211	8.	50.	111.	19.	0.072	0.45
225	32.	37.	20.5	20.	1.56	1.81
235	22.	27.	15.	21.	1.47	1.81
239	12.	11.	14.5	21.5	0.82	0.78
253	20.	13.	17.	18.5	1.18	0.74
267	70.	31.	22.	11.	3.18	1.39
274	36.	17.	25.	13.	1.44	0.69
281	45.	12.	37.	12.	1.22	0.32
288	55.	22.	50.	11.	1.1	0.5
295	40.	15.	39.	9.	1.0	0.38
302	25.	12.	28.	7.5	0.89	0.41

U_{max} is (µg-C)/(µg-chlo-a)/hr Chlo-a is in µg/ℓ
PP is in µg/ℓ
T is in ℃

The constant P cell quota formulation is not considered since it is apparent from the field measurement that no detectable amount of phosphorus was available and therefore, it will not be possible to find the correlation between primary productivity and ortho-P concentration.

The regression results are presented in Table 5.16. Function I can only explain 20% of the observed variance in the data while divergence occurred for Functions II and III during the process of searching for the best fitted parameters. An alternative approach to parameter estimation is simulation. By specifying the range of each parameter and the increments for the parameters in the simulation, a best set of parameter values within the specified ranges may readily be found. The simulation results are shown for Functions II and III and again, neither of the functions can satisfactorily explain the data variation.

Following the addition of the limiting nutrient, there is a transition period in which the hyperbolic relationship between the net carbon uptake rate and the cell quota of the limiting nutrient does not apply. Healey (1979) excellently illustrates the phytoplankton physiology changes after nutrient enrichment. For example, a phosphorus-deficient cell (P/C = 0.0049 by weight) was enriched with ortho-P so that the P/C ratio was raised to 0.065 after three hours. Since the uptake of ortho-P is an active process, it may compete with the photosynthesis reaction for the use of ATP. Therefore, photosynthesis might even be depressed during the uptake of ortho-P, which was what Healey (1979) observed. During the uptake period, the net photosynthesis was depressed by 40%. Only some eight hours after the addition of the phosphate did the net photosynthetic rate begin to show

Table 5.16

Regression of Specific Primary Productivity Rate
as a Function of Temperature and Nutrient

Dependent variable: u_{max}

Independent variables: T,Q

Parameters: q, T_{opt}, T_{div}, a

	Function I	*Function II	*Function III
a	2.42	0.8	1.6
q	0.187	-	0.2
T_{opt}	-	50.	35.
T_{div}	-	50.	50.
r	20%	3%	22%

*Divergence occurred during the search of best fitted parameters, values shown are from simulation analysis with the following specifications:

$0.1 \leq a \leq 3.0$ $\quad \Delta a = 0.1$

$0.1 \leq q \leq 2.0$ $\quad \Delta q = 0.1$

$10. \leq T_{opt} \leq 50.$ $\quad \Delta T_{opt} = 5.$

$10. \leq T_{div} \leq 50.$ $\quad \Delta T_{div} = 5.$

large increases over its pre-enrichment period. Dark respiration is stimulated by the addition of nutrient. The length of this transition period was at least the length of the nutrient uptake period but may very well have extended beyond the nutrient uptake period depending on the degree of nutrient deficiency. In general, the larger the nutrient/biomass ratio or the more severe the nutrient deficiency, the longer the transition period. For this transition period, there is no good description for the biomass variation.

In view of the often delayed and variable response of the photosynthesis to the nutrient addition, care must be taken in fitting the short term photosynthesis measurement. It is assumed that a better fit for the period before the sharp decline of the phytoplankton biomass may exist for the following two reasons:

(1) The ratio of added nutrient to biomass is smaller due to the higher biomass in the earlier period, and

(2) The effect of zooplankton on ortho-P cycling is insignificant.

The possibility of zooplankton presence cannot be eliminated in the latter period. Although the amount of zooplankton present is uncertain, zooplankton may be conceived to be present in a more abundant number and the grazing/excretion activity of zooplankton causes phytoplankton standing crops to continuously take up ortho-P. The increase of phytoplankton P cell quota during this period could be significant as suggested by the excessive ortho-P concentration in the water column obtained from Model II' which uses constant P cell quota formulation. This will induce a longer and more frequent transition period of photosynthetic activity, and the

photosynthetic rate may not be related to the P cell quota by the hyperbolic form. Therefore, a regression was performed for the first 7 values which were taken from the period before the occurrence of chlorophyll-a peak. The result is summarized in Table 5.17. In this case, Function I is able to explain 80% of the variance; while the regression package was unable to find any realistic parameter values for both Function II and Function III. The insignificant relationship between temperature and the primary productivity may be due to the fact that there is little difference in the temperatures for the 7 data sets (16 to 21°C). Although the small number of data sets (7) prevents the making of statistically profound judgements on the estimation of 2 parameters, this result certainly suggests the possibility of a significant relationship between the specific primary productivity and P-cell quota.

The value of minimum cell quota obtained from the regression of primary productivity under the optimum light condition is 0.30 μg-p/μg-(chlo-a), while the value of the minimum P cell quota obtained from the field data is 0.4 μg-P/μg-(chlo-a). The agreement of the two may be considered satisfactory. The estimated μ_{max} from the regression is 5 μg-C/μg-(chlo-a)/hr corresponding to 60 μg-C/μg-(chlo-a)/day for 12 day-time hours. Since it was assumed that chlorophyll-a is approximately 1/100 of the phytoplankton biomass (see Table 5.6) and the carbon content is estimated to be 53 ± 5% of the ash-free dry weight (Wetzel, 1975), the estimated maximum primary productivity then corresponds to a growth rate of 1.0-1.2 per day which is also considered to agree satisfactory to the value 1.0/day used in the model. The reasonable agreement between

Table 5.17

Regression of Specific Primary Productivity
as a Function of Temperature and Light

The Pre-Peak Period

Dependent variable: u_{imax}

Independent variables: T_i, Q_i

Parameters: q, T_{opt}, T_{div}, a

	Function I		*Function II	*Function III
a	5.3	0.7		
q	0.3	0.03		
T_{opt}	-			
T_{div}	-			
r	80%			

*For both Function II and Function III, the regression package was unable to find any realistic values for the parameters, and the best fitted parameters found resulted in a function which has variance greater than the original variance.

the growth rate and minimum cell quota used in the model and the same parameters estimated from primary productivity data suggest that carbon excretion rate was small during the pre-peak period since the measured primary productivity represents the sum of net carbon increase rate and excretion rate. This confirms the assumption used in performing the parameter estimation for the growth function from the U_{ij} data. However, this regression gives no information on the respiration rate.

5.4 Parameter Transferability to Year 1974

5.4.1 Data Analysis

In 1974, L227 received the same nutrient addition pattern as in 1973. The lake was fertilized from May 21 to October 9 with 21 weekly additions. During each fertilization, 1.14 kg and 14.97 kg of PO_4-P and NO_3-P, respectively, were dissolved and mixed in the water taken from the lake surface. These mixtures were then added to the lake surface from a boat.

The lake response to these additions can be seen from the measurement of ortho-P, TDP, PP and chlorophyll-a concentrations. Epilimnion ortho-P, measured by Rigler's bioassay method, was in the order of 0.1 µg/l which is similar to the concentration of the ortho-P measured in 1973 by the same method (Fig. 5.38) (Levine, 1975). Epilimnion TDP concentration, measured by regular chemical analysis, remained fairly constant (~8 µg/l) from May to October of 1974 which is also similar to the TDP concentration trend of the previous year (Fig. 5.39). However, there were considerable differences in the epilimnion PP concentration and dramatic difference in the epilimnion chlorophyll-a concentration between 1974 and 1973 (Figs. 5.40 and 5.41). By July 2 (the 183rd day), 41 days after the first addition, significant difference in chlorophyll-a had occurred. Instead of continuing to increase as in 1973, chlorophyll-a began to drop in 1974 and the maximum epilimnion chlorophyll-a concentration in 1974 was only 50 µg/l or 25% of the maximum chlorophyll-a concentration in the year 1973. The maximum epilimnion concentration of PP in 1974 was 50 µg/l which was slightly lower than the maximum epilimnion PP concentration in 1973. However, the general pattern of the epilimnion PP concentration is quite different.

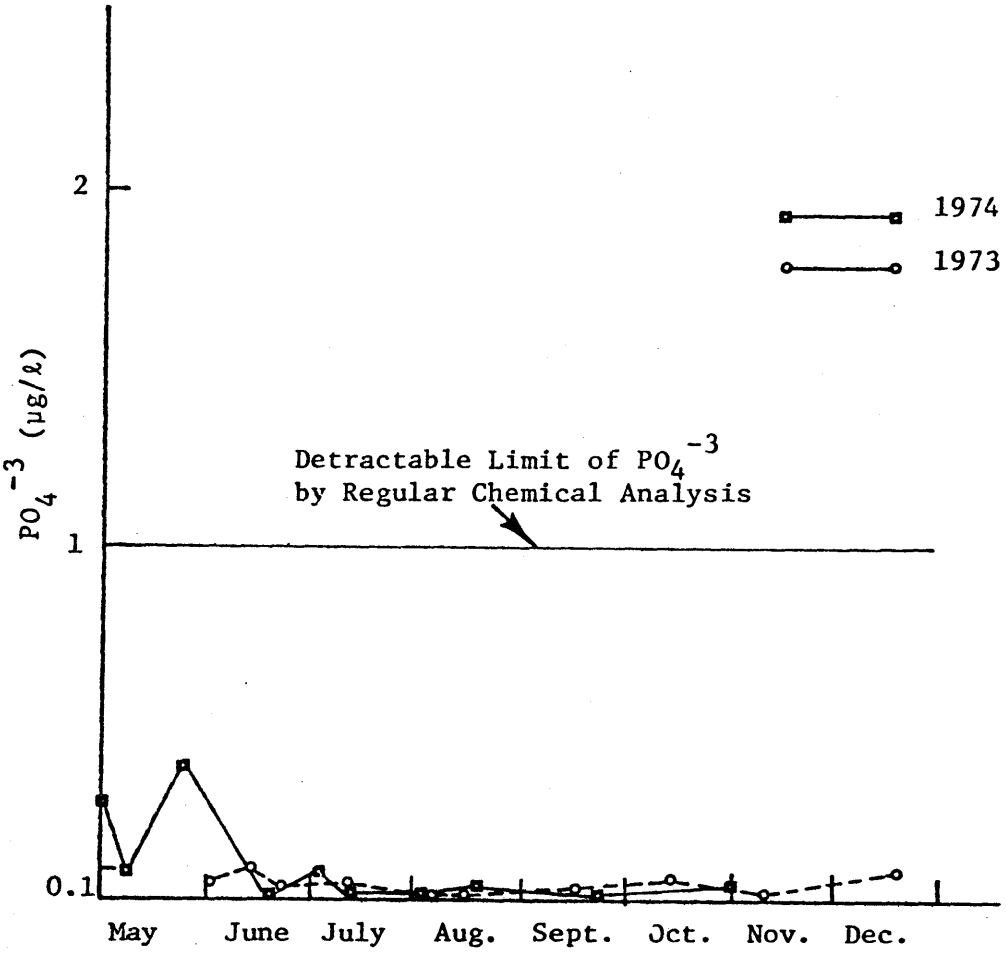

Figure 5.38: Epilimnion Ortho-P Concentration - 1974 vs. 1973

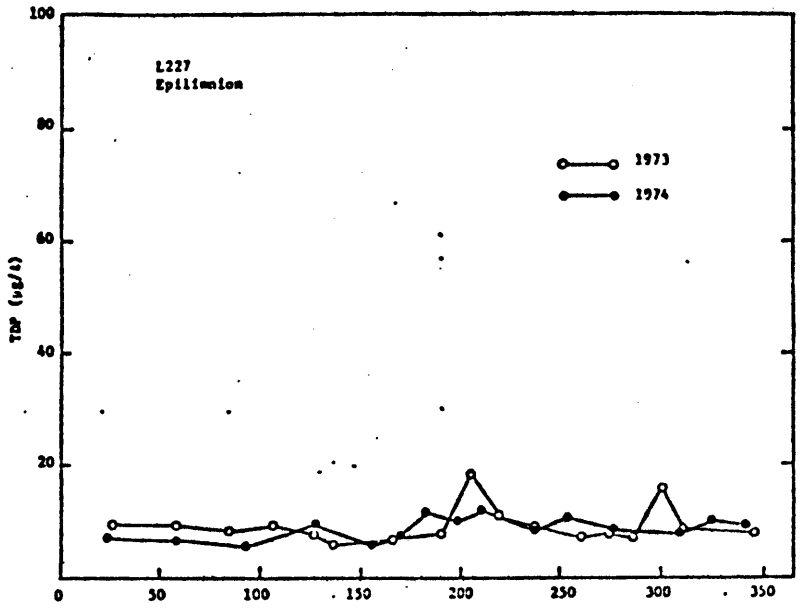

Figure 5.39: Epilimnion TDP Concentration - 1974 vs. 1973

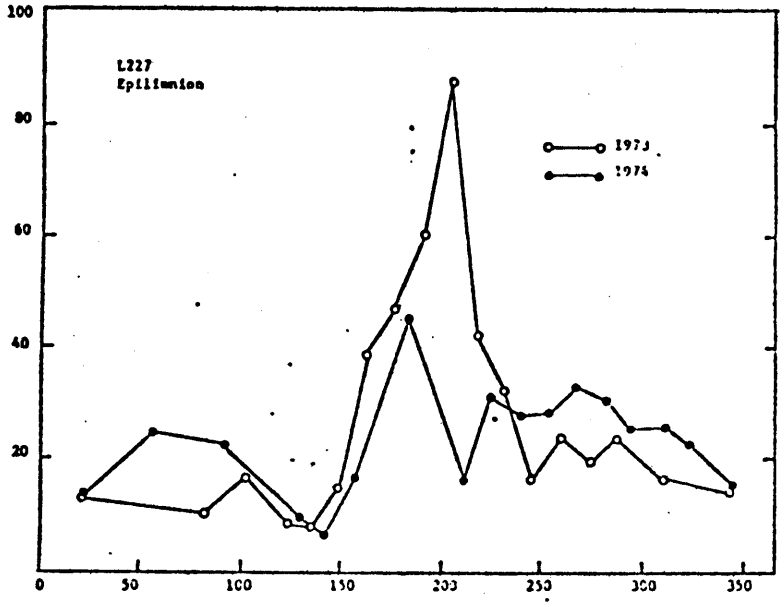

Figure 5.40: Epilimnion PP Concentration - 1974 vs. 1973

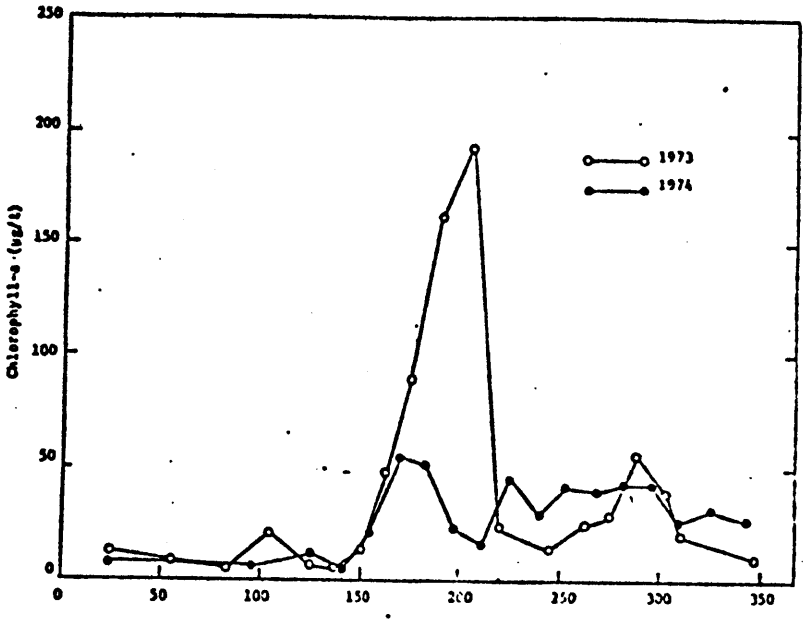

Figure 5.41: Epilimnion Chlorophyll-a Concentration - 1974 vs. 1973

5.4.2 Phytoplankton Simulation

As in the previous year, the simulation started with the temperature simulation obtained using the MIT wind mixing model described in Section 2. The required input data for the temperature simulation are the same as those described in Section 5.2.1. The daily record of direct solar radiation which is one of the most important input data was missing for most of the period from August 8 to November 31 due to instrument failure. Therefore, the simulation is confined to the period from May 21 to July 30 which covers the occurrence of the first chlorophyll-a peak. The daily values of extinction coefficient needed for the simulation were obtained by linearly interpolating the published extinction coefficienct taken at biweekly intervals by Shearer (1976). To account for the sheltering effect of the tall jackpines surrounding the small L227, a wind speed reduction factor of 0.7, which had been used in the 1973 temperature simulation, was also applied for this 1974 simulation.

Shown in the four panels of Fig. 5.42 are the comparisons of model temperature simulation with field measurement. In general, the wind mixing model satisfactorily simulates the measured lake temperature. The simulated FML is shown in Fig. 5.43. L227 exhibited an earlier strong stratification in 1974 than in 1973, with the FML depth from May to early July generally smaller in 1974 than in 1973. The simulated temperature for the upper 4 m is shown in Fig. 5.44. Compared with the 1973 temperature time series plot (Fig. 5.6), the FML temperature is high in 1974 by approximately 5°C.

Model II, described in Section 5.3.2.2 was used for phosphorus and

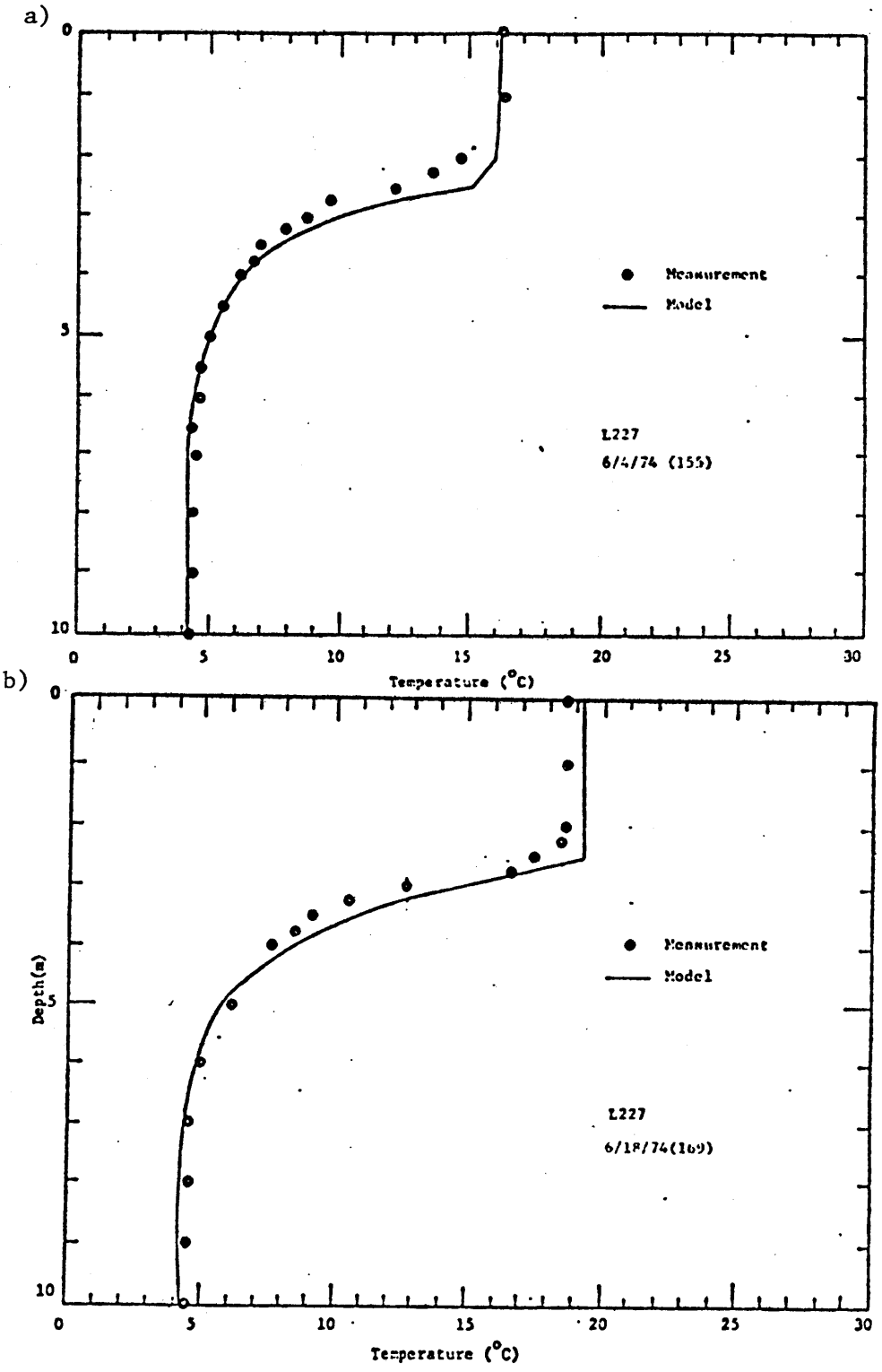

Figure 5.42: 1974 Temperature Simulation Results

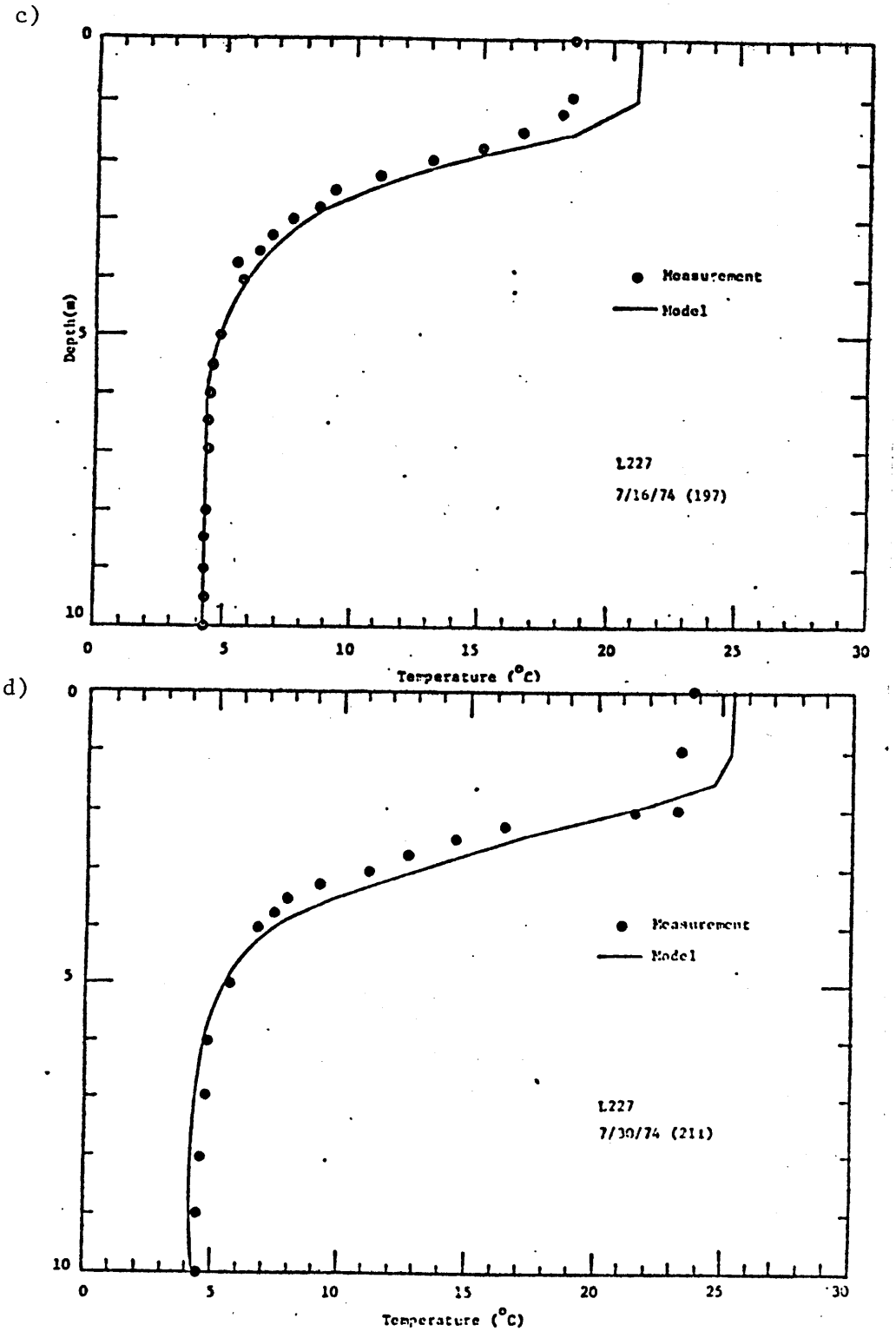

Figure 5.42: Continued

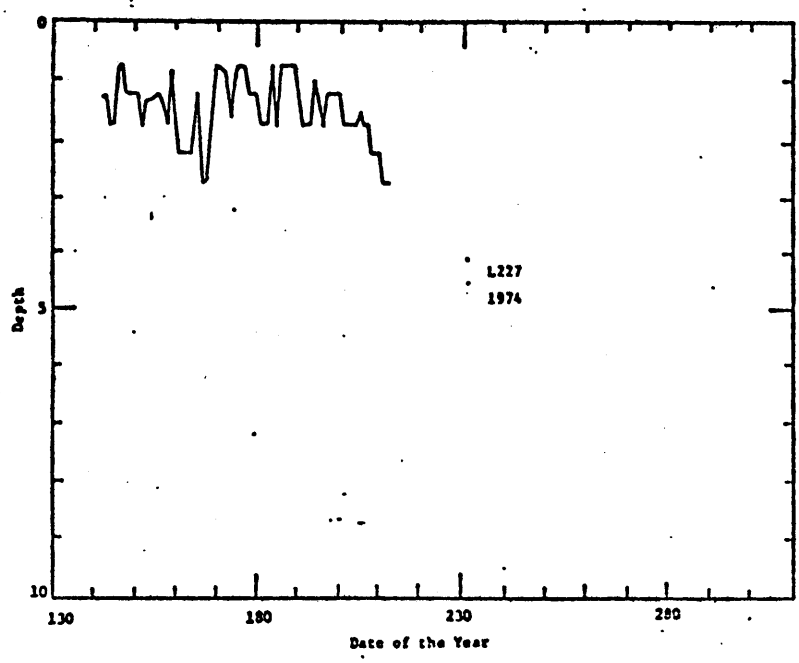

Figure 5.43: FML Variation - 1974

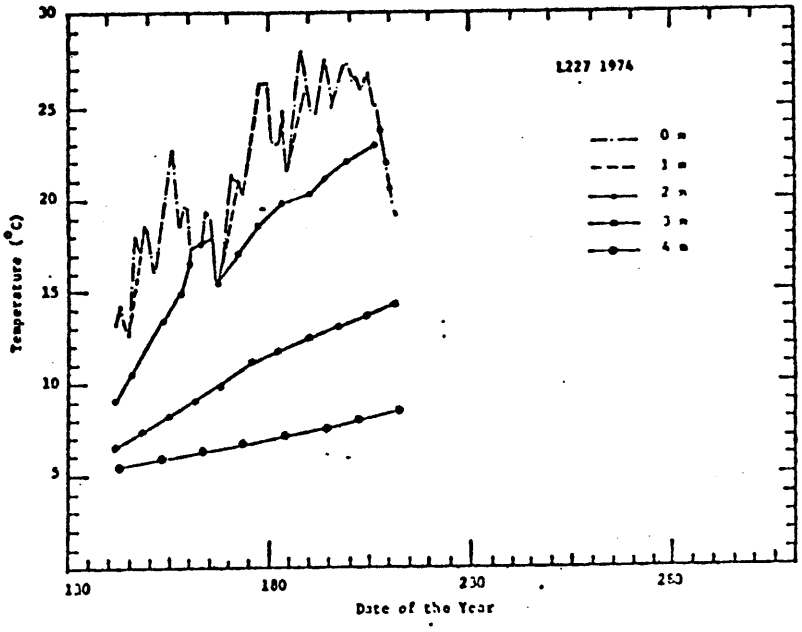

Fiugre 5.44: Simulated Temperature for the Upper 4 m Depth

simulations. Although the structure of Model II has the potential to continue the simulation from 1973 to 1974, the lack of data during the winter does not allow us to feel confident about our ability in correctly simulating the zooplankton population changes for the post-chlorophyll-a peak period, and the initial zooplankton concentration needed for 1974 simulation remains as a model parameter.

Model simulation results are shown in Figures 5.45 and 5.46 and as in the previous year, the zooplankton initial concentration is assumed to be one fifth of phytoplankton initial concentration. The model predicts a continuous increase of both PP and chlorophyll-a concentration in the FML until the 210th day which is simular to the trend of the previous year but it fails to predict a decrease of PP and chlorophyll-a occurring after the 176th day. The model currently predicts maximum chlorophyll-a and PP in the FML higher than that of the year 1973 which resulted from the shallower FML depth in 1974 for the period 176th to 204th. Clearly, the field measurement of 1974 can not be simulated without any modification of the model parameters. The dramatic difference of the two years' epilimnion chlorophyll-a and PP concentration cannot be explained by the difference of the hydrothermal conditions alone.

Information on the phytoplankton response to the nutrient addition may be gained from primary productivity data for 1974. Table 5.18 compares four pairs of maximum specific primary productivity under the optimum light condition and the corresponding phosphorus cell quota during the period covering the 148th to the 190th day of 1973 and 1974. The maximum specific primary productivity is expressed as P_{max}/chl-a in

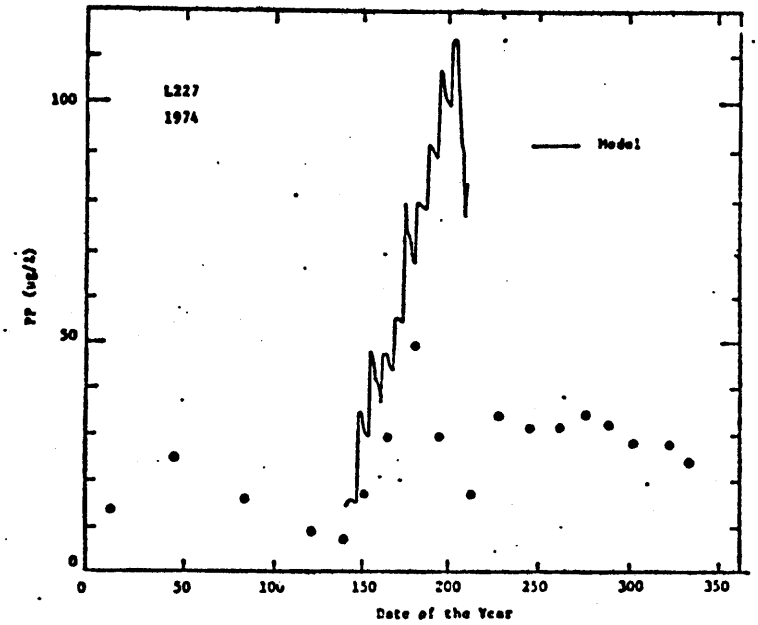

Figure 5.45: FML PP Concentration, 1974 - Model II Results with the Same Parameters as Used in 1973

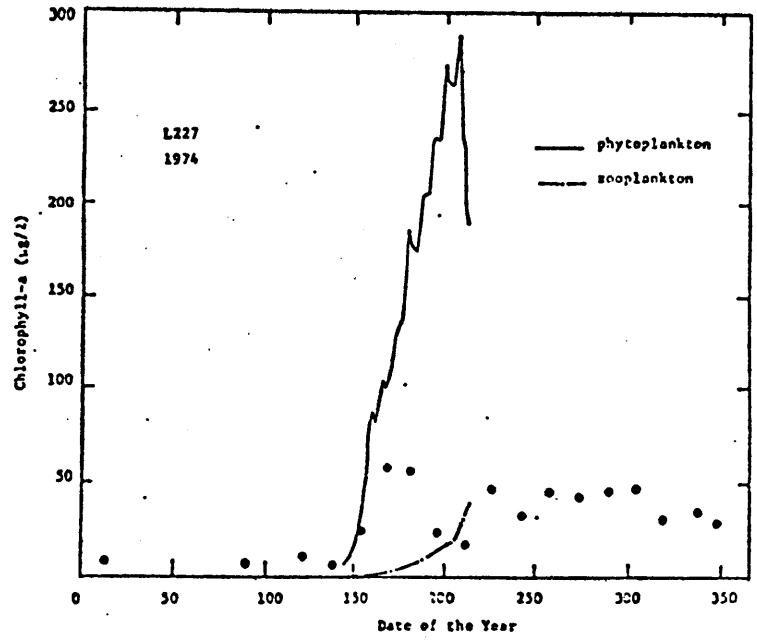

Figure 5.46: FML Chlorophyll-a Concentration, 1974 - Model II Results with the Same Parameters as Used in 1973

Table 5.18

Primary Productivity for L227

1973 vs. 1974 (for the period 5/28 - 7/9)

Year 1973				Year 1974			
Date	Temp. (C)	P_{max}/chl-a (μg-C/μg-(chl-a)/hr))	PP/chl-a (μg-P/μg-(chl-a))	Date	Temp. (C)	P_{max}/chl-a (μg-C/μg(chl-a)/hr))	PP/chl-a (μg-P/μg-(chl-a))
151	17	3.4	0.8	148	12	1.8	1
158	16	3.0	0.7	162	16	1.6	0.7
166	18.5	2.2	0.5	184	20	2.4	1.
183	21	1.44	0.4	190	21	1.5	1.

Table 5.18 with P_{max} estimated from the published incubation test data from Shearer and Fee (1975) and Shearer (1976). Chlorophyll-a is either obtained from field chemistry measurement or from linear interpolation of the field measurement. Phosphorus cell quota is expressed as PP/chl-a in Table 5.18 with PP obtained from field measurement or model simulation. Temperatures are taken from incubation results (Shearer and Fee, 1975; Shearer, 1976). The recorded temperature for the 148th day in 1974 is 12°C which is considered low and could be an error in the record since the upper 2 m of the lake was warmer in 1974 than in 1973 for this period of the year. If the difference in temperature between the 148th day of 1974 and the 151st day of 1973 is disregarded (since the other three pairs, i.e., 162nd 1974 vs. 158th 1973; 184th 1974 vs. 166th 1973; and 190th 1974 vs. 183rd 1973, have very similar temperatures), it may be concluded that the difference in their P_{max}/chl-a is due to the difference in their response to nutrient condition. Comparing 148th 1974 vs. 151st 1973 and 162nd 1974 vs. 158th 1973, it may be observed that the values of P_{max}/chl-a in 1974 are only half of the corresponding values of 1973 while the values of PP/chl-a are approximately the same in both years. For the remaining two pairs -- 184th 1974 vs. 166th 1973 and 190th 1974 vs. 183rd 1973 -- the P_{max}/chl-a values are the same for the two years while PP/chl-a in 1974 are twice the corresponding values in 1973. In other words, for the same nutrient condition, phytoplankton in 1973 were able to have higher specific primary productivity than phytoplankton in 1974. If there is no difference in the responses of other carbon fluxes to nutrient condition, then this result suggests that the minimum cell quota in 1974 is higher than that in 1973.

The increase of the value of q alone cannot simulate the field measurement for chlorophyll-a and PP. L227 only retained 60% of its PP in the FML in 1974 while in 1973, the FML practically retained all the added phosphorus for the corresponding period. Phosphorus in 1974 was lost at a faster rate in the earlier period than in 1973. There are two mechanisms through which phosphorus can be lost from the water column: settling and zooplankton grazing. There is no available information on the phytoplankton settling behavior during the simulation periods of the two years but zooplankton concentratinn was observed to be higher in 1974 (Malley, Cheng and Schindler, manuscript).

Different combinations of higher zooplankton concentration and higher q for the 1974 simulation were tested and a combination of zooplankton initial concentration same as the phytoplankton concentration and a q value of 0.005 was found to simulate the field measurement of PP and chlorophyll-a (Figs. 5.47 and 5.48). The possibility of a higher settling rate for phytoplankton in 1974, however, cannot be excluded. The taxonomy composition of phytoplankton of the two years are shown in Fig. 5.49 (Findlay and Kling, 1975; Findlay, 1976). From mid-May to the end of July, Chlorophyceae dominated in both years. The common species of Chlorophyceae in 1974 are reported to be Scenedesmus sp., Oocystis submarina var. variablis, Dictyosphaerium simplex, Ankistrodesmus falcatus var. spiralis, and Chlamydonas. These species were also present in the year 1973. Therefore, the cause of these differences in phytoplankton responses in the two years remains unknown since there was no apparent species variation for the two years.

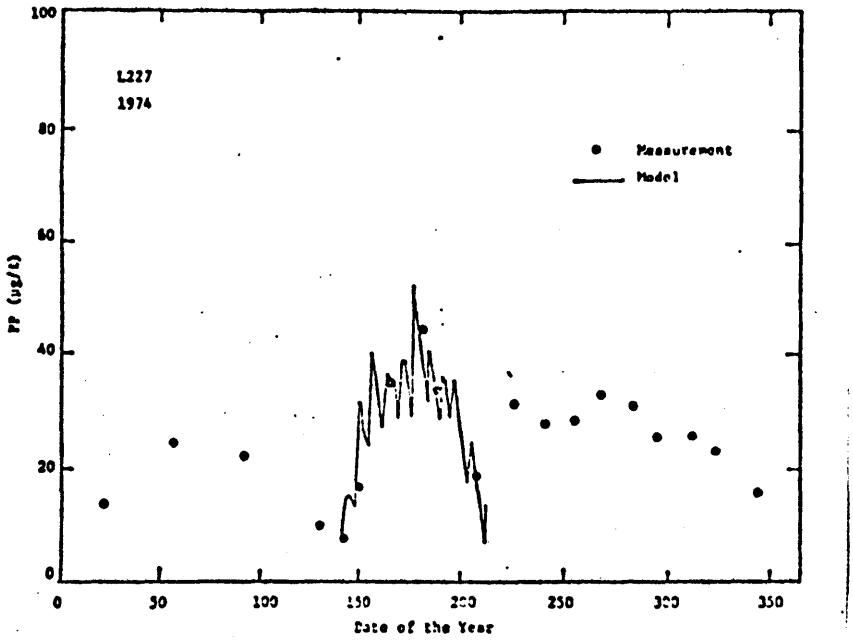

Figure 5.47: FML PP Concentration, 1974 - Model II with Modified Parameters

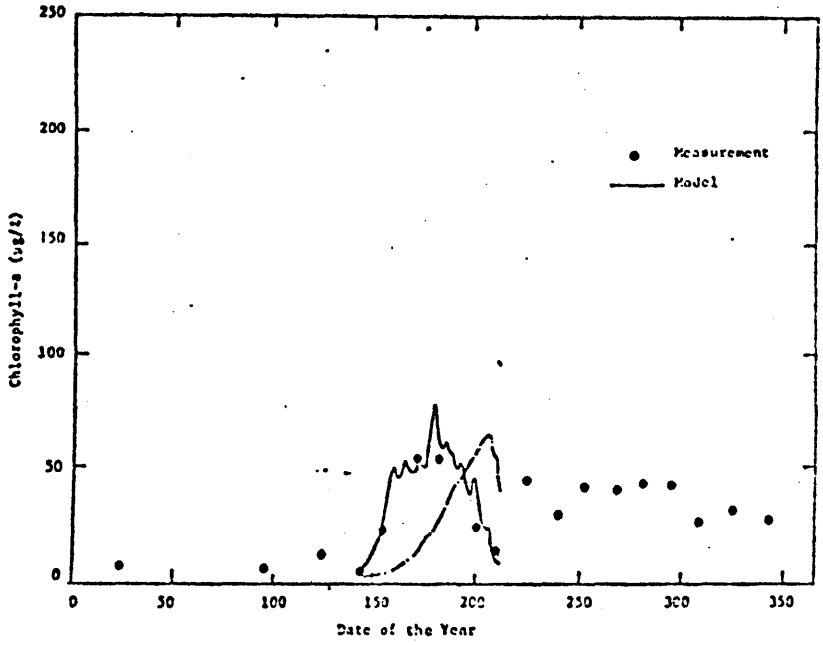

Figure 5.48: FML Chlorophyll-a Concentration - Model II with Modified Parameters

a)

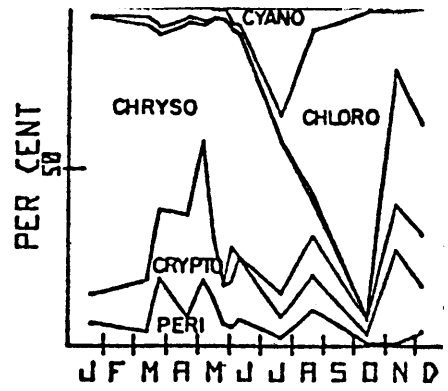

b)

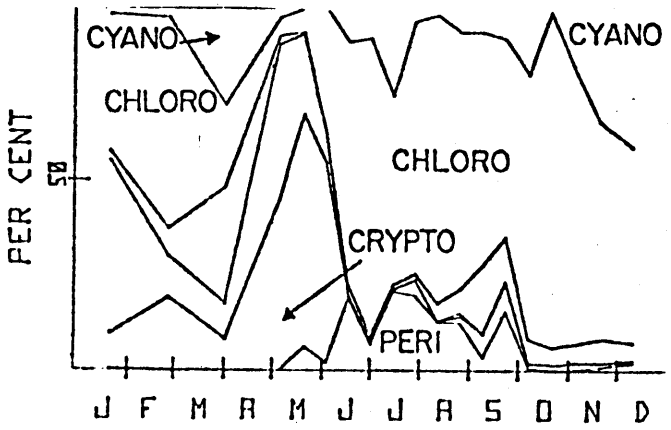

Figure 5.49: Phytoplankton Species Composition for the Year 1973 (a) and Year 1974 (b) (From Findlay and Kling, 1975; Findlay, 1978)

Chapter 6

THE IMPORTANCE OF FML DYNAMICS IN LAKE PHYTOPLANKTON MODELING

6.1 Introduction

The theme of this chapter is a more detailed discussion of the effect of hydrothermal structure upon lake phytoplankton modelling. Specifically, this is illustrated by comparing the response of phytoplankton in a phosphorus limited environment when the calibrated Model II of Chapter 5 is linked with three hydrothermal models with various specifications of the FML dynamics.

6.1.1 The Interaction Between the Hydrothermal Model and the Biological Model

A deterministic phytoplankton model is composed of two basic components: hydrothermal and biological.

The hydrothermal component, based on the one-dimensional (vertical) heat transport equation, describes the advection, mixing processes and the temperature distribution within the lake.

The biological component, based on mass transport equations (one for each biological or chemical variable), describes the vertical distribution of these biological or chemical variables within the lake.

There is a strong forward coupling between the hydrothermal model and the biological model, since most of the biological and chemical substances are passively transported by the fluid movement. In addition, temperature affects biological activity. A backward coupling between the biological model and hydrothermal model also exists: the distribution of the suspended and dissolved substances affects the extinction

coefficient which affects the thermal stratification through its influence on the absorption of solar radiation within the water column.

In the case study presented in Chapter 5, extinction coefficients have been measured and therefore, are regarded as input variables to the model. The availability of the extinction coefficient measurement allows the effect of hydrothermal structure upon phytoplankton to be studied without suffering the inaccuracy induced from an empirical relationship which expresses the extinction coefficent as a function of the suspended material. It shall be stressed that the omission of the discussion on the backward coupling between the biological model and the hydrothermal model by no means implies a lesser importance of this coupling effect. If an empirical formulation which relates the extinction coefficient as a function of dissolved and suspended variables is confidently known, then this effect can be readily studied. A first order linear regression between the measured extinction coefficients and the measurement of chlorophyll-a or PP indicates that L227 has a high background turbidity resulting from its long history of eutrophication. The regression result and the comparisons of the measurement with other empirical formulations are presented in Appendix C.

6.1.2 Focus on the Hydrothermal Structure Comparison

The hydrothermal characteristics of a stratified lake have been discussed in Chapter 2 along with the description of various one-dimensional models to simulate this phenomenon. All models, except the 2-box model, recognize the quiescent nature of the hypolimnion and accordingly approximate it by multi-diffusion layers. The unrealistic representation

of an overall stable hypolimnion by a fully mixed layer, as employed in the 2-box model, has been discussed in section 2.2.2.

In the hypolimnion, where little light penetrates and the temperature profile is almost vertical, the temperature profile gives practically no information on the vertical diffusivity. Thus, a correct representation of the hypolimnion diffusivity and other vertical transport processes has to be based on hydrodynamic principles. Although the hypolimnion diffusivity has been estimated by conducting field measurement of the vertical profiles of tracers such as Radium-226 and Tritium (Imboden et al., 1978; Quay, 1977), the question remains on the validity of extrapolating these values to other meteorological and hydraulic conditions or to lakes with different geometries. Therefore, a more specific simulation and comparison of the hypolimnion modeling other than those discussed in section 2.2.2 is not attempted here because we do not have a detailed analysis of these mechanisms which lead to a satisfactory parameterization of sporadic, local mixing events into an effective vertical diffusivity term. In this chapter we continue to use molecular diffusivity in the hypolimnion and examine the importance of the modeling the dynamics of the surface fully mixed layer (FML).

Except for the wind mixing model, the models reviewed in Chapter 2 are descriptive in nature since they consider the vertical diffusivity as a model parameter and calibrate it with field temperature measurements. A descriptive model has no capability to serve as a predictive tool because it does not explicitly formulate a causal relationship between the important model parameter and environment conditions. Therefore, a descriptive model is limited to the analysis of field data in a retrospective manner.

Moreover, the identification of the vertical transport process from analyzing temperature data in a retrospective manner may suffer from the inadequacy of sampling. The most important, but often neglected effect is the dynamics of the FML. The thickness of the eplimnion is often considered as a slowly varying process and the time scale of variation is regarded in the order of the summer stratification season. The daily variability of the FML has not been fully appreciated. This misconception of the FML movement has led to bi-weekly or monthly temperature sampling schemes that provide no information on short term movements.

The recent development of the mixed layer model allows long term simulations of the daily FML movement from given meteorological conditions. The importance of capturing the daily dynamics of the FML movement is investigated in section 6.4 by comparing the phytoplankton response of a phytoplankton model which uses the wind mixing model as its hydrothermal structure with that of phytoplankton models which use hydrothermal models specifying the FML dynamics from linear interpolation of the thermocline locations from bi-weekly temperature measurements.

6.2 The Importance of the FML Dynamics on the Phytoplankton Population

6.2.1 The Effect on the Limiting Nutrient Distribution

The keystone of a phytoplankton model is the correct description of the limiting nutrient distribution. In a phosphorus limited lake, which is a typical temperate lake, the phytoplankton population responds briskly to the variation of the phosphorus; therefore, it is convenient to start by considering the effect of the FML on the distribution of the external P and internal P inputs. This section will show that the distribution of the P input is known only if detailed knowledge of the

vertical temperature profile and of the FML dynamics are available.

6.2.1.1 The Effect on the Distribution of the External P Input

External nutrients are nutrients which originate from outside the lake; they have four means of entering the lake: (1) direct precipitation onto the lake surface; (2) surface runoff through the lake periphery (non point sources); point sources such as (3) influx by the stream and/or (4) discharge through a sewage outfall. The direct precipitation onto the lake surface is neglected in this discussion for two reasons:

(1) The amount of P concentration in rain is small,

(2) The lake surface is much smaller than the watershed area.

The problem of identifying the vertical placement of nutrient inputs within the lake is complicated because these inputs enter with flows whose temperature differs from the lake temperature at the apparent entrance point of these P inputs. The temperature difference results in vertical movement of the inflow.

Stream inflows usually enter the lake at the surface. However, the temperarure of the stream flow is usually lower than that of the lake surface. Therefore, the stream flow plunges after the entrance and entrains the ambient flow until it reaches a depth at which its density matches that of the ambient fluid (Figure 6.1.a). On the other hand, a sewage outfall may discharge near the lake bottom with a temperature higher than the hypolimnion temperature during most of the year. During the process of rising due to buoyancy, it entrains ambient fluid until it reaches the height at which the density of the ambient fluid is the same as that of the rising plume (Figure 6.1.b).

a)

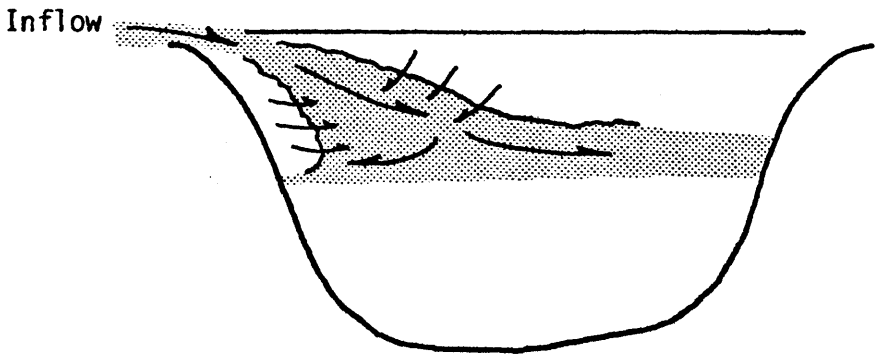

b)

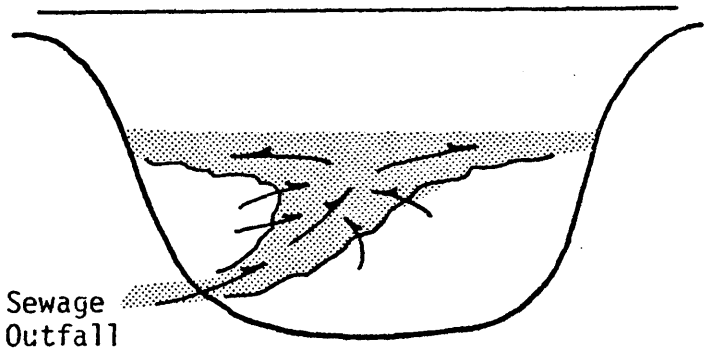

Figure 6.1: Vertical Placement of the External Phosphorus Input
(a) Streamflow
(b) Sewage

Not all of the external P enters the region where light and temperature conditions are most favorable for phytoplankton growth. The P cycling is governed by the combination of the diffusion and entrainment process which is caused by the deepening of the FML. The final location of the input depends on many factors, of which one of the most important is the time varying temperature distribution within the lake.

A pre-impoundment study of the Lafarge Lake in Wisconsin by Thornton et al. (1976) excellently illustrates the effect of lake vertical temperature structure on the inflow nutrient distribution. Figure 6.2 is a comparison of inflow temperature and lake surface temperature. The inflow temperatures range from zero to 5°C lower than the lake surface temperature. After entrance mixing, the location of the inflow was calculated to be from zero to 12 m below the lake surface as shown by the shaded region in Figure 6.3. From June to September the inflow and consequently the nutrient carried by it, entered the region below the thermocline.

The lake vertical temperature structure exerts an important influence on the vertical placement of the inflow in the water column. This becomes especially important when the major nutrient source is the surface run-off carried in during short term intervals.

6.2.1.2 The Effect on the Distribution of the Internal Nutrient

Internal nutrient refers to the ortho phosphorus which is released from lake sediment under anoxic conditions. In many lakes, especially those with a long history of eutrophication, this is the dominant source of phosphorus. Even for lakes where phosphorus from external sources is the dominant phosphorus on an annual basis, the internal phosphorus

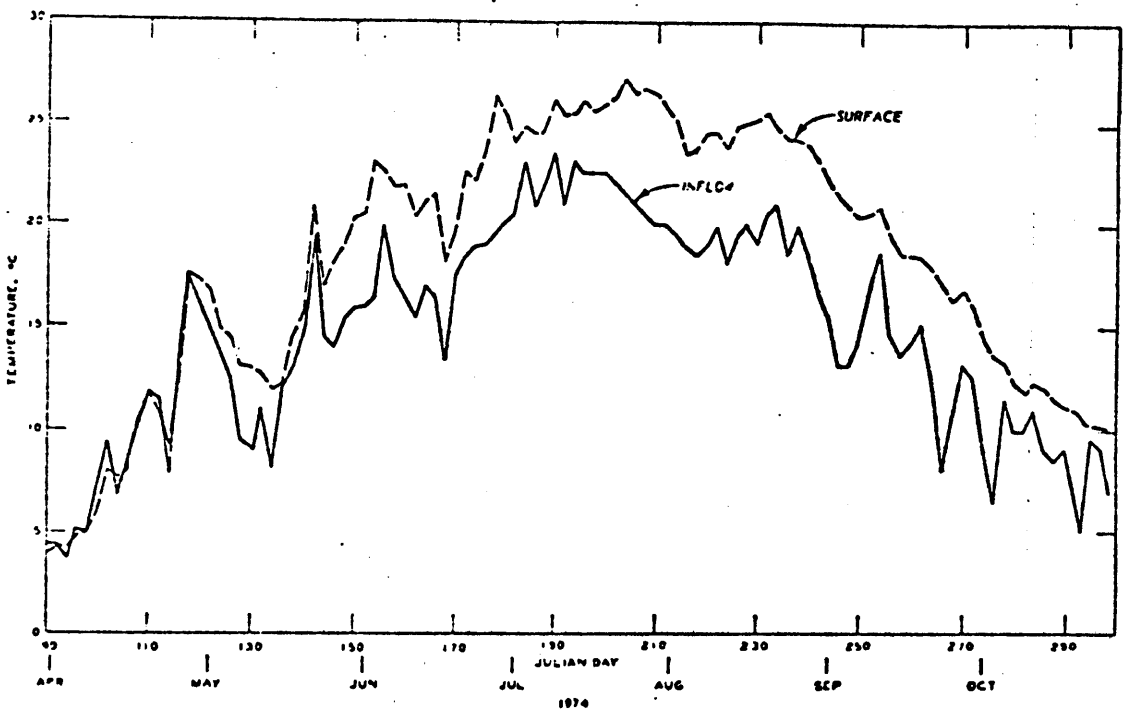

Figure 6.2: Comparison of Inflow Temperature and Lake Surface Temperature (from Thornton et al., 1976)

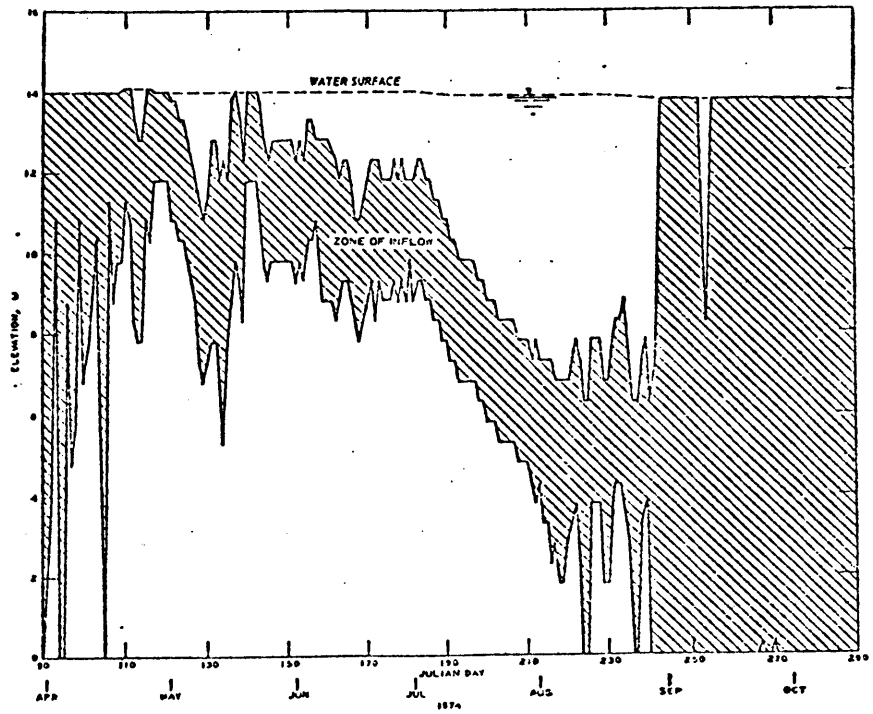

Figure 6.3: Zone of the Inflow (from Thornton et al., 1976)

could still be important for the seasonal phosphorus budget. Imboden and Gachter (1978) estimated that in Greefensse the ratio of phosphorus from internal sources to phosphorus from external sources, F_i/F_e, was between 0.6 to 1.0 for the period June to November, 1968 (Table 6.1).

Table 6.1

Internal Loading of Phosphate F_I (Flux through the Thermocline) Compared to the External Nutrient Loading F_E (taken from measurements in 1968) in Greifensee for the Summer 1975 (Imboden and Emerson, 1978).

	F_E (mgP m^{-2} day^{-1})	F_I	$F_I:F_E$
April/May	24	2	0.1
May/June	24	5	0.2
June/Sept.	24	15±7	0.6
Oct./Nov.	24	25	1

This sediment-released P accumulates in the hypolimnion where an anoxic condition prevails. This hypolimnetic accumulated ortho-P can only become available to the epilimnion by diffusion and/or entrainment. The process of entrainment is linked with sporadic wind mixing events. Evidence of this linking was provided by Stauffer (1974). He observed on July 12 - 13, 1971 a cold front passage accompanied by a strong enduring wind. The event caused the thermocline to deepen by approximately one

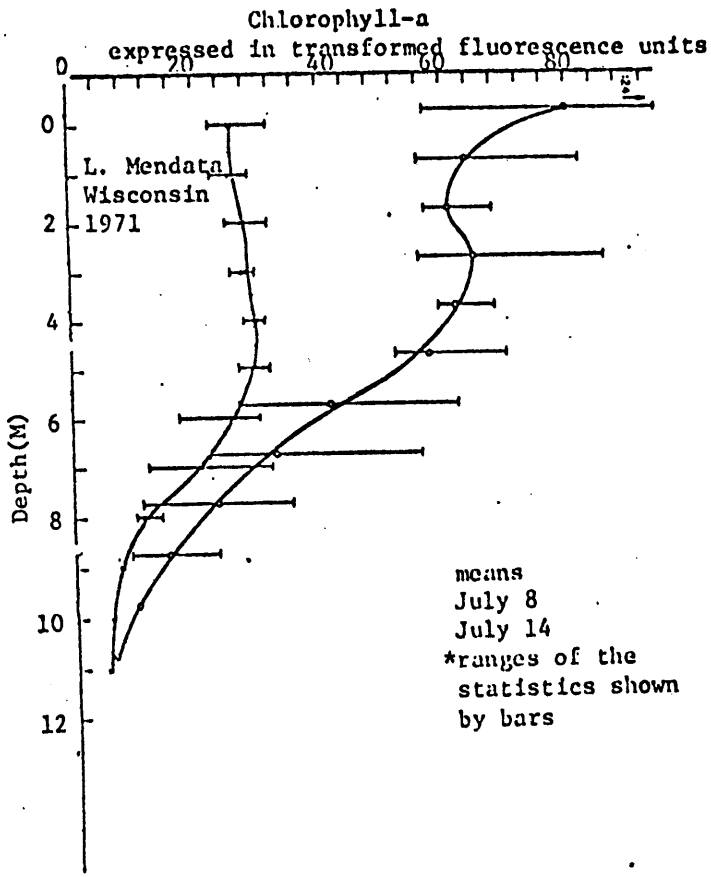

Figure 6.4: Progression of Average Temperature Profile after a Storm Event, Lake Mendoza, 1971 (from Stauffer, 1974)

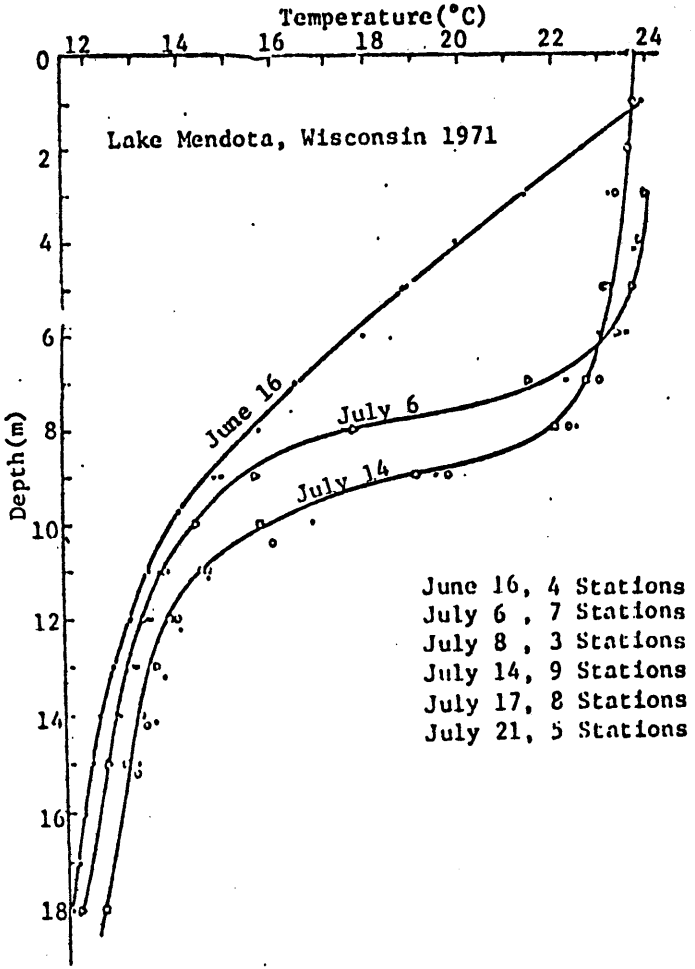

Figure 6.5: The Variation of Chlorophyll-a after a Storm EVent, Lake Mendoza, 1971 (from Stauffer, 1974)

one meter (Figure 6.4) and the epilimnion chlorophyll-a to more than double after this event (Figure 6.5). This short term increase of the epilimnion chlorophyll-a was a response to the phosphorus entrainment from the hypolimnion caused by the thermocline deepening.

6.2.2 The Effect on the Light Condition to which the Phytoplankton is Exposed

Another effect occurs when the FML varies. One of the naturally occurring limiting factors for phytoplankton growth in deep lakes is light. Since the light intensity in the lake decreases exponentially with the distance from the surface, no phytoplankton growth can take place in the deep region of the lake. If the effect of photoinhibition is not considered and if all other factors influencing the phytoplankton growth are uniform with depth, then the growth rate of phytoplankton would remain constant for the upper few meters and then decrease with depth. For example, using a hyperbolic function (equation 4.8) to describe the phytoplankton growth dependence on light, the depth averaged growth rate over the FML under optimal nutrient and temperature conditions is:

$$\tilde{f}(I) = \frac{\mu}{\eta H} \ell n\left(\frac{I' + K_I}{I' \exp(-\eta H) + K_I}\right) \qquad (6.1)$$

where μ = specific growth rate under optimal nutrient and temperature conditions, H = depth of the FML and $I' = I_o(1 - \beta)$. The asymptotic values for equation (6.1) are:

$$\tilde{f}(I) = \mu \quad \text{if} \quad I' \exp(-\eta H) >> K_I \quad \text{or if} \quad H << \frac{1}{\eta} \ell n\left(\frac{K_I}{I'}\right) \qquad (6.2)$$

$$\tilde{f}(I) = \frac{\mu}{\eta H} \ln \left(\frac{I'+K_I}{K_I}\right) \qquad \text{if } I' \exp(-\eta H) << K_I \text{ or if } H >> \frac{1}{\eta} \ln \left(\frac{K_I}{I'}\right) \tag{6.3}$$

That is, as the FML depth becomes larger than the depth defined by $\frac{1}{\eta} \ln \left(\frac{K_I}{I'}\right)$ the deepening of the FML results in a reduction of the overall depth averaged growth rate in the FML.

6.3 The FML Dynamics and its Effect on the Vertical Distribution of the Water Quality Parameters - Simulated by the Wind Mixing Model

6.3.1 The Dynamics of the FML

The FML movement of L227 in 1973 as simulated by the wind mixing model from daily meteorological conditions has been previously shown in Figure 5.5 which indicates variations of the FML at time intervals of a day. These short term variations of the FML depth are usually much larger than those of longer time scales. The variation of the monthly average FML is presented as Figure 6.6 which indicates the seasonal variation of the FML: from May to August as the stratification progressed the FML became shallower; from August to October as the destratification progressed, the FML became deeper. From May to June, the monthly average FML depth remained constant; from June to August, the depth increased at a rate of 0.5 m/month; from August to October, the depth increased at a rate of 2 m/month.

In this section, two incidents will be presented for a more detailed description of the FML movement. One illustrates a short term deepening of the FML during the summer heating period and the other illustrates the short term decrease of FML depth during the fall cooling season.

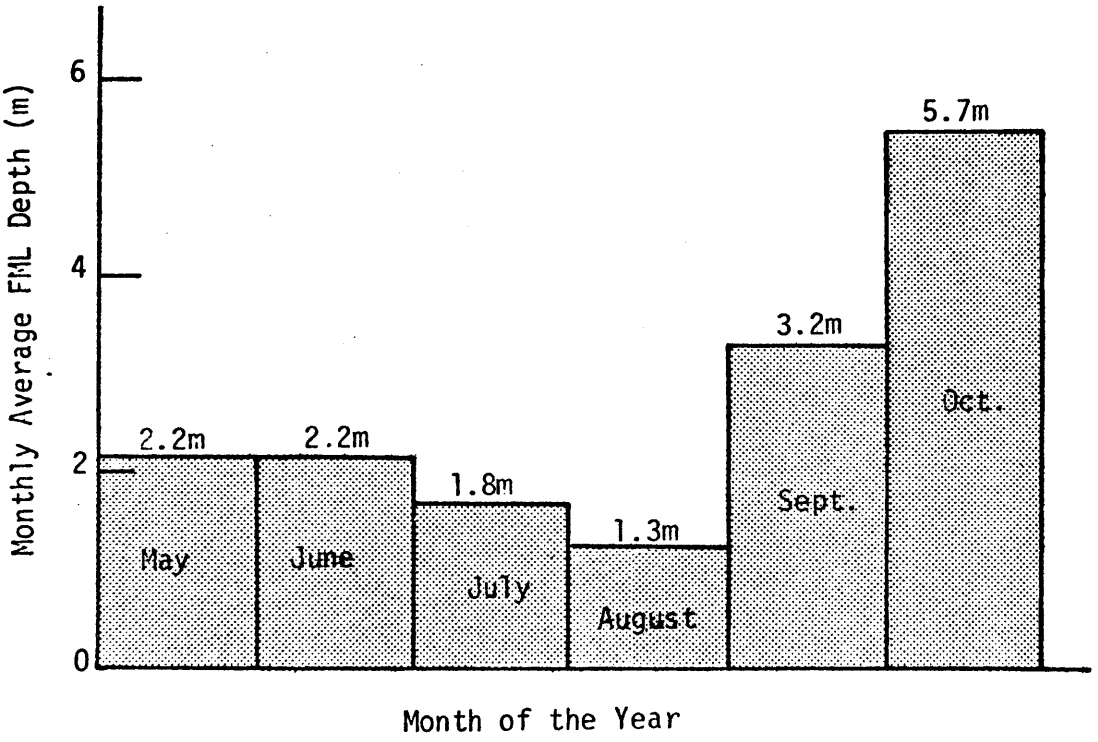

Fig. 6.6: Variation of the Monthly Average FML L227, 1973

6.3.1.1 Short Term Deepening of the FML During the Heating Period

The model simulated temperature profiles for the period from May 23 to May 27 are shown in Figure 6.7. The FML deepended from 1.5 m on May 23 to 3.7 m on May 26 with an overall change of 2.2 m over the three-day period. In order to explain the causes of these variations, a review of

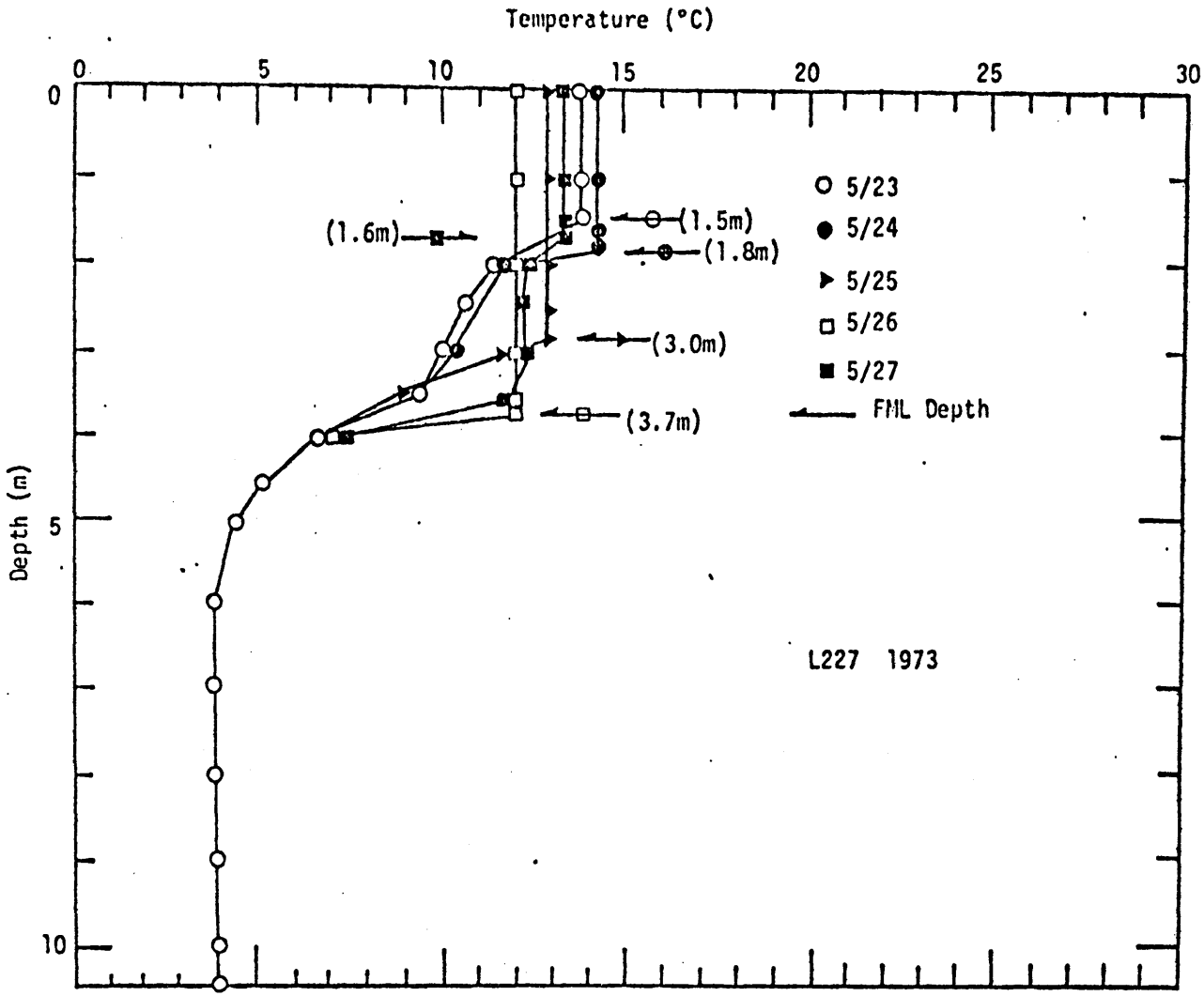

Figure 6.7: Short Term Deepening of the FML During the Summer Heating Period

the surface heat fluxes is presented in Figure 6.8 using the notations defined in section 2.3.1. The absorption of the direct solar radiation, ϕ_1, always gives an increase of the heat content of the surface element while the sum of other fluxes varies. If we define ϕ_2 as the sum of other fluxes, then whether ϕ_2 is positive or negative largely depends on the difference between the air temperature and water surface temperature. If the air temperature is larger than the water surface temperature then ϕ_2 is likely to be positive and vice versa. The sum of ϕ_1 and ϕ_2 represents the net change of heat content of the surface element.

On May 23, the water surface temperature was higher than the air temperature by 1°C and there was a loss of heat through ϕ_2 (i.e., ϕ_2 is negative). The amount of heat increase by ϕ_1 in the surface element, however, was large enough to overcome the loss of heat by ϕ_2 and subsequently caused an increase of water surface temperature by 0.5°C. This weak shallow stratification between the surface element and the element below was short-lived because the wind, which was at a speed of 5.2 miles/hr, transferred enough kinetic energy into the water column to overcome this stability and stirred this amount of heat into a depth of 1.8 m, which was the simulated FML depth of May 24, until the Richardson number, Ri, became in the order of 1500 which was large enough to cause most of the remaining kinetic energy to be locally dissipated (see section 2.3.3). On May 24, the air temperature was lower than the surface water temperature by 2°C and the surface heat loss due to ϕ_2 was larger than the heat input due to the absorption of the direct solar radiation. Therefore, the temperature of the surface element dropped by 1.5°C, the density instability induced by this surface cooling resulted in a FML depth of 2 m,

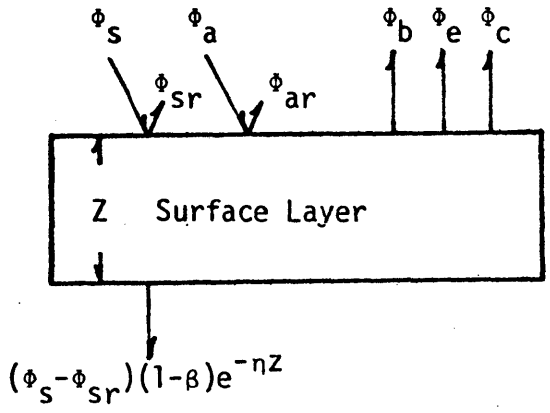

$$\Phi_1 = (\Phi_s-\Phi_{sr}) - (\Phi_s-\Phi_{sr})(1-\beta)e^{-\eta Z}$$

$$\Phi_2 = (\Phi_a-\Phi_{ar}) - \Phi_b - \Phi_e - \Phi_c$$

Figure 6.8: Surface Heat Fluxes

and the strong wind which was at a speed of 10.3 miles/hr caused the FML to move downward by an additional 1.0 m. As the FML reached a depth of 3.0 m, the Ri at the interface between the FML and the layer below was in the order of 450 and the energy remaining for stirring could no longer cause additional entrainment. A similar combination of convective cooling and wind stirring of May 25 caused a FML depth of 3.7 m for May 26.

6.3.1.2 Short Term Decrease of the FML Depth During the Fall Cooling Period

An example of the FML depth dynamics during the fall cooling period may be found in the period from October 21 to October 24. The temperature profiles as simulated by wind mixing model for this period are presented in Figure 6.9. The depth of the FML decreased from 9.3 m on October 21 to 0.6 m on October 24, with an overall reduction in the FML depth of 8 m in 3 days. Following this reduction of the FML depth, the FML depth increased by 4.5 m in one day.

On October 21, the air temperature was higher than the water surface temperature by 6°C; therefore, there was an increase of heat content of the surface element due to ϕ_2, and the direct absorption of the solar radiation caused a further increase of the heat content. The temperature of the surface element was increased by 1.5°C; the wind which was at 6 miles/hr stirred this heat downward to a depth of 1.8 m. On October 22 the air temperature was higher than the surface water temperature by 6°C and a similar heating/mixing reaction as on October 21 resulted in a FML depth of 0.6 m. On October 23 the air temperature dropped to 3^{o}C less than the water surface temperature, resulting in a heat loss of the surface element by ϕ_2, 10 times larger than the increase caused by

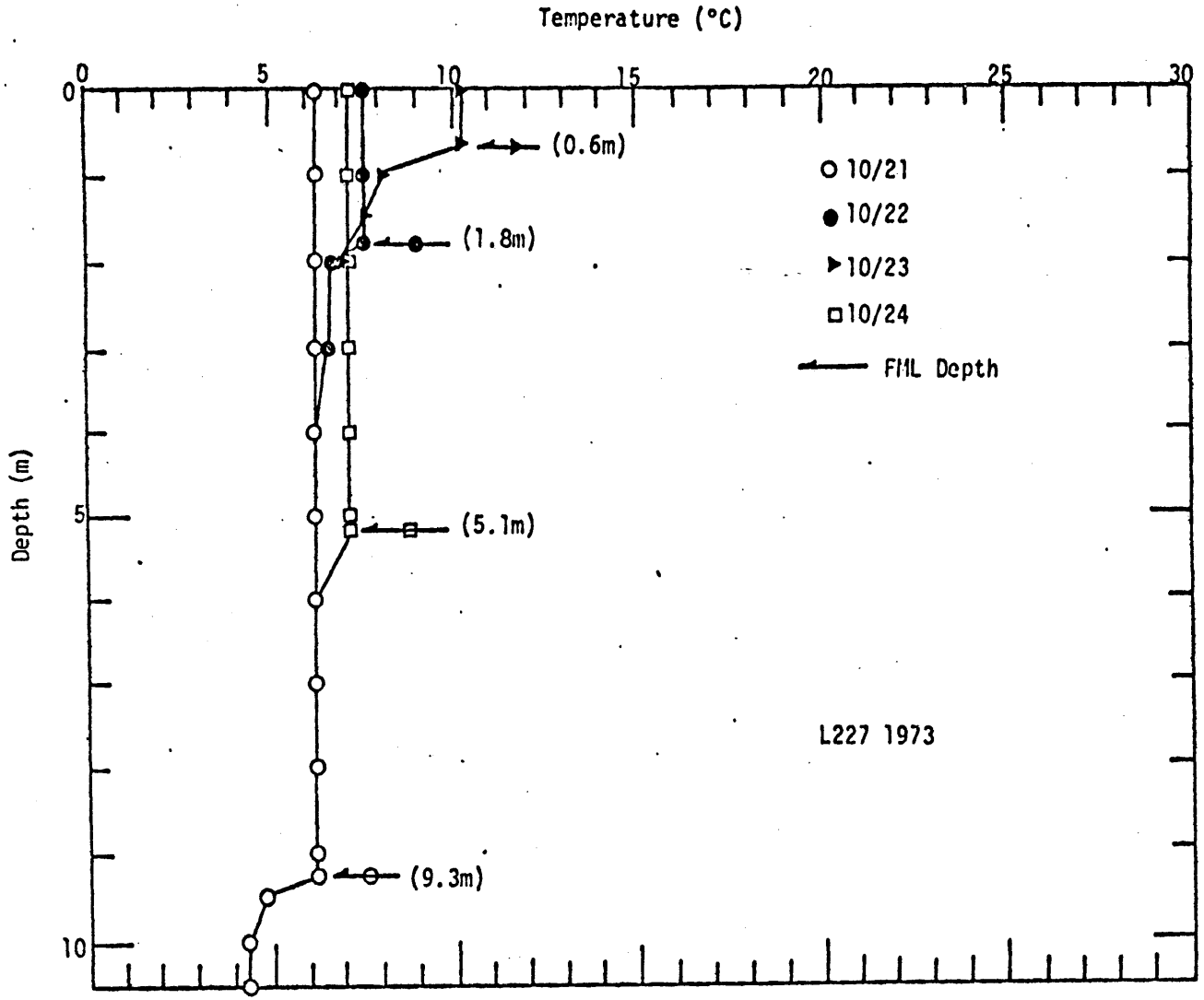

Figure 6.9: Short Term Decrease of the FML Depth During the Fall Cooling Period

absorption of the direct solar radiation and the surface water temperature was reduced by 3°C. The convective cooling resulted in a FML depth of 2.5 m; the stirring effect of the wind caused an additional entrainment and the FML was moved down to a depth of 5.1 m.

6.3.1.3 Summary

Although the temperature measurements of L227 in 1973 were not taken frequently enough to allow a full verification of the FML movement simulated by the wind mixing model, the existence of this short term FML variation is supported by Ford (1980). Ford measured the daily temperature profiles of three lakes in the Minneapolis-St. Paul area from April to June 1974 and concluded that:

> The onset of stratification was not, as traditionally described, a simple, graduate response of a lake to the annual solar radiation cycle. Rather it depends on a series of alternating heating, cooling and mixing cycles similar to annual and diel cycles but with a period of approximately five days. These were in direct response to the passage of major weather systems and displayed no apparent time lag.

Field measurement taken at bi-weekly or monthly intervals do not provide information on short time scale variations and the inference on vertical transport processes drawn from these temperature measurements may not be correct.

6.3.2 The Effect of FML Dynamics on PP and Chlorophyll-a Distributions

The role of the FML movement in the vertical distribution of the water quality parameters may be illustrated by a closer examination of the succession of daily profiles of PP and chlorophyll-a. The first example is taken from the period May 23 - May 27 of 1973 from the earlier L227

simulation presented in Chapter 5. Figure 6.10 shows the PP and chlorophyll-a profiles with the depths of the FML indicated by arrows.

The PP vertical profile on May 23 is shown as the line connecting open circles; the concentration in the FML is 25 μg/ℓ and decreased monotonically to a value of 10 μg/ℓ at 4 m depth (Figure 6.10.a). The following day, the FML deepended to a depth of 1.7 m which is about 0.2 m deeper than the depth on May 23. The resulting entrainment of water from below which has a smaller PP concentration caused a slight reduction of the FML PP concentration on May 24. The concentration of PP in the FML decreased from 25 μg/ℓ on May 23 to 18 μg/ℓ on May 26 coinciding with the deepening of the FML during this period. The reduction of the PP concentration in the FML depends on the relative concentration and volume difference between the FML and the entrained water during the deepening event. On May 27, a combination of higher air temperature, higher direct solar radiation and smaller wind speed caused a shallower FML of 1.6 m. However, the reduction of the FML from 3.7 m on May 26 to 1.6 m on May 27 caused no difference in the vertical PP profiles of these two days. It is important to realize that the reduction of a FML does not concentrate the mass which was previously distributed in a deeper FML to a smaller FML. That is, there is no concentration of the mass during the reduction of the FML.

For substance A, which is either so nonactive that there is no appreciable change during the time course of observation or which is so active that over the time course of measurement it is in kinetic equilibrium, the effect of the FML movement on its concentration in the FML may

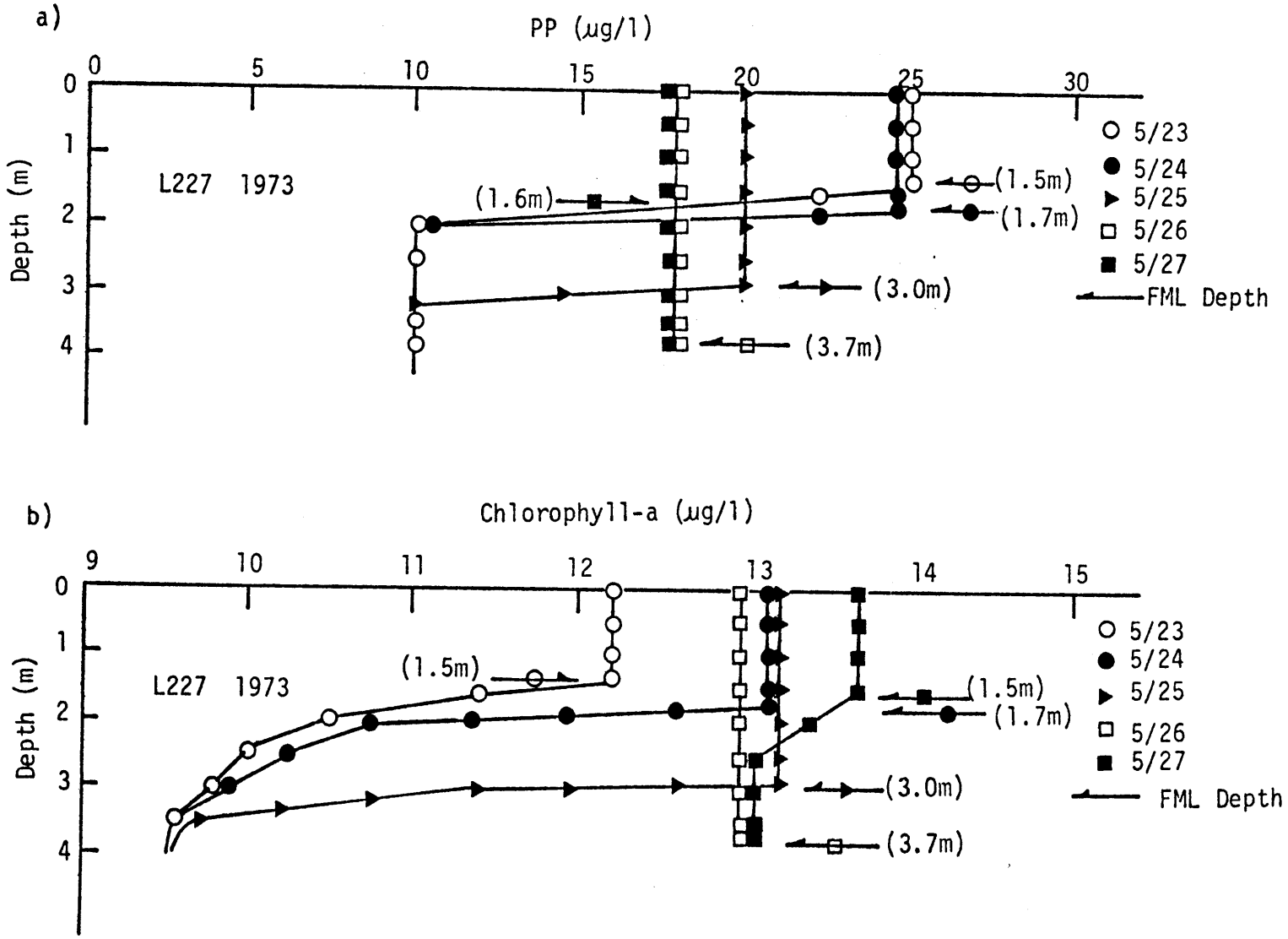

Figure 6.10: The Effect of FML Movement on the Vertical Distribution of PP and Chlorophyll-a (May 23 to May 27)

be illustrated by the panels of Figure 6.11. The concentration of substance A in the FML is governed by the maximum FML depth of the period in the absence of any input.

The chlorophyll-a gradients in the upper 4 m during the period May 23 to May 27 are small (only 20% difference between the surface and 4 m depth), therefore, the scale is enlarged to showed the effect caused by FML variations (Figure 6.10.b). On May 23, the concentration of chlorophyll-a in the FML is 12.2 μg/ℓ and decreases to 9.5 μg/ℓ at 4 m depth. The deepening of the FML will cause a reduction of the FML concentration as shown in the case of PP distribution. However, the phytoplankton growth increases the chlorophyll-a concentration, therefore, the final concentration depends on the combined effect of the FML variation and growth. As reflected in the profile of May 24, the deepening of the FML caused a slight reduction which is overcome by the increase due to the growth effect; therefore, the concentration of chlorophyll-a in the FML is increased when compared with that of May 23. The reduction of FML depth from May 26 to May 27 shows no change in the PP vertical profile (see Figure 6.10.a), however, this is reflected in the chlorophyll-a profiles. On May 26, the chlorophyll-a concentration is uniformly 13 μg/ℓ for the upper 3.7 m water column which is the depth of the FML of the day; the next day, the chlorophyll-a concentration is only uniform for the upper 1.6 m with a value of 13.7 μg/ℓ and shows a gradient for the depth below. In summary, the chlorophyll-a concentration which is subject to additional reaction terms is more sensitive to the FML movement than the PP.

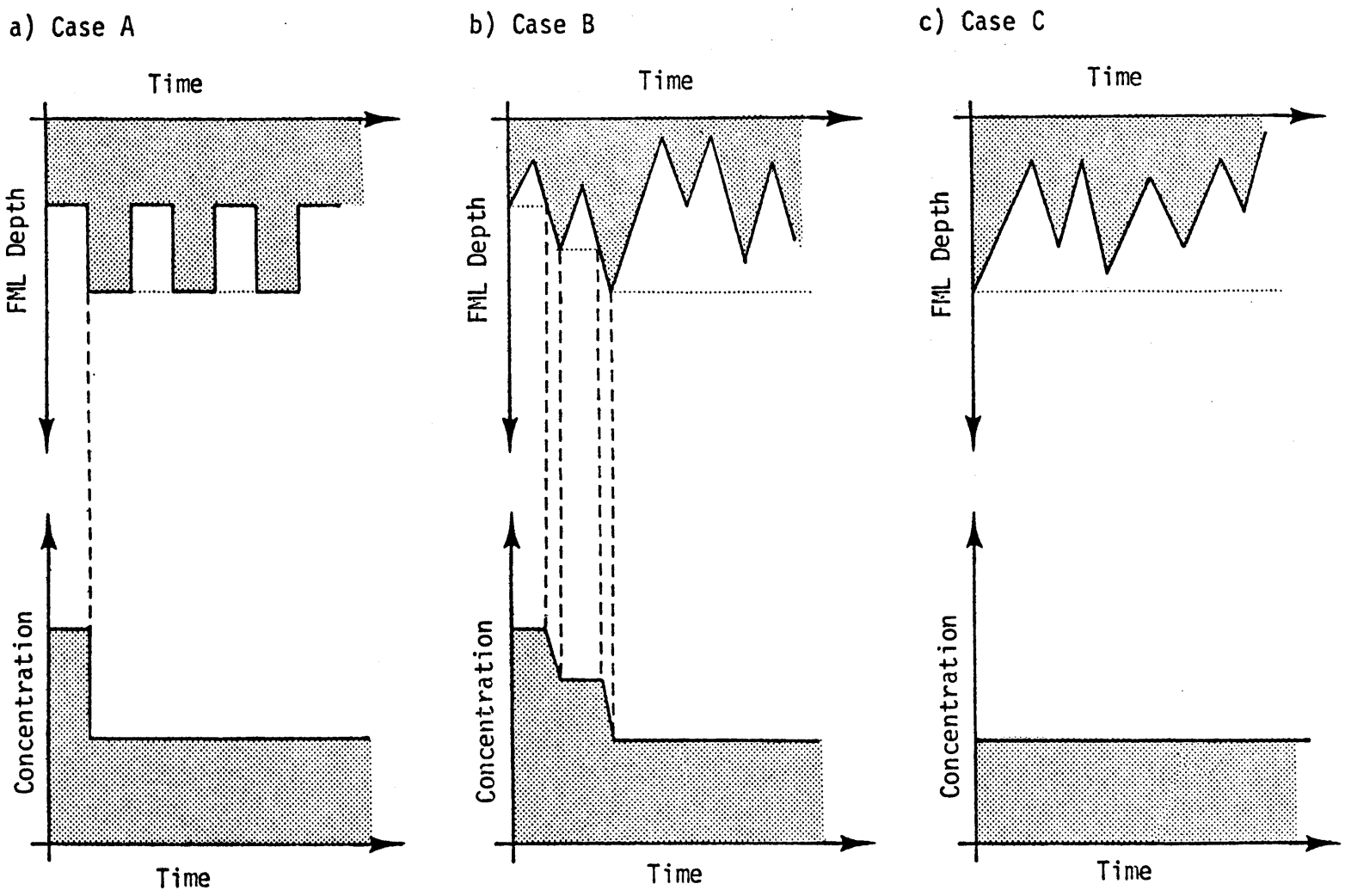

Figure 6.11: The Effect of the FML Movement on Substance A Which is Either Nonactive or in Kinetic Equilibrium

The second set of consecutive daily profiles of PP and chlorophyll-a is presented in Figure 6.12 for the period from October 21 to October 24. The PP profile remains unchanged for the whole period. The reason is clear from the illustration of Case C in Figure 6.11. The FML depth of the first day is 9.3 m and the PP is uniformly distributed over this depth. The fluctuation of the FML in the following 4 days is within the water column which lies above the FML depth of the first day and therefore, no change in the PP profiles. The chlorophyll-a profiles, shown in the enlarged scales, reflect the depth of the FML since the vertical homogeneity only exists in the FML.

6.4 Comparison of Phytoplankton Predictions of Lake Phytoplankton Models with Different Hydrothermal Models

The objective of this section is to compare quantitatively the differences in predicted phytoplankton concentrations in L227 that result when the same biological model is linked to three different hydrothermal models under identical meteorological and nutrient input conditions. In the base case the phytoplankton model is linked to the wind mixing model (in which the FML is predicted on a daily basis) as used throughout Chapter 5. In the other two hydrothermal models the depth of the FML layer is specified (i.e., as an input to the hydrothermal model) from lake temperature measurements made at two week intervals. The daily values needed for simulation are obtained by linear interpolation these two models differ only in their definition of the depth of the FML as explained below. They are similar to the specified thermocline depth model used by Imboden (1978).

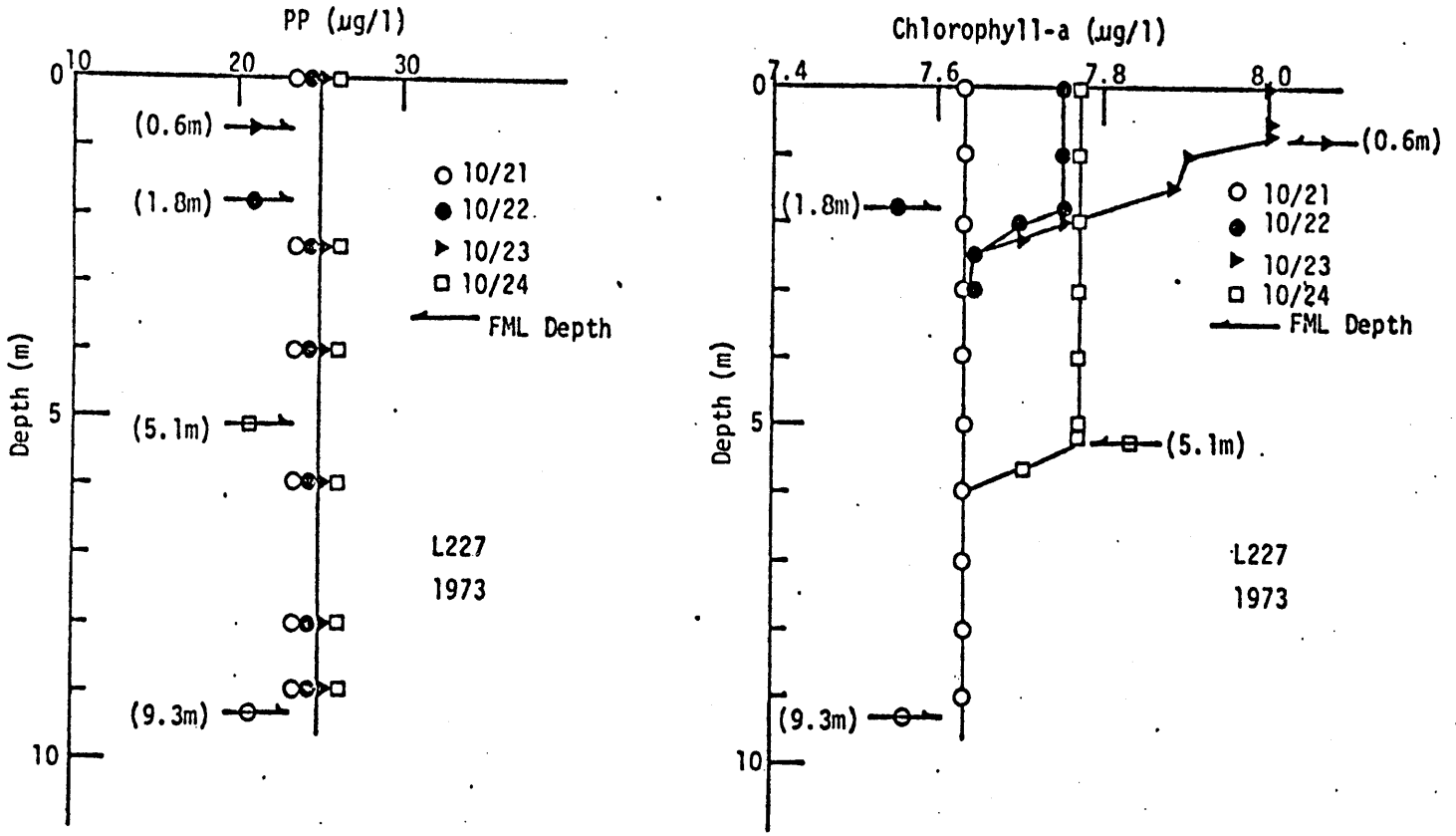

Figure 6.12: The Effect of FML Movement on the Vertical Distribution of PP and Chlorophyll-a (October 21 to October 24)

The following two cases of nutrient input are considered:

(a) Surface nutrient input; nutrient enters the fully mixed layer and is retained in the FML.

(b) Nutrient interflow case, that is, nutrients enter the lake at an intermediate depth and is entrained into the FML by the deepening of the FML.

6.4.1 Model Description

The structures of the three lake phytoplankton models are illustrated in Figure 6.13. Model II, the biological model with the inclusion of zooplankton grazing previously presented in section 5.3.1.4 is used as the common biological model of the three lake phytoplankton models. The three models are formed by linking Model II with the wind mixing model, specified depth model 1, and specified depth model 2. The three hydrothermal models use an alternating heating/mixing algorithm for temperature simulations. They are identical in their treatment of the heating processes, that is, they solve the same one-dimensional heat balance equation (equation 2.12). They only differ in their definitions of the daily FML depths:

(a) WDMIX Model

The MIT Wind Mixing Model: The daily FML is computed from the given meteorological data as well as information on the water column stability. The FML is characterized by the absolute thermo-homogeneity in the model output of temperature.

(b) SD1 Model

The Specified Depth Model 1: The depth of the FML is defined as the

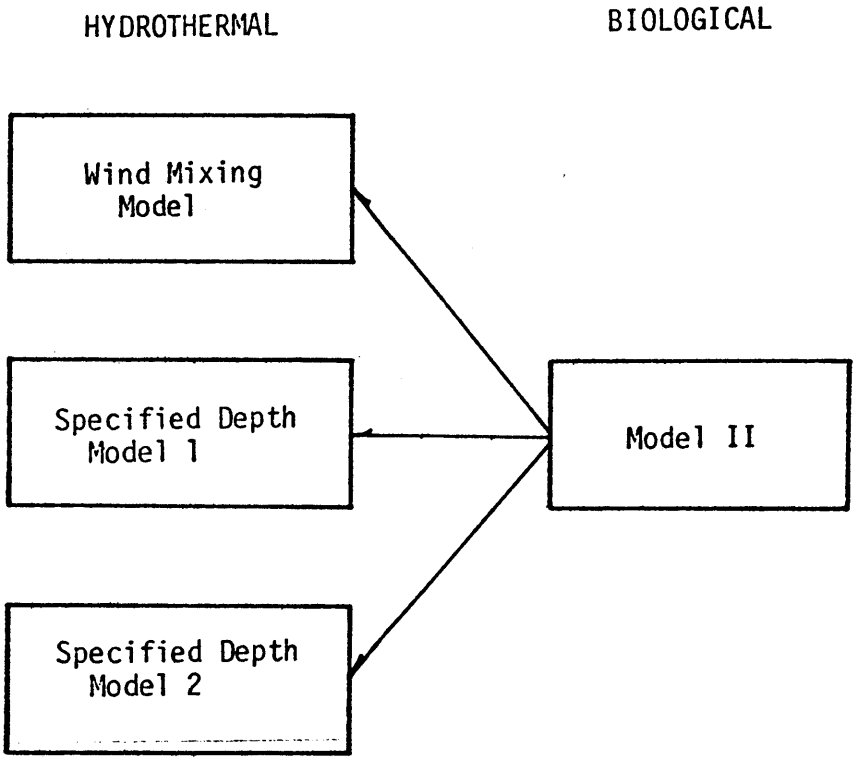

Figure 6.13: Structures of the Three Lake Phytoplankton Models Chosen from Comparison

depth of the thermocline location. The daily thermocline location needed for model computation is obtained from linearly interpolating the thermocline locations from the bi-weekly temperature measurements. Following Birge's (1897) suggestion, the location of the thermocline from any of the bi-weekly temperature profiles is defined as the shallowest depth at which the temperature gradient is greater than 1° C/m.

(c) SD2 Model

The Specified Depth Model 2: The daily FML depth is also obtained from linearly interpolating the locations of the thermoclines defined from bi-weekly temperature measurement. However, the location of the thermocline is defined as the depth at which the maximum temperature gradient occurs, following Brönsted and Wesenburg-Lund (1911).

It should be noted here that the three hydrothermal models differ not only in their specifications of the daily variation of the FML, but also in their definitions of the FML. In theory, the FML should be characterized by absolute thermo-homogeneity in any temperature profile. The WDMIX model, which employs this definition, should always define an FML location shallower or equal to that defined by either the SD1 model or the SD2 model from a given temperature profile. Similarly, the FML location in any given temperature profile defined by the depth at which the temperature gradient is greater than 1°C/m should always be equal to or less than the FML defined by the depth at which the maximum temperature gradient occurs, unless the maximum temperature gradient is less than 1°C/m.

Figure 6.14 shows the temperature profile on the 204th day of 1973 for L227. The depth of the FML according to each of the above definitions

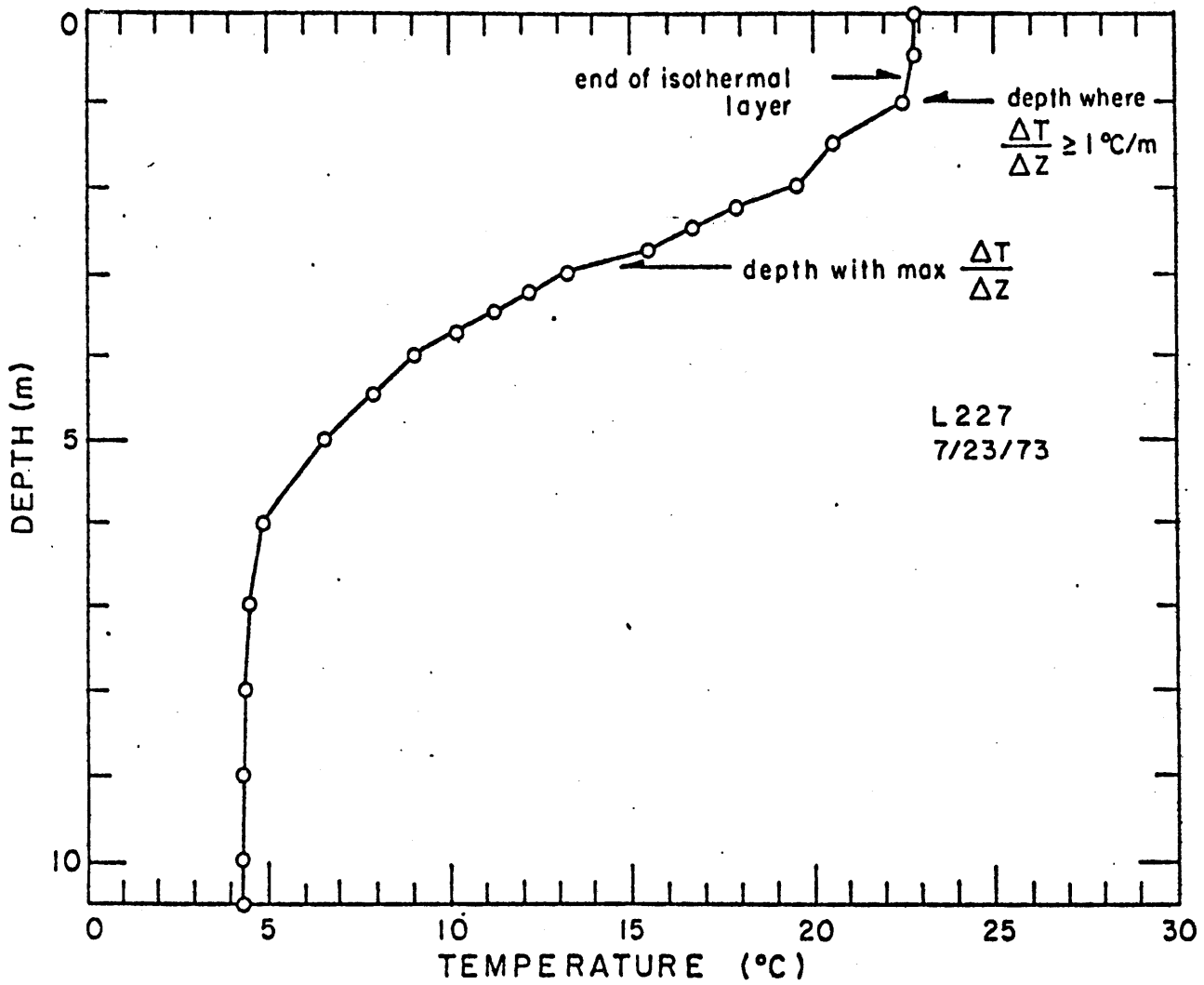

Figure 6.14: Comaprisons of the Three Model Definitions of FML from a Given Temperature Profile

is also marked on the figure. The isothermal layer was 0.5 - 1.0 m deep (the exact location is unknown due to the 0.5 m depth sampling interval in this region on that day); at 1 m depth the temperature gradient becomes greater than 1°C/m; and the maximum temperature gradient occurred at 2.75 - 3.0 m depth interval with a value of 9°C/m. The temperature difference between the lake surface and the 3 m depth was 9.5°C/m; clearly, the upper 3 m of the lake was not fully mixed on that day. We may conclude from this example that the depth of maximum temperature gradient is not necessarily the depth of the actually fully mixed layer at that instant.

The daily FML used for computation in three hydrothermal models are presented in Figure 6.15. The SD2 model which linearly interpolates the biweekly depth of maximum temperature gradient, always specifies deeper FML than the SD1 model, which linearly interpolates the bi-weekly depth with temperature gradient greater than 1°C/m. The only exception is the period between the 288th to the 302nd day. On the 302nd day the lake was only weakly stratified and the maximum temperature gradient was less than 1°C/m (see Figure 6.16) so that the location of the FML on this day is 10 m according to the SD1 model but only 7 m according to the SD2 model. The WDMIX model simulates a highly fluctuating FML during this simulation period from May 15 to October 29. Whenever there are measurements available, the FML simulated by the WDMIX model coincide well with the location of FML defined by the SD1 model. If the actual movement of the fully mixed layer is well represented by the simulation of the WDMIX model, then this time series plot seems to suggest that the location of the maximum temperature gradient bears memory from the

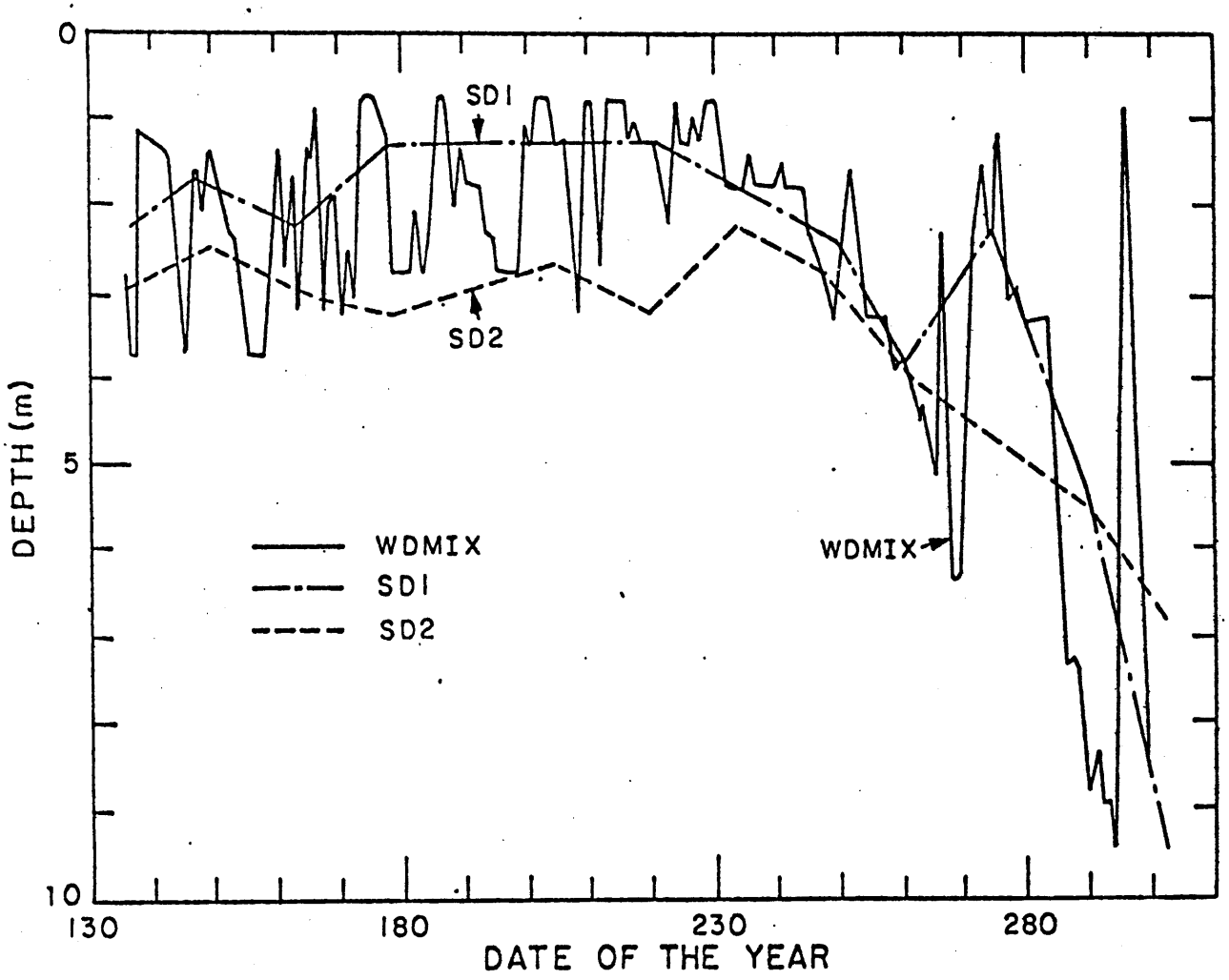

Figure 6.15: Definitions of the Daily FML Depth in Three Models

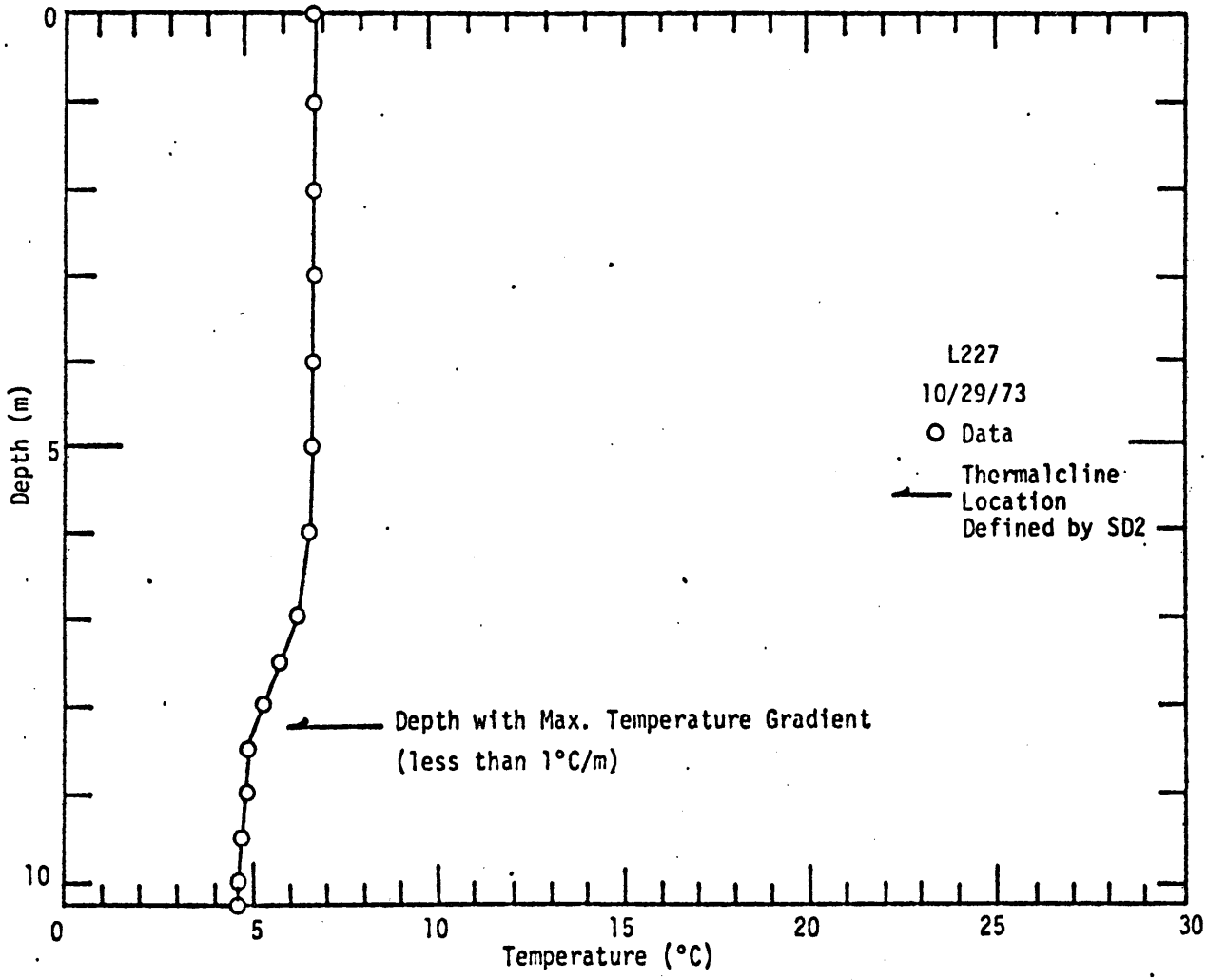

Figure 6.16: Measured Temperature Profile on the 302th Day, 1973 L227

preceding mixing event. For example, on the 176th day, the SD2 model defines a FML depth of 3.25 m which is much deeper than the actual FML of the day (1 m), but which closely resembles the location of the FML of the 170th day. Similar occurrences can also be observed for the 190th, 204th and 218th day. After the 274th day, the WDMIX model overpredicts the depth of the FML; the possible cause of this overprediction has been discussed in section 5.2.2.

6.4.2 Case A - Surface Nutrient Addition

6.4.2.1 Problem Statement

The example used for this comparison in based on data for L227, 1973. As previously described in section 5.1, L227 received its nutrient input from weekly surface additions and this added nutrient was retained in the upper layer of the lake because the nutrient was dissolved in water taken from the surface of the lake (Schindler, 1971). Therefore, the phytoplankton simulation will not suffer from the difficulty of identifying the zone of inflow which is caused by the temperature difference between the lake surface temperature and the inflow temperature of the nutrient. The strong stratification of L227 resulted in very clear locations of thermoclines; there was no indication of multiple thermocline formation from the available field temperature measurement (see section 5.2). In other words, it is comparatively easy to identify the location of the thermocline for L227. There is only one remaining uncertainty from linearly interpolating the location of thermocline from intermittent temperature measurements; that is, the dynamics of the FML movement. The objective of this simulation is to compare quantitatively the

difference in phytoplankton prediction with various specifications of the FML location.

6.4.2.2 Simulation Results, Comparison and Discussion

(A) Temperature Simulation

Despite the difference in their specifications of the FML depths, the three hydrothermal models show remarkable agreement in their predictions of surface temperature and hypolimnion temperatures. Figure 6.17 compares three model simulations for the 190th day with field measurements. All the models satisfactorily simulate the surface temperature and temperature for depths below 4 m, showing a difference between model simulation and field measurement of no more than 2°C.

The good agreement between the WDMIX model simulation and the field temperature measurement has been shown earlier in section 5.2.2. Examples of temperature simulation by the SD1 model and SD2 model are shown in Figure 6.17 with the field measurements. The result indicates that the SD1 model is considerably better than the SD2 model in simulating the field temperature measurements. The inadequacy of the SD2 model's definition of the FML depth is clearly demonstrated in its temperature simulation results. For example, on the 190th day, the difference between the SD2 model simulation and field measurement is as much as 10°C at 3 m depth (see Figure 6.17.a). Significant differences between the SD2 model's result and the field measurements for the depth interval between 1-4 m can also be observed in Figure 6.1.7.b.

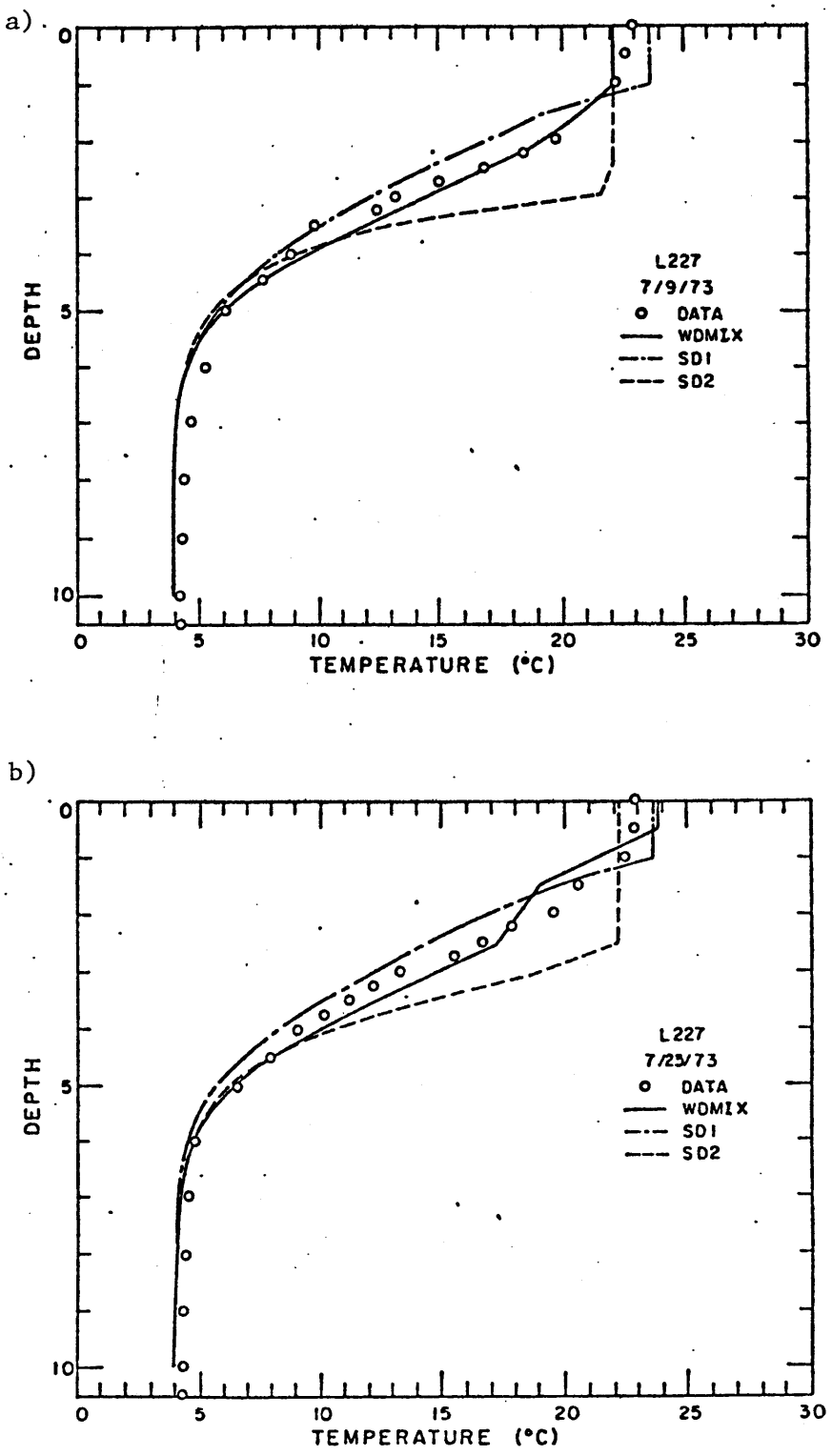

Figure 6.17: Comparison of the Models' Temperature Simulation Result (a) July 9 (b) July 23

(B) Phytoplankton Simulation

The simulated phytoplankton concentrations represented as chlorphyll-a concentration, are shown in Figures 6.18 and 6.19. In all three models the same initial conditions and parameter values listed in Table 5.8 and Table 5.11 are used. Since in all three models, the FML does not extend below 3.5 m depth until after the 260th day, the model simulations are almost identical for the 4 m depth and depths below. Therefore, only the concentration in the FML and the 3 m depth are compared.

(a) Comparison of the Phytoplankton Concentration

Figure 6.18 is a comparison of the FML chlorophyll-a concentration simulations. The SD1 model predicts the highest value and the SD2 model predicts the lowest value. Compared with the simulation results of the WDMIX model, the SD1 overpredicts by as much as 50% (peak chlorophyll-a value of 300 μg/ℓ for SD1 vs. 200 μg/ℓ for WDMIX) while the underprediction by SD2 model is moderate at only 15% (peak chlorophyll-a value of 170 μg/ℓ for SD2 vs. 200 μg/ℓ for WDMIX). The simulated chlorophyll-a concentration at 3 m depth is presented in Figure 6.19. Here, the trend observed in Figure 6.18 is reversed: the SD1 model predicts the lowest value and the SD2 model predicts the highest value, with more pronounced differences in the predictions of the three model at the 3 m depth. Again, using the prediction by the WDMIX model as the reference, the other two models either overpredict or underpredict by more than 50% for most of the period.

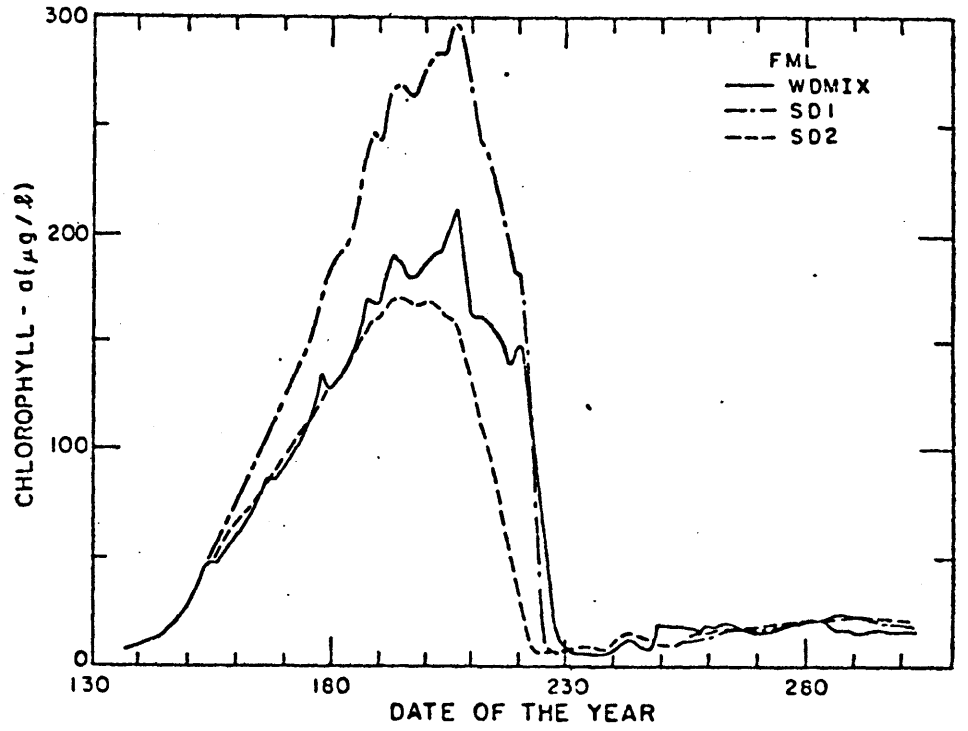

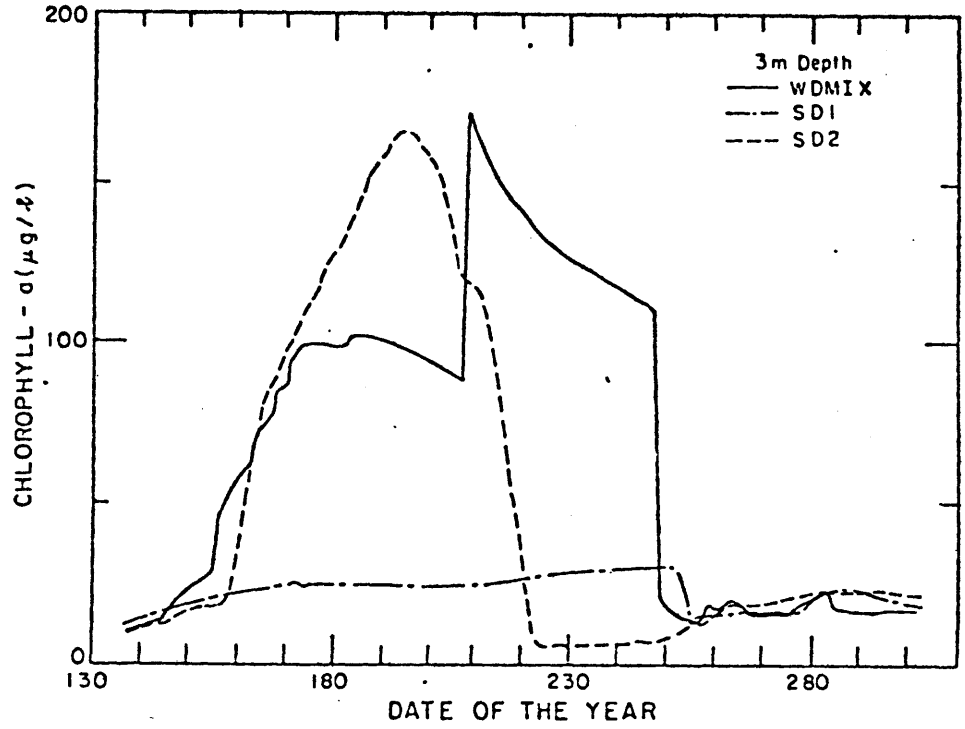

Figure 6.18: Comparison of Models' Simulation Result on Phytoplankton (FML)

Figure 6.19: Comparison of the Models' Simulation on Phytoplankton at 3 m Depth

(b) Discussion

The difference in the simulated chlorophyll-a values mainly stems from the difference in the model's simulations of the PP distribution. Figure 6.20 and Figure 6.21 compare the models' simulated PP values in the FML and at 3 m depth respectively. The parallel between each model's prediction of PP values and chlorophyll-a values are clear from comparing Figure 6.18 with Figure 6.20 and Figure 6.19 with Figure 6.21.

In all three models, the uptake of ortho-P is so rapid that within a few hours after the nutrient addition, all added ortho-P is taken up by phytoplankton and then converted to particulate P. We may approximate this condition by considering that 1.14 kg of PP is added to the lake on a weekly basis. Moreover, since in all these simulations the settling rates of PP are assumed to be zero, PP has no means of entering the deeper layers other than through the process of entrainment. We may very well explain the differences in the models' predictions of PP distribution by considering the effect of FML specification on the distribution of an inert substance.

In the FML:

The difference in PP concentration predicted by the SD1 model and the WDMIX model becomes pronounced after the 180th day. The period between the 176th and the 204th days may be conveniently divided into 4 weekly intervals coinciding with the nutrient addition intervals: 176-183, 183-190, 190-197, 197-204. Re-examining the time series plot of the FML (Figure 6.15) we may observe that in each of these intervals, the WDMIX model predicts a maximum FML depth on the order of 2.5 m while the SD1

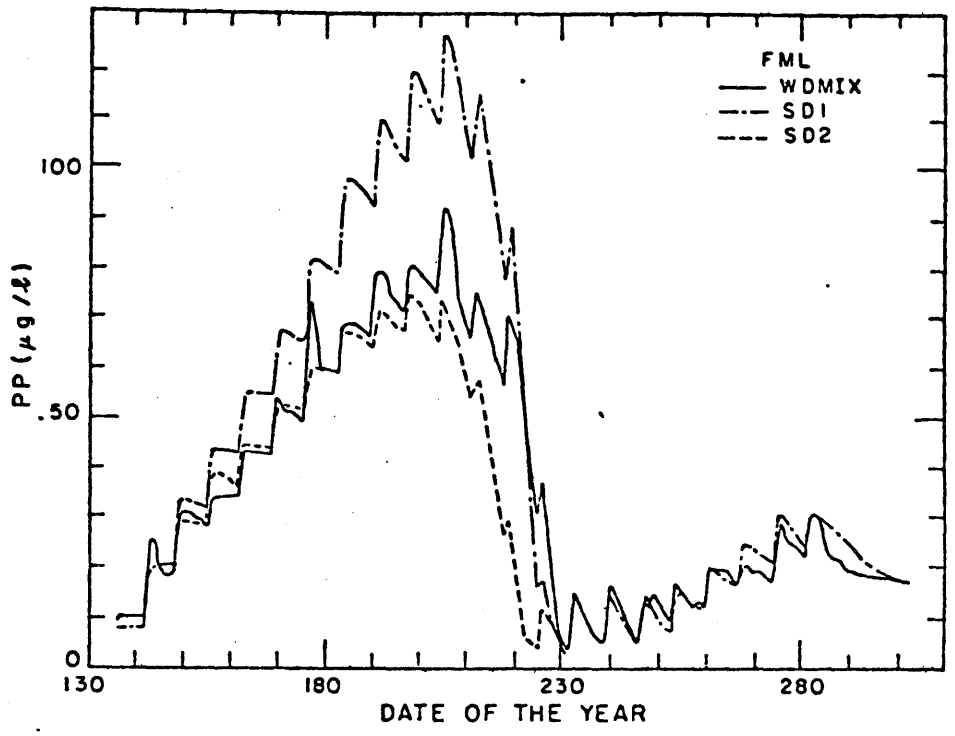

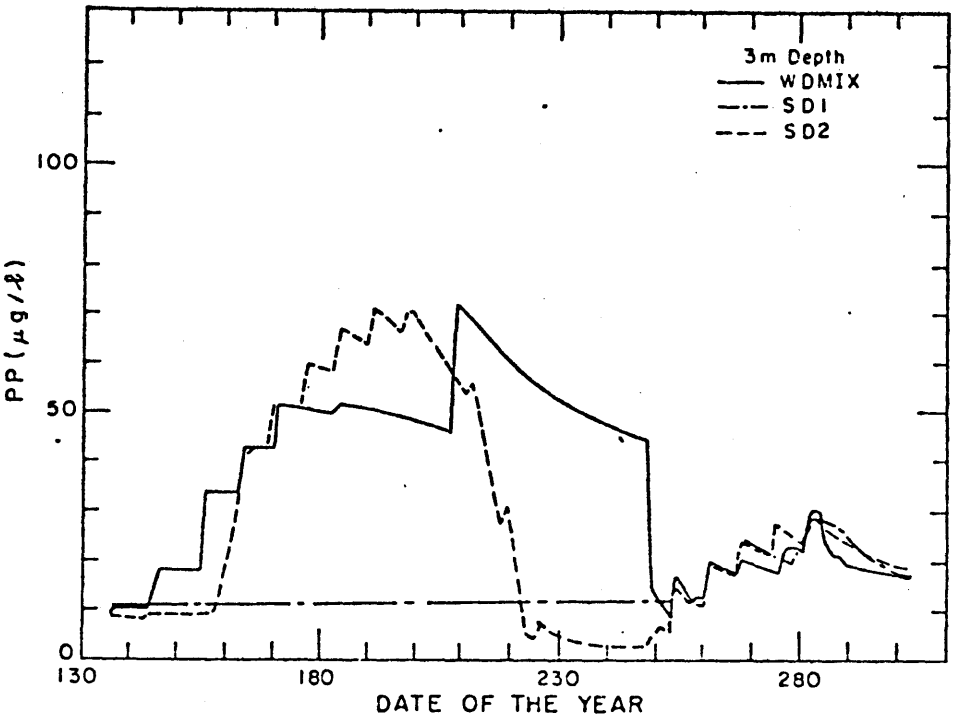

Figure 6.20: Comparison of the Models' Simulation on PP in the FML

Figure 6.21: Comparison of the Models' Simulation of PP at 3 m Depth

model predicts a maximum FML of 1.2 m. Therefore, according to the SD1 model the amount of nutrient added into the lake surface during this period will not be distributed into depths lower than 1.2 m, but according to the WDMIX model, these added nutrients will be distributed down to 2.5 m depth. As described in section 6.3.3, the maximum FML during the inerval of nutrient addition is most important. For example, if the WDMIX model predicts a dynamic FML shown as the shaded region in Figure 6.22 for this period, the model similation of PP will be similar and the difference between SD1 model and the WDMIX model will be the same for this hypothetical case. Even the mean value of the FML depth in the SD1 model is larger than the mean value in this hypothetical case. Following this analogy, we may easily see why the SD2 model and the WDMIX model are similar in their predictions of the PP values. The FML depths in the SD2 model closely follow the maximum FML depth in weekly intervals with slightly higher values for the period between the 180th and 204th day. Consequently, this results in a close prediction of PP values between the SD2 model and WDMIX model with only a slight underprediction in the period between the 180th and 204th day.

The very interesting point is that in this case study, the SD2 model whose definition of FML depth bears little resemblance to the physically defined fully-mixed depth (see Figure 6.14), does a better job in simulating the concentration of an inert PP substance in the FML than the SD1 model whose definition of FML is closer to the physically defined fully mixed layer.

Phytoplankton in the FML of the three models grow without any light limitation due to the low half saturation constant for light function

(15 ly/day) used for the simulation. The temperature of the FML predicted by three models are similar as in Figure 6.17. As a result of similar light effect on phytoplankton and temperature condition in the FML for the three models, models which predict similar PP concentration in the FML predict similar chlorophyll-a concentration in the FML as indicated by the results between the WDMIX model and the SD2 model. A sensitivity analysis of light effect is done by increasing the half saturation constant from 15 ly/day to 150 ly/day. The comparison of the simulated chlorophyll-a concentrations in the FML are shown in Figure 6.23. The difference between the three models predictions is enhanced when compared with the results presented in Figure 6.18.

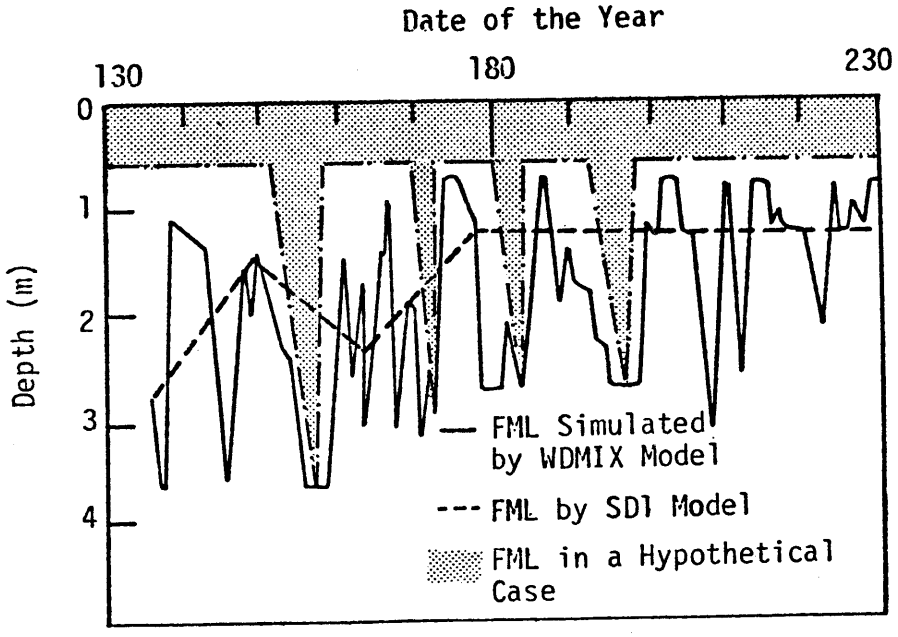

Figure 6.22: Hypothetical FML Variation Which Will Produce the FML Phytoplankton Concentration as Simulated by WDMIX Model

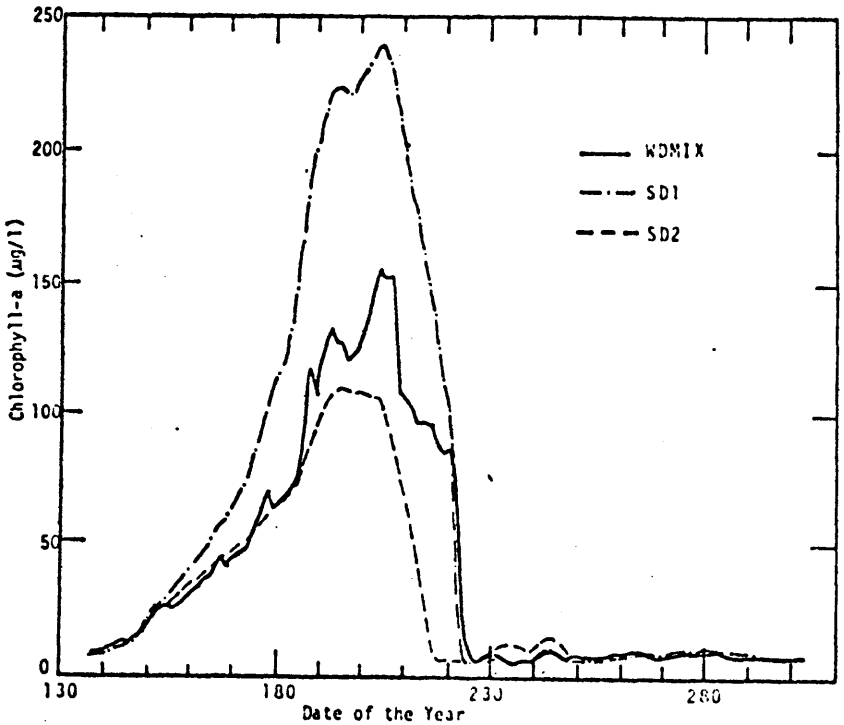

Figure 6.23: Comparison of the Models' Simulation on Phytoplankton at FML $\bar{\omega}$ K_1 = 150 1y/day

At 3 m depth:

Due to the 0.5 m grid size used in the model, we should consider a depth interval between 2.75 - 3.25 m instead of an exact depth of 3 m. Since the total amount of nutrient added is the same in the three models, the model which gives higher values of PP concentration in the FML undoubtedly gives lower values of PP concentration in the adjacent lower layer. Thus the SD1 model now predicts the lowest values of PP while the SD2 model predicts the highest value for this depth.

According to the SD1 model, the 3 m depth is the non-fully mixed layer for the whole period between the 140-240th day. Since the first nutrient addition was on the 142nd day, the 3 m depth in the SD1 model will not receive any additional nutrient until after the 240th day. On the other hand, the 3 m depth is regarded as the FML according to the SD2 model except for periods around the 148th and 204th day, and the longer period of approximately 20 days beginning on the 225th day. The two earlier non-fully mixed periods have little influence on the PP concentration distribution since they are quickly followed by the fully mixed periods. Therefore, the PP concentration in the 3 m depth is almost identical to the PP concentration in the FML, except for the period between the 235th-245th day.

With the WDMIX model, the 3 m depth is intermittently defined as being within the FML, but from the 114th day untile the 208th day the layer between 2.75-3.25 m is considered as a layer below the FML and this prevents the water in this depth and depths below to receive the nutrient added onto the lake surface during this period. Thus the significant difference in PP values between the SD2 model and the WDMIX model occurs.

6.4.3 Case B - Interflow Nutrient Addition

6.4.3.1 Problem Statement

This simulation is based on the same L227 1973 data used in Case A. However, in order to simulate the interflow case, the nutrient addition method has to be modified. In reality, the nutrient was added to the surface of L227 but in this simulation, the nutrient is assumed to be brought in by inflow whose temperature is 2°C less than the lake surface temperature. For computational convenience, the frequency of nutrient addition is also changed; instead of weekly additions, we now assume a bi-weekly addition. The amount of nutrient added each time remains the same, i.e., 1.14 kg PO_4-P per addition. Table 6.2 lists the schedule of nutrient addition for the present simulation. The inflow temperature, obtained by subtracting 2°C from the lake surface temperature as simulated by the WDMIX model, is also shown in Table 6.2.

The lower temperature of the inflow, when compared with the lake surface temperature, causes the inflow to enter subsurface layers. The exact location has to be defined by the lake vertical temperature structure at the moment of inflow entrance. The objective of this simulation is to compare quantitatively the effect of the specification of FML depth upon phytoplankton dynamics.

6.4.3.2 Model Modification

Modifications to the three hydrothermal models have to be made in order to account for subsurface nutrient input. Presently, the inflow placement is handled in the following simple manner: the inflow is assumed to enter the water column centered at an elevation at which the

Table 6.2

Nutrient Addition Schedule and the Inflow Temperature For Nutrient Interflow Case

Date of Nutrient Addition	Inflow Temperature (°C)
148	13.5
162	12.0
176	17.5
204	20.0
218	21.5
232	20.0
246	18.0
260	10.0
274	10.5
288	6.0

density is equal to the inflow density and the zone of the inflow is assumed to be of a uniform 1.5 m thickness, which equals three 0.5 m thick elements that are currently used in all three hydrothermal models. That is, the computer program first determines the central element of inflow placement (j) by comparing the inflow temperature and the lake temperature profile on the date of each nutrient addition. Then, it computes the induced PO_4-P concentration increase in the three elements by:

$$\Delta PO_4\text{-}P = \frac{1.14 \text{ kg}}{\sum_{i=j-1}^{i=j+1} VOL(i)} \qquad (6.2)$$

where: ΔPO_4-P = the increase of PO_4-P concentration in element j-1, j, and j+1; VOL(i) = volume of element i.

6.4.3.3 Simulation Result, Comparison and Discussion

Since the nutrient is assumed to be brought in by inflow whose temperature is 2°C below the lake surface temperature, all three models predict inflow/nutrient to enter a region centered at a sub-surface layer. However, due to the difference in the FML specification of each model, the absolute location of the inflow/nutrient placement could vary with each hydrothermal model.

Figure 6.24 shows the three models' temperature simulation for the 204th day. The corresponding center of 22°C inflow zone in each model is indicated by the arrow. The depth of the center of the inflow zone is 1 m in the WDMIX model, 1.5 m in the SD1 model, and 2.5 m in the SD2 model. Shown in the three panels of Figure 6.25 are the time series plots of the FML with the zone of inflow, the solid circle representing the center of

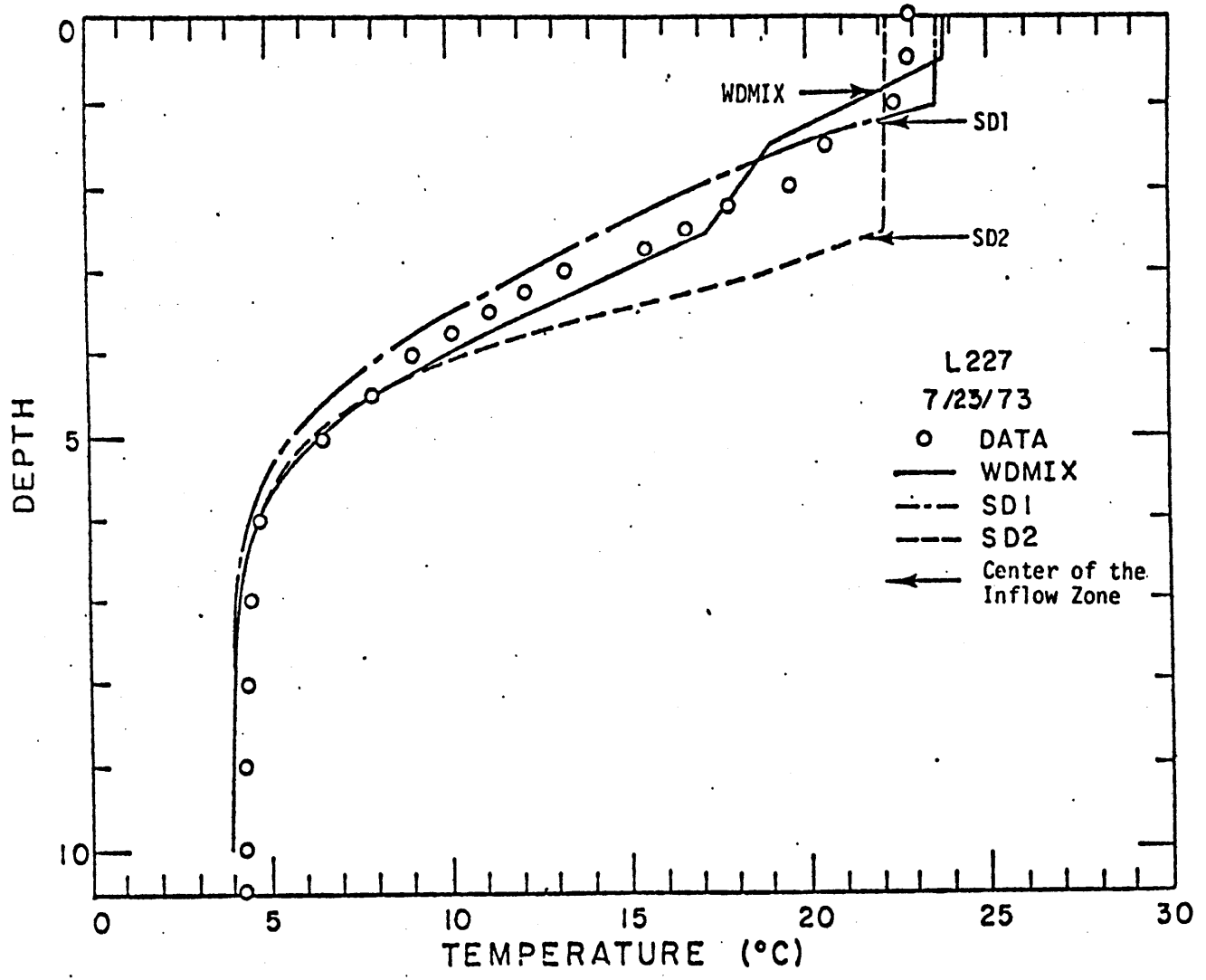

Figure 6.24: The Effect of FML Specification on the Definition of the Inflow Placement

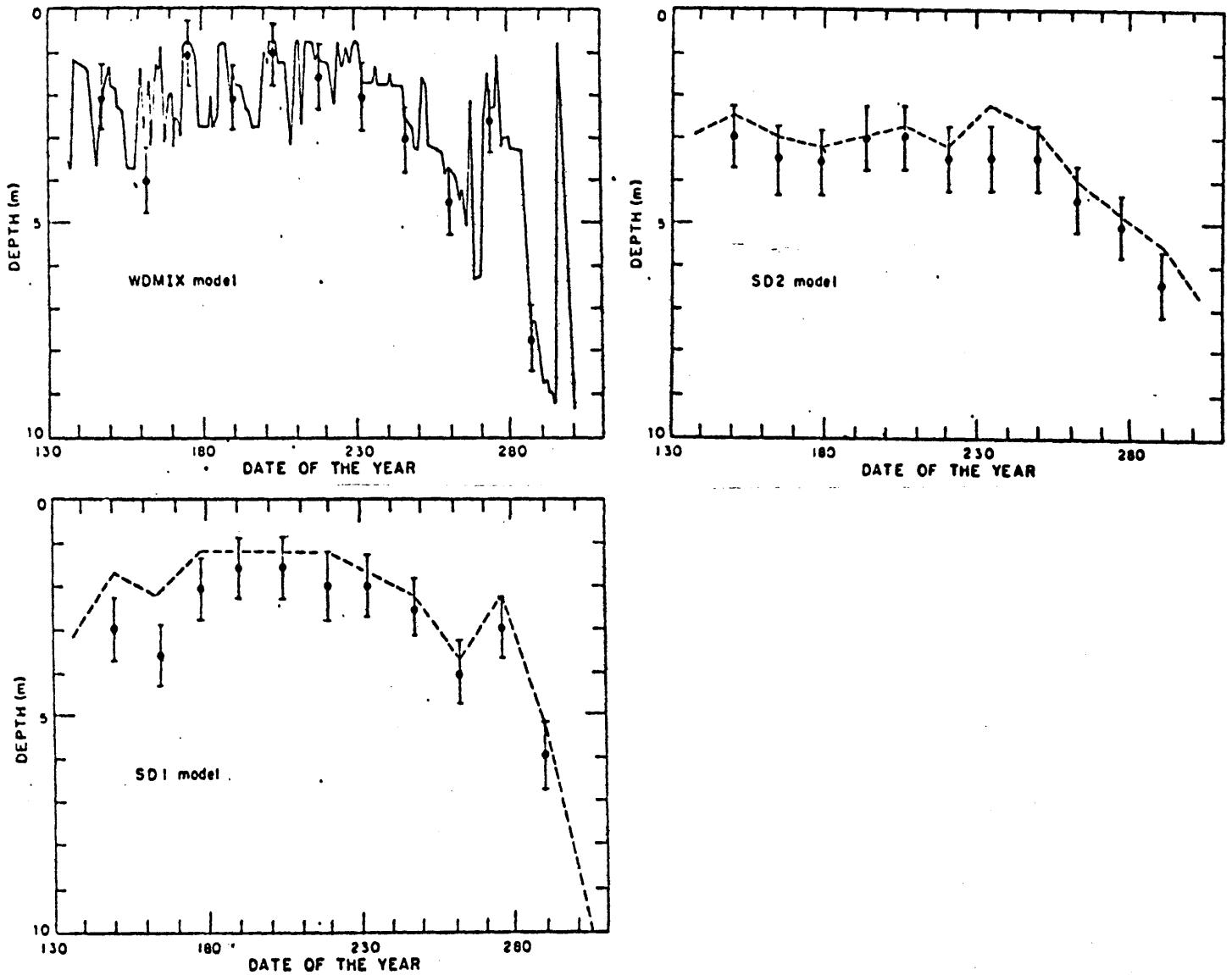

Figure 6.25: The FML Time Series Plot and the Zone of Inflow (a) WDMIX (b) SD1 Model (c) SD2 Model

inflow zone and the bar indicating the range of the inflow zone. The model simulations of phytoplankton concentration, represented as chlorophyll-a concentration, are shown in Figure 6.26 and Figure 6.27. These results are obtained by applying the same initial conditions and parameter values listed in Tables 5.8 and 5.11.

Figure 6.26 compares the simulated FML chlorophyll-a concentration by the three models. Although all three models predict a general pattern of dual chlorophyll-a peak, their predicted values of chlorophyll-a peak concentration and the time of peak occurrence are very different. According to the WDMIX model, the first chlorophyll-a peak occurs on the 204th day with a value of 90 μg/ℓ. In both the SD1 model and the SD2 model, chlorophyll-a reaches a plateau of 45 μg/ℓ, which is 50% less than the first peak value in the WDMIX model. Chlorophyll-a reaches the plateau 30 days earlier in the SD2 model than in the SD1 model (175th day in SD1 vs. 205th day in SD2). The second peak in the WDMIX model occurs on the 280th day and is 35 μg/ℓ, approximately 40% of its first peak. The SD1 model indicates the occurrence of the second peak on the 260th day with a value of 20 μg/ℓ which is also 40% of its first peak. The second peak in the SD2 model is predicted to occur on the 280th day and is, however, more pronounced than its first peak at 80 μg/ℓ.

The model simulation results for the 3 m depth are given in Figure 5.27. There is little difference in the three model results until after the 210th day. Using the WDMIX model simulation as the reference, the other two models either overpredict or underpredict by 50% from the 210th day and thereafter.

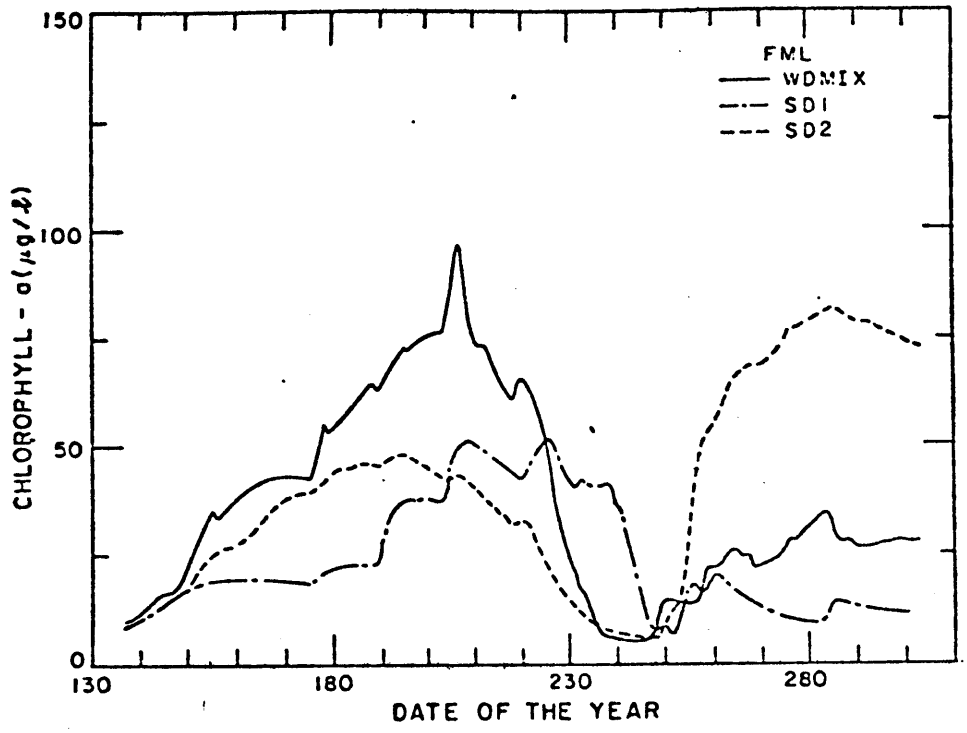

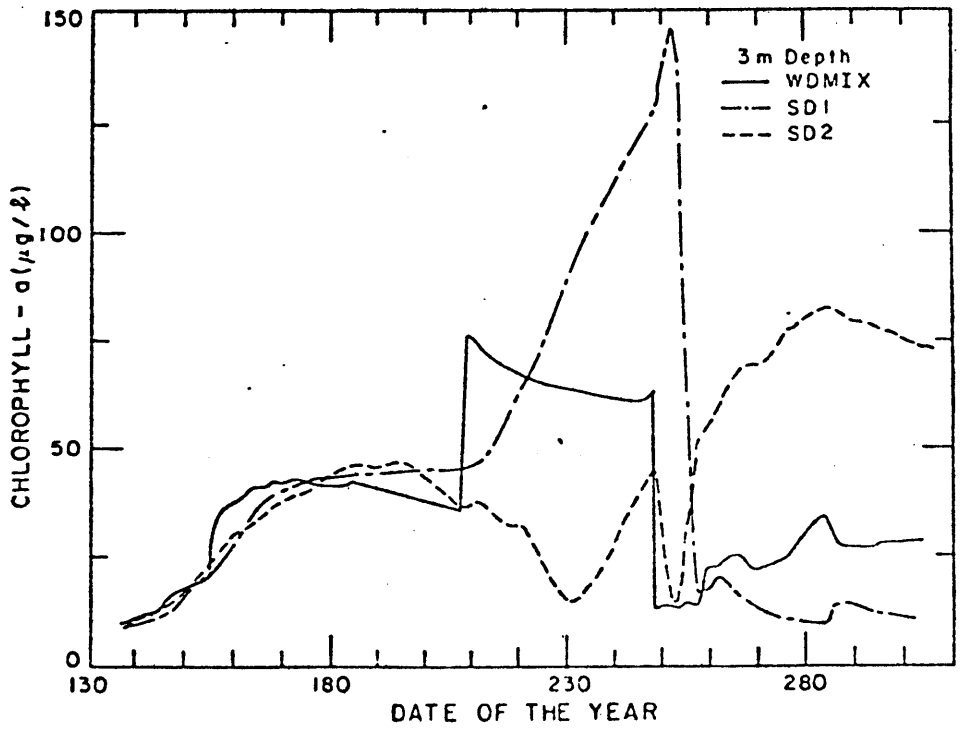

Figure 6.26: Comparison of the Models' Simulation on Phytoplankton Concentration in the FML

Figure 6.27: Comparison of the Models' Simulation on Phytoplankton Concentration at the 3 m Depth

As in Case A, a general analysis of the models' simulation on particulate-P serves as the starting point in explaining the difference in the models' simulation of chlorophyll-a. Figure 6.25, the time series plot of the FML and the zone of inflow, can serve as a convenient guideline for analyzing the PP variation.

In the FML:

Comparison of Figures 6.27 and 6.28 clearly shows the strong resemblance between the simulated chlorophyll-a and PP distribution for all three models. This resemblance suggests that all three models simulate the situation where the phytoplankton concentration in FML is mainly limited by the availability of phosphorus.

The WDMIX model, which gives the highest value of the first chlorophyll-a peak, also gives the highest value of PP during the corresponding period. The relative magnitude of the PP value during the period of the first chlorophyll-a peak may be explained by Figure 6.25. By the 210th day, the FML in the WDMIX model has received most of the nutrient added prior to this date, whereas the FML in the SD2 model has received approximately half of the added nutrient and the FML in the SD1 model has received less than one-third of the amount added. The compound effect of lesser nutrient entrained in the FML and the larger volume of FML causes the SD2 model to predict a PP concentration smaller than that of the WDMIX model. On the other hand, when the SD2 model is compared with the SD1 model, although a larger amount of phosphorus is entrained in the FML of the SD2 model, its larger volume (11×10^4 m^3 in SD2 vs. 5.6×10^3 m^3 in SD1) cause the simulated PP concentration of the SD1 and SD2 models

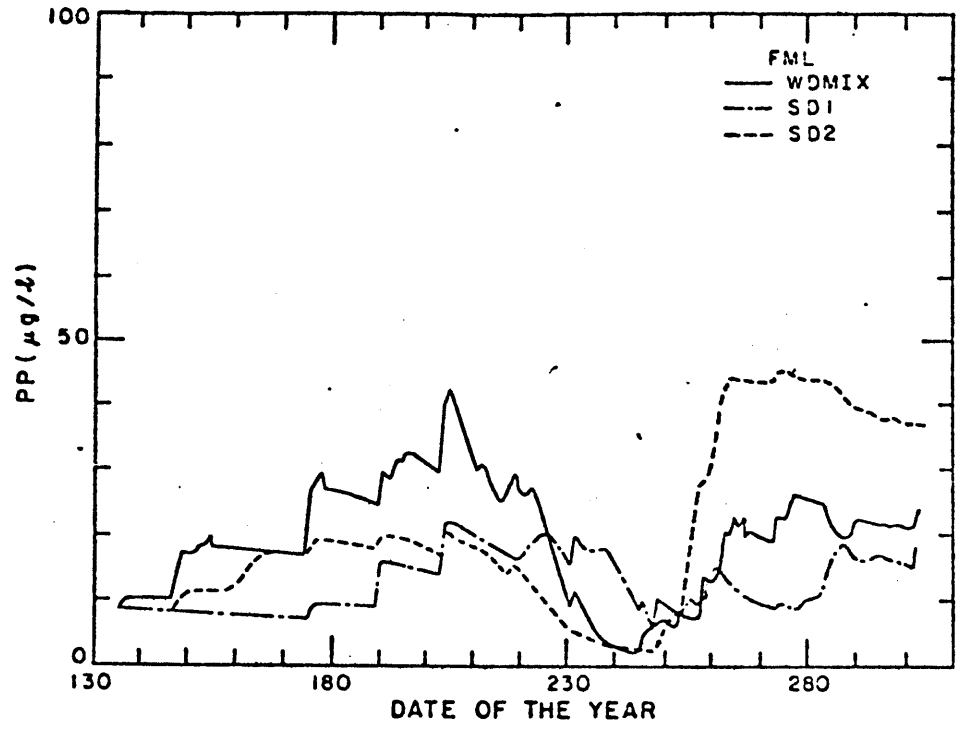

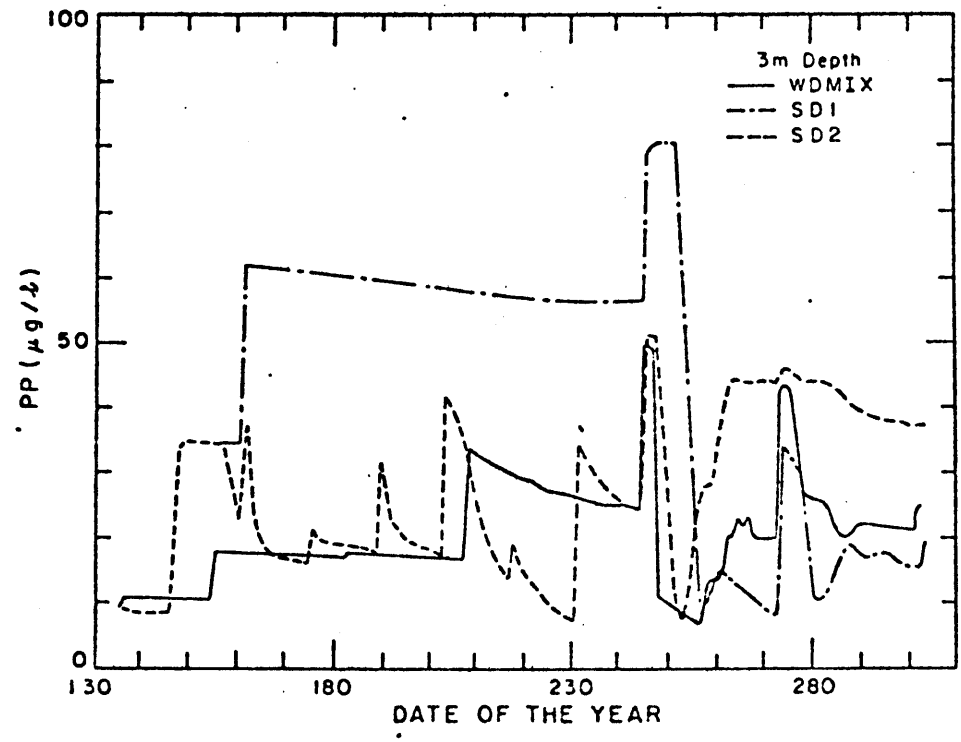

Figure 6.28: Comparison of the Models' Simulation on PP Concentration in the FML

Figure 6.29: Comparison of the Models' Simulation on PP Concentration at 3 m Depth

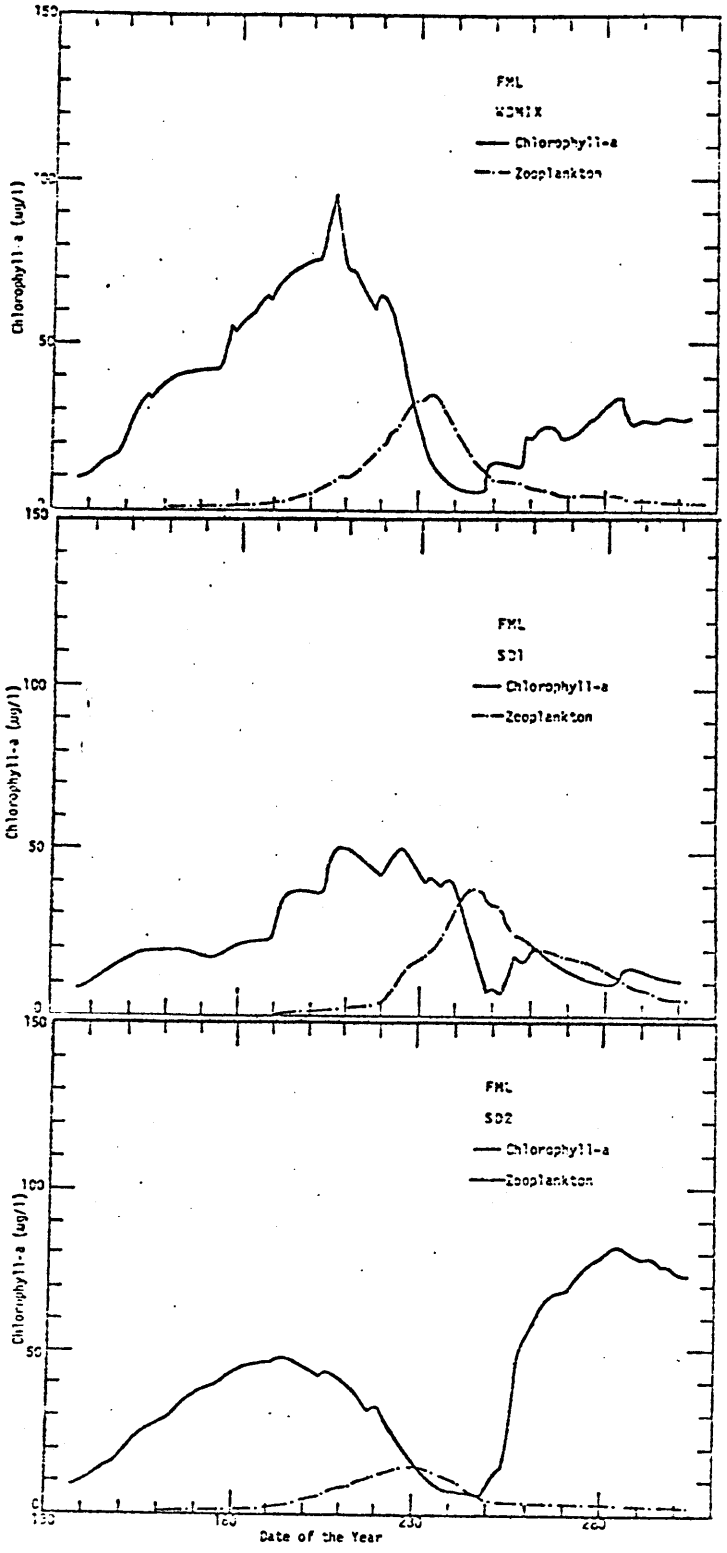

Figure 6.30: Model Simulation Result of Phytoplankton and Zooplankton in the FML

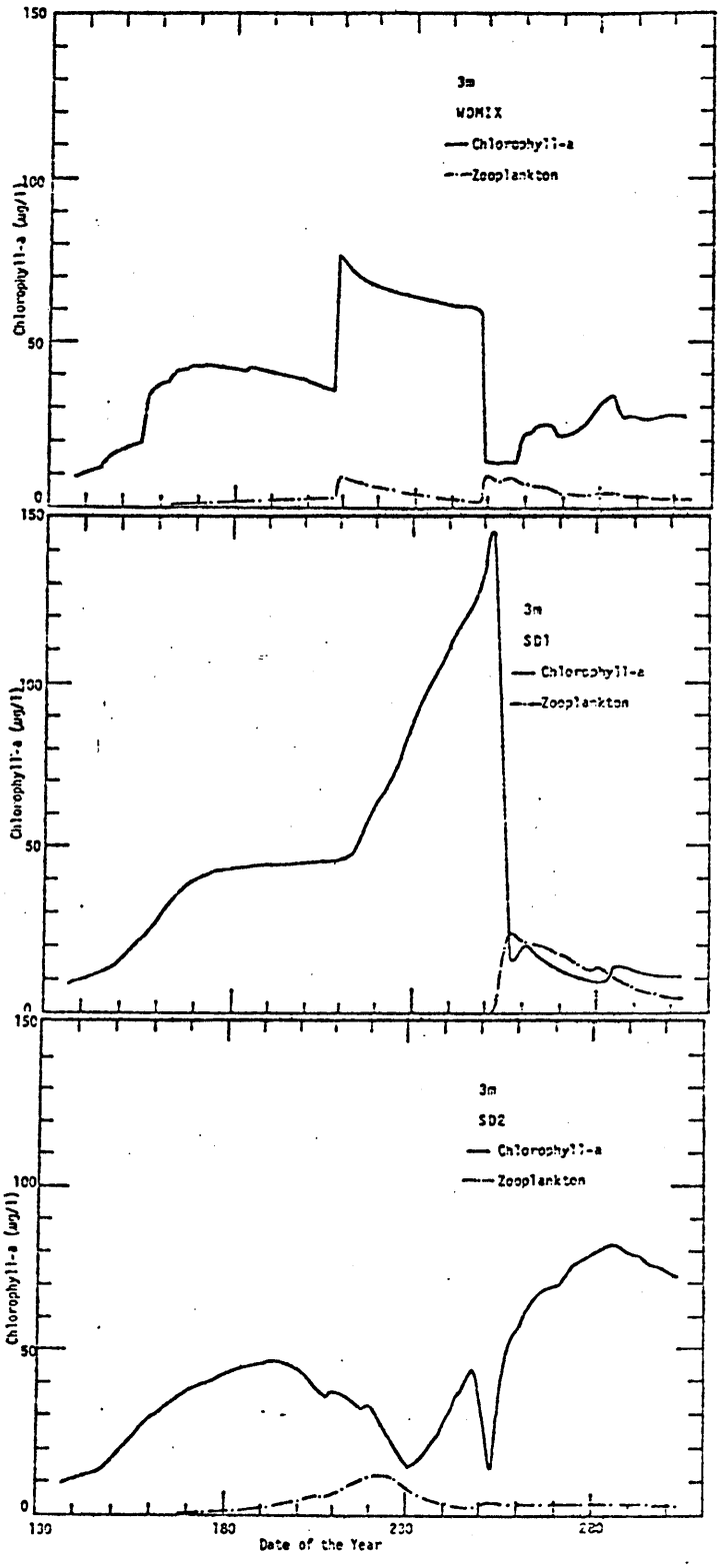

Figure 6.31: Model Simulation Result of Phytoplankton and Zooplankton at 3 m depth.

to be similar.

After the 260th day, the deepening of the FML causes an entrainment of phosphorus from the sub-surface layer. The amount of phosphorus entrained is largest in the SD1 model and is least in the WDMIX model. However, the observed apparent increase of phytoplankton concentration does not follow the trend of nutrient increase. This is because the apparent increase of phytoplankton in the period of second bloom is governed by the zooplankton/phytoplankton (zo/phr) ratio during the entrainment. The SD2 model, which has the lowest zoo/phy ratio predicts the highest second chlorophyll-a peak. Conversely, the SD1 mode, which has the highest zoo/phy (greater than 1) predicts the lowest second chlorophyll-a peak (Figure 6.30).

At the 3 m Depth:

After the 260th day, the 3 m depth becomes part of the FML in all three models. Since we have already discussed the differences of the models' prediction in the FML, we will limit our discussion here to the period before the 260th day.

The concentration of PP at 3 m depth is highest in the SD1 model's result since the amount of phosphorus added to the lake is the same in three models and the SD1 FML has the lowest PP concentration. A sharpt decline of the PP occurs in the period between the 250th to the 260th day during which the FML descends to 4 m depth. The PP concentration at 3 m depth decreases from 80 μg/ℓ to 10 μg/ℓ (Figure 6.29). Two reasons for this drastic reduction are:

(1) The volume of the elements at 3 m depth is 1.5×10^5 m^3 which

is only 1/10 of the volume of a 4 m deep FML, and the PP concentration in the FML is 5 μg/ℓ before the entrainment. It takes at least a 3 meter element of 50 μg/ℓ to increase the FML concentration to 10 μg/ℓ.

(2) The zooplankton concentration is higher than the phytoplankton concentration during this period (Figure 6.31), and this causes a significant portion of newly entrained PP to be stored in the zooplankton. Since PP does not include the zooplankton bound phosphorus, the grazing activity will appear as a reduction of PP. The presence of higher zooplankton concentration in the FML in the SD1 model continuously suppresses the increase of phytoplankton concentration caused by the subsequent nutrient addition.

Although the characteristics of PP concentration as predicted by the SD2 model and the WDMIX model are quite different, the magnitude of the PP concentration are much closer in these two models. Both the SD2 and WDMIX models give a maximum PP value of 40 μg/ℓ which is 50% of the SD1 model's prediction. It may be recalled from Figure 6.27, the chlorophyll-a concentration at the 3 m depth are similar in 3 models for a period up to the 210th day. One reason is that in the SD1 model, 3 m depth has always been the non-fully mixed region so that the growth of phytoplankton is limited by light. To test this hypothesis, we try a case of no phytoplankton growth dependence on light. The models' simulation result is shown in Figure 6.32. The difference in their predictions of PP concentration is now immediately reflected in their predictions of chlorophyll-a concentration.

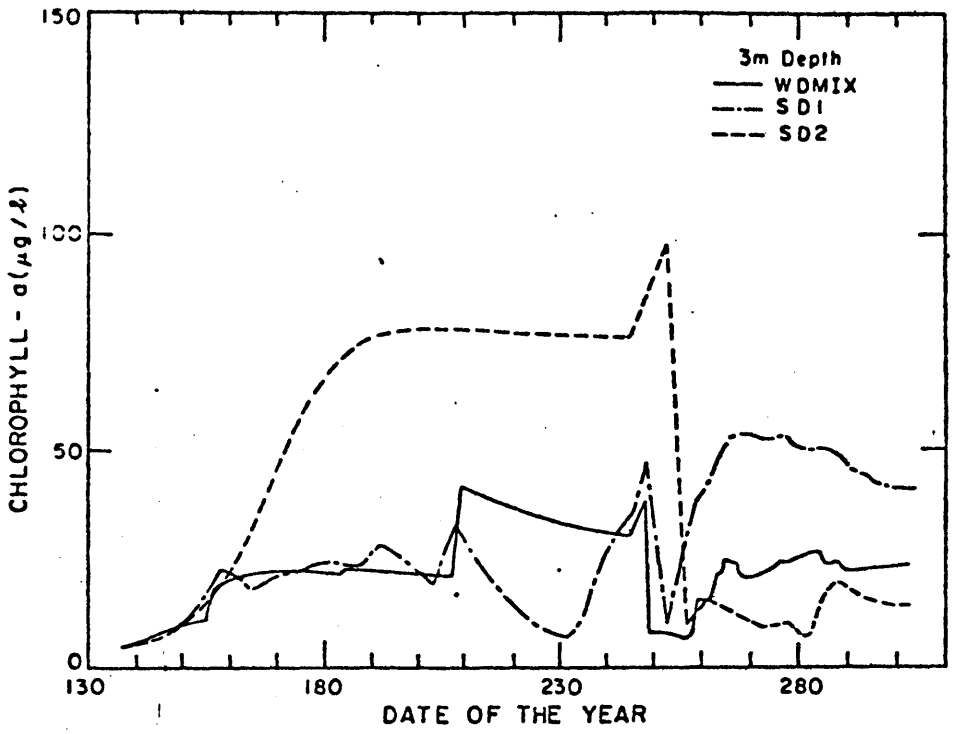

Figure 6.32: The Simulation Result of Phytoplankton and Zooplankton Concentration at 3 m Depth

(a) WDMIX Model

(b) SD1 Model

(c) SD2 Model

6.5 Conclusion

Significant differences in the prediction of phytoplankton concentration have been shown in section 6.4 among three phytoplankton models. The three models have the same biological model - Model II, the same model parameters, and the same nutrient inputs; the only difference is in their hydrothermal models: one with wind mixing model, the others use specified depth models - SD1 and SD2. The difference in the three models prediction on the phytoplankton concentration stems from the difference in three models hydrothermal structure.

Alternatively, we could have attempted to calibrate the biological parameters for three phytoplankton models from the same data set and thereby examined the difference in the calibrated biological parameters. Obviously, the alternative approach is a much more time consuming task than the simulation approach which we have taken. It is expected that if the multiple calibration effort had been followed the calibrated model biological parameters would have indicated high degree of variation.

A correct representation of the hydrothermal processes in the water body is the premise in analyzing or modeling any aquatic system. The important effect may often be associated with short term, extreme events such as a sudden deepening of the FML during the storm event, which may often escape field sampling. Therefore, even in analyzing field data in a retrospective manner, the unnecessary simplification in the hydrothermal model should be avoided.

Chapter 7

SUMMARY AND CONCLUSIONS

7.1 Summary

A deterministic model provides a convenient method for evaluating management strategies in the attempt to control lake eutrophication. Such a mathematical model should be capable of describing changes in the state of a lake as recorded by a time series of data as well as predicting future states caused by changes in hydrologic conditions or by control of nutrient inputs. A complete eutrophication model requires linkages between the biological transformation processes (at the trophic level of plankton) and the environmental (temperature and light) and transport processes (advection, mixing, diffusion and settling).

The formulation of a euthrophication model requires decisions on the complexity of the biological model (i.e., number of state variables) and model structure (i.e., transformations between biological state variables) as well as on the type of hydrothermal transport model to which the biological model is linked.

The thesis includes a summary of the state-of-the-art of hydrothermal modeling and biological modeling of the phosphorus cycle. It is demonstrated that a mixed-layer hydrothermal model, employing meteorological data, that calculates the vertical temperature profile and thickness of the upper fully mixed layer at a daily time step is capable of simulating the transport and diffusive process in a stratified lake with a minimum number of calibrated parameters. A methodology is developed for arriving at the degree of biological model complexity that

is consistent with the available field data. A procedure is outlined for extracting certain biological model rate constants from laboratory measurements of primary productivity. The extent to which the linked hydrothermal-biological model can be calibrated to seasonal phytoplankton variations is demonstrated for Lake 227. The ability of the calibrated model to simulate the eutrophication cycle in the following summer season is discussed. Finally, the importance of capturing the short term dynamics of the fully mixed layer in the modeling of phytoplankton variations is illustrated by simulation runs with the linked model for cases in which nutrient inputs occur at the lake surface or at intermediate depths. The studies described above are summarized in more detail in the following sections.

The model running cost is minimal because of the simple numerical scheme currently employed. The normal running cost of the developed model is about five dollars (with a compiled version of the Fortran IV source program) on an IBM 370 for a period of approximately six months for five model state variables (temperature, ortho-P, phytoplankton-P, phytoplankton biomass and zooplankton biomass).

7.1.1 The Hydrothermal Model

In a small- to medium-sized lake in the temperate region, the major vertical transport process is caused by the turbulence induced by wind and convective cooling. This transport process has been represented in earlier hydrothermal models by various combinations of vertical exchange coefficients and eddy diffusivities. Because of the descriptive

nature of these hydrothermal models, the number of calibrated parameters increases with the model complexity. The simpler models, such as the two-layer model, have fewer calibrated coefficients but lack the ability to represent realistically the hydrothermal characteristics that are important to modeling biological processes in the lakes. Some of these important characteristics are the movement of the FML and the exchange of mass energy fluxes with the lake boundaries (surface and water-air interface). While the multi-layer diffusion model gives a realistic hydrothermal structure for a stratified lake, it introduces a large number of calibrated parameters because of the difficulty in specifying, a priori, the temporal and spatial variation of the vertical eddy diffusivity. The necessity of calibrating parameters makes model application difficult and, most importantly, introduces an uncertainty that may undermine the reliability of the calibrated biological parameters and subsequently, the reliability of the model's predictions.

The current state of knowledge allows us to represent realistically the hydrothermal variability of a stratified water body with a minimum number of calibrated parameters. Therefore, improvement in the hydrothermal component of a lake eutrophication model can be achieved by introducing a recently developed mixed layer model that overcomes some of the difficulties inherent in specifying the vertical diffusivity by explicitly modeling the underlying wind driven entrainment mechanisms.

There are two major components in the MIT Wind Mixing Model:

(1) Heating

The basic equation for heat transport in the vertical direction is

obtained by considering heat and mass flow through an internal control volume taken as a horizontal layer of the water body. In the hypolimnion the molecular diffusivity of heat is used as the vertical diffusion coefficient. The equation is solved by using an explicit finite difference scheme.

(2) Mixing

(a) Convective cooling

After the solution of the heat transport equation, the model checks the density stability of the resulting profile. Whenever there is a density instability, the adjacent layers of the unstable region are mixed until the stability of the water column is restored.

(b) Wind mixing

The wind mixing algorithm takes into account the stirring effect induced by wind. The ratio of the change in potential energy due to entrainment, into the mixed layer, dE_p, to the change in turbulent kinetic energy due to wind shear, dE_k, during the time interval dt is given by

$$\frac{dE_p}{dE_k} = 0.057 \text{ Ri } \left(\frac{29.5 - \text{Ri}^{1/2}}{14.2 + \text{Ri}}\right) \tag{2.21}$$

with Ri, the Richardson number, defined as

$$\text{Ri} = \frac{\Delta\rho g h}{\rho_o u_*^2} \tag{2.21}$$

Following the computation for the internal heat transfer (see section 2.3.1) and the convective cooling (see section 2.3.2), the wind mixing rule given in equation 2.26 is applied to redistribute the heat

and adjust the temperature profile.

7.1.2 The Biological Model

In modeling the effect of external nutrient P input on phytoplankton growth, a knowledge of the P transfer among its various forms in the lake is necessary. There must be consistency in the definition and use of the various P compartments and the terms that refer to the biological processes describing the P movement. Unfortunately, many of the models reviewed in this thesis have not exhibited this consistency which is necessary in the formulation of a coherent structure. Once this structure has been achieved, the model should also be able to simulate the reported large variations in the ratio of phytoplankton-P to biomass.

A final requisite for a successful eutrophication model is ease of calibration and verification. This can be accomplished by choosing as model state variables those variables that can be directly measured in the field. The direct extrapolation of laboratory pure culture results to the field is not always justified. Therefore, the success of a eutrophication model does not depend on the incorporation of a large number of state variables but in its consistent and coherent application of the governing conservation of mass principle and its construction around experimentally verifiable quantities.

In the construction of a model that simulates phytoplankton biomass variations in a phosphorus limited environment, emphasis was placed on eliminating the existing confusion in terminology by rigorously defining biological reactions in terms of mass fluxes. Model construction started with the choice of P compartments. Based on our current understanding of

the P cycle and the conventional chemical methods of P measurement, the recommended number of P compartments is 2 to 4, with ortho-P and phytoplankton P as necessary state variables and soluble unreactive phosphorus (i.e., non-ortho-P dissolved phosphorus) and zooplankton-P as possible additional state variables. The inclusion of zooplankton-P as state variable is necessary when there is a significant increase of total P that cannot be accounted for by an external source of sediment return. When the total P budget shows a decrease or balance, the choice of incorporating zooplankton as a model state variable or employing a variable phytoplankton settling rate is left to the discretion of the modeler. The results of a simple mass balance on the soluble unreactive phosphorus can serve as the basis for the inclusion of SUP as a state variable. If the difference between the external supply of SUP and the variations of the in-lake SUP is significant compared to the phytoplankton bound P, then the inclusion of SUP as a state variable is necessary.

In the model, phytoplankton growth rate is defined as the net carbon increase rate and is expressed as a multiplicative effect of light, temperature and phosphorus cell quota (see section 5.3.2.1):

$$\mu = \mu_{max} \frac{I}{k_2+I} \cdot \exp\left(-2.3 \left|\frac{T-T_{opt}}{T_{div}}\right|\right) \cdot \frac{Q-q}{Q}$$

A hyperbolic function is used to express the light dependence and the variable cell quota formulation is used to describe the dependence on nutrient. The temperature dependence function is similar to that used by Jørgensen (1976, 1978).

7.1.3 Model Application to L227

The eutrophication model developed was applied to L227 which has received artificial fertilization of P and N since 1969. It was free from any other nutrient input and this level of control of nutrient budget provided an opportunity to evaluate the model's applicability. The period chosen for the simulation and calibration was May 15, 1973 to October 29, 1973.

The value of the parameter $\frac{AE}{QD}$ (see section 2.2.4), which compares the rate of vertical heat transport by diffusion to the rate of heat transport by advection, was approximately 13 with E equal to the molecular diffusivity. This suggests that the vertical temperature profile for L227 was sensitive to vertical mixing processes rather than to vertical advection due to inflow and outflows. Therefore, L227 was ideal for verifying the model formulation of vertical mixing.

The measured soluble unreactive phosphorus during the simulation period remained fairly constant ($\sim$10 µg/ℓ) while particulate phosphorus (PP) varied from 8 to 65 µg/ℓ. Since L227 was artificially fertilized with ortho-P, there was no significant input of SUP. It was therefore assumed that SUP represented a fraction of dissolved P that is not actively involved in the ortho-P $\rightarrow$ PP dynamics and therefore, contributed very little to the particulate phosphorus fluctuation. The number of P compartments was then further reduced to either 2 (ortho-P and phytoplankton-P) or 3 (with the inclusion of zooplankton-P). Both cases were considered in the 1973 simulation. The possibility of utilizing the parameter values obtained from the 1973 calibrations for prediction

of eutrophication in the following year was tested by doing a simulation for a similar period in 1974. Because 1974 solar radiation data were not complete, the simulation for 1974 extended only from May 21 to July 30.

7.2 Conclusions

The application of our model to simulate the temperature structure and phytoplankton response to the phosphorus enrichment of L227 has led to the following conclusions:

- The MIT wind mixing model is able to simulate satisfactorily lake temperature profiles from meteorological data. The use of the model is relatively easy since it contains no calibrated parameter other than the wind speed reduction factor to account for the sheltering effect of trees near the lake.

- The movement of the fully mixed layer is not, as traditionally described, a simple gradual response to the annual solar cycle. Instead, it respons to a series of alternating heating, cooling and mixing cycles in a characteristic time step of a day. L227, a strongly stratified and well-protected small lake, which should be less sensitive to the mixing effect of the wind, still shows variations of the fully mixed layer at intervals of a day.

- The variation of the ratio of two phytoplankton measurements, particulate P and chlorophyll-a, suggests the need of capturing the variable P cell quota by formulating the phytoplankton growth dependence on nutrient in two sequential steps -- the uptake of ortho-P and the

direct dependence of growth rate on the P cell quota.

- The computation of the total-P budget indicated that L227 effectively retained the added phosphorus in the fully mixed layer until the peak of the phytoplankton concentration. After the phytoplankton peak, the added phosphorus was lost at a rate that could be expressed as a phytoplankton settling rate of between 0.07 m/day to 0.45 m/day. A 2-P compartment model (Model I) was used to simulate successfully the observed PP and chlorophyll-a concentrations up to the occurrence of the phytoplankton peak; however, in order to simulate the decline of the peak, a variable settling velocity (as noted above) had to be used. Two possible explanations of the time variable settling velocity were considered: one considers that change caused by phytoplankton species variation and the change caused by phytoplankton nutrient status (i.e., cell quota) variation. Neither of the two would allow a successful prediction of the change in the settling velocity as suggested by the field measurement of particulate-P. Therefore, the alternative of including additional model state variable -- zooplankton -- was considered (Model II).

- The inclusion of zooplankton grazing of phytoplankton followed by the excretion of ortho-P and subsequent re-assimilation of the excreted ortho-P by phytoplankton, explained the rapid decline of the phytoplankton biomass in a two week period and the increase of phytoplankton P cell quota during the peak crash period. However, the penalty is that with an additional variable -- zooplankton -- Model II introduced 6 additional parameters. The available data do not allow a

unique determination of these 6 parameters by calibration.

The field measurement of the biological variables are best described by Model II, which is the phytoplankton model with the inclusion of zooplankton as a state variable. This suggests that zooplankton grazing is an important factor in controlling the phytoplankton population in a natural aquatic environment. However, the correct modeling of zooplankton population dynamics is an extremely difficult task. Therefore, in the model application for management purpose, at the present time, it is perhaps better to first model the phytoplankton population in the absence of zooplankton grazing. The result so simulated will give a margin of safety since it will always predict the upper limit of the phytoplankton population. The effect of zooplankton grazing upon phytoplankton may be studied with sensitivity analysis of a model which includes zooplankton as state variable (such as Model II in this research). Further refinement of the zooplankton model depends on the desired safety margin.

- Comparison of the results of Model II (variable P cell quota) and Model II' (constant cell quota) indicates that it is impossible to find constant values of μ_m, k_s and PP/chl-a (under the assumption of constant cell quota) for Model II that can produce identical results as Model II for all ortho-P, PP and chlorophyll-a concentrations simultaneously.

- Primary production data were also used for parameter estimation and evaluation of the phytoplankton growth function. The light function and the half saturation constant so obtained are considered reasonable.

The direct evaluation of the temperature and nutrient function is not possible due to the absence of information on chlorophyll-a and P/chl-a field values. The values of chlorophyll-a and PP from the model simulation were used instead. For the pre-peak period, the regression result indicated a significant correlation between the specific primary productivity and the phosphorus cell quota. The regression result, however, was unable to identify a significant correlation with temperature. The insignificant correlation between temperature and the primary productivity may be due to the fact that there is little temperature difference in the temperature of the 7 data sets (16°C - 21°C). Zooplankton might have been present in a more abundant number in the latter period and the grazing/excretion activity of zooplankton will cause phytoplankton standing crops to take up the ortho-P continuously excreted by zooplankton. The increase of P cell quota due to this uptake of the zooplankton excreted ortho-P might be significant, as reflected in the excessive ortho-P concentration simulated by Model II' which uses constant P cell quota formulation (see section 5.3.3). This significant change in P cell quota might induce a longer and more frequent transition period where no good description is available for biomass variation, and the photosynthesis may not be related to the P cell quota by the hyperbolid form.

- Although nutrient additions were identical for both the years 1973 and 1974, the observed chlorophyll-a and PP concentrations were very different. Both were lost at much higher rates in 1974 than those observed in 1973 and the peak values of the PP to chlorophyll-a ratios

are 25% and 60% for 1973 and 1974, respectively. At the time of the chlorophyll-a peaks, the ratio PP/chl-a is unity in 1974, this is approximately 2.5 times the corresponding value in 1973. These differences cannot be explained by differences in the hydrothermal structure of the lake. A combination of a higher initial zooplankton concentration and a 30% increase in the minimum phosphorus cell quota is required to simulate the 1974 observation. The modifications needed to be made in the biological model parameters were calibrated from 1973 analysis, for 1974 simulation might be partially explained by the observation that zooplankton concentration was higher in 1974; however, why the phytoplankton responded differently to the nutrient condition in 1974 remains unresolved since there was no apparent species variation between the two years.

- Movement of the fully mixed layer, primarily dominated by wind mixing and convective cooling effects, is the major vertical transport process in a horizontally-stratified small- to medium-sized lake. Since the basis of a lake eutrophication model is the ability to simulate the distribution of the limiting nutrient, the validity of a dynamic lake eutrophication model is often impaired by errors resulting from: (a) lack of detailed information on lake temperature distribution, (b) the difficulty of identifying the FML from a given temperature profile and (c) the unknown FML dynamics which are very sensitive to the meteorological conditions. Two simulation cases presented in Chapter 6 which consider the cases of surface nutrient input and nutrient interflow, demonstrate the importance of correctly modeling the lake vertical

temperature profile and the FML dynamics.

In order to demonstrate the importance of the linkage between the hydrothermal and biological components of a eutrophication model we could have attempted to calibrate the biological parameters for phytoplankton models that have different hydrothermal structures, from the same data set and thereby examined the difference in the calibrated biological parameters. Obviously, this approach is a much more time consuming task than the simulation approach taken in Chapter 6. In the simulation approach we have retained the calibrated biological parameters of Model II (in which the biological component is linked to the daily mixed layer hydrothermal model). The same biological component was then linked to two other hydrothermal models in which the mixed layer thickness was specified, from field temperature measurements, on a bi-weekly basis. These models employed two different definitions of the mixed layer thickness. The importance of the linkage was demonstrated by comparing the predictions of algae response for the three linked models.

7.3 Recommendations for Future Research

A meaningful quantitative evaluation of phytoplankton biomass is the fundamental requirement in the modelling of water quality of any aquatic system. Among the various phytoplankton biomass measured, the total organic dry weight is a better indicator of the phytoplankton biomass in an aquatic system with composite species (see section 4.2). The variation of the phytoplankton organic dry weight may be linearly related to the variation of the phytoplankton organic carbon. The

model developed in this thesis was calibrated using field chlorophyll-a measurement due to the lack of measurement of phytoplankton organic carbon. Although chlorophyll-a is the most common field measurement of phytoplankton, questions have been raised concerning the reliability of using chlorophyll-a as a measure of the total phytoplankton biomass. For example, diurnal variations of chlorophyll-a have been observed; the significant change of the chlorophyll-a to phytoplankton carbon ratio under nitrogen limited conditions has been reported. Therefore, attention should be given in developing a method which can be conveniently applied to measure the phytoplankton organic carbon in natural aquatic systems, whose variation also reflects a parallel variation of the phytoplankton dry weight.

After the choice of a meaningful phytoplankton biomass measurement, the next step is to design a sampling scheme which captures the dynamics of the whole lake system. In this study, the modeling of the hydrothermal characteristics is based on our understanding of the physical processes which govern the heat and momentum transport in lakes. The application of the wind mixing model showed a large amplitude short term variation of the fully mixed layer occurring a daily time scales. The failure to capture this short term variation by bi-weekly temperature measurement and the importance of capturing this variation have been addressed previously. The short term fully mixed layer variation is only supported indirectly by measurement taken at other sites by other researchers. However, a proper verification of the model needs measurement which allows a direct comparison of the daily model output. The hydrothermal model may be regarded as a case in which the theory

surpasses field measurements. On the other hand, the biological model development is based on the available field data; that is, the biological modeling of this research is limited by the availability of field data and does not produce new facts or dynamics other than that suggested by field measurement. The following recommendations on a sampling scheme design for the biological variables is based on studies by other researchers. Phytoplankton in lakes have often been observed to occur in lakes in patches whose sizes have been observed to range from centimeters to kilometers. Several explanations have been suggested but the conclusive field test of these hypotheses is still missing. The one-dimensional model output should be compared with the averaged concentration of the horizontal plane; phytoplankton spatial heterogeneity casts doubt on obtaining a whole lake representative value from vertical measurements at one station. The necessary spatial and temporal intervals of sampling depend on our understanding of the factors which cause the variations. Once the factors are identified, a model which synthesizes this information into formulation and quantitative representation, can be used to set up the framework of the sampling scheme with properly designed sensitivity runs.

Additionally, since the basis of model formulation is laboratory studies, attention should be given to the study of processes that are relevant to the modeling purpose. For example, the nutrient effect on phytoplankton growth has often been predominantly studied with chemostate experiments that measure cell division rate. If the phytoplankton organic carbon is considered as the most meaningful biomass indicator,

then emphasis should be on studying the changes of phytoplankton organic carbon as a function of environmental factors and nutrient conditions. Moreover, steady state studies contain no kinetic information, the application of a relationship derived from chemostate studies to a dynamic condition is open to question.

In addition to the field measurement of phytoplankton biomass, primary productivity data may be used for independent estimation of biological rates and subsequent evaluation of the model formulation. The importance of rate measurements as part of the model calibration and verification warrant the development of an accurate measurement of the primary productivity. Although at least four carbon fluxes have been identified (i.e., photosynthesis, respiration, photorespiration and excretion) between a phytoplankton cell and its environment, the classic primary productivity measurement is built on the concept of two carbon fluxes -- photosynthesis and respiration, with emphasis on photosynthesis. From the viewpoint of modeling phytoplankton biomass variations, the interest is on the net carbon increase rate. The effect of factors, other than light, on photosynthetic rates are relatively unknown. Therefore, it is difficult to relate experimental results to the four identified carbon fluxes, and consequently, to apply the functional relationship derived from these experimental results. The simultaneous measurement of carbon fluxes, phytoplankton cell nutrient content, and temperature will allow an evaluation of the model formulation.

There is an additional time scale to be added to the present model -- the diurnal variation. Diurnal variations are important in both

physical and biological systems. Light, which is one of the major facotrs in controlling the carbon production of phytoplankton, undergoes major variations at the diurnal time scale. The diurnal variation of the light intensity causes loss of heat at night inducing the convective cooling at night. Therefore, a study of the response of both physical and biological systems to this major variation of their forcing function is important.

REFERENCES

Al Kholy, 1956. On the assimilation of phosphorus in Chlorella pyrenoidosa. Physiologia Pl., 9: 135-143.

Atkins, W.R.G., 1923. The phosphate content of fresh and salt water in its relationship to the growth of the algal plankton. J. Mar. Biol. Assoc. U.K., 13:119-150.

Bachman, R.W. and C.R. Goldman, 1975. Hypolimnetic heating in Castle Lake, California. Limnol. Oceanogr. Vol. 10, No. 2, April, 1965.

Becker, J.D., G. Döhler and K. Egle, 1968. Die Wirkung Monochromatischen Lichts ouft die extrazelluläre Glykoläure-Ausscheidung bei der Photosynthese von Chlorella Z. Pflphysiol. 58:212-221.

Bloss, S. and D.R.F. Harleman, 1979. Effect of wind mixing on the thermocline formation in lakes and reservoirs. Ralph M. Parsons Laboratory Technical Report No. 249, Massachusetts Institute of Technology, Nov. 1979.

Birge, E.A., 1910. On the evidence for temperature seiches. Trans. Wis. Acad. Sci. Arts. Lect. 16:1005-1016.

Bowers, J.A., 1979. Zooplankton grazing in simulation models: the role of vertical migration. In D. Scatia and A. Robertson (eds.) Perspectives on Lake Ecosystem Modeling, Ann Arbor Science, p. 53-74.

Brock, T.D., 1970. Biology of microorganisms. Prentice-Hall.

Brönsted, J.N. and C. Wesenberg-Lund, 1911. Chemisch-physikalische Untersuchungen der dänkscher Gerwässer nebst Bermerkungen über ihre Bedentung für unsere Auffassung der Temporalivariationen. Int. Rev. Hydrobiol., 4:251-290, 437-492.

Brylinksy, M. and Mann, K.H., 1973. An analysis of factors governing productivity in lakes and reservoirs. Limnol. Oceanogr. 18:1-15.

Buchan, A., 1871. Remarks on the deep-water temperature of Lochs Lomond, Katrine and Tay. Proc. Roy. Soc. Edinb., 7:791-795.

Burmaster, D.E., 1978. Steady and unsteady continuous culture of Monochrysis lutheri under phosphorus limitation. Ph.D. thesis, Massachusetts Institute of Technology.

Burnison, B.K., 1980. Personal communication.

Canter, H.M. and J.W.C. Lund. New phytologist, 47, 238, (1943).

Caperon, J., 1968. Population growth response of Isochrysie galbana to nitrate variation at limiting concentrations. Ecol. 49:866-872.

Caperon, J. and J. Meyer, 1972. Nitrogen-limited growth of marine phytophlankton. I. Changes in population characteristics with steady-state growth. Deep-Sea Res. 19:601-618.

Chamberlain, W.M., 1968. A preliminary investigation of the nature and importance of soluble organic phosphorus in the phosphorus cycle of lakes. Ph.D. thesis, Univ. of Toronto, Canada.

Chamberlain, W.M. and J. Shapiro, 1969. On the biological significance of phosphate analysis; comparison of standard and new methods with a bioassay. Limnol. Oceanogr., 14:921-927.

Chapil, R.G., 1973. Canada Centre for Inland Waters. Annual Radiation Summary.

Chen, C.W. and G.T. Orlob, 1972. Ecologic simulation for aquatic environments. Final report to OWRR by Water Resoruces Engineers, Inc., Dec. 1972. OWRR C-2044, WRE 1-0500.

Chen, C.T. and F.J. Millers, 1977. The use and misuse of pure water PVT properties for lake waters. Nature, 266:707-708.

Confer, J.L., 1969. The interrelationship among plankton, attached algae, and the phosphorus cycle in artificial open systems. Ph.D. thesis, Univ. of Toronto, Canada.

Dake, J.M.K. and D.R.F. Harleman, 1966. An analytical and experimental investigation of thermal stratification in lakes and ponds. Technical report no. 99, Ralph M. Parsons Laboratory, Massachusetts Institute of Technology, Cambridge, Mass.

De Saussure, H.B., 1779. Voyages dans les Alpes, précédés d'un essai sur l'historie naturelle des environs de Genève. Tome 1, chap. 1 and 2. Neuchacel, S. Fauche (quarto; octavo reprint, 1803).

Deniges, G., 1921.

Détermination quantitative des plus faibles quantitiés de phosphate dans les produits biologiques par la méthode cérulemolybique. Compts. Rend. Soc. Biol. (Paris) 84(17): 75-877.

DiToro, D.M., D.J. O'Connor, R.V. Thomann, 1971. A dynamic model of phytoplankton populations in the Sacremento - San Joaquin Delta. Advan. in Chem. Series. 106, 131-180.

DiToro, D.M. and W.F. Matystik Jr., 1977. Mathematical models of water quality in large lakes, Part 1: Lake Huron and Saginaw Bay. Final report to Environmental Protection Agency. Manhattan College, Environmental Engineering and Science Program, Bronx, N.Y. 10471.

DiToro, D.M. and G. Van Straten, 1979. Uncertainty in the parameters and predictions of phytoplankton models. WP-79-027 IIASA, Laxenburg, Austria.

DiToro, D.M., 1980. Applicability of cellular equilibrium and monod theory to phytoplankton growth kinetics. Ecological Modelling, 8(1980), 201-218.

Droop, M.R., 1968. Vitamin B12 and marine ecology. IV. The kinetics of uptake, growth, and inhibition in Monochrysis lutheri. J. Mar. Biol. Assn. U,K., 48:689-733.

Droop, M.R., 1970. Vitamin B12 and marine ecology. V. Continuous culture as an approach to nutritional kinetics. Helgolander Wiss-Meeresunters, 20:629-636.

Droop, M.R., 1974. The nutrient status of algal cells in continuous culture. J. Mar. Biol. Assoc. U.K., 54:825-855.

Eagleson, P.S., 1976. Dynamic hydrology. McGraw-Hill.

Edmonson, W.T., 1972. The present condition of Lake Washington. Verh. Internat. Verein. Limnol., 18:284-291.

Environmental Protection Agency, 1971. Guidelines - water quality management planning. Water Quality Office, Washington, D.C., January.

Eppley, R.W., 1972. Temperature and phytoplankton growth in the sea. Fishery Bulletin, Vol. 70, No. 4.

Eppley, R.W., R.W. Holmes, and J.D.H. Strickland, 1967. Sinking rates of marine phytoplankton measured with a fluorometer. J. Exp. Mar. Biol. Ecol., 1:191-208.

Eppley, R.W. and E.H. Renger, 1974. Nitrogen assimilation of an oceanic diatom in nigrogen limited continuous culture.

J. Phycol. 10:15-23.

Fee, E.J., 1969. A numerical model for the estimation of photosynthetic production, integrated over time and depth in natural waters. Limnol. Oceanogr., 14(6)a:906-911.

Fee, E.J., J.A. Shearer and D.R. DeClercq, 1979. In vivo chlorophyll profiles from lakes in the experimental lakes area, northwestern Ontario. Technical Report No. 703. Fisheries and Marine Service, Canada.

Fee, E.J., 1978. Studies of hypolimnion chlorophyll peaks in the experimental lakes area, northwestern Ontario. Can. Fish. Mar. Serv., Tech. Rept. 752:iv.

Findlay, D.L. and H.J. Kling, 1975. Seasonal successions of phytoplankton in seven lake basins in the experimental lakes area, northwestern Ontario following artificial eutrophication. Can. Fish. Mar. Serv. Tech. Rept. 513.

Findlay, D.L., 1978. Seasonal successions of phytoplankton in seven lake basins in the experimental lakes area, northwestern Ontario, following artificial eutrophication. Data from 1974 to 1976. Can. Fish. Mar. Serv. Manuscript Report No. 1466.

Fischer, H.B., E.J. List, R.C.Y. Koh, J. Imberger, N.H. Brooks, 1979. Mixing in inland and coastal waters. Academic Press.

Fogg, G.E., 1958. Extracellular products of phytoplankton and the estimation of primary productivity. Rapp. P.-V.-Reun., Gons. Int. Explor. Mer., 144:56-60.

Fogg, G.E., C. Nalewajko and W.D. Watt, 1965. Extracellular products of phytoplankton photosynthesis. Proc. R. Soc. Lond. Ser. B 162: 517-534.

Fogg, G.E., 1973. Phosphorus in primary aquatic plants. Water Research, Pergamon Press. Vol. 7, pp. 77-91.

Fogg, G.E., 1977. Comment: Excretion of organic matter by phytoplankton. Limnol. Oceanogr., 22(3):576-577.

Ford, D.E., 1976. Water temperature dynamics of dimictic lakes: Analysis and prediction using integral energy concepts. Ph.D. thesis, Univ. of Minnesota, Minneapolis, Minn.

Ford, D.E. and H. Stetan, 1980. Stratification variability in three morphometrically different lakes under identical meteorological forcing. Water Resources Bulletin, Vol. 16, No. 2, April, 1980.

Franzen, W.A.W., 1932. Ein Versuch der physiologisches Erforschung der Productions - fahigkeit des Moskauflosswassers. Microbiologiya 1:122-130.

Fuhs, G.W., 1969. Phosphorus content and rate of growth in the diatoms Cyclocella nana and Thalassiosira fluviatilis. J. Phycol 5:312-321.

Gardiner, A.C., 1937. Phosphate production by planktonic animals. J. Const. Int. Explor. Mer., 12:144-146.

Goldman, J.C. and J.H. Ryther, 1976. Temperature-influenced species competition in nass cultures of marine phytoplankton. Biotechnology and Bioengineering, Vol. XVIII, pp. 1125-1144.

Goldman, J.C., 1977. Steady-state growth of phytoplankton in continuous culture: comparison of internal and external nutrient equations. J. Phycol., 13:251-258.

Golterman, H.L., 1960. Studies on the cycle of elements in freshwater. Acta Bot. Neerl., 9:1-58.

Golterman, H.L., 1973. Vertical movement of phosphate in freshwater, In Environmental phosphorus handbook, edited by E.J. Griffith et al., John Wiley and Sons, pp. 507-538.

Golterman, H.L., 1975. Physiological limnology. Elsevier.

Haan, C.T., 1977. Statistical methods in hydrology. Iowa State Univ.

Healey, F.P., 1979. Short-term responses of nutrient-deficient algae to nutrient addition. J. Phycol. 15:289-299.

Harleman, D.R.F., 1980. Hydrothermal analysis of lakes and reservoirs. First Hunter Rouse hydraulic engineering lecture. Proceedings of ASCE Hydraulics Division Conference on Computer and Physical Modeling. August 6, 1980, Chicago, Illinois.

Harris, G.P. and B.B. Piccinin, 1977. Photosynthesis by natural phytoplankton populations. Arch. Hydrobiol. 80(4):405-457.

Hatch, M.D., C.B. Osmond and R.O. Slatyer, eds., 1971. Photosynthesis and photorespiration. Wiley-Interscience.

Hebert, D., R. Elsworth and R.C. Telling, 1956. The cominuous culture of bacteria: A theoretical and experimental study. J. Gen. Microbiol. 14:601-622.

Hellebust, J.A., 1965. Excretion of some organic compounds by marine phytoplankton. Limnol. Oceanogr. 10:192-206.

Hellebust, J.A., 1974. Extracellular products, In W.D. Stewart (ed.) Algal physiology and biochemistry. Univ. Calif.

Hobbie, J.E., R.J. Barsdate, V. Alexander and D.W. Stanley, 1972. Carbon flux through a tundra pond ecosystem at Barrow, Alaska. J.S. Tundra Biome Report. 72-1.

Hoffman, C., 1956. Untersuchangen über die Remineralisation des Phosphors im Plankton. Kieler Meeresforsch., Bd 12, 25-36.

Holling, C.S., 1966. The functional response of invertebrate predators to prey density. Mem. Ent. Soc. Can. 48:1-85.

Hooper, F.F., 1973. Origin and fate of organic phosphorus compounds in aquatic systems, In Environmental phosphorus handbook, edited by E.J. Griffith et al., John Wiley and Sons, pp. 179-201.

Huber, W.C. and D.R.F. Harleman, 1968. Laboratory and analytical studies of thermal stratification of reservoirs. MIT Hydrodynamics Laboratory Technical Report No. 112. October 1968.

Hoogenhout, H., and J. Amesz, 1965. Growth rates of photosynthetic microorganisms in laboratory cultures. Arch. Mikrobiol. 50:10-24.

Hutchinson, G.E., 1969. Eutrophication, past and present, In Eutrophication: causes, consequences, correctives, Proceedings of a symposium, National Academy of Science.

Hutchinson, G.E., 1975. A treatise on limnology. Vol. 1, Part 1: Geography and physics of lakes. 2nd edition, John Wiley and Sons.

Ignatiades, L., and G.E. Fogg, 1973. Studies on the factors affecting the release of organic matter by Skeletonema costatum (Greville) Cleve in culture. J. Mar. Biol. Assoc. U.K. 53:937-956.

Imboden, D.M. and S. Emerson, 1978. Natural radon and phosphorus as a limnological tracer: horizontal and vertical eddy diffusion in Greifensee. Limnol. Oceanogr. 23:77-90.

Imboden, D.M. and R. Gächter, 1978. A dynamic lake model for trophic state prediction. Ecological Modelling 4 (1978) 77-98.

Imboden, D.M. and R. Gätcher, 1979. The impact of physical processes on the trophic state of a lake, In, O. Ravera (ed.), Biological aspects of freshwater pollution, Pergamon Press, Oxford, pp. 93-110.

Ivlere, V.S., 1945. The biological productivity of waters. Uspekhi Sorrem. Biol. 19:98-120.

Jassaby, A., 1973. The ecology of bacteria in the hypolimnion of Casele Lake, California. Ph.D. thesis, Univ. Calif., Davis. 186pp.

Jensen, J.L.W.V., 1905. Om Konvexe Funktioner og Ulighedermellem Middelvaerdier. Nyt. Tidsskr. Math. 16B:49-69.

Johnson, W.E. and J.R. Vallentyne, 1971. Rationale, background and development of experimental lake studies in northwestern Ontario. J. Fish. Res. Bd., Canada 28:123-128.

Jørgensen, S.E., 1976. A eutrophication model for a lake. Ecol. modelling. 2:147-165.

Jørgensen, S.E., H. Mejer and Friis Mogens, 1978. Examination of a lake model. Ecol. Modelling, 4:253-278.

Kantha, L.H., O.M. Phillips and R.S. Azad, 1977. On turbulent entrainment at a stable density interface. J. Fluid Mechanics, 79:753-768.

Kato, H. and O.M. Phillips, 1969. On the penetration of turbulent layer into a stratified fluid. J. Fluid Mechanics. 37:643-655.

Kersting, K. and W. van der Leeuw, 1976. The use of coulter counter for measuring the feeding rates of Daphnia magna. Hydrobiol. 49(3):233-237.

Ketcham, B.H., 1939. The development and restoration of deficiencies in the phosphorus and nitrogen composition of unicellular plants. J. Cell. Comp. Physiol. 13:373-381.

King, P.H., 1970. A test of the hypothesis that vacuum filtration of lakewater releases orthophosphate. M.Sc. thesis, Univ. of Toronto, Canada. 82 pp.

Kraus, E.B. and J.S. Turner, 1967. A one-dimensional model of the seasonal thermocline. Tellus XIX.

Kremer, J.M. and S.W. Nixon, 1978. A coastal marine ecosystem simulation analysis. Spinger-Verlag.

Kuenzler, E.J. and B.H. Ketchum, 1962. Rate of phosphorus uptake by Phaedactylum tricornutum. Biol. Bull. 123:134-145.

Kuenzler, E.J. and B.H. Ketchum, 1962. Rate of phosphorus uptake by Phaedactylum tricornutum. Biol. Bull. 123:134-145.

Kuenzler E.J. and L.E. Greer, 1980. Phosphorus dynamics in a North Carolina piedmont reservoir. Rept. No. 154, Water Resources Research Institute of the Univ. of North Carolina. January.

Lean, D.R.S., 1973a. Phosphorus dynamics in lake water. Science 179:678-680.

Lean, D.R.S., 1973b. Movements of phosphorus between its biologically important forms in lake water. J. of Fish. Res. Board of Canada 30:1526-1536.

Lean, D.R.S., 1976. Phosphorus kinetics in lake water: influence of membrane filter pore size and low-pressure filtration. J. Fish. Res. Board Canada 33:2800-2804.

Leppard, G.G., A. Massalski and D.R.S. Lean, 1977. Electron-opaque microscopic fibrils in lakes: their demonstration, their biological derivation and their potential significance in the redistribution of cations. Protoplasma 92:289-309.

Levine, S.N., 1975. A preliminary investigation of orthophosphate connection and the uptake of orthophosphate by seston in two Canadian shield lakes. M.S. thesis, Univ. of Manitoba.

Levine, S.N. and D.W. Schindler, 1980. Radiochemical analysis of orthophosphate concentrations and seasonal changes in the flux of orthophosphate to seston in two Canadian shield lakes. Can. J. Fish. Aquat. Sci. 37:479-487.

Lord, J.M, G.A. Codd and M.J. Merrett, 1970. The effect of light quality on glycolate formation and excretion in algae. Pl. Physiol., Lancaster, 46:855-856.

Lotka, A.J., 1925. Elements of physical biology. Williams and Wilkins, Baltimore, pp. 88-94. (reprinted as Elements of mathematical biology, Dover, N.Y., 1956.)

Lund, J.W.G., 1950. Studies of Ascerionella formosa Hass II. Nutrient depletion and the spring maximum. Part I: Observations on Windermere, Esthwaite Water and Bleham Tarn. Part II: Discussion. J. Ecol. 38:1-14, 15-35.

Lund, J.W.G. and J.F. Talling, 1957. Botanical limnological methods with special reference to the algae. Bot. Rev. 23:489-583.

Lund, J.W.G, 1969. Phytoplankton, pp. 306-330. In Eutrophication, causes, consequences, correctives. National Academy of Science.

Mackereth, F.J., 1953. Phosphorus utilization by Asterionella formosa Hass. J. Exp. Bot. 4:296-313.

Mague, T.H., E. Friberg, D.J. Hughes and I. Morris, 1980. Extracellular release of carbon by marine phytoplankton; a physiological approach. Limnol. Oceanogr. 25(2):262-279.

Malley, D.F., P.S.S. Chang and D.W. Schindler. Decline of zooplankton of Lake 227, Expreimental Lakes Area, Ontario: 1969-1974. Manuscript (to be published).

Marra, J. 1978. Phytoplankton photosynthetic response to vertical movement in a mixed layer. Marine Biology 46:203-208.

Marra, J. 1980. Vertical mixing and primary production, In Falkowski, P.G. (ed.) Primary productivity in the sea.

Marshall, S.M. and A.P. Orr, 1955. On the biology of Calanus firmarchicus, VIII. Food uptake, assimilation and excretion in adult and stage V Calanus. J. Mar. Biol. Assoc. U.K., 34:495-529.

Millers, F.J. and R.T. Emmet, 1976. The effect of dissolved air and natural isotopic distribution on the density of water. J. Mar. Res. 34:15-24.

Monod, J., 1942. Recherches sur la croissance des cultures bacteriennes. Paris: Herman et Cie.

Moore, M.J. and R.R. Long, 1971. An experimental investigation of turbulent stratified shearing flow. J. Fluid Mechanics 49.

National Academy of Science, 1969. Eutrophication: Causes, consequences, correctives. Proceedings of the International Symposium of Eutrophication at the Univ. of Wisconsin, Madison, June 11-15, 1967.

Naumann, E., 1919. Nagra synpunkter angaende planktons ökologi. Ned särskild hänsyn till fytoplankton. Svensk. Bot. Tidskr. 13:129-158.

Naumann, E., 1927. Ziel und Hauptprobleme der regionale Limnologie. Bot. Notiser 1927:81-103.

Octavio, K.A.H., G.H. Jirka and D.R.F. Harleman, 1977. Vertical heat transport mechanisms in lakes and reservoirs. MIT Ralph M. Parsons Laboratory Technical Report No. 227, August 1977.

Ohle, W., 1938. Zur Vervollkommung der hydrochemischen Analyse III. Die Phosphorbestimmung. Z. Angew. Chem. 51:906-911.

Olsen, S., 1966. Recent trends in the determination of orthophosphate in water, p. 63-104, In H.L. Golterman and R.S. Clyme (eds.), Chemical environment in the aquatic habitat. Proc. I.B.P. Symp. Amsterdam N.V., Noord-Hollandsche Utigevers Maatschappij, Amsterdam.

Orlob, G.T., and L.G. Selna, 1967. Progress report on development of a mathematical model for prediction of temperatures in deep reservoirs - Phase 3: Castle Lake investigation. Water Resources Engineers Inc., Lafayette, California, January 1967.

Orlob, G.T. and L.A. Roesner et al., 1969. Mathematical models for prediction of thermal energy changes in impoundments. Final report to Water Quality Office, EPA, by Water Resources Engineers, Inc.

Overbeck, J., 1963. Untersuchungen zum phosphathaushalt von Grünalgen VI, Ein Beitrag zum Polyphosphatstoftwechsel des Phytoplanktons. Bor. Deutch Bot. Gesell 76(8):276-286.

Paasche, E., 1975. Growth of the plankton diatom Thalassiosira nordenskiaelcii cleve at low silicate concentrations. J. Exp. Mar. Biol. Ecol. 18:173-183.

Park, R.A., R.V. O'Neil and J.A. Bloomfield, et al., 1974. A generalized model for simulating lake ecosystems. Simulation 23(2):33-50.

Peters, R.H., 1972. Phosphorus regeneration by zooplankton. Ph.D. thesis, Univ. of Toronto.

Quay, P.D., 1977. An experimental study of turbulent diffusion in lakes. Ph.D. thesis, Faculty of Pure Science, Columbia Univ.

Radmer, R. and B. Kok, 1977. Photosynthesis: Limited yields, unlimited dreams. Bioscience, 27(9):599-605.

Reeve, M.R., 1963. The filter-feeding of Artemia I. in pure cultures of plant cella. J. Exp. Biol. 40:195-205.

Reid, R.A., D.W. Schindler and R.V. Schmidt, 1975. Light measurements in the experimental lakes area, 1969-1973. Technical Report No. 559, Fisheries and Marine Service, Canada.

Rhee, G-Yull, 1972. Competition between an alga and an aquatic bacterium for phosphate. Limnol. Oceanogr., July 1972, Vol.XVII No. 4:505-514.

Rhee, G-Yull, 1978. Effect of N:P atomic ratios and nitrate limitation on algal growth, cell composition and nitrate uptake. Limnol. Oceanogr. 23(1):10-25.

Richardson, M., 1974. Microbodies (glyoxysomes and peroxisomes) in plants. Sci. Prog. 61:41-61.

Richey, J.E., 1977. An empirical and mathematical approach toward the development of a phosphorus model of Castle Lake, California. In Ecosystem modeling in theory and practice, edited by C.A.S. Hall and J.W. Day. Wiley-Interscience.

Rigler, F.H., 1961. The uptake and release of inorganic phosphorus by Daphnia magna Straus. Limnol. Oceanogr. 6:165-174.

Rigler, F.H., 1961b. The relation between concentration of food and feeding rate of Daphnia magna Straus. Can. J. Ecol. 39:857-868.

Rigler, F.H., 1964. The phosphorus fractions and turnover time of phosphorus in different types of lakes. Limnol. Oceanogr. 9:511-518.

Rigler, F.H., 1966. Radiobiological analysis of inorganic phosphorus in lakewater. Verh. Int. Verein. Limnol. 16:465-470.

Rigler, F.H., 1968. Further observations inconsistent with the hypothesis that the molybdenum blue method measures orthophosphate in lakewater. Limnol. Ocenaogr. 13:7-13.

Rigler, F.H., 1973. A dynamic view of the phosphorus cycle in lakes, In Environmental phosphorus handbook, edited by E.J. Griffith, A. Beeton, J.M. Spencer and D.T. Mitchell, pp. 539-568. John Wiley and Sons.

Rodhe, W., 1948. Environmental requirements of freshwater plankton algae. Symbol. Bot. Upsalienses 10(1):1-149.

Rouse, H. and J. Dodu, 1955. Diffusion turbulence à traverse une discontinué de densité. La Houille Blanche 10:522-532.

Ryan, P.J. and D.R.F. Harleman, 1971. An analytical and experimental study of transient cooling pond behavior. MIT Ralph M. Parsons Laboratory Technical Report No. 161, January 1973.

Ryther, J.H., 1956. Photosynthesis in the ocean as a function of light intensity. Limnol. Oceanogr. 1:61-70.

Saunder, G.W., . The transformation of artificial detritus in lake water. Mem. 1st. Ital. Idrokiol., 29(suppl):261-288.

Schindler, D.W., F.A.J. Armstrong, S.K. Holmgren and G.J. Brunskill, 1971. Eutrophication of Lake 227, experimental lake area, northwestern Ontario, by addition of phosphate and nitrate. J. Fish. Res. Bd. Canada 28:1763-1782.

Schindler, D.W., D.R.S. Lean and E.J. Fee, 1972a. Productivity of world ecosystems. National Academy of Science, Proc. of Symposium.

Schindler, D.W., R.V. Schmidt and R.A. Reid, 1972b. Acidification and bubbling as an alternative to filtration in determining phytoplankton production by the ^{14}C method. J. Fish. Res. Bd. Canada 29:1627-1631.

Schindler, D.W., 1974. Eutrophication and recovery in experimental lakes: impolications for lake management. Science, Vol. 184, pp. 897-899. May 24, 1974.

Schindler, D.W. and E.J. Fee, 1975. The role of nutrient cycling and radiant energy in aquatic communities, from Photosynthesis and productivity in different environments, J.P. Cooper (ed.) Cambridge Univ. Press.

Schindler, D.W. and K.G. Beaty, 1976. Meteorological records for Rawson Lake watershed areas. (unpublished data).

Senft, W.H., 1978. Dependence of light-saturated rates of algal photosynthesis on intracellular concentrations of phosphorus. Limnol. Oceanogr. 23(4):709-718.

Shananhan, P., 1981. Linked hydrodynamic and biogeochemical models of shallow lake water quality.

Sharp, J.H., 1977. Excretion of organic matter by marine phytoplankton: do healthy cells do it? Limnol. Oceanogr. 22(3):381-399.

Shearer, J.A. and E.J. Fee, 1974. Phytoplankton primary production in the experimental lake area using an incubator technique -- 1973 data. Can. Fish. Mar. Serv., Tech. Rep. No. 474.

Shearer, J.A., 1976a. Light extinction measurements in the experimental lakes area -- 1974 data. Can. Fish. Mar. Tech. Rept. No. 615.

Shearer, J.A., 1976b. Phytoplankton primary production in the experimental lakes area using an incubator technique -- 1974 data. Can. Fish. Mar. Serv. Tech. Rept. No. 616.

Shen, C.Y. and F.W. Morgan, 1973. Hydrolysis of phosphorus compounds, In Environmental phosphorus handbook, edited by E.J. Griffith et al., pp. 241-264. John Wiley and Sons.

Shiao, M.C., 1976. Mathematical modeling of water quality dynamics in a deep reservoir. Ph.D. thesis, Univ. of Tennessee, Knoxville, June 1976.

Smith, E.L., 1936. Photosynthesis in relation to light and carbon dioxide. Proc. Natl. Acad. Sci. U.S.A., 22:504.

Snodgrass, W.J., 1974. A predictive phosphorus model for lakes -- development and testing. Ph.D. dissertation, Univ. of North

Carolina, Chapel Hill, N.C. 27514.

Snodgrass, W.J., and C.R. O'Melia, 1975. Predictive model for phosphorus in lakes. Environ. Sci. Technol. 9:937-944.

Solórzano, L., and J.D.H. Strickland, 1968. Polyphoste in seawater. Limnol. Oceanogr. 13:515-518.

Stainton, M.P., M.J. Capel and F.A.J. Armstrong, 1977. The chemical analysis of fresh water. 2nd ed. Can. Fish. Mar. Serv. Misc. Spec. Publ. 25:180 pp.

Stainton, M.P., 1980. Errors in molybdenum blue methods for determining orthophosphate in fresh water. Can. J. Fish. Aquat. Sci. 37:472-478.

Stauffer, R.E., 1974. Thermocline migration -- algal bloom relationships in stratified lakes. Ph.D. thesis, Univ. of Wisconsin.

Steele, J.H., 1962. Environmental control of photosynthesis in the sea. Limnol. Oceanogr. 7:137-150.

Strickland, J.D.H., 1960. Measuring the production of marine phytoplankton. Bull. Fish. Res. Bd. Canada 122:172 pp.

Strickland, J.D.H. and T.R. Parsons, 1960. A manual of sea water analysis. Bull. Fish. Res. Bd. Canada 125.

Stumm, W. and J.J. Morgan, 1970. Aquatic chemistry -- an introduction emphasizing chemical equilibrium in natural waters. Wiley-Interscience.

Sundaram, T.R. and R.G. Rehm, 1973. The seasonal thermal structure of deep temperate lakes. Tellus, XXV, 2.

Swinbank, W.C., 1963. Long wave radiation from clear skies. Quart. J. of the Royal Met. Soc. of London, Vol. 89, July 1963.

Talling, J.F., 1957. Photosynthetic characteristics of some fresh water plankton diatoms in relation to underwater radiation. New Phytol. 56:29-50.

Thomann, R.V. and D.M. DiToro et al., 1975. Mathematical modelling of phytoplankton in Lake Ontario. EAP-660/3-75-005, March 1975.

Thornton, K.W., D.E. Ford and D.L. Robey, 1976. Preliminary evaluation of water quality of proposed Lafarge Lake, Kickpoo River, Vernon County, Wisconsin. U.S. Army Corps of Engineers, Vicksburg, Mississippi, Oct. 1976, Miscellaneous paper y-76-5.

Thornton, K.W. and A.S. Lessen, 1976. Sensitivity analysis of the water quality for river-reservoir system model. U.S. Army Corps of Engineers, Vicksburg, Mississippi, Misc. paper y-76-4, 1976.

Titman, D. and P. Kilham, 1976. Sinking in freshwater phytoplankton: some ecological implications of cell nutrient status and physical mixing processes. Limnol. Oceanogr. 21(3):409.

Tolbert, N.E., 1971. Microbodies -- peroxisomes and glyoxysomes. A. Rev. Pl. Plysiol. 22:45-74.

Tolbert, N.E., 1974. Photorespiration. W.D. Stewart (ed.), Algal physiology and biochemistry. Univ. of Calif. Press, Berkeley and Los Angeles.

Turner, J.S., 1968. The influence of molecular diffusivity on turbulent entrainment across a density interface. J. of Fluid Mechanics 33.

van Niel, C.B., 1944. Bact. Reus. 8:1-11.

Vollenweider, R.A., 1965. Calculation models of photosynthesis --

depth curve and some implications regarding day rate estimates in primary production measurements. Men. 1st. Ital. Idrobiol., 18(suppl):425-457.

Vollenweider, R.A., 1969. A manual on methods for measuring primary production in aquatic environments. Int. Biol. Program Handbook 12. Oxford. Blackwell Scientific Publications. 213 pp.

Volterra, V., 1926. Memoria della R. Accademia Nazionale dei Lincei 2.31 (translated by M.E. Wells in R.N. Chapman, Animal ecology, McGraw-Hill, pp. 409-448, 1931).

Water Resources Engineers, Inc., 1972. Ecologic simulation for aquatic environments. Prepared for the Office of Water Resources Research, U.S. Department of the Interior, Dec. 1972.

Watt, W.D., 1966. Release of dissolved organic material from the cells of phytoplankton populations. Proc. R. Soc. Lond. Ser. B 164:521-551.

Watt, W.D. and G.E. Fogg, 1966. The kinetics of extracellular glycollate production by Chlorella pyrensidosa. J. Exp. Bot. 17:117-134.

Wetzel, R.G., 1975. Limnology. W.B. Saunders Company.

Wu, J., 1973. Wind-induced turbulent entrainment across a stable density interface. J. Fluid Mechanics 61.

Wunderlich, W.O., 1972. Heat and mass transfer between a water surface and the atmosphere. T.V.A. Engineering Laboratory. Report No. 14. Norris, Tennessee.

Zeman, O. and H. Tennekes, 1977. Parameterization of the turbulent energy budget at the top of the daytime atmospheric boundary layer. J. Atmos. Sci. 34.

Appendix A

MEASUREMENT OF THE PRIMARY PRODUCTION IN ELA

Since 1973, primary production of ELA has been measured with an incubator technique. The results of these measurements have been published as technical reports of the Canada Fisheries and Marine Service. Detailed descriptions of the techniques and the subsequent modifications of the techniques can be found in these reports:

(a) Phytoplankton Primary Production in the ELA Using an Incubator Technique - 1973 Data, by J.A. Shearer and E.J. Fee.

(b) Phytoplankton Primary Production in the ELA Using an Incubator Technique - 1974 Data, by J.A. Shearer.

The following section summarizes some of the important information on the field sampling techniques and the laboratory procedures for the period from 1973 to 1974.

1. Field Sampling

During the ice-free period water samples were taken from the lakes bi-weekly, and during the ice-cover period water samples were taken monthly. Whenever possible, samples were collected in the morning or at least by early afternoon. This was to avoid the severe diurnal fluctuation of the primary production as reported by Fee (1974).

Normally, at any sampling date, two samples were taken from each lake, one from the epilimnion and the other from the hypolimnion. Water samples from discrete depths were collected with either an opaque PVC Van Dorn bottle or a battery=powered peristaltic pump. A new sampling technique was developed due to the discovery of the hypolimnetic chlorophyll peaks (Fee, 1976). This new technique, which is referred to as the integrated

sampling, allows the water sample to be taken continuously over a given depth interval. From August 7, 1974, the integrated sampling was employed as the regular field sampling technique. The limit of these intervals were determined from the in situ temperature profiles and light extinction data. The integrated epilimnion samples were taken from the lake surface to the top of the thermocline, and the integrated hypolimnion samples were taken from the middle or the bottom of the thermocline slighly below the depth where 1% of the surface light penetrated.

Once taken, samples were transported to amber 2 liter polypropylene screw-top bottles. During the filling of the bottles, efforts were made to avoid the bubbling. And the bottles were filled so as to minimize the remaining bubbles after the transport. In general, great care was taken during the sampling and the transport of the samples so that no part of the samples was exposed to surface irradiance at any time. Also, whenever the ambient air temperature differed markedly from the in situ temperature of samples, samples were transported back to the laboratory in styrofoam insulated boxes even though the transport time from the field to the laboratory was less than an hour in most cases.

2. Laboratory Procedures

Upon their arrival at the laboratory, samples were processes ad quickly as possible for DIC measurement and for incubation. From June 25th, 1973, it became a regular procedure to enrich the epilimnion samples with carbon with a stock solution of 800 mg NaHCO/100 ml. This procedure was to eliminate the temporary diurnal DIC depletion in those water samples (Schindler and Fee, 1973). The enriched samples were mixed thoroughly on

a magnetic stirrer before being partitioned.

2.1 DIC Measurement

The procedure used for DIC measurement was as follows:

(a) The sample bottle was homogenized by shaking.

(b) Replicate 500 cc syringe samples were taken. These syringes were filled with a long canula to prevent any bubbling.

(c) The DIC of the sample was analyzed by the gas chromatography in the years 1973, 1974 (Stainton, 1973). (From the year 1975 on, an automatic conductimeter system has been used.)

The variance of the DIC analysis was reported to be much reduced with the introduction of the new method in 1975 (Stainton, 1976). It should be mentioned here that the DIC values for the year 1973 were not reported.

2.2 The Incubation

Preparation of the Incubation Bottles

(a) Nine 125 ml Pyrex reagent bottles were filled with water samples from the 2 liter polypropylene bottle. When the in situ temperature of the sample was low, the 125 ml reagent bottles were cooled before filling. Of the nine incubation bottles, eight were clear bottles (light bottles) and one was wrapped in aluminum foil and black PVC tape to eliminate light (dark bottle).

(b) The glass stoppers were replaced and the bottles were shaken to remove excess water from around the neck of the bottle.

(c) The stopper was removed, then aliquotes of water were removed whose volume equals the volume of the C-14 solution to be added.

(d) The C-14 solution was added to each of the nine bottles with a

Cornwall syringe fitted with a canula that extends to the bottom of the bottle.

(e) The incubation bottles were restopped and the dark bottle was sealed from the light.

(f) All the nine bottles were placed in the incubator to begin the incubation.

The Incubator

The incubator was located in a dark room to eliminate light other than that from the light bank of the incubator. Shown in Figure 1 is the incubator used for these experiments. The incubator was patterned after that used by Fee for shipboard studies on Lake Michigan (Fee, 1973). The incubation bottles were held horizontally on four vertical discs at four separate chambers which rotate at 5 rounds per minute. Two light bottles were placed in each of the four chambers; the dark bottle was placed in the chamber farthest from the light bank. Each chamber was filled with water and the temprature of each chamber could be adjusted to be within 2 of the sample in situ temperature by adding ice or hot water.

The light source was a light bank which consists of six 500 w tungsten-in-iodine-vapor lamps and this light bank was mounted vertically at one end of the incubator. At the beginning of 1974, four 100 W mercury-vapor lamps were added to the light bank in order to introduce more blue light to the incubator. A 5 cm thick Pyrex chamber, positioned between the light bank and the first incubation chamber, serves as a cooling shield to prevent the excessive heat produced by these lamps. In September 1974 this cooling shield was replaced by an air-cooled chamber composed of two

cooling sheets of 6.5 mm thick transparent polycarbonate sheet. A fan moved the cooling air across these sheets and out the top of the chamber. There is a white acrylic sheet located between the cooling shield and the first incubation chamber; this acrylic sheet diffuses the light to create a uniform light field and it attenuates the light. The additional attenuation of the light in each chamber is a result of the distance from the light bank and the single layer window screen between any two adjacent chambers.

The Measurement of the Light

The light in each chamber was recorded for the visual spectrum (400-700 nm). In eyar 1973, the light was reported in energy units of Langley per minute. In eyars 1974 and 1975, the Lambda Li-185 meter and the LI-1925 underwater quantum sensor were used for the light measurement. The new sensor measures the photosynthetically active radiation (PAR) for the visual range and the light was reported in quantum units as micro-einstein per square meters per second.

Determination of the Carbon Assimilation Rate by C-14 Method

Standard C-14 Solution

NaCO was diluted with distilled water to approximately 8 uCi/ml; the standard solution was then sealed in 20 ml ampules and autoclaved.

Procedure

(i) To each incubation bottle 1.00 cc of standard solution was added. In winter when the primary production rate was low, the added standard solution was up to 1.5 ml.

(ii) The activity of the standard solution was determined by taking 5 replicate standards and using liquid scintillation counting in a dioxane fluor (Schindler, 1966).

(iii) At the end of the incubation period, the incubation bottles were removed from the chambers and placed in a light-tight aluminum box for transfer to the processing area.

(iv) A 20 ml aliquot from each bottle was acidified and bubbled for 20 minutes according to the method described by Schindler (1972).

(v) 2.5 ml aliquots of the bubbles solution was placed in plastic liquid scintillation vials. 10-15 ml of a dioxane base flour was added to each vial (Schindler, 1966; Schindler and Holmgren, 1971).

(vi) The radioactivity was determined using a Picker Nuclear Liquimat 220 liquid scintillation counter.

(vii) The primary production rate was determined by (Fee, 1973):

$$\text{Photosynthetic rate} = \frac{(R_s - R_b) \times C \times 1.06}{H \times E \times A} \qquad (A.1)$$

where R_s = the radioactivity of the sample, R_b = the radioactivity of the dark bottle; C = the total carbon available for uptake in the water sample; A = the radioactivity added to the sample; E = the counting efficiency of the counter; H = the incubation period. The factor 1.06 accounts for the slower uptake of the tracer C-14 relative to C-12.

Appendix B

STATISTICAL METHOD OF ANALYSIS

If the primary production rate were linearly related to the environmental factors, the task of parameter estimation would be much simpler. Unfortunately, most of the researchers suggested that the primary production is nonlinearly related to the important environmental factors. The nonlinearity renders the linear regression technique useless.

It is always a better practice to preserve the functional relationship which has some physical meaning than arbitrarily fitting the dependent variable with various combinations of independent variables. Therefore, our approach in the statistical anlaysis is first using the formulations which were suggested by researchers based on laboratory osbservations. These formulations are nonlinear and the best fitted parameters are estimated by both the nonlinear parameter estimation technique and the simulation technique. If the fitting is nice, no further steps will be taken. However, if the fitting is poor then various linear regression models will be tested.

Many researchers used the step linear regression to test the importance of various environmental factors. In fact, this approach has a fundamental flaw. The non-existence of a significant linear relationship between the dependent variable and an independent variable only means what it is: the lack of linear dependence between the independent variable and the dependent variable. This should not be confused with "the lack of dependence between the independent variable and the independent variable". Hanns (1979) illustrated this point very well be presenting two nonlinear models

with their respective linear regression result.

In Figure B.1(a) the two variables are related by function: $Y = x^2/4$ for $x \geq 0$ and in Figure B.2(b) the two variables are related by function: $Y = I\sqrt{q-x^2}$ for $-3 \leq x \leq 3$. In both figures the two variables are functionally dependent. However, the correlation coefficient in Figure B.1(a) is 0.963, indicating that the two variables are strongly linearly correlated while in Figure B.1(b), $\gamma = 0$, indicating that the two variables are linearly uncorrelated. The case represented in Figure B.1(b) illustreates that one cannot conclude that x and y are unrelated based on the fact of small correlation coefficient of their linear regression result.

In the following sections, we will discuss difficulties involved in the nonlinear parameter estimation and we will describe the methods employed for this study.

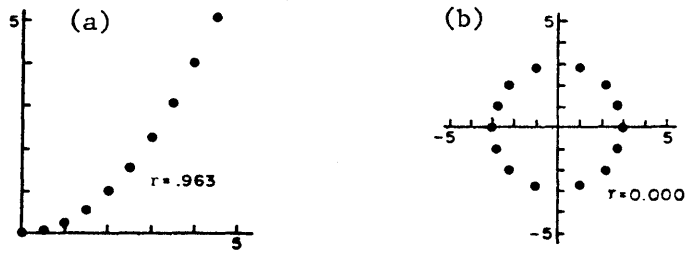

Figure B.1: Examples of the Correlation Coefficient (from Hann, 1979)

1. The Nonlinear Parameter Estimation

Two methods have been used to estimate the best fitted parameters that gives the least residual sum of the squares. The first one is the regression method and the second one is the simulation method.

The nonlinear parameter can only be solved by iterations. And the nonlinear parameter estimation technique can only give us the parameter value that is locally optimum. None of the current searching technique for nonlinear parameter estimation guarantees that this locally optimum value can be found within finite steps of iterations. There is always a possibility that the iteration would not converge after finite trials of iterations. Additionally, the statistical tests which are appropriate for linear models cannot be applied to the nonlinear models. We can only feel the goodness-of-fit of the nonlinear model by examining the residual sum of the squares. But, we cannot use any test to obtain the conclusion at any specified level of confidence.

To compensate for the insufficiency of the current nonlinear parameter estimation technique, we have decided to take an additional approach. This additional approach is the simulation method. The simulation method is to compute values of the dependent variable for all possible combinations of parameters values within our specified ranges. This method is cumbersome and time consuming, but it does give us the best possible combination of parameters within our specifications.

2. The Computer Program

We use the regression package in TROLL system for both linear and nonlinear parameter estimations. TROLL was developed by the Center for

Computational Research in Economic and Management Science of MIT. In general, the regression task uses an ordinary least-squares algorithm to compute parameter values. The parameters in linear regression models are solved directly. For nonlinear regression models, the regression task solves the parameters by continuous iterations until the difference between successive iterations for each parameter is less than 0.1% or less than a tolerance range assigned by the user. It uses the singular-value decomposition to solve for the parameters. The method is numerically very stable, even when data are highly collinear. The detailed technical discussion of TROLL's parameter estimation was presented by Eisner and Pindyck (1973).

For the simulation task, we wrote a computer program which computes values of the dependent variable from regression models for all possible combinations of parameters values. We can define the ranges of parameter values and the increment intervals. The standard output from this simulation program gives us values of 10 sets of parameters which yield the 10 minimum residual sum of the squares.